EPA-660/2-73-012
October 1973

Environmental Protection Technology Series

Negatively Buoyant Jets In A Cross Flow

Office of Research and Development
U.S. Environmental Protection Agency
Washington, D.C. 20460

RESEARCH REPORTING SERIES

Research reports of the Office of Research and Development, U.S. Environmental Protection Agency, have been grouped into five series. These five broad categories were established to facilitate further development and application of environmental technology. Elimination of traditional grouping was consciously planned to foster technology transfer and a maximum interface in related fields. The five series are:

1. Environmental Health Effects Research
2. Environmental Protection Technology
3. Ecological Research
4. Environmental Monitoring
5. Socioeconomic Environmental Studies

This report has been assigned to the ENVIRONMENTAL PROTECTION TECHNOLOGY STUDIES series. This series describes research performed to develop and demonstrate instrumentation, equipment and methodology to repair or prevent environmental degradation from point and non-point sources of pollution. This work provides the new or improved technology required for the control and treatment of pollution sources to meet environmental quality standards.

EPA REVIEW NOTICE

This report has been reviewed by the Office of Research and Development, U.S. Environmental Protection Agency, and approved for publication. Approval does not signify that the contents necessarily reflect the views and policies of the U.S. Environmental Protection Agency, nor does mention of trade names or commerical products constitute endorsement or recommendation for use.

EPA-660/2-73-012
October 1973

NEGATIVELY BUOYANT JETS IN A CROSS FLOW

By

Jerry Lee Anderson
Frank L. Parker
Barry A. Benedict

Grant # R-800613
Project 16130 FDQ
Program Element 1BA032

Project Officer

Mr. Frank Rainwater
Pacific Northwest Water Laboratory
National Environmental Research Center
Corvallis, Oregon 97330

Prepared for
OFFICE OF RESEARCH AND DEVELOPMENT
U. S. ENVIRONMENTAL PROTECTION AGENCY
WASHINGTON, D.C. 20460

For sale by the Superintendent of Documents, U.S. Government Printing Office, Washington, D.C. 20402 - Price $2.50

ABSTRACT

Negatively buoyant jets, or sinking jets, can be observed in many problems of pollutant discharge. Any chamical waste that is heavier than the receiving water into which it is discharged may act as a negatively buoyant jet. In addition, when water is taken from the hypolimnion of a deep lake or reservoir and used as cooling water, the temperature, and, consequently, the discharge may behave like a negatively buoyant jet.

Two existing jet diffusion models have been utilized to predict the trajectory and dilution of a positively buoyant jet, or a rising jet, and have been modified to account for the sinking effect.

Twenty-four experimental investigations were conducted involving different combinations of densimetric Froude number , velocity ratios, and initial angle of discharge. Salt was used as the tracer, yielding a fluid that was denser than the ambient receiving water and facilitated measuring concentration profiles of the jet plume. The coefficient of entrainment, the major mechanism of dilution, was determined as a function of the densimetric Froude number, velocity ratio, and initial angle of discharge.

The reducted drag coefficient was chosen as zero for both models since any other value would predict a trajectory whose rise would be less than experimentally observed. For all angles of discharge the entrainment coefficient increased with a decrease in the velocity ratio and with an increase in densimetric Froude number. Additionally, there was a marked decrease in the entrainment coefficient with a decrease in the initial angle of discharge.

TABLE OF CONTENTS

LIST OF FIGURES

LIST OF TABLES

ACKNOWLEDGMENTS

The successful completion of this investigation owes a great deal to a great many - more individuals than can be mentioned here. The undertaking of the laboratory investigation would have been virtually impossible without the cooperation and assistance of the faculty, staff, and students of the Environmental and Water Resources Engineering Department at Vanderbilt University. Special thanks is due to several fellow students who not only made helpful suggestions for successful completion of this investigation, but aided in taking the laboratory data, especially Ed Yandell, Bob Reimers, Eung Bai Shin, Greg Waggener, and Aaron Parker. Thanks is also due Peggie Bush for superb typing and Larry Jones for his drafting. Above all, the author wishes to express his appreciation to his wife, Patsy, for her unwavering support, encouragement, and financial assistance.

The investigations described herein were principally supported by the National Center for Research and Training in the Hydrologic and Hydraulic Aspects of Water Pollution Control in the Department of Environmental and Water Resources Engineering at Vanderbilt University, which was funded by the Environmental Protection Agency, Contract Number 16130 FDQ. The senior author was also supported for one year by an Air Pollution Traineeship and for three years by a NASA Traineeship. Grateful acknowledgment is made for the financial support from these groups.

The authors are also indebted to Mr. Frank Rainwater, Chief, National Thermal Pollution Research Program and Dr. Bruce Tichenor, of the National Thermal Pollution Research Program for their helpful discussions during the course of the work.

The investigation also served as partial fulfillment of the Ph.D. requirements of the senior author.

I CONCLUSIONS

A laboratory investigation of negatively buoyant jets using two models originally derived for the prediction of characteristics of a positively buoyant jet has been completed. The results presented predict trends rather than exact dilutions and jet trajectories. The author feels that the utilization of Fan's model for the negatively buoyant jet is theoretically more valid than the use of Abraham's model. Abraham's model can also be used to predict the dilution of jet trajectory. However, Abraham's model considers the direction of flow of the jet to be parallel to the direction of flow of the ambient fluid at some distance downstream from the discharge port. This is not the case for a negatively buoyant jet, particularly one whose densimetric Froude number is small, i.e., one in which the negative buoyancy term is large. In the case of a jet with a small densimetric Froude number, the jet will deflect downward towards the discharge level after reaching a maximum height. However, Abraham's model is advantageous in that the entrainment coefficients are constant and are not restricted to a fixed relationship with the densimetric Froude number, velocity, ratio, and initial angle of discharge.

Values of α, the entrainment coefficient, and C_d, the reduced drag coefficient, have been presented. It was found from fitting the predicted curves to the experimental data that the best fit occurred when a value of C_d equal to zero was used. Moreover, a relationship which

will predict the entrainment coefficient used in the modified Fan's model for negatively buoyant jets as a function of densimetric Froude number, velocity ratio, and initial angle of discharge has been presented. Field studies of negatively buoyant jets in a cross-flow are needed to verify appropriate values of α. This study has increased the understanding and application of the integral theory of jet dispersion to situations other than positively buoyant jets in cross-streams.

II RECOMMENDATIONS

The use of Fan's model for prediction required a priori knowledge of both the length of the zone of flow establishment and the reduced angle of inclination at the end of the zone of flow establishment. Much more information detailing the effects of a cross-stream is needed so that one can adequately describe or predict the length of the zone of flow establishment as a function of k, the velocity ratio. Heretofore, investigation on the length of the zone of flow establishment as a function of k and β_o' has been limited to discharges of 90° for submerged jets. Motz and Benedict (25) investigated the effect of the initial angle of discharge and velocity ratio on the length of the zone of flow establishment for a heated surface jet and found that the length of flow establishment was strongly dependent upon the velocity ratio. This was the approach taken by this author. However, since data was only available for a discharge of 90° for submerged jets, there should be further investigation on the effect on the length of the zone of flow establishment caused by a discharge angle other than 90°.

The reduced angle of inclination is also an important parameter for the utilization of Fan's model. Scant data exists for the effect of the velocity ratio on the value of the reduced angle of inclination. Present information indicates that the ratio of the reduced angle of inclination to the initial angle of discharge should decrease with a decrease in velocity ratio; however; the data is very scattered as

evidenced by Figure 39. Hence, no statement can be made regarding the confidence with which one should use data now available.

Fan's and Abraham's models predict the dilution and jet trajectory information for a single port injection system only. In practice, the method of injection may vary from a single port system to a multiport diffuser system. Hence, additional work is necessary to delineate the effect of interference as the jet spreads and is intersected by an adjacent jet.

Larsen and Hecker (39) investigated jet interaction for the case of submerged diffusers with a heated effluent. They found that the surface dilution due to jet interference was reduced for the case of a multi-jet discharge. However, for a negatively buoyant jet, the case of jet interference has not been investigated. The reduced dilution will probably occur and give cause for some concern since the waste will tend to sink back to the discharge level and subject the benthic organisms to higher concentrations of the waste than were predicted by a single jet discharge. Therefore, further investigations are needed to characterize the extent of dilution for a multiport discharge system.

Another feature of the negatively buoyant jet model that should receive additional attention is the maximum height of rise of the jet. Holly and Grace (40) present data for the maximum height of rise of a negatively buoyant jet in a flowing stream. However, no information is available concerning the effects of the initial angle of discharge since the studies conducted by Holly and Grace involved only a discharge

angle of 90°. The equation developed by Holly and Grace utilized an ambient densimetric Froude number which could possibly be related to a velocity ratio.

The height of rise of the jet in a river or lake may be a limiting criteria for the use of a particular initial angle of discharge. As noted by Holly and grace (40), a primary consideration in designing an outfall system for dense waste is deciding whether the dense plume will be allowed to reach the surface, or whether it will be controlled so that it remains submerged. One would like to be able to maximize the dilution and still keep the jet submerged. The jet may have to be discharged at some angle other than 90° to keep it submerged. Therefore, a relationship difining the maximum height of rise of a negatively buoyant jet as a function of the velocity ratio, jet densimetric Froude number, and initial angle of discharge, is needed.

CHAPTER I
III
INTRODUCTION

Jet dilution is one of the techniques that may be used to meet stream quality standards in order to disperse dense waste waters. However, a basic understanding of this flow phenomenon of a negatively buoyant jet is needed to adequately control this type of pollution problem and meet the stream quality standards. This thesis is expected to enhance the general understanding of the flow phenomenon of a negatively buoyant jet.

Today, as never before, the nation's attention is focused on ecology and the many parameters that affect an ecosystem. This is true whether the ecosystem is found in a pond, lake, or in the very air we breathe. This is exemplified by the increase in time, effort, and money being utilized to alleviate some of the more pressing problems. A challenge to all individuals was issued by President Johnson in 1968 in his assessment of the Nation's water resources under the Water Resources Planning Act of 1965 when he said, "A nation that fails to plan intelligently for the development and protection of its precious water will be condemned to wither because of its shortsightedness" (1).

The Water Resources Council has reported that the conterminous United States has a natural runoff averaging about 1,200 billion gallons per day (bgd). Withdrawals have been estimated at 270 bgd in 1965 and 1,368 bgd in 2020. The large withdrawals estimated for 2020 in relation to runoff indicate that even with increased inplant recycling, a large

increase in reuse of water will be required. Hence, there will be an ever-increasing need for increased investment in water development, water conditioning, waste treatment, and water management to meet the estimated requirements (1).

The ultimate disposal of man-made wastes is a major environmental problem of today. Pollution of the receiving waters has to be controlled effectively and reduced to such a level as to preserve the delicate balance of the natural biological processes. This is true for all kinds of waste for which an upper limit of pollutant can be defined. Where a limit on the concentration of a particular pollutant exists, the most advantageous method of discharging the waste would be one in which complete-mixing was accomplished instantaneously. However, the method may be limited due to the money available, hydraulic configuration of the place of discharge, or other space restrictions. Yet a waste cannot simply be discharged into a receiving stream in a manner in which its dilution would be inhibited. Hence, a method of discharging a waste must be found that lies between these two extremes, i.e., one that will approach a completely-mixed concentration below the permitted upper limit of the concentration of the particular pollutant within some specified or known distance from the discharge point.

The use of jet diffusion has received much attention in the past as a means of disposing of domestic sewage in marine areas. Brooks (2), Fan and Brooks (3), and Cederwall (4,5) present solutions of a jet diffusing into an ocean. The degree of treatment and the choice of outfall site, as well as the design of the outfall structure, must be carefully considered so that water quality requirements of the receiving

water can be met. More and better information will be needed to adequately design outfall sites and describe the dilution of waste water discharges.

In the past, much work has been conducted on the trajectories and dilution of positively buoyant jets in a flowing stream as exemplified by the work of Fan (3), Abraham (6), and Cederwall and Brooks (7). Cederwall (5), Abraham (8), and Turner (9) present solutions for the maximum height of rise of a vertical negatively buoyant jet in a stagnant environment and the concentration at its terminal height. However, no work has been conducted on negatively buoyant jets discharged into a flowing stream.

Negatively buoyant jets, or sinking jets, can be observed in many problems of pollutant discharge. Any chemical waste heavier than the receiving water may form a negatively buoyant jet. In addition, the negatively buoyant jet is found in releases of cold hypolimnic waters to the warmer receiving stream, and the release of a gaseous waste which is heavier than the receiving ambient air. It is also expected that this study on negatively buoyant jets will increase general understanding about mass and heat transfer across density gradients, a factor of vital concern in many pollution problems.

This study will include a laboratory investigation of negatively buoyant jets in a cross-flow. Various combinations of velocity ratios, densimetric Froude numbers, and initial angles of discharge will be considered. Models for positively buoyant jets in a flowing stream developed by Fan (3) and Abraham (6) will be modified and extended to

include the negatively buoyant case. Values of α, the entrainment coefficient, and, if applicable, C_d, the drag coefficient, will be determined.

CHAPTER II

IV

REVIEW OF THE LITERATURE

Jets in General

In the past, more research attention has been devoted to the problem of buoyant jets where the discharge fluid is lighter than the receiving fluid and will rise. Fan (3) presents a comprehensive review of the research heretofore accomplished. His review encompasses the field of simple jets (Figures 1a and 1b), simple plumes (Figures 2a and 2b), vertical buoyant jets and inclined or horizontal buoyant jets (Figures 3a and 3b). The variables found on the figures are defined as:

O' = origin of the coordinate system (x',y'), point of jet discharge

O = origin of the coordinate systems (x,y), beginning of the zone of established flow (The zone of flow establishment will be discussed in detail in a later section.)

Q_o = initial volume flux at the nozzle

D_o = diameter of jet at orifice and orifice diameter

r = radial distance measured from the jet axis

x' = coordinate axis in horizontal direction on the same plane as jet axis with origin at O'

y' = coordinate axis in vertical direction, with origin at O'

U_a = ambient uniform velocity

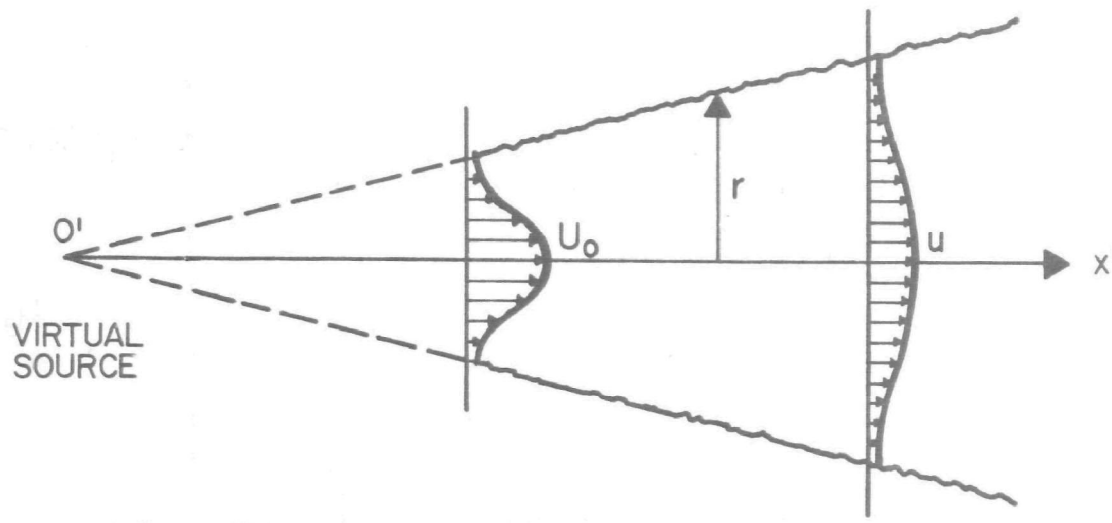

a. CONCEPT OF A VIRTUAL SOURCE

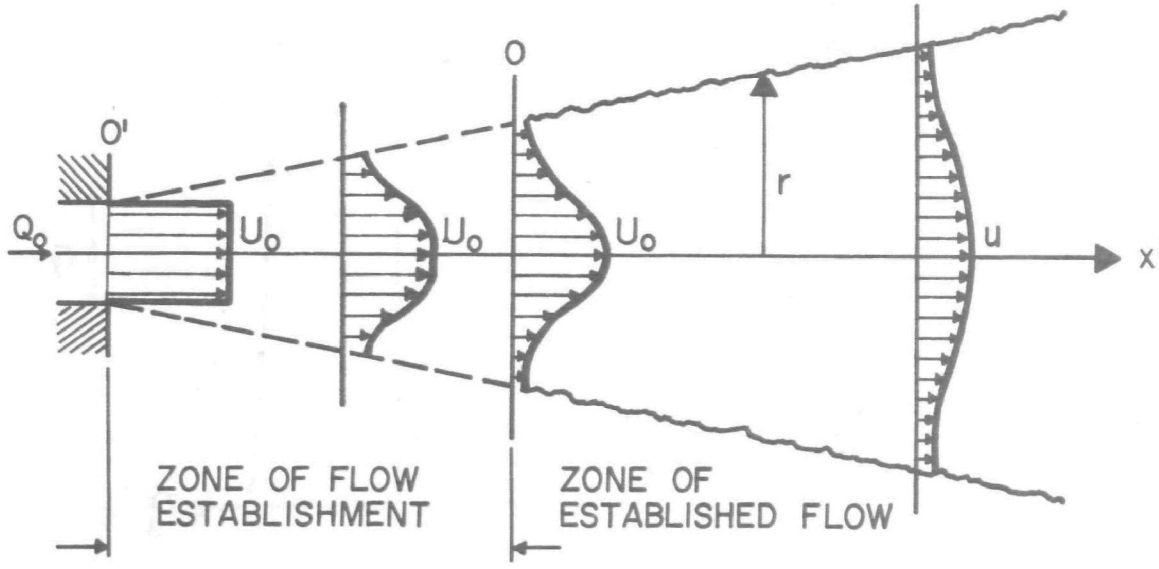

b. ZONE OF FLOW ESTABLISHMENT AND ZONE OF ESTABLISHED FLOW

FIGURE 1 - A SIMPLE JET (AXISYMMETRIC CASE)

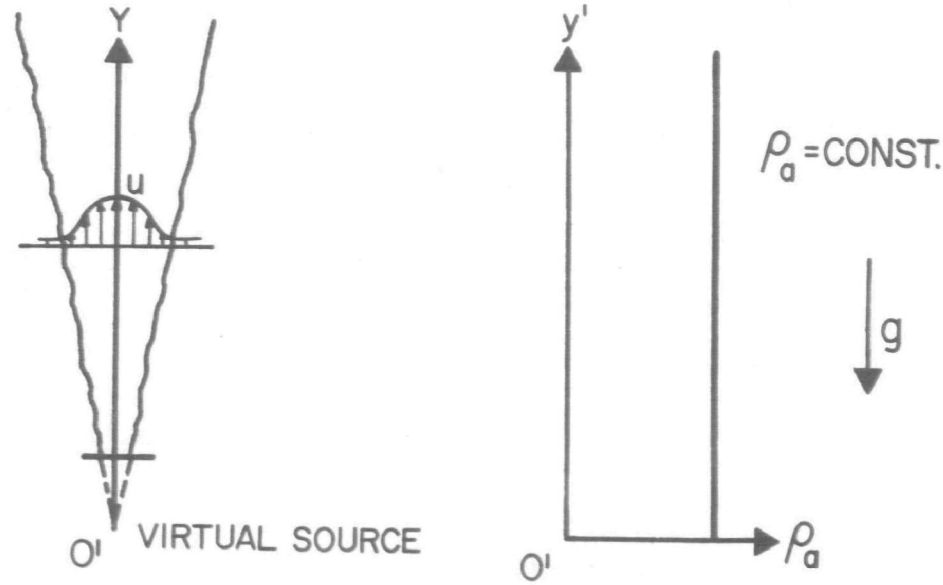

a. A SIMPLE PLUME IN A UNIFORM ENVIRONMENT

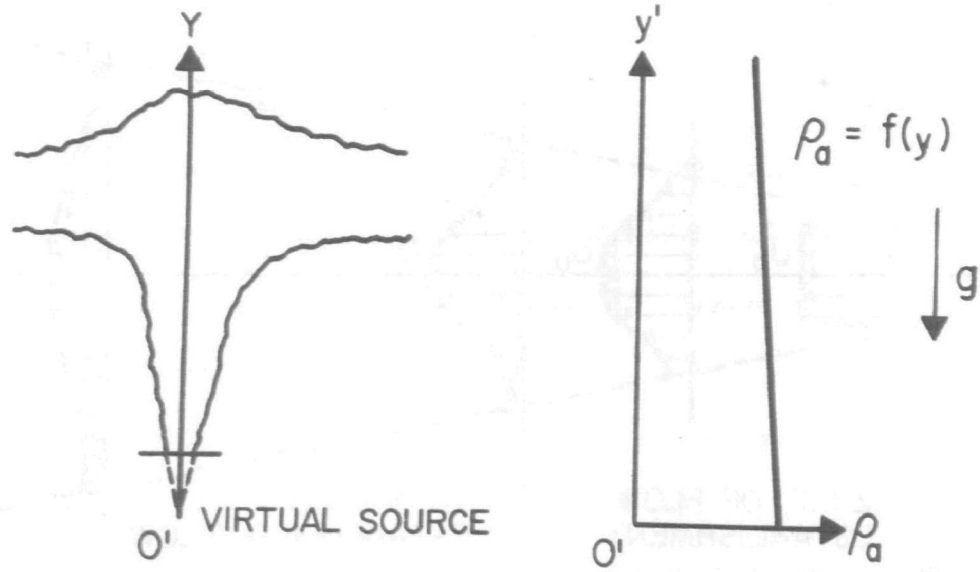

b. A SIMPLE PLUME IN A LINEARLY STRATIFIED ENVIRONMENT

FIGURE 2 - PROFILE VIEWS OF SIMPLE PLUMES IN UNIFORM AND STRATIFIED ENVIRONMENTS

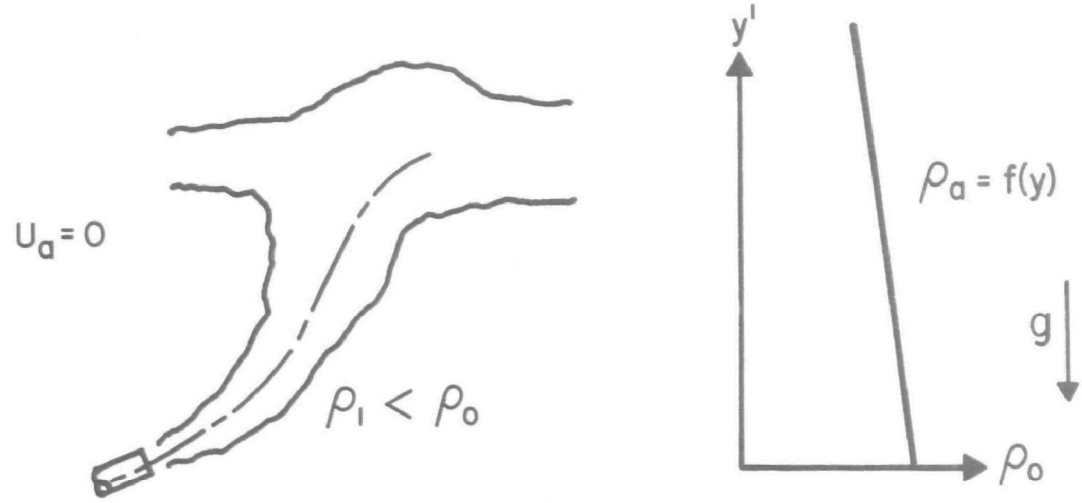

a. AN INCLINED ROUND BUOYANT JET (FORCED PLUME) IN A STAGNANT ENVIRONMENT WITH LINEAR DENSITY STRATIFICATION

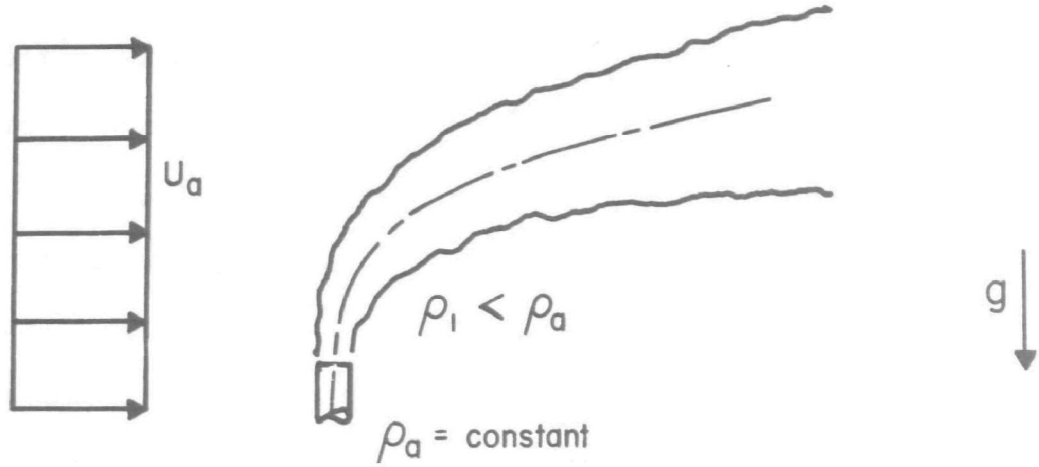

b. A VERTICAL ROUND BUOYANT JET IN A UNIFORM HORIZONTAL WIND (CROSS STREAM)

FIGURE 3 - PROFILE VIEWS OF BUOYANT JETS
[AFTER FAN (3)]

U_o = initial jet discharge velocity

u = jet velocity at the centerline of the jet

ρ_a = density of the ambient fluid

ρ_o = reference density taken as $\rho_a(0)$

ρ_1 = initial jet density

g = gravitational acceleration

A simple jet (or ordinary momentum jet) is the turbulent flow pattern generated by a continuous source of momentum. Albertson, Dai, Jensen, and Rouse (10) have presented a model which describes the behavior of a simple jet, whereas a simple plume is characterized by a turbulent flow pattern generated by a continuous source of buoyancy. The more common case that has received most of the attention in the past is a steady release of heat. The plume has no initial momentum flux. Hence, the main direction of flow of the plume is in the direction of the buoyancy force. Due to continuous action of the buoyancy force, the momentum flux of the plume increases with increasing height in the case of a heated plume. A buoyant jet (or forced plume) is characterized both by a steady release of mass, "momentum," and buoyancy from a source. The source may be situated in either a uniform environment or stably stratified fluid. Hence, the simple jet and simple plume are limiting cases of buoyant jets.

Morton (11) and Fan (3) have presented solutions for buoyant jets. Fan presents a solution for an inclined round buoyant jet in a stagnant environment with linear density stratification and for a round buoyant jet in a uniform cross-stream of homogeneous density. Development of the round buoyant jet in a uniform cross-flow of homogeneous density

will be discussed at length in the following pages.

Parker and Krenkel (12) present a more recent review of analytical models of jet studies. In their report the integral approach of Morton, Taylor, and Turner (13) is reviewed with Morton's (14) basic assumptions:

a. The fluids are incompressible

b. Flow is fully turbulent, implying no Reynolds number dependence and that molecular diffusion is negligible compared to turbulent diffusion.

c. Longitudinal diffusion is negligible compared to lateral diffusion.

d. The largest variation of fluid density through the flow field is small compared with the reference density. Hence, variations of density can be neglected when considering inertial terms, but must be included in gravity terms. As Fan (3) notes, this small density variation implies that the conservation of mass flux can be approximated by the conservation of volume flux. The assumption of small density variation is commonly called the Boussinesq assumption.

e. Velocity profiles are similar in consecutive transverse sections of the jet in the zone of established flow. Fan (3) also assumed a similarity for profiles of buoyancy and concentration of tracer. Buoyancy and concentration profiles are given by the relation:

$$\rho_a - \rho^*(s,r,\phi) = [\rho_a - \rho(s)]\, e^{-r^2/b^2} \qquad (1)$$

and

$$c^*(s,r,\phi) = c(s)\ e^{-r^2/b^2} \tag{2}$$

where ρ_a = density of the ambient fluid

ρ^* = local density within a jet

s = distance along the jet axis from the zone of establishment

r = radial distance measured from the jet axis on A

A = jet cross-section normal to the jet axis

ϕ = angular coordinate on a cross-section normal to the jet axis

b = local characteristic length of half-width of the jet

c^* = local concentration value

c = concentration at the jet axis

Figure 4 shows a round buoyant jet discharging at a velocity u_o into a uniform cross-stream of velocity U_a. In addition to the above variables, the other variables shown on Figure 4 are defined below:

θ = angle of inclination of the jet axis (with respect to the x-axis)

The x-axis is formed by passing a plane through the origin, O, in the same direction as the flow of the ambient stream.

β_o' = initial angle of inclination

β_o = angle of inclination at the end of zone of flow establishment

s_e' = length of zone of flow establishment

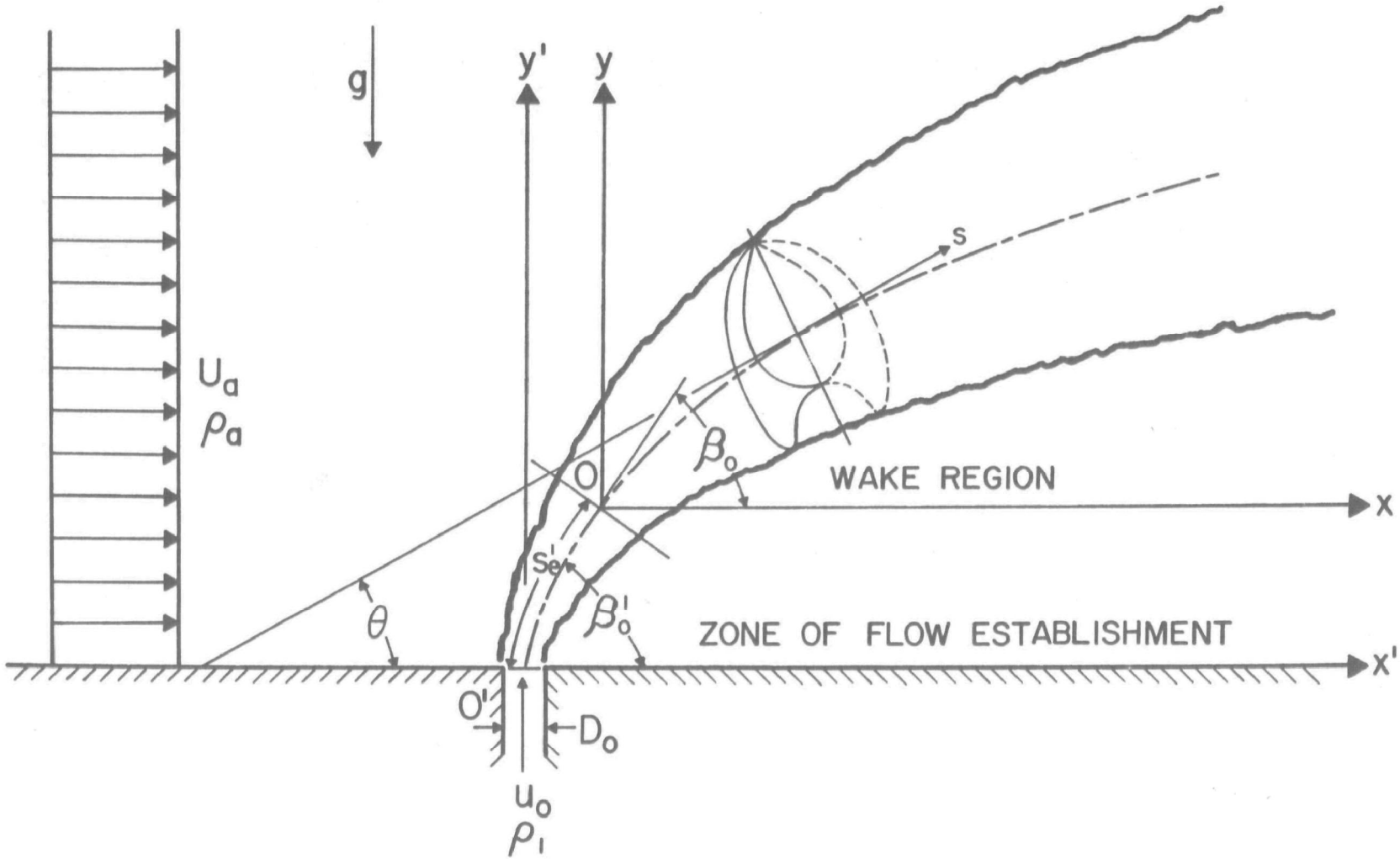

FIGURE 4 - SCHEMATIC DIAGRAM OF A PROFILE VIEW OF A ROUND BUOYANT JET IN A UNIFORM CROSS STREAM OF HOMOGENEOUS DENSITY

In addition to the above assumption, Fan made two additional assumptions which are also appropriate in this study. They are:

f. Within the range of variation, the density of the fluid is assumed to be a linear function of either salt concentration or heat content above the reference level. However, Morton (13) did consider the density difference expressed as a linear function of temperature difference and cubical expansion coefficient. This is a reasonable assumption as can be seen in Appendix A. It is appropriate in this case since measurements of the conductivity of the fluid were used to obtain the concentration of salt along the jet axis. The procedure will be dealt with in a later chapter.

g. Curvature of the trajectory of the jet is small. That is, the ratio of the local characteristic length to the radius of curvature is small. Hence, the effect of curvature is neglected. In the case of the negatively buoyant jet, for small Froude numbers, the radius of curvature is small. Hence, the ratio of the local characteristic length to the radius of curvature may be large, but as a first approximation of the system, the effect of curvature is also neglected.

Zone of Flow Establishment

It can be shown that a zone of flow establishment must exist beyond the efflux section of either a two-dimensional jet or a three-dimensional submerged jet (10). With reference to Figures (1b) and (4),

the fluid discharged from the boundary opening may be assumed to be of relatively constant velocity. At the efflux section there will necessarily be a pronounced velocity discontinuity between the jet and the surrounding fluid. The eddies generated in the region of high shear will immediately result in a lateral mixing which progresses both inward and outward with distance from the efflux section. Fluid within the jet is gradually decelerated; fluid from the surrounding region is gradually accelerated and entrained into the jet. The limit of the zone of flow establishment is reached when the mixing region has penetrated to the centerline of the jet. Albertson, et al. (10), reported that the zone of flow establishment for a three-dimensional submerged jet in a stagnant non-stratified environment is $x_o/D_o = 6.2$ where x_o = distance along the axis of the jet from the efflux (discharge) section to point of established flow. In the case of a jet in a cross-flow, x_o will be replaced by s_e'.

Fan (3) reported values obtained from Gördier (15), Jordinson (16), and Keffer and Baines (17) for the length of the zone of flow establishment for different velocity ratios. Fan developed a plot of s_e'/D_o versus k for k values of 4, 6, and 8 where

s_e' = the distance along the jet axis from the discharge point to the point of established flow and

k = velocity ratio = U_o/U_a

where

U_o = jet discharge velocity and

U_a = ambient velocity.

The equation of the data presented by Fan is

$$s_e'/D_o = 6.2\ e^{-3.22/k} \tag{4}$$

as reported by Parker and Krenkel (12). Note that s_e'/D_o approaches 6.2, which is the same coefficient reported by Albertson, as 1/k approaches zero.

Since the above equation was developed from using only 4 points, it was felt necessary to seek additional sources of information. Pratte and Baines (18) have presented results as shown in Figure 5.

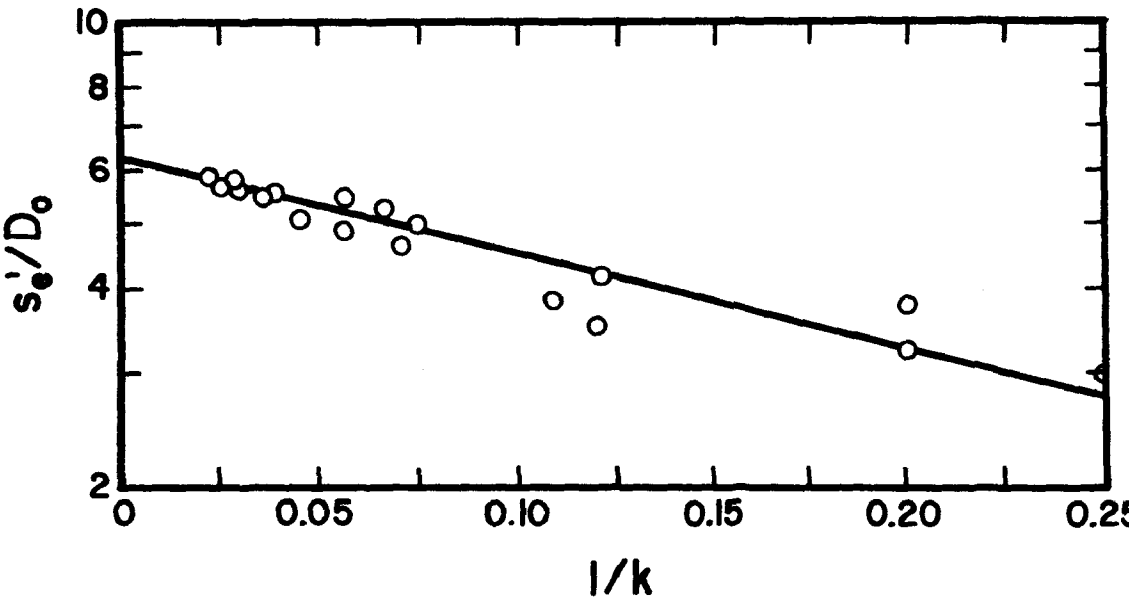

FIGURE 5 - LENGTH OF ZONE OF ESTABLISHMENT VERSUS 1/k

These authors felt that the different diameters used in their studies affected the length of the potential core (zone of flow establishment). However, it is altogether possible that experimental error could have just as easily been the villain, since the diameters of the orifices used were all less than 1/2-inch. Hence, a least

squares fit of the data was performed, and as a result the equation $s'_e/D_o = 5.91\ e^{-2.57/k}$ was developed. Hence, this lends credence to the equation developed by Parker and Krenkel (12) and will be used in this report.

Mechanisms of Entrainment in Turbulent Flow

The mechanism of entrainment has received much attention over the last 20 years in determining buoyant jet behavior. Tollmien (19) and Schmidt (20) studied the problems of turbulent non-buoyant and buoyant jets, issuing vertically upwards into a homogeneous fluid at rest. It was noted that the similarity of velocity and concentration profiles provided sufficient information to solve for a jet's trajectory with either negligible or predominant influence of buoyancy. However, as noted by Abraham (21), for jets which are characterized by a varying influence of buoyancy effects within the field of motion, the entrainment principle is necessary.

Morton, Taylor, and Turner (13) first proposed an entrainment mechanism for the dilution of a maintained plume. They proposed the equation

$$\frac{dQ}{dx} = 2\ \pi\alpha ub \tag{5}$$

where $\frac{dQ}{dx}$ represents the rate of change of volume flux and α is the coefficient of entrainment. This equation states that the rate of entrainment at the edge of the plume is proportional to some characteristic velocity at that point. They noted that when a stream is in contact with another stream the eddies which cause transfer of matter

between them are characterized by velocities proportional to the relative velocity of the two streams. They developed equations for (a) a maintained plume in a uniform ambient stagnant fluid, (b) a point source in a stratified fluid, and (c) a uniformly stratified fluid. The entrainment coefficient was considered constant at about 0.093.

Morton (11) states that the structure of the turbulence within a plume (jet in the case of a forced plume from a point source of momentum) and the rate of entrainment at its mean edge depends only on the difference in mean density and mean velocity between the plume axis and the ambient fluid.

Fan (3) used this technique in the analysis of a turbulent round buoyant jet in a flowing stream. The entrainment for a jet in a cross stream is assumed to be represented by the equation

$$\frac{dQ}{ds} = 2\,\pi\alpha b\,|\vec{U}_j - \vec{U}_a| \tag{6}$$

where b is again a characteristic length defined by the assumed velocity profile. The variables $\vec{U}_j$ and $\vec{U}_a$ are defined by the following equations:

$$\vec{U}_i = \vec{i}(U_a \cos\theta + u) \tag{7}$$

$$\vec{U}_a = \vec{i}(U_a \cos\theta) + \vec{j}(U_a \sin\theta) \tag{8}$$

where $\vec{i}$ is a vector in the direction tangent to the jet axis and $\vec{j}$ is a vector perpendicular to the jet axis. Hence, $|\vec{U}_j - \vec{U}_a|$ is the magnitude of the vector difference in the two velocities. Fan assumed α to be constant in the analysis.

Abraham (21) investigated the principle of entrainment and discussed

its restrictions in solving problems of jets. It was maintained that the entrainment coefficient, as defined above, was not constant. Abraham introduced a new constant, E, which relates the rate at which work is done by turbulent shear per unit time in a layer with some thickness, dx, at some level, x, per rate of vertical flow, Q_v.

However, Fan and Brooks (22) in the discussion of Abraham (23), considered the rate of entrainment to be proportional to the local characteristic (or maximum) velocity and the local characteristic radius of the jet or plume. They noted that the value of α for buoyant plumes based on data of Rouse, Yih, and Humphreys (24) was 0.082, while for momentum jets the value was 0.057 based on data by Albertson, Dai, Jensen, and Rouse (10). Fan and Brooks recognized that the entrainment coefficient could not be a universal constant, but varied as the relative buoyancy or local Froude number changed. However, for simplicity's sake, it was assumed constant. Fan (3) considered the entrainment coefficient to be constant along the jet trajectory for a particular set of values of velocity ratio and densimetric Froude number, but was a variable dependent on each different set of values of velocity ratios and densimetric Froude number. The densimetric Froude number is defined as:

$$F = \frac{U_o}{\sqrt{g\left|\frac{\Delta\rho}{\rho_a}\right| D_o}} \tag{9}$$

where $U_o = u_o + U_a \cos \beta_o$ = initial jet discharge velocity

U_a = ambient uniform velocity

u_o = jet discharge velocity at orifice

β_o = angle of inclination at the end of the zone of flow establishment

g = gravitational constant

$$\left|\frac{\Delta\rho}{\rho_a}\right| = \frac{\rho_a - \rho_1}{\rho_a} \tag{10}$$

also

$$k = \frac{U_o}{U_a} = \frac{u_o + U_a \cos \beta_o}{U_a} \tag{11}$$

For the case under study, i.e., negatively buoyant jets, it is advantageous to use the absolute value of the density difference. A more explicit definition of the above variables is given in Figure 4.

Fan (3) found that values for α for a round buoyant jet in a cross flow varied from 0.4 to 0.5 for a range of velocity ratios from 4 to 16 and a range of densimetric Froude numbers from 10 to 80. Benedict and Motz (25) reported values of the entrainment coefficient varying from 0.13 to 0.46 for heated surface jets discharged into flowing ambient streams. Abraham (6) modified Fan's approach and considered the solution of a round buoyant jet with two distinct regions of entrainment. This modification will be discussed in more detail in Chapter III.

Abraham suggests that the jet velocity, at a sufficiently great distance downstream from the nozzle of the jet fluid, is about equal to the velocity of the ambient fluid. Hence, the entrainment may be described as if the jet was a cylindrical thermal. Richards (26) describes a

cylindrical thermal as a body of fluid of cylindrical shape with its horizontal axis moving through a stagnant surrounding fluid due to a density difference between the surrounding fluid and the particular body of fluid under consideration. Hence, Abraham describes the volumetric flux and momentum flux of a round buoyant jet in terms of the entrainment of a simple jet and the entrainment of a cylindrical thermal. The values of the entrainment coefficients used for the simple jet and cylindrical thermal were 0.057 and 0.5, respectively. These values of the entrainment coefficient were considered constant for all combinations of densimetric Froude numbers and velocity ratio.

It can be seen that there are many different values for the entrainment coefficient, dependent upon the case under study. However, in most cases the value of the entrainment coefficient is unique for a specific combination of densimetric Froude number and velocity ratio. This approach is used in this study.

Negatively Buoyant Jets

The first attempt to deduce the path followed by a jet of initial density different from its surroundings was reported by Groume-Grjimailo (27). However, this formula neglected all consideration of viscosity or entrainment and was really based on the parabolic path of a projectile.

Bosanquet, et al. (27), studied the effect of density difference on the paths of jets. Equations were developed to predict the trajectories. However, since these experimental tests were conducted in a transparent box with baffles, they were essentially conducted in a

stagnant environment. Hence, the applicability to a negatively-buoyant jet in a cross-flow is limited.

Turner (9) studied jets and plumes with negative or reversing buoyancy. In an attempt to explain the oscillation occurring at the top of a cumulus cloud due to evaporation, Turner injected salt water vertically into a stagnant basin. The most feasible explanation put forth was that the evaporation produced a reversal of the buoyant force.

In these experiments the salt water was injected upwards. Initially the pulse of fluid looked like a buoyant plume with a vortex-like front and steady plume behind. The velocity decreased more rapidly with height and instead of rising indefinitely with constant shape, the whole plume broadened, came to rest, and then started to fall back. The steady-state position was reached with the top at a lower height than that attained initially, with an upflow in the center, and a downflow surrounding this. Figure 6 is a sketch showing the relative shape of a jet with negative buoyancy.

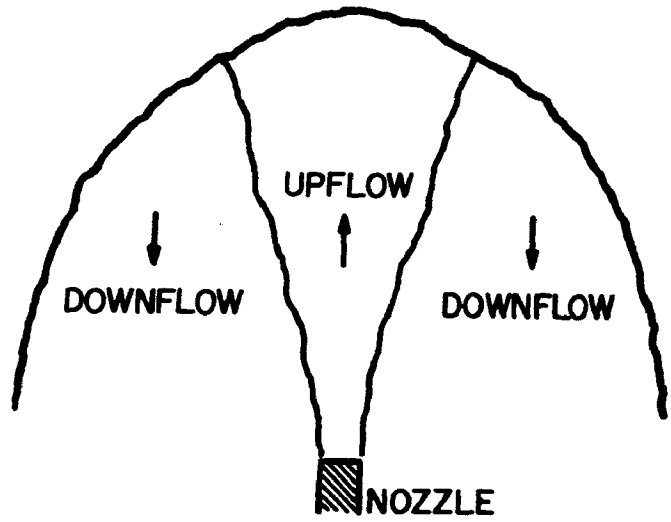

FIGURE 6 - JET WITH NEGATIVE BUOYANCY

The three phases distinguished were (a) a 'starting plume', advancing and growing by mixing over its top and sides, (b) the cap stopped rising while it continued to grow; negative buoyancy is being accumulated here, and (c) the cap collapsing. Turner studied two different cases, a heavy jet injected upward and the plumes with reversing buoyancy. Turner's results concerning the heavy jet were of particular interest to this study. For a heavy jet injected upwards, two parameters, M (momentum flux) and F_2 (buoyancy flux) were used to define the flow from a small source (essentially a point source). The developed equation took the form

$$y_t = CM^{0.75}F_2^{-0.5} \tag{12}$$

where C = a constant

y_t = the mean vertical height of rise of the plume

$$M = \frac{\pi D_o^2 U_o^2}{4} \tag{13}$$

$$F_2 = \pi g\left(\frac{\rho_1 - \rho_a}{\rho_a}\right)\frac{D_o^2}{4}\ U_o = \pi D_o \frac{U_o^3}{4F^2} \tag{14}$$

Evaluation of the experimental data shows that C = 1.85. Hence, substituting the value of C and Equations 13 and 14 into Equation 12 and dividing both sides of Equation 12 by D_o, Equation 15 is developed.

$$\frac{y_t}{D_o} = 1.74\ F \tag{15}$$

The main conclusion that can be drawn from the above research is that jets in which the buoyancy force always act downward, and which must be driven upward by momentum at the source, reach a steady height

and fluctuate randomly about this height.

Abraham (8) has studied the problem of jets with negative buoyancy in homogeneous fluids. He made a distinction between a zone with positive entrainment near the orifice and a zone with negative entrainment near the ceiling level. Abraham developed an expression for the ceiling level of a heavy jet injected upward, which is

$$\frac{y_t}{D_o} = 1.94\ F \tag{16}$$

In the above Equations 15 and 16, the densimetric Froude number, F, is calculated by dividing the density difference, $\Delta\rho$, by the density of the jet fluid, ρ_1, which is different from the definition of F in Equation 9. However, the resulting value of F will not be significantly changed if it is divided by either ρ_a or ρ_1 since $\rho_a \simeq \rho_1$.

Fan (28) used his model to theoretically predict the dilution and trajectory of waste gas discharges from campus buildings. The mixing of waste gas discharged from a vertical fumehood exhaust in a wind is basically a phenomenon of turbulent jet mixing in a crosswind. The waste gas jet bends over toward the downwind direction due to the action of ambient wind motion. In the process, the jet entrains the ambient air, growing in volume and width.

Fan also considered a sinking jet in a calm atmosphere. The governing dimensionless parameters were velocity ratio and jet densimetric Froude number. The cases for a negatively buoyant jet considered were for combinations of densimetric Froude numbers of 80, 40, and 20, and velocity ratios of 4, 8, 12, 20, 24, and 32.

In a calm atmosphere ($U_a = 0$ or $k = \infty$), a jet rises indefinitely if it has positive buoyancy or $F > 0$, but a jet with negative buoyancy would eventually sink back to the discharge level and spread over the roof or ground after reaching a maximum height. For a negatively buoyant jet, the initial upward momentum of the jet is gradually reduced by the constant downward action of the gravitational force. Using the integral approach of Turner (9), Fan made an estimate of the height of rise of the jet as

$$\frac{y_t}{D_o} = 1.9\ F \tag{17}$$

and the dilution ratio S_t at $y = y_t$ as

$$S_t \approx \sqrt{\frac{4\alpha}{5}}\ F \qquad \text{(for } F > 10\text{)} \tag{18}$$

or

$$S_t \approx 0.25\ F \qquad \text{(for } \alpha = 0.082\text{)} \tag{19}$$

Morton (11) investigated the height of rise of a negatively buoyant forced plume issuing vertically into a stagnant environment. He considered the effect of the discharge of momentum from a virtual source of buoyancy and presented a solution in non-dimensional parameters. An equation was developed for the maximum height of rise in terms of the non-dimensional parameters. However, as noted by Morton, Turner, and Taylor (13), a correction must be made for a jet or forced plume emitted from an orifice when a point source is considered.

Cederwall (5) states that, in the case of a jet issued vertically upwards into a homogeneous, lighter ambient fluid, the initial momentum

and buoyancy force are opposing each other. However, the basic considerations are essentially the same as for a positively buoyant jet, as long as the vertical momentum of the jet is sufficient to maintain positive entrainment. Equations 20 and 21 were developed to describe the velocity and concentration profile for a negatively buoyant jet.

$$\frac{U}{U_o}(y') = 6.2 \frac{D_o}{y'} \left(1 - 0.22 \frac{y'}{D_o^2 F^2}\right)^{-0.33} \tag{20}$$

and

$$\frac{c(y')}{c_o} = 5.6 \frac{D_o}{y'} \left(1 - 0.22 \frac{y'}{D_o^2 F^2}\right)^{-0.33} \tag{21}$$

Equation 22 was also developed to predict the maximum height of rise for a negatively buoyant jet.

$$\frac{y_t}{D_o} = 2.9 \, F^{0.67} \tag{22}$$

However, Cederwall noted that for small values of F, Equation 22 will not hold. Figure 7 is a comparison of experimental data (Table 1) obtained by Cederwall and is compared to the previously developed Equations 15 and 16. Also, Cederwall compared Equation 23, from the work of Priestley and Ball (29), in Figure 7 with data obtained at Chalmers Institute of Technology (5).

$$\frac{y_t}{D_o} = 1.85 \, F \tag{23}$$

The equations that Cederwall compared for the height of rise of a negatively buoyant jet in a stagnant fluid are listed below:

TABLE 1 - HEAVY VERTICAL JET EXPERIMENTS IN HOMOGENEOUS AMBIENT FLUID

Run	F	$\frac{y_t}{D_o}$	$\frac{y_t}{D_o}$ Flowing Ambient Fluid	$\frac{y_t}{D_o F}$	$\frac{y_t}{D_o F}$ Flowing Ambient Fluid
1	9.3	14	--	1.50	--
2	10.5	17	--	1.62	--
3	20.4	30	--	1.47	--
4	28.8	32	54	1.11	1.88
5	31.8	43	58	1.35	1.82
6	20.6	26	38	1.26	1.84

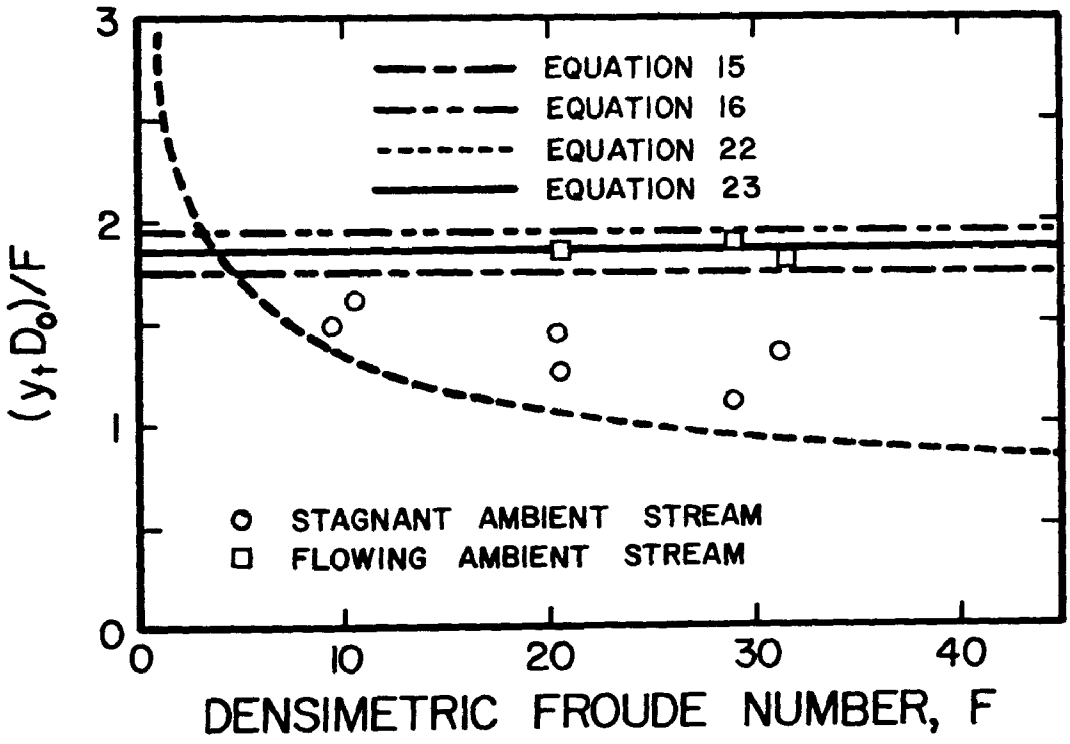

FIGURE 7 - MAXIMUM HEIGHT OF NEGATIVELY BUOYANT JETS [AFTER CEDERWALL (5)]

1. $y_t/D_o = 1.74\ F$ (15)

2. $y_t/D_o = 1.94\ F$ (16)

3. $y_t/D_o = 2.9\ F^{0.67}$ (22)

4. $y_t/D_o = 1.85\ F$ (23)

Cederwall noted that the equations developed by Abraham (Equation 16) and Priestley and Ball (Equation 23) gave better prediction of the maximum height of rise of a negatively buoyant jet in a flowing stream. However, the velocity of the flowing ambient stream [Cederwall (5)] is not given, nor is the value of the jet discharge velocity given. Hence, no statement can be made concerning the effect of the velocity ratio or the relative strength of the jet on the terminal height of rise of a negatively buoyant jet in a flowing ambient stream.

A review of the literature concerning negatively buoyant jets indicates a paucity of information concerning the experimental verification of any models which predict the dilution and trajectory of the jet. However, Cederwall (5) noted that the theoretical considerations for a negatively buoyant jet are essentially the same as these for a positively buoyant jet. Cederwall noted that the only difference between a negatively buoyant jet and a positively buoyant jet is that the initial momentum and buoyancy force are opposing each other. Hence, the models for a positively buoyant jet, with an appropriate modification to the buoyancy force terms, should be able to predict the dilution and trajectory of a negatively buoyant jet. Thus, the integral approach of Morton, Taylor, and Turner (13) applied to a negatively

buoyant jet in the same manner as Fan (3) and Abraham (6) treated a positively buoyant jet should yield a satisfactory and usable means of evaluating the characteristics of a negatively buoyant jet. These two models are developed in more detail in Chapter III.

1. $y_t/D_o = 1.74\ F$ (15)

2. $y_t/D_o = 1.94\ F$ (16)

3. $y_t/D_o = 2.9\ F^{0.67}$ (22)

4. $y_t/D_o = 1.85\ F$ (23)

Cederwall noted that the equations developed by Abraham (Equation 16) and Priestley and Ball (Equation 23) gave better prediction of the maximum height of rise of a negatively buoyant jet in a flowing stream. However, the velocity of the flowing ambient stream [Cederwall (5)] is not given, nor is the value of the jet discharge velocity given. Hence, no statement can be made concerning the effect of the velocity ratio or the relative strength of the jet on the terminal height of rise of a negatively buoyant jet in a flowing ambient stream.

Briggs (42) presents an excellent review of existing plume rise observations and formulas. Nine formulas are reviewed and compared with data from sixteen different sources. Briggs chose Equation 94 as the best predictive equation. However, Equation 94 must be modified by assuming that a ceiling height is reached at a distance of ten stack heights downwind. Other equations are presented which are dependent upon different stability conditions.

$$\Delta h = 1.6\ F\ U_a^{-1}(X')^{.667} \quad (94)$$

in which Δh = plume rise above top of stack.

A review of the literature concerning negatively buoyant jets indicates a paucity of information concerning the experimental verification of any models which predict the dilution and trajectory of the

jet. However, Cederwall (5) noted that the theoretical considerations for a negatively buoyant jet are essentially the same as these for a positively buoyant jet. Cederwall noted that the only difference between a negatively buoyant jet and a positively buoyant jet is that the initial momentum and buoyancy force are opposing each other. Hence, the models for a positively buoyant jet, with an appropriate modification to the buoyancy force terms, should be able to predict the dilution and trajectory of a negatively buoyant jet. Thus, the integral approach of Morton, Taylor, and Turner (13) applied to a negatively buoyant jet in the same manner as Fan (3) and Abraham (6) treated a positively buoyant jet should yield a satisfactory and usable means of evaluating the characteristics of a negatively buoyant jet. These two models are developed in more detail in Chapter III.

CHAPTER III

V

ANALYTICAL DEVELOPMENT OF FAN'S AND ABRAHAM'S MODEL

In this chapter both Fan's and Abraham's models will be reviewed and normalized so that they can be used to describe negatively buoyant jets.

Fan's Model for a Round Buoyant Jet in a Uniform Cross Stream

Fan (3) applies the integral approach of Morton, Taylor, and Turner (13) to solve the problem of a round buoyant jet in a cross stream. Figure 8 shows a round buoyant jet discharging at a velocity u_o into a uniform cross stream of velocity U_a. The densities of the discharged fluid and the ambient fluid are ρ_l and ρ_a, respectively. The flow becomes fully developed at a short distance s_e' from the nozzle, 0' is taken at the beginning of the zone of flow establishment, and 0 is taken at the beginning of the zone of established flow. θ is the angle of the inclination of the trajectory with respect to the horizontal x-axis.

For the case of a positively buoyant jet, there are two reasons for the deflection of the jet toward the downstream direction - the low pressure region established behind the jet and the entrainment of ambient horizontal momentum as the jet entrains the fluid of the cross stream. Yet, in the case of the negatively buoyant jet, the jet will reach a maximum height and then bend over toward the region of y = 0

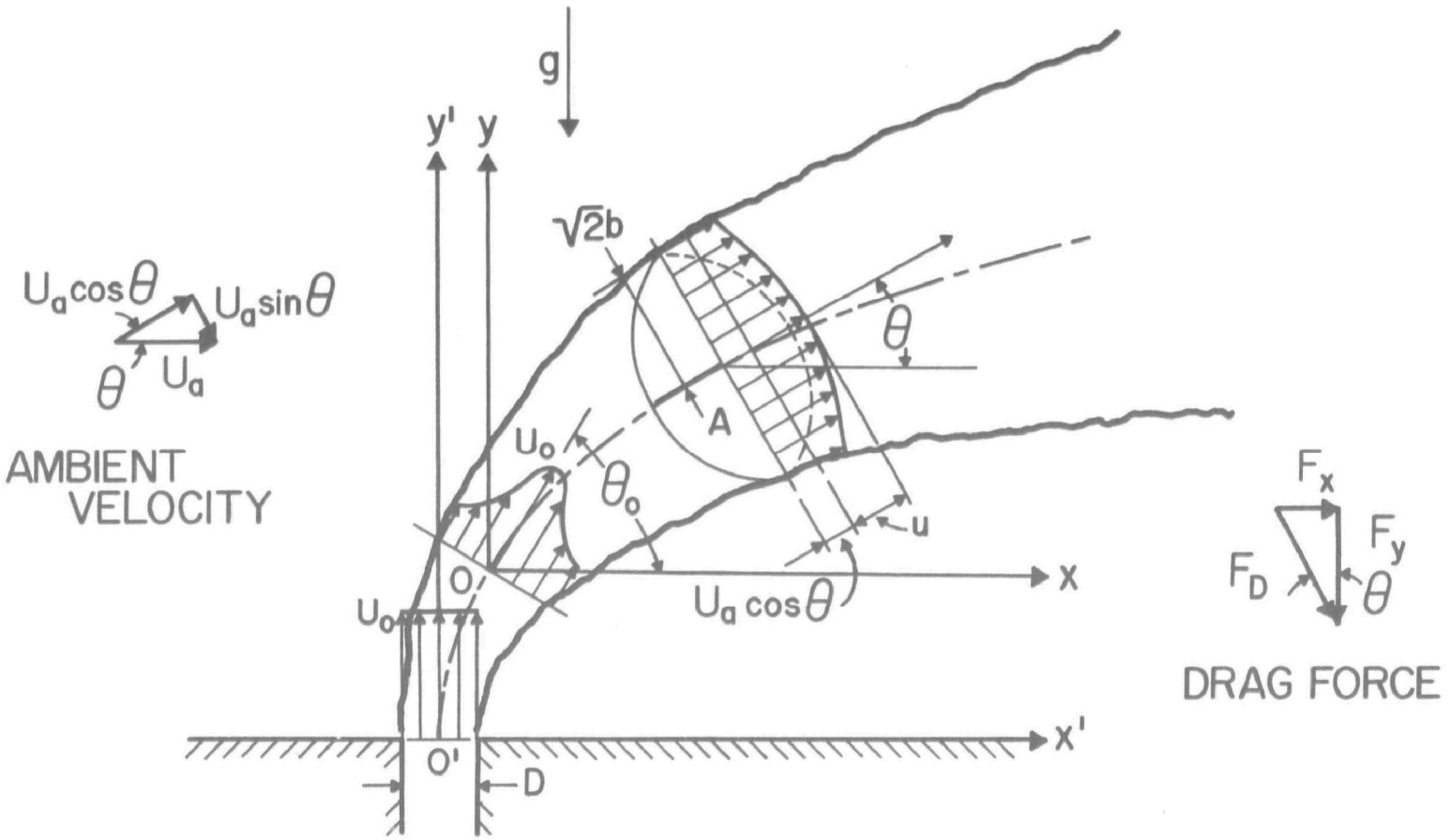

FIGURE 8 - SCHEMATIC DIAGRAM FOR THE ANALYSIS OF A ROUND BUOYANT JET IN A CROSS STREAM

or towards the discharging level or lower. The jet will rise due to its vertical momentum flux, but at the same time the negatively acting buoyancy flux will tend to reduce the jet's initial momentum in such a manner that it bends over and returns towards the discharge level.

Fan found by dimensional analysis that the flow of a positive buoyant jet was characterized by the densimetric Froude number (Equation 9) and by a velocity ratio which represents the relative strength of the jet into a cross flow as defined by Equation 3.

Basic Assumptions

The assumptions adopted by Fan are outlined below.

1. Velocity profiles are assumed to be similar and Gaussian above the component of the ambient velocity $U_a \cos \theta$

$$u^*(s,r,\phi) = U_a \cos \theta + u(s)\, e^{-r^2/b} \tag{24}$$

where u^* = velocity at a local point and b = local characteristic length.

2. The entrainment relation for a jet in a cross stream is assumed to be represented by the equation

$$\frac{dQ}{ds} = 2 \pi \alpha b \left|\vec{U}_j - \vec{U}_a\right| \tag{6}$$

where Q is the volumetric flux.

3. Buoyancy profiles are assumed to be Gaussian

$$\rho_a - \rho^*(s,r,\phi) = [\rho_a - \rho(s)]\, e^{-r^2/b^2}$$

where ρ^* = local density within a jet.

4. Concentration profiles of a certain tracer are assumed to be

Gaussian

$$c^*(r,s,\phi) = c(s)\ e^{-r^2/b^2}$$

where c^* = local concentration value.

5. The effect of the presence of the pressure field can be lumped into a gross drag term proportional to the square of the velocity component of the ambient stream normal to the jet axis. The drag coefficient is assumed constant.

Development of Equations

Fan makes use of the equation of conservation of mass, the equation of conservation of momentum, and geometric equations to describe the round buoyant jet in a cross stream. The equations developed are outlined below.

1. Conservation equations - Equation 6 is integrated to attain an expression for the continuity of fluid.

$$\frac{dQ}{ds} = 2\pi\alpha b\left|\vec{U}_j - \vec{U}_a\right|$$

where Q is the volumetric flux.

$$Q = \int_A u^*\ dA \tag{25}$$

where A is jet cross section normal to the jet axis.

Fan defines the boundary of this jet as $\sqrt{2}b$. Then, substituting Equation 24 for u^* into Equation 25 and integrating between the limits of $r = 0$ and $r = \sqrt{2}b$, Equation 25 becomes

$$Q = \int_r 2\pi r(U_a \cos\theta + ue^{-r^2/b^2})\ dr$$

After the substitution of the limits

$$Q = \int_0^{\sqrt{2}b} 2\pi r(U_a \cos\theta + ue^{-r^2/b^2})\, dr$$

which can be approximated as

$$Q \quad 2\pi\left[\int_0^{\sqrt{2}b} r\, U_a \cos\theta\, dr + \int_0^{\infty} ure^{-r^2/b^2}\, dr\right]$$

After integration,

$$Q = \pi b^2(2U_a \cos\theta + u)$$

Hence,

$$\frac{dQ}{ds} = \frac{d}{ds}[\pi b^2(2U_a \cos\theta + u)] = 2\pi\alpha b|\vec{U}_j - \vec{U}_a| \qquad (26)$$

Thus, $|\vec{U}_j - \vec{U}_a|$ is the vector difference of the jet velocity and the ambient velocity.

$$\vec{U}_j = \vec{i}(U_a \cos\theta + u)$$

and

$$\vec{U}_a = \vec{i}\, U_a \cos\theta + \vec{j}\, U_a \sin\theta$$

Therefore,

$$|\vec{U}_j - \vec{U}_a| = \sqrt{(U_a \cos\theta + u - U_a \cos\theta)^2 + (0 - U_a \sin\theta)^2}$$

Hence,

$$|\vec{U}_j - \vec{U}_a| = \sqrt{(u^2 + U_a{}^2 \sin^2\theta)}$$

Dividing Equation 26 by π,

$$\frac{d}{ds}[b^2(2U_a \cos\theta + u)] = 2\alpha b\sqrt{(U_a{}^2 \sin^2\theta + u^2)} \qquad (27)$$

2. The momentum equations can be written by assuming a gross drag coefficient, C_d. In the x-direction, the rate of change of momentum flux is equal to the rate of entrainment of ambient momentum flux plus the drag force acting on the jet.

$$\frac{d}{ds}\int_A \rho^* u^* (u^* \cos\theta) dA = 2\pi\alpha b\, \rho_a\, U_a |\vec{U}_j - \vec{U}_a| + F_D \sin\theta \qquad (28)$$

where F_D is the drag force per unit length assumed to be

$$F_D = C_d \frac{\rho_a U_a^2 \sin^2\theta}{2} 2\sqrt{2}b \qquad (29)$$

The left side of Equation 28, after substitution of Equation 24 and making use of Boussinesq's assumption that $\rho^* \approx \rho_a$, becomes

$$\frac{d}{ds}\int_0^{\sqrt{2}b} \rho_a\, 2\pi r (U_a \cos\theta + u e^{-r^2/b^2})^2 \cos\theta\, dr$$

After integration,

$$\rho_a \pi \frac{d}{ds}\left[\frac{b^2}{2}(2U_a \cos\theta + u)^2 \cos\theta\right] \qquad (30)$$

Substituting Equation 29 and 30 into Equation 28 and dividing by $\rho_a\pi$, the x-momentum equation becomes

$$\frac{d}{ds}\left[\frac{b^2}{2}(2U_a \cos\theta + u)^2 \cos\theta\right] = 2\alpha b\, U_a \sqrt{(U_a^2 \sin^2\theta + u^2)} + \frac{C_d\sqrt{2}}{\pi} U_a^2 b \sin^3\theta \qquad (31)$$

3. In the y-direction, the rate of change of the momentum flux is equal to the gravity force acting on the jet cross-section minus the y-component of the drag force. For a negatively buoyant jet, the buoyant force will be acting in a manner to

reduce momentum in the y-direction. Hence, a negative sign correction to the buoyancy term will be made on Fan's equation for y-momentum so that the absolute value of the Froude number can be used later.

$$\frac{d}{ds}\int_A \rho^* u^* (u^* \sin\theta) dA = -\int_A g(\rho_a - \rho^*) dA - F_D \cos\theta \qquad (32)$$

The left-hand side of the equation is treated in the same manner as the left-hand side of Equation 28, as shown by Equation 30. The first term of the right-hand side of the equation is treated as below substituting Equation 1.

$$-\int_A g(\rho_a - \rho^*) dA = -\int_A g(\rho_a - \rho) e^{-r^2/b^2} dA$$

$$-\int_A g(\rho_a - \rho^*) dA = -\int_0^\infty 2\pi r(\rho_a - \rho) e^{-r^2/b^2} dr$$

$$-\int_A g(\rho_a - \rho^*) dA = -\pi b^2 g(\rho_a - \rho)$$

Therefore,

$$\rho_a \pi \frac{d}{ds}\left[\frac{b^2}{2}(2U_a \cos\theta + u)^2 \sin\theta\right] = -\pi b^2 g(\rho_a - \rho) - C_d \frac{\rho_a U_a^2 \sin^2\theta \, 2\sqrt{2}b}{2} \qquad (33)$$

Dividing Equation 33 by $\rho_a \pi$ yields, for the y-momentum equation,

$$\frac{d}{ds}\left[\frac{b^2}{2}(2U_a \cos\theta + u)^2 \sin\theta\right] = -b^2 g \frac{(\rho_a - \rho)}{\rho_a} - \frac{C_d \sqrt{2}}{\pi} b U_a^2 \sin^2\theta \cos\theta \qquad (34)$$

4. The density deficiency flux induced is conserved since the ambient fluid is homogeneous, so

$$\frac{d}{ds}\int_A u^*(\rho_a - \rho^*)dA = 0 \tag{35}$$

Substituting Equations 1 and 24 into Equation 35 yields

$$\frac{d}{ds}\int_0^{\sqrt{2}b} 2\pi r(U_a \cos\theta + ue^{-r^2/b^2})\ (\rho_a - \rho)e^{-r^2/b^2}dr = 0$$

$$2\pi\frac{d}{ds}\left[\frac{b^2}{2}U_a \cos\theta(\rho_a - \rho) + \frac{b^2}{4}u(\rho_a - \rho)\right] = 0$$

$$2\pi\frac{d}{ds}\left[\frac{b^2}{2}(2U_a \cos\theta + u)\ (\rho_a - \rho)\right] = 0 \tag{36}$$

Therefore, Equation 36 yields

$$\frac{d}{ds}\left[b^2(2U_a \cos\theta + u)\ (\rho_a - \rho)\right] = 0 \tag{37}$$

5. The flux of any specific tracer of concentration, c*, contained in the jet flow will be conserved in a fashion similar to the density deficiency, as shown below.

$$\frac{d}{ds}\int_A u^*\ c^*\ dA = 0 \tag{38}$$

Substituting Equations 2 and 24 into Equation 38 and integrating yields

$$\frac{d}{ds}\left[b^2(2U_a \cos\theta + u)c\right] = 0 \tag{39}$$

6. There exist two geometric relationships due to the jet trajectory which are utilized.

$$\frac{d}{ds}x = \cos\theta \tag{40}$$

and

$$\frac{d}{ds} y = \sin \theta \tag{41}$$

Hence, there are 7 unknowns - u, $\rho_a - \rho$, c, b, θ, x, and y - that can be solved for with seven simultaneous ordinary differential equations - Equation Numbers (27), (31), (34), (37), (39), (40), and (41).

Initial Condition for Fan's Model

Fan considers his model applicable after the zone of flow establishment. The initial conditions at the origin, 0, at the end of the zone of flow establishment are given below.

$$\begin{aligned} u(0) &= u_o \\ b(0) &= b_o \\ \rho(0) &= \rho_1 \\ \theta(0) &= \theta_o = \beta_o \\ c(0) &= c_o \\ x(0) &= 0 \\ y(0) &= 0 \\ \text{at } s &= 0 \end{aligned} \tag{42}$$

where u_o = initial jet discharge velocity at orifice

b_o = jet half-width at the end of the zone of flow establishment as defined in Equation 24

ρ_1 = jet density

c_o = initial concentration at the end of the zone of flow establishment

x = horizontal coordinate measured from the end of the zone of flow establishment

y = vertical coordinate measured from the end of the zone of flow establishment

s = parametric distance along jet axis measured from the end of the zone of flow establishment

By considering the conservation of the flux of density deficiency between the two cross-sections at point 0 and 0',

$$\frac{1}{2}\pi b_o^2 (2U_a \cos\theta_o + u_o) \frac{\rho_a - \rho_1}{\rho_a} = \frac{\pi D_o^2}{4} U_o \frac{\rho_a - \rho_1}{\rho_a}$$

$$b_o = D_o \frac{1}{\sqrt{2}} \sqrt{\frac{U_o}{2U_a \cos\theta_o + u_o}}$$

where $k' = \dfrac{2U_a \cos\theta_o + u_o}{U_a} = k + \cos\theta_o$ (43)

Hence, $b_o = D_o \sqrt{\dfrac{k}{2k'}}$ (44)

In addition, the initial angle, θ_o, is the reduced angle of inclination. It will always be less than the initial angle of discharge due to deflection in the zone of flow establishment. Fan developed a functional relationship involving k to express the value of θ_o. However, for the negatively buoyant jet, no functional relationship exists. So, in each case, the jet trajectory is plotted, the zone of establishment is measured along the axis using values calculated from Equation 4, and then the angle at the end of the zone of flow establishment is measured. Hence, when Fan uses θ_o in his derivation, it is equivalent to β_o in

this report. In addition, β_o' is the initial angle of inclination at the orifice.

Dimensionless Parameters

Fan's equations are normalized by defining dimensionless parameters as follows, using initial values.

Volumetric flux parameter,

$$\mu = \frac{b^2(2U_a \cos\theta + u)}{b_o^2(2U_a \cos\theta_o + u_o)} \tag{45}$$

momentum flux parameter,

$$m = \frac{b^2(2U_a \cos\theta + u)^2}{b_o^2(2U_a \cos\theta_o + u_o)^2} \qquad \text{(s-direction)} \tag{46}$$

$$h = m \cos\theta \qquad \text{(x-direction)} \tag{47}$$

$$v = m \sin\theta \qquad \text{(y-direction)} \tag{48}$$

velocity ratio,

$$k = \frac{u_o + U_a \cos\theta_o}{U_a} = \frac{U_o}{u_a} \tag{3\&11}$$

$$k' = k + \cos\theta_o \tag{43}$$

buoyancy parameter,

$$f = b_o\, g\, \frac{\rho_a - \rho_1}{\rho_a} / (\alpha\, k'^2\, U_o^2) \tag{49}$$

$$f = \left[\frac{1}{2\alpha}\ \frac{k}{k'}^{2.5}\right]/F^2 \tag{50}$$

where F = densimetric Froude number,

coordinates,

$$s : \zeta = \frac{2\alpha}{b_o}\, s$$

$$x : \eta = \frac{2\alpha}{b_o} \; x$$

$$y : \xi = \frac{2\alpha}{b_o} \; y \tag{51}$$

where α = coefficient of entrainment.

Normalization of Fan's Equations

Fan's equations are normalized using the dimensionless parameters on pages 39 and 40, resulting in Equations 52-56, 60, and 61. Fan's equations 27, 31, 34, 37, 39, 40 and 41:

1. $$\frac{d\mu}{d\zeta} = \frac{1}{k'} \mu \psi / \sqrt{m} \tag{52}$$

2. $$\frac{dh}{d\zeta} = \frac{1}{k'^2} \frac{\mu}{\sqrt{m}} (2 \psi + C_d' \sin^3 \theta) \tag{53}$$

3. $$\frac{dv}{d\xi} = - f \frac{\mu}{m} - \frac{C_d'}{k'^2} \frac{\mu}{\sqrt{m}} \sin^2 \theta \cos \theta \tag{54}$$

4. $$\frac{d\eta}{d\zeta} = \cos \theta \tag{55}$$

5. $$\frac{d\xi}{d\zeta} = \sin \theta \tag{56}$$

where $$\psi = \left[\sin^2 \theta + (k' \frac{m}{\mu} - 2 \cos \theta)^2 \right]^{.5} \tag{57}$$

and $$C_d' = C_d \sqrt{2} / \alpha \pi \tag{58}$$

6. The equations of continuity of a tracer, 38, and density deficiency, 37, may be solved immediately. The continuity of a tracer is expressed as

$$b^2 (2U_a \cos \theta + u) c = \text{constant} \tag{59}$$

Therefore,

$$\frac{c}{c_o} = \frac{b_o^2(2U_a \cos \theta_o + u_o)}{b^2(2U_a \cos \theta + u)} = \frac{1}{\mu} \tag{60}$$

7. The conservation of density deficiency integrated as

$$b^2(2U_a \cos \theta + u)(\rho_a - \rho) = \text{constant} \tag{61}$$

Hence, values of both c and $(\rho_a - \rho)$ can be determined easily from the solutions of the terms $b^2(2U_a \cos \theta + u)$. This leaves only five unknowns contained in five simultaneous ordinary differential equations.

The initial conditions for $\zeta = 0$ are

$$\begin{aligned} \mu(0) &= 1 \\ m(0) &= 1 \\ \theta(0) &= \theta_o = \beta_o \\ n(0) &= 0 \\ \xi(0) &= 0 \end{aligned} \tag{62}$$

Abraham's Model for Round Buoyant Jets Issuing Vertically into a Flowing Stream

Abraham (6) has modified Fan's model by using entrainment coefficients that are constant, i.e., they are not functions of either F, k, or β_o'. For Fan's model the value of the entrainment coefficient and the drag coefficient is a function of the velocity ratio and densimetric Froude number. Abraham recognizes that this may preclude the use of Fan's model beyond the range of conditions covered by the experiments.

Basic Assumptions

Abraham considers two regions of the jet. In the vicinity of the nozzle the trajectory of a round buoyant jet in a cross flow may be

described as a vertical line, provided that the cross flow is weak and that the initial momentum of the jet is strong. The region near the nozzle may be described as a jet primarily influenced by its initial momentum, and thus the volumetric flux may be expressed as

$$\frac{dQ}{ds'} = \alpha_{mom} 2\pi bu \tag{63}$$

where α_{mom} = coefficient of entrainment for jets primarily influenced by initial momentum

α_{mom} = 0.057 according to Albertson, et al. (10)

The variables u and b are the same as described earlier.

The second region is a great distance downstream from the nozzle where the velocity of the jet fluid is about equal to the velocity of the ambient fluid. Here, entrainment may be described by the relationship for a cylindrical thermal in a stagnant fluid as described by Richards (26). The entrainment satisfies the relationship,

$$\frac{dV_q}{dy'} = \alpha_{th} 2\pi B_{th} \tag{64}$$

where y' = vertical coordinate indicating position of center of thermal jet

V_q = quantity of fluid contained in a thermal jet per unit of length

B_{th} = radius of thermal defined by Equation 66

α_{th} = coefficient of entrainment for thermals moving through stagnant ambient fluid [0.5 according to Richards (26)] (65)

The entrainment of a cylindrical thermal may be described by Equation 64 when the concentration of a tracer carried by the thermal

is expressed as

$$c^*(s',r,\phi) = c(s')\, e^{-r^2/B_{th}^2} \tag{66}$$

This expression is equivalent to the one used by Fan shown in Equation 2. Abraham assumes the same velocity profile as described by Fan in Equation 24,

$$u^*(s',r,\phi) = U_a \cos\theta + u(s')\, e^{-r^2/b^2} \tag{24}$$

Abraham combines Equations 63 and 64 and describes the volumetric flux as

$$\frac{d}{ds'} \int_A u^* dA = 2\pi b(\alpha_{mom}\, u + \alpha_{th}\, U_a \sin\theta \cos\theta) \tag{67}$$

where dy' has been replaced by sin θ ds'.

The cosine function in Equation 67 was arbitrarily introduced in the term involving α_{th} to avoid this term contributing to entrainment in the initial region near the orifice where the jet is primarily a momentum jet. In addition, the prime notation is used to indicate the coordinates of the jet from the discharge point. Hence, comparing Fan's notation with Abraham's notation, the relationship for the coordinates is as follows:

$$\begin{aligned} s' &= s'_e + s \\ x' &= x'_e + x \\ y' &= y'_e + y \end{aligned} \tag{68}$$

where s'_e, x'_e, and y'_e are the distances from the discharge point to the end of the zone of flow establishment [Figure (9)].

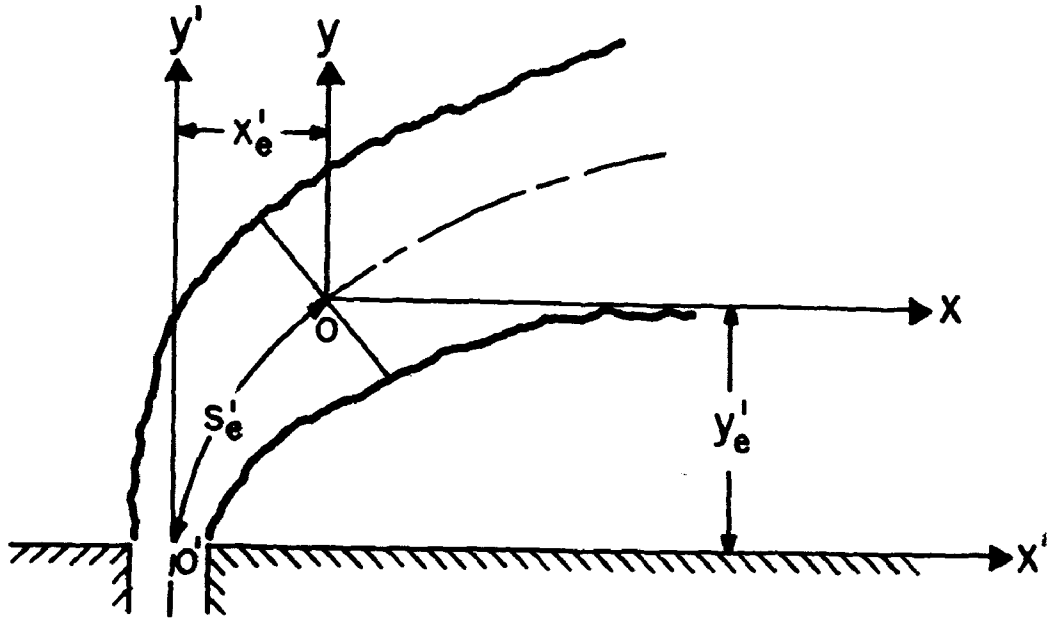

FIGURE 9 - SCHEMATIC RELATIONSHIP BETWEEN INITIAL DISCHARGE POINT AND END OF ZONE OF FLOW ESTABLISHMENT

Development of Equations

The following equations were developed by Abraham using Equation 67 to describe the volumetric and momentum flux equations. Where the equations are the same as developed by Fan, they will receive the same number. The equations are outlined below.

1. Continuity,

$$\frac{d}{ds'}\left[b^2(2U_a \cos\theta + u)\right] = 2b(\alpha_{mom}\, u + \alpha_{th}\, U_a \sin\theta \cos\theta) \qquad (69)$$

2. x-momentum,

$$\frac{d}{ds'}\left[\frac{b^2}{2}(2U_a \cos\theta + u)^2 \cos\theta\right] =$$

$$2bU_a(\alpha_{mom}\, u + \alpha_{th}\, U_a \sin\theta \cos\theta) + \frac{C_d\sqrt{2}}{\pi} U_a^2\, b \sin^3\theta \qquad (70)$$

3. y-momentum - The equation for y-momentum is essentially the same as developed by Fan as shown by Equation 34 with

modification for the buoyancy force in the negative y-direction.

$$\frac{d}{ds'}\left[\frac{b^2}{2}(2U_a \cos\theta + u)^2 \sin\theta\right] =$$

$$-b^2 g \frac{\rho_a - \rho}{\rho_a} - \frac{C_d\sqrt{2}}{\pi} U_a^2 b \sin^2\theta \cos\theta \qquad (34)$$

4. Continuity of tracer,

$$\frac{d}{ds'}[b^2(2U_a \cos\theta + u)c] = 0 \qquad (39)$$

5. Density deficiency,

$$\frac{d}{ds'}[b^2(2U_a \cos\theta + u)(\rho_a - \rho)] = 0 \qquad (37)$$

6. Geometric relationships,

$$\frac{d}{ds'} x' = \cos\theta \qquad (40)$$

$$\frac{d}{ds'} y' = \sin\theta \qquad (41)$$

It is important to note that the values of x', y', and s' for Abraham's equation are measured from the orifice rather than the end of the zone of flow establishment and are defined as

x' = horizontal coordinate, measured from orifice

y' = vertical coordinate, measured from orifice

s' = distance along jet axis, measured from orifice

Initial Conditions

There are seven unknowns for Abraham's model (u, b, c, $\rho_a - \rho$, θ, x', and y') with seven equations (69, 70, 34, 39, 37, 40, and 41). The initial conditions are:

$$u(0) = u_o$$

$$c(0) = c_o$$

$$\rho(0) = \rho_1$$

$$b(0) = D_o/2$$

$$x'(0) = 0$$

$$y'(0) = 0 \qquad (71)$$

$$\theta(0) = \theta_o = \beta'_o$$

$$\text{at} \quad s' = 0$$

where c_o = initial concentration,

u_o = initial jet discharge velocity,

β'_o = initial angle of inclination at discharge point, and

D_o = diameter of orifice.

Dimensionless Parameters

Abraham's equations are normalized in the same manner as Fan's equations with the following exceptions:

Buoyancy parameter:

$$f = b_o g \frac{\rho_a - \rho_1}{\rho_a} / (k'^2 U_a^2) \qquad (72)$$

$$f = (k/k')^2/2F^2 \qquad (73)$$

coordinates:

$$s : \zeta' = \frac{2}{b_o} s'$$

$$x : \eta' = \frac{2}{b_o} x' \qquad (74)$$

$$y : \xi' = \frac{2}{b_o} y'$$

Normalization of Abraham's Equation

Abraham's Equations 69, 70, 34, 40, and 41 are normalized using the dimensionless parameters listed on page 46, resulting in Equations 75-79.

$$1.\quad \frac{d\mu}{d\zeta'} = \alpha_{mom}\sqrt{m} - \frac{\mu}{k'\sqrt{m}}(2\,\alpha_{mom} - \alpha_{th}\sin\theta)\cos\theta \tag{75}$$

$$2.\quad \frac{dh}{d\zeta'} = \frac{\mu}{\sqrt{m}}\,\frac{1}{k'^2}\left[2\alpha_{mom}\left(\frac{k'm}{\mu} - 2\cos\theta\right) + 2\alpha_{th}\sin\theta\cos\theta + C_{da}\sin^3\theta\right] \tag{76}$$

$$3.\quad \frac{dv}{d\zeta'} = -f\frac{\mu}{m} - C_{da}\frac{1}{k'^2}\frac{\mu}{\sqrt{m}}\sin^2\theta\cos\theta \tag{77}$$

$$4.\quad \frac{d}{d\zeta'}\eta' = \cos\theta \tag{78}$$

$$5.\quad \frac{d}{d\zeta'}\xi' = \sin\theta \tag{79}$$

$$\text{where } C_{da} = \frac{C_d\sqrt{2}}{\pi} \tag{80}$$

The density deficiency and continuity of tracer are solved in the same manner as Fan's equation for density deficiency and continuity of tracer.

The initial conditions for $\zeta' = 0$ are:

$$\begin{aligned} \mu(0) &= 1 \\ m(0) &= 1 \\ \theta(0) &= \beta_o' \\ \eta'(0) &= 0 \\ \xi'(0) &= 0 \end{aligned} \tag{81}$$

Solution of Equations

A system of simultaneous differential equations can be solved using a Fourth-Order Runge Kutta technique. Such a program is available at the Vanderbilt University Computer Center in the Scientific Subroutine library. The listing of the computer program used to solve Fan's model is included in Appendix B, and the computer program used to solve Abraham's model is included in Appendix C. The subroutine that contains the Fourth-Order Runge Kutta solution to solve a system of simultaneous ordinary differential equations is the same for both Fan's model and Abraham's model and is included in Appendix D. However, the main programs, which contain the individual equations for the two different models, are different.

CHAPTER IV
VI
METHODS AND MATERIAL

Introduction

The objective of this research was to measure the vertical profile of a negatively buoyant jet at points downstream from the jet discharge point in order to obtain dilution data, jet half-width data, and jet trajectory data for a negatively buoyant jet. Salt solutions of different concentrations were used to model the jet for two reasons. First, a salt solution is heavier than water and can easily be used to model a negatively buoyant jet. Secondly, the vertical profiles of the jet could be measured very easily by using a conductivity probe with appropriate monitoring devices.

Conductivity Probe

The conductivity probe was similar to the one used by Krenkel (30) and Burdick (31) with a few modifications. The electrode consisted of a 16-gage blunt stainless steel hypodermic needle as the outer electrode and a length of 0.01 in. diameter platinum wire as the inner electrode. The platinum wire was insulated from the hypodermic needle by a small capillary of plastic tubing into which it was threaded. Both ends of the electrode were sealed with a non-conducting epoxy cement. The bottom portion of the needle and the exposed portion of the platinum were then plated with platinum black to provide a large surface area.

However, the hypodermic needle was first plated with copper as shown by Krenkel (32) so that the platinum black would adhere more strongly. Copper was plated on the stainless steel by using a length of cleaned copper wire as one electrode and the needle as the other electrode. A 5-volt power supply with variable output was used as the driving force in the plating operation. A voltage output of 1.5 volts was used. This circuit was completed by using 1 N copper sulfate as the electrolyte. The copper wire was helically wound to increase the surface area in the copper sulfate solution. After the copper plating had been thoroughly washed, the needle was placed in a 100-milliliter solution containing 3 grams of platinic chloride and 0.02 grams of lead acetate. The needle leads were then connected to about three volts direct current as shown by Clements (33). The direction of current was reversed every 15 seconds until a uniform coating was deposited on both electrodes. (Two or three minutes is suggested.) The electrodes were then rinsed in running tap water for half an hour and stored in distilled water when not in use. It was necessary to keep the probe wet at all times in order to keep the platinum black coating in proper condition.

The probes were finally covered with a non-conducting rubber coating to insure insulation and to give the soldered leads more strength. Detailed views of the probe are shown in Figure 10 and 11.

Conductivity Monitor and Recorder

The conductivity monitor was designed as described by Clements (31). The basic premise of construction involved using a series resistance arrangement with an a.c. source having a low internal

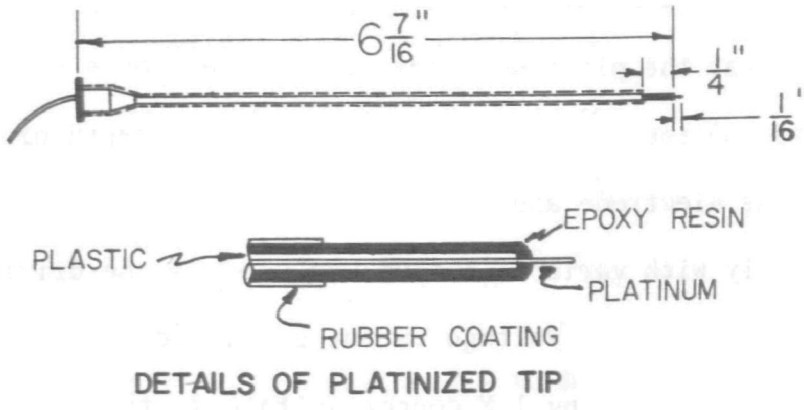

FIGURE 10 - DETAILS OF PROBE CONSTRUCTION

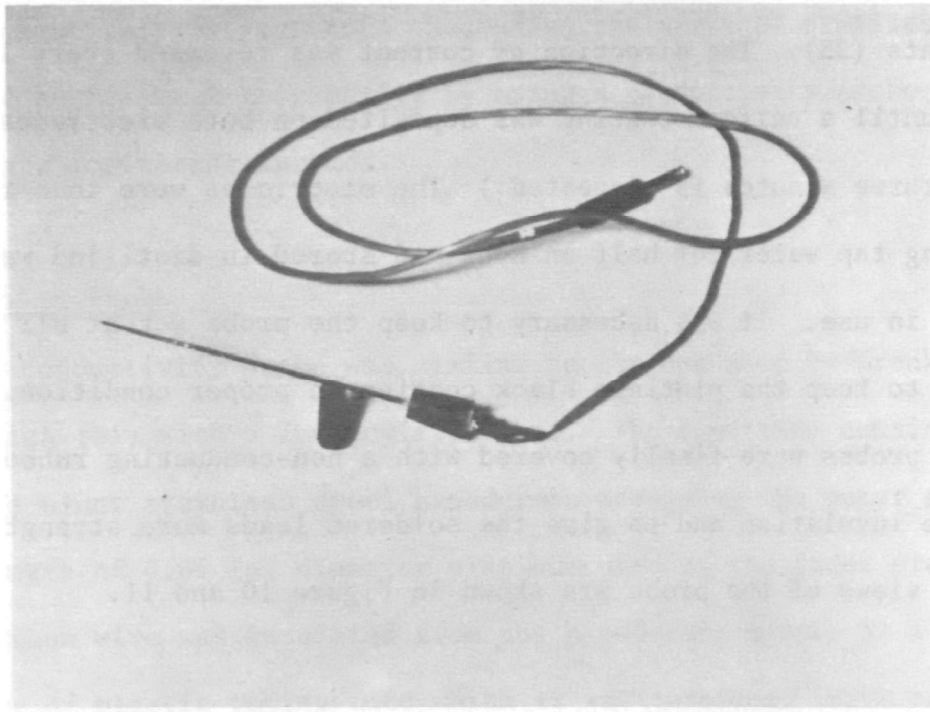

FIGURE 11 - PHOTOGRAPH OF CONDUCTIVITY PROBE

impedance as shown in Figure 12. This type of circuit provided an output

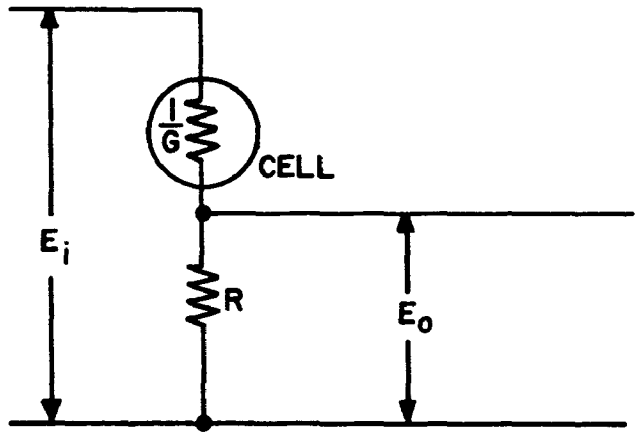

FIGURE 12 - BASIC MEASURING CIRCUIT
[AFTER CLEMENTS (35)]

voltage, E_o, which was nearly linearly proportional to the conductivity G, of the test solution, where E_i was a constant supply voltage of 5 volts and G was the reciprocal of probe resistance, R_c. The linearity may be seen by considering Equation 82.

$$E_o = \frac{E_i R}{1 + GR} \quad G \tag{82}$$

If $GR \approx .01$, E_o is directly proportional to G. This type of monitor was chosen for the following characteristics.

1. Low cost - approximately $25.00 for parts.
2. Drift was low - about 0.12 percent per hour with normal ventilation.
3. Calibration was linear over a large range.
4. Polarization effects at the conductivity cell electrodes were negligible due to the 1 kHz excitation frequency.

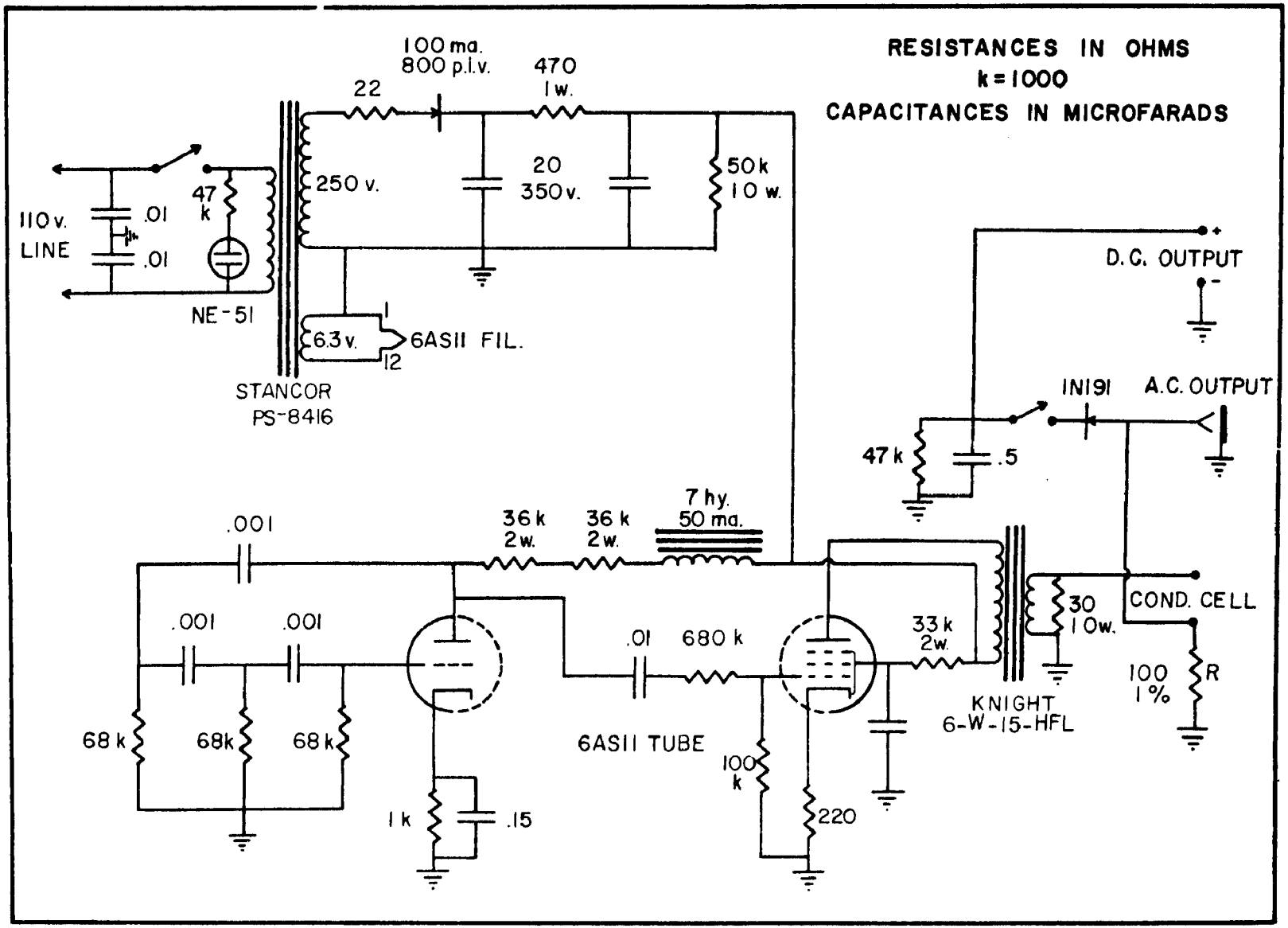

FIGURE 13 - SCHEMATIC OF CONDUCTIVITY MONITOR [AFTER CLEMENTS (34)]

5. Response was fast, with an average time constant of 0.025 second.

The combination of 1-kHz excitation frequency and the large surface area exposed by the platinum black made the polarization effects at the conductivity probe neglible. Figure 13 is a diagrammatic sketch of the monitor and Figure 14 is a photograph of the conductivity monitor.

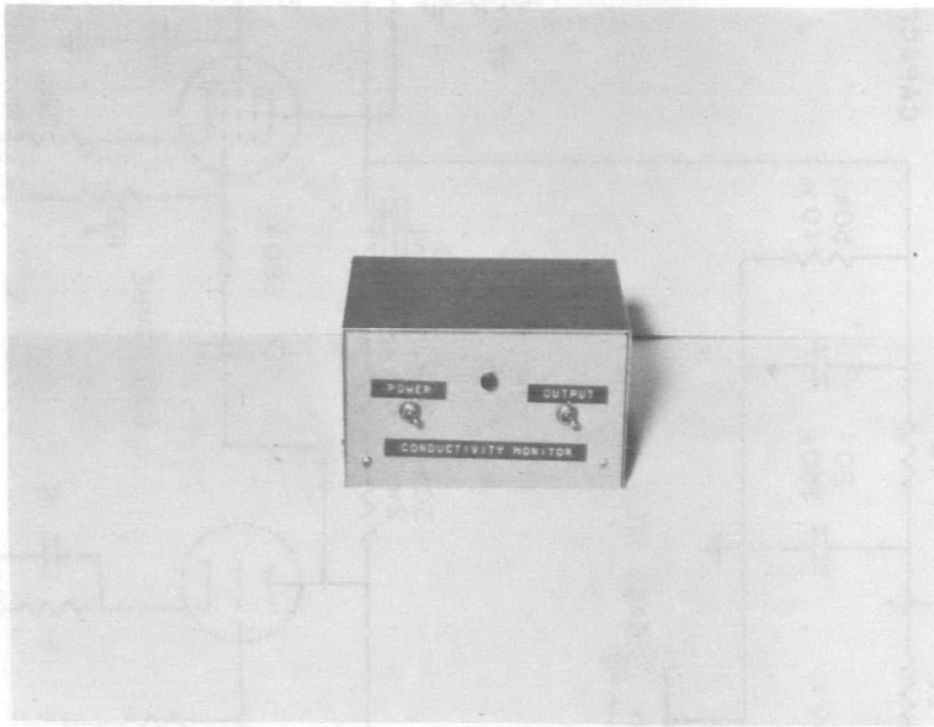

FIGURE 14 - CONDUCTIVITY MONITOR

The recorder chosen was an Esterline-Angus Model T171B, Port-A-Graph recorder. The input resistance for the recorder was 1.8 to 2 mega ohms. The wide range of 2,5,10,20,500,200 MV, 0.5, 1,2,5,10,20,50 V afforded the needed flexibility for measuring various outputs with the needed sensitivity. Figures 15 and 16 show the Esterline-Angus Recorder and the combination of conductivity monitor and recorder, respectively.

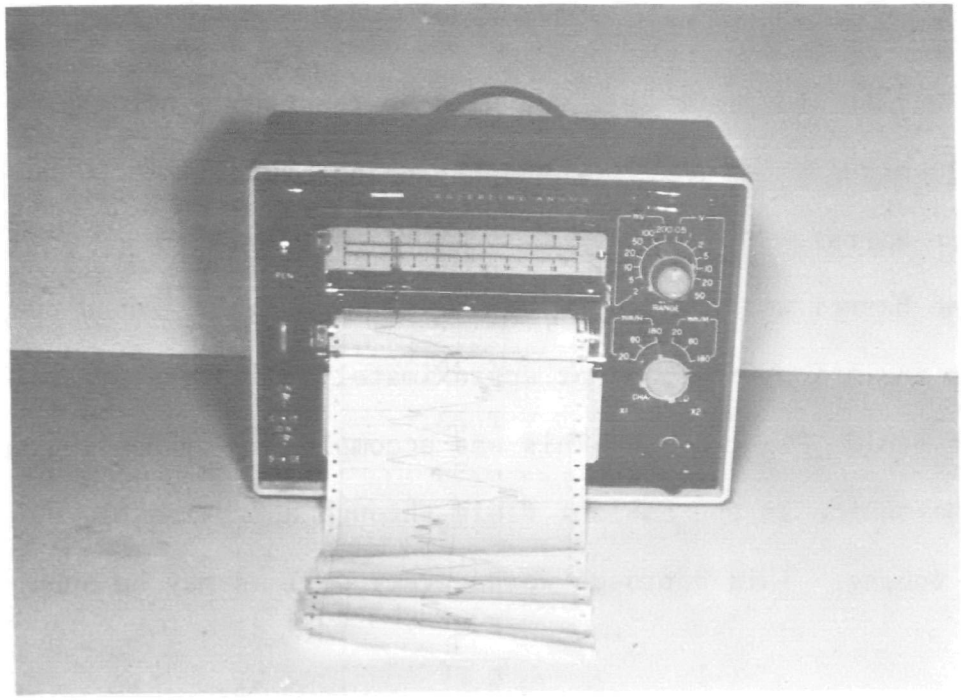

FIGURE 15 - ESTERLINE-ANGUS RECORDER

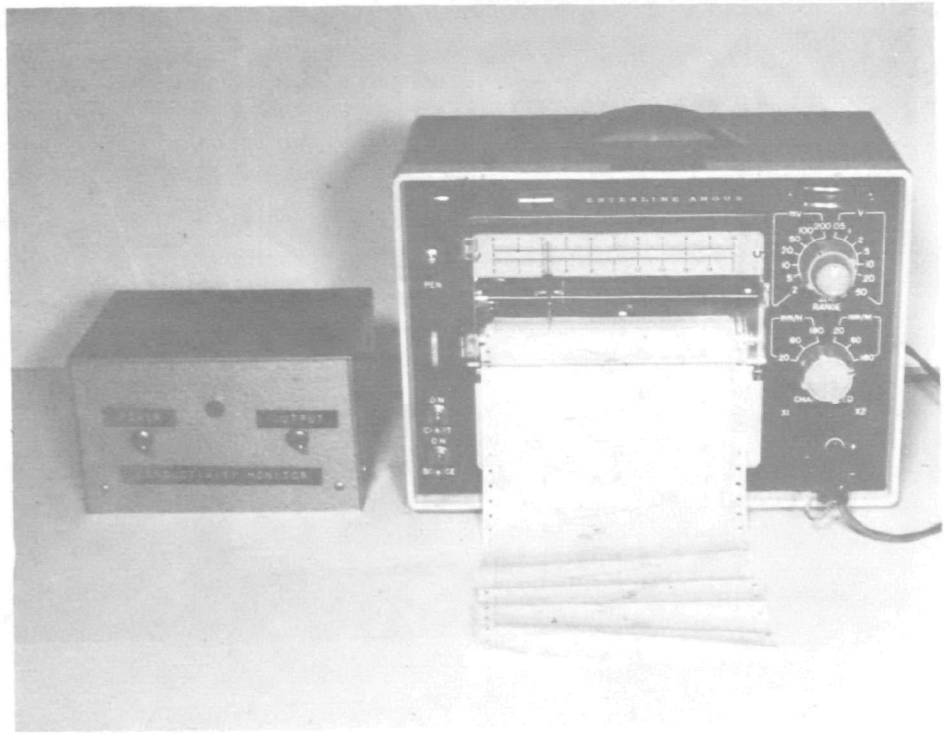

FIGURE 16 - COMBINATION OF CONDUCTIVITY MONITOR AND RECORDER

Injection and Flow Control

A commercial grade salt was used as the trac material. The salt was well-mixed using a 1500-gpm stirring apparatus in a 50-gal polyethylene barrel.

The barrel was equipped with internal helically wound copper coils to keep the tracer material at approximately the same temperature as the ambient fluid (Figure 17). This was accomplished by passing water from the same source as the ambient fluid through approximately 60 feet of copper tubing. This approach worked very well as may be seen in Table 2.

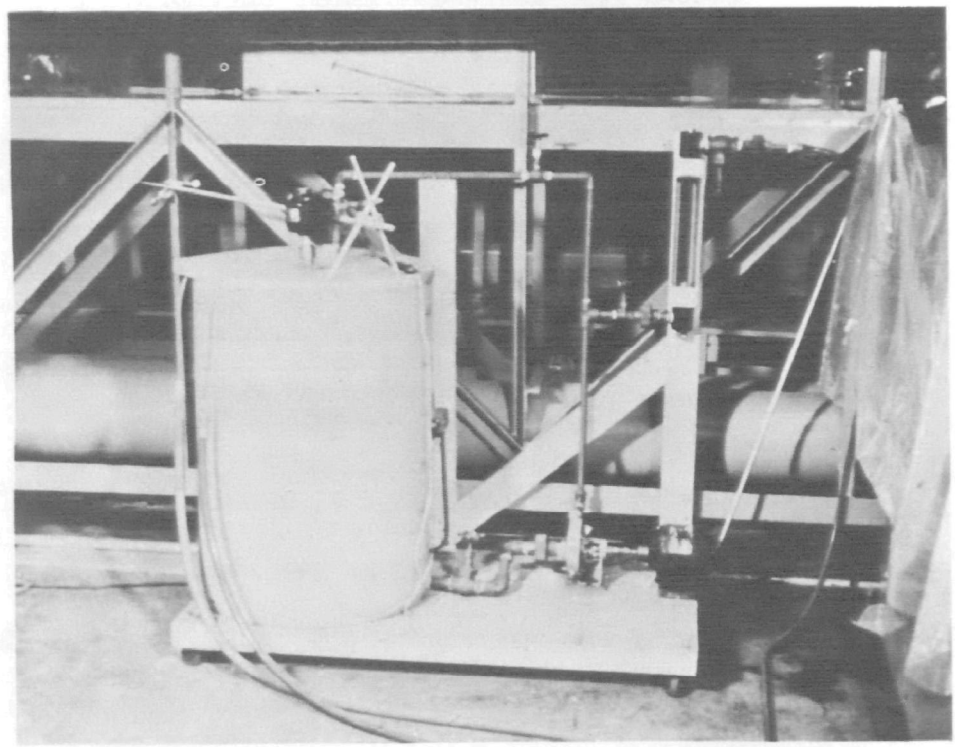

FIGURE 17 - POLYETHYLENE BARREL WITH FLOW AND TEMPERATURE CONTROL

TABLE 2 - COMPARISON OF JET TEMPERATURE WITH AMBIENT FLUID TEMPERATURE

Run No.	Temperature Ambient (°F)	Temperature Jet (°F)
9	64.6	65.4
10	66.3	67.5
11	66.3	67.5
12	66.8	67.6
13	67.6	68.5
15	68.7	69.0
16	68.5	69.1
18	70.5	71.0
19	73.3	73.7
20	73.3	73.7
21	73.2	73.4
22	73.2	74.4
23	75.5	75.6
24	76.0	76.0
25	76.0	76.0
26	72.2	72.2
27	76.2	76.4
28	76.2	76.4
29	77.6	77.8
30	77.6	77.8
31	77.6	77.2
32	76.1	75.9
33	76.1	76.6
34	75.5	75.9

A student's t-test for the comparison of the means shows that there is no significant difference in the two populations. Hence, the conclusion can be drawn that the data obtained came from the same population. Figure 18 shows how temperature control was obtained.

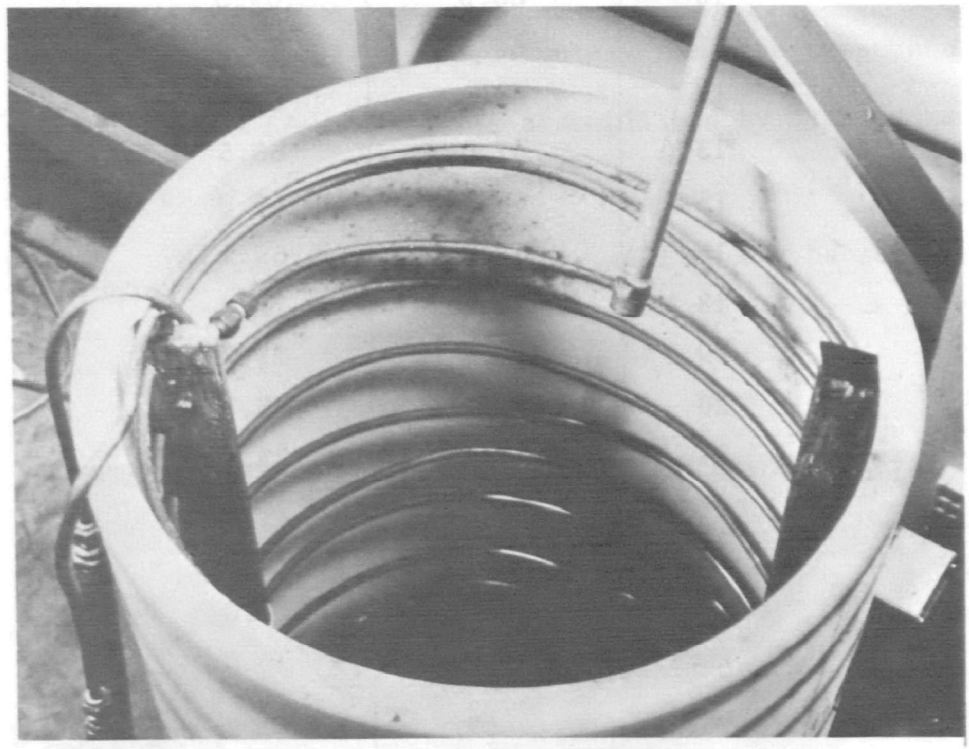

FIGURE 18 - JET TEMPERATURE CONTROL

The salt solution was then pumped through a PVC piping system by a 12-gpm pump through a 0.5-gpm Fisher-Price rotameter to measure the flow rate. The excess was recirculated back into the mixing chamber. The rotameter calibration curve is presented in Appendix E. The desired flow-rates were obtained by adjustment of valves located in the piping network. The piping network was then connected to the injection port located in the bottom of the laboratory flume.

Laboratory Flume

The flume used is located in the hydraulics laboratory of the Department of Environmental and Water Resources Engineering at Vanderbilt University. The flume is 60 feet long, 1.0 foot deep, and 2.0 feet wide. The channel walls consist of glass panels, and the steel bottom was painted with an epoxy-based paint to prevent chemical corrosion. The entire flume system is supported at two points, one of which has a mechanical screw jack mechanism for changing the channel slope. However, all experiments were made with a horizontal slope. A variable-speed recirculating pump is located at the lower end of the flume by which water may be recirculated if it is necessary. At times it was necessary to recirculate to obtain the desired ambient flow rate in the flume at the required depth. The maximum flow rate with recirculation was 0.48 cfs. The maximum flow rate available for a single pass through the flume was 0.15 cfs. The flow rate was measured by a 60° V-notch weir installed at the upstream end of the flume. A calibration curve of flows over the weir was used which appears in Appendix F and is very close to the theoretical equation of

$$Q_a = 1.4076\ H_w^{2.5}$$

where Q_a = flow, cfs

H_w = head of water above apex of notch, feet

A bank of ripple siding was installed near the upstream end to aid in straightening the flow. A point gauge mounted on a traversing mechanism was used to measure the flume depth and local positions of the jet with an accuracy of 0.001 foot. The required depth of flow was

controlled by means of a perforated baffle installed at the downstream end of the flume. A diagrammatic sketch of the flume and appurtenances may be seen in Figure 19.

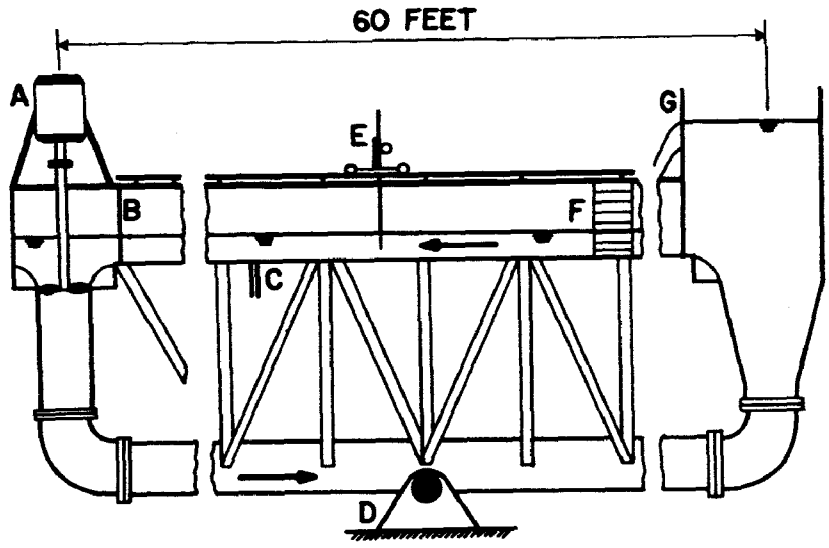

FIGURE 19 - PARTIAL CUTAWAY VIEW OF RECIRCULATING FLUME

The injection of the salt solution was obtained either by using a length of standard 3/8-inch copper tubing as the port or injecting vertically from a port in the bottom of the flume. For the 90° jet, the salt water was injected vertically from the bottom of the flume using a previously installed withdrawal tap. The diameter of the jet at this point is 0.80 centimeter. The 45° jet was a standard 45°-3/8-inch copper ell inserted into the withdrawal port. This essentially raised the elevation of the jet 0.106 feet above the bottom of the flume.

The diameter of the 45° jet was 0.95 cm. The 60° jet was constructed by bending a length of 3/8-inch copper tubing to an angle of 60° from the horizontal. The jet was then inserted into the withdrawal port, thus raising the elevation of the jet 0.081 feet above the bottom of the flume. The diameter of the 60° jet was 0.72 cm. The location of the withdrawal tap is in the center of the flume 1.0 feet from each wall.

Procedure for Obtaining Correct Salt Concentration

The limiting factors for determining the various parameters during the experiments were the ambient flow rate and the depth of the water in the flume. The usual depth of water in the flume was between 10 and 12 inches. A depth of 10 inches and a maximum flow rate for a single pass of 0.15 cfs was used for preliminary calculations. This set the preliminary ambient velocity. Then, using the required velocity ratio, the preliminary jet velocity was determined. Knowing the required jet velocity and densimetric Froude number, the preliminary density difference was calculated for a particular jet diameter. The salt was added to water and sufficient time was allowed for complete mixing. The density of the solution was then determined using previously weighed specific gravity bottles. After the density difference was accurately determined, the jet velocity was again determined using the required densimetric Froude number. Then, using the required velocity ratio, the ambient velocity was calculated. Using the maximum flow rate of 0.15 cfs, the depth of flow in the flume was calculated.

If recirculation was required to obtain the desired combination of parameters, a salt solution was initially mixed and then the density

difference was determined as for a single pass. Then, the required jet velocity and ambient velocity were calculated. Using a depth of 12 inches, the ambient flow rate was calculated. The required flow rate was then obtained using the recirculating pump.

CHAPTER V
VII
ANALYSIS OF DATA AND PRESENTATION OF RESULTS

The objective of this research was to ascertain the applicability of two different jet models which describe the dilution, jet half-width, and jet trajectory of positively buoyant jets in flowing streams to the case of a negatively buoyant jet in a flowing stream. The specific objectives are outlined below:

1. Determine if Fan's model could be used to predict the dilution, jet half-width, and jet trajectory for a negatively buoyant jet.
2. Determine if Abraham's model could be used to predict the dilution, jet half-width, and jet trajectory of a negatively buoyant jet.
3. Determine the range of values of the coefficient of entrainment, α, and drag coefficient, C_d.
4. Seek the functional relationship of α and C_d as a function of the velocity ratio, k, and the densimetric Froude number, F, and the initial angle of discharge, β_o'.
5. If both models can be used, determine the best model.

A chronological schedule for obtaining and evaluating the data is outlined below:

1. Determine the actual conditions for a particular laboratory investigation.
   a. jet velocity

b. ambient velocity

c. density of salt water

2. Obtain probe calibration curve of millivolt output versus concentration of salt in jet.

3. Obtain concentration profile data measured in millivolt output from laboratory investigation.

4. Reduce millivolt output data describing the profile to actual concentration data using the calibration curve found in step 2 above.

5. Determine the centerline concentration, the vertical position, y, and the standard deviation, σ_k, for a particular profile which is located at a known distance downstream, x, from the discharge point.

6. Measure the length of the zone of flow establishment along the axis of the jet trajectory using Equation 4.

7. Determine β_o from plotted jet trajectory data obtained using the profile data.

8. Obtain theoretical dilution, jet half-width, and jet trajectory for initial guesses of α and C_d.

9. Fit theoretical data to experimental data to obtain the best values of α and C_d.

A laboratory investigation was used to answer the specific objectives of this research. Experiments were conducted for various combinations of k, F, and β_o, with values of k ranging from 5 to 20, F ranging from 10 to 40, and initial angles of discharge of 90°, 60°, and 45°. A laboratory run consisted of an experimental investigation of one

particular combination of the above parameters, e.g., k ~ 5, F ~ 10, and $\beta_o' = 90°$. The exact combinations are found in Table 3 for Fan's definitions and in Table 4 for Abraham's definitions. The laboratory conditions were set up as discussed in Chapter IV.

Procedure for Obtaining Salt Concentration Profiles

For each laboratory run, a calibration curve of millivolts output versus salt concentration was made for various dilutions. Hence, there was no need for a temperature correction, since the probe was calibrated each time a run was made. Concentration profile data was initially taken starting at the downstream end of the jet. This procedure was followed so that any disturbance created by the probe would be felt only downstream of the profile under investigation. Figure 20 is a typical example of the data taken over one cross-section.

The strip charts of millivolt output at each sampling point were analyzed for each individual run. Values of the average millivolt output at a point in a cross-section for various time increments, Δt, were estimated by eye from the trace on the strip chart. These were then averaged according to Equation 83 to obtain the time-averaged millivolt output for that point.

$$\bar{m}_{j,k} = \frac{\sum_{i=1}^{n} (m_{i,j,k})(\Delta t_i)}{\sum_{i=1}^{n} \Delta t_i} \tag{83}$$

where $\bar{m}_{j,k}$ = time-averaged millivolt output at location j in cross-section, k

$m_{i,j,k}$ = millivolt output at location (j,k) over time increment Δt_i

$s'/D = 3.54$

$x'/D = 2.00$

$c/c_o = 0.48$

$\sigma = 0.55$

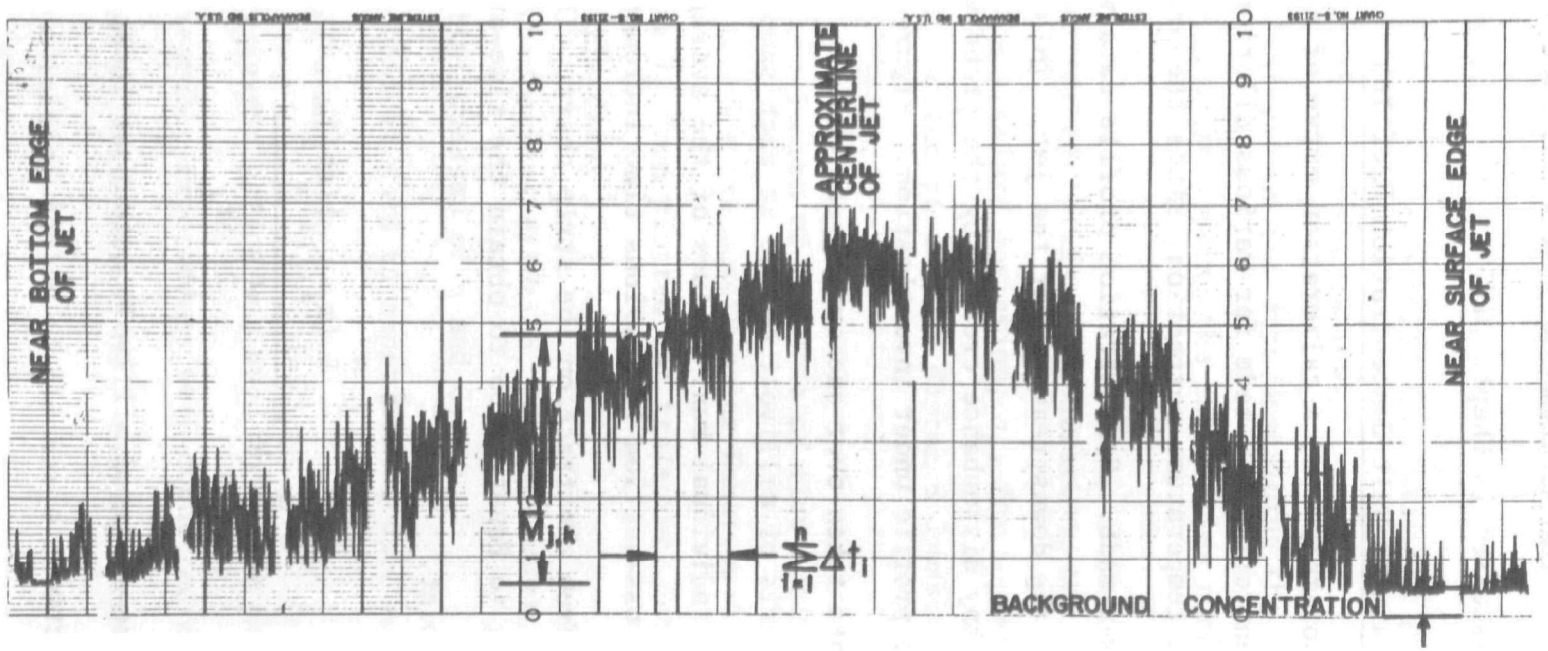

FIGURE 20 - CONCENTRATION PROFILE AT $s'/D_o = 3.54$ FOR RUN NO. 34

TABLE 3 - COMBINATION OF DENSIMETRIC FROUDE NUMBER, VELOCITY RATIO, AND INITIAL ANGLE OF DISCHARGE ACCORDING TO FAN'S DEFINITIONS

Run No.	Froude No., F	Velocity Ratio $k = U_o/U_a$	Initial Angle of Discharge β'_o	Angle at End of Zone of Flow Establishment β_o	Reynolds No. R_e
9	10.3	10.3	90	74	1650
10	10.9	5.5	90	62.5	1190
11	20.4	10.2	90	78	2200
12	21.1	5.3	90	74.8	1050
13	40.7	10.2	90	76.3	2030
15	10.1	20.1	90	81.8	1110
16	20.2	20.2	90	78.3	2240
18	44.2	5.5	90	58.3	4700
19	11.7	5.9	45	31.8	1730
20	21.6	10.8	45	36.5	3200
21	23.5	5.9	45	28.0	1600
22	43.2	10.8	45	36.3	3140
23	10.9	10.9	45	28.0	2540
24	20.8	20.8	45	34.5	4980
25	10.4	20.9	45	29.3	1590
26	46.9	5.9	45	30.0	4580
27	11.3	5.7	60	48.8	1180
28	21.3	10.6	60	51.3	2220
29	10.6	10.6	60	52.0	1870
30	20.6	20.6	60	53.0	3636
31	10.3	20.6	60	53.8	1035
32	22.5	5.6	60	52.0	1080
33	42.7	10.6	60	53.8	2040
34	45.4	5.7	60	47.8	2940

TABLE 4 - COMBINATION OF DENSIMETRIC FROUDE NUMBER, VELOCITY RATIO, AND INITIAL ANGLE OF DISCHARGE ACCORDING TO ABRAHAM'S DEFINITIONS

Run No.	Froude No. F	Velocity Ratio $k = U_o/U_a$	Initial Angle of Discharge β'_o	Reynolds Number R_e
9	10.0	10.0	90	1580
10	10.0	5.0	90	1090
11	20.0	10.0	90	2180
12	20.0	5.0	90	1900
13	40.0	10.0	90	2000
15	10.0	20.0	90	1110
16	20.0	20.0	90	2220
18	40.0	5.0	90	4250
19	11.4	5.7	45	1700
20	21.4	10.7	45	3170
21	22.8	5.7	45	1555
22	42.8	10.7	45	3110
23	10.7	10.7	45	2440
24	20.7	20.7	45	4930
25	10.4	20.7	45	1580
26	45.7	5.7	45	4320
27	11.0	5.5	60	1150
28	21.0	10.5	60	2200
29	10.5	10.5	60	1840
30	20.5	20.5	60	3610
31	10.3	20.5	60	1000
32	22.0	5.5	60	1060
33	42.0	10.5	60	2030
34	44.0	5.5	60	2850

i = index number of time period

j = index number denoting a given location in a given cross-section, k

k = index number denoting a given cross-section

n = number of time increments used

Δt_i = time period used in time-averaging

The time-averaged millivolt outputs were then used as input data for a computer program called Analysis. A listing of the computer program, Analysis, is included in Appendix G. This program used the calibration curve to convert the time-averaged millivolt output, $\bar{m}_{j,k}$, to a time-averaged concentration, $\bar{c}_{j,k}$. Knowing $\bar{c}_{j,k}$, which was the concentration at location (j,k), y'_k, the y-location of the mean value of the concentration profile, $\bar{c}_k$, the mean values of the concentration profile, and the standard deviation, σ_k, were calculated using Equations 84, 85, and 86, respectively.

$$y'_k = \frac{\sum_{j=1}^{N} \bar{c}_{j,k} \cdot y'_{j,k}}{\sum_{j=1}^{N} \bar{c}_{j,k}} \tag{84}$$

$$\bar{c}_k = \frac{\left(\sum_{j=1}^{N} \bar{c}_{j,k}\right) \cdot CI}{\sigma_k \sqrt{2\pi}} \tag{85}$$

$$\sigma_k = \sqrt{\frac{\sum_{j=1}^{N} \bar{c}_{j,k} \cdot (y'_{j,k})^2 - \frac{\left(\sum_{j=1}^{N} \bar{c}_{j,k} \cdot y'_{j,k}\right)^2}{\sum_{j=1}^{N} \bar{c}_{j,k}}}{\sum_{j=1}^{N} \bar{c}_{j,k}}} \qquad (86)$$

where N = number of j location in a given cross-section, k

$y'_{j,k}$ = the vertical distance from the discharge point

CI = Δy, the incremental distance between each $y_{j,k}$

It is important to note that $\bar{c}_{j,k}$ and $\bar{c}_k$ are equivalent to $c^*(s,r,\phi)$ and $c(s)$, respectively, where $c^*(s,r,\phi)$ is a local concentration value for any given y-distance from the centerline and for any given cross-section, k, and $c(s)$ is the centerline concentration for any given cross-section, k. This is equivalent to the nomenclature used in Equation 2 for Fan's model and Equation 66 for Abraham's model. The values of $\bar{c}_k$, y'_k, and σ_k are then used as input to the computer programs for comparison with the theoretical predictions. Using Equation 24, the relationship between σ_k and b, the jet half-width, is defined as

$$b = \sqrt{2}\,\sigma_k \qquad (87)$$

Hence, the centerline concentration, $\bar{c}_k$, was calculated. For each $\bar{c}_k$, there was both an x'-coordinate and a y'-coordinate. The x'-coordinate represented the horizontal distance from the discharge point, whereas the y'-coordinate was the vertical location of the centerline concentration measured from a horizontal plane passed through the discharge point. Figure 21 gives a more explicit description of the location of a jet's trajectory.

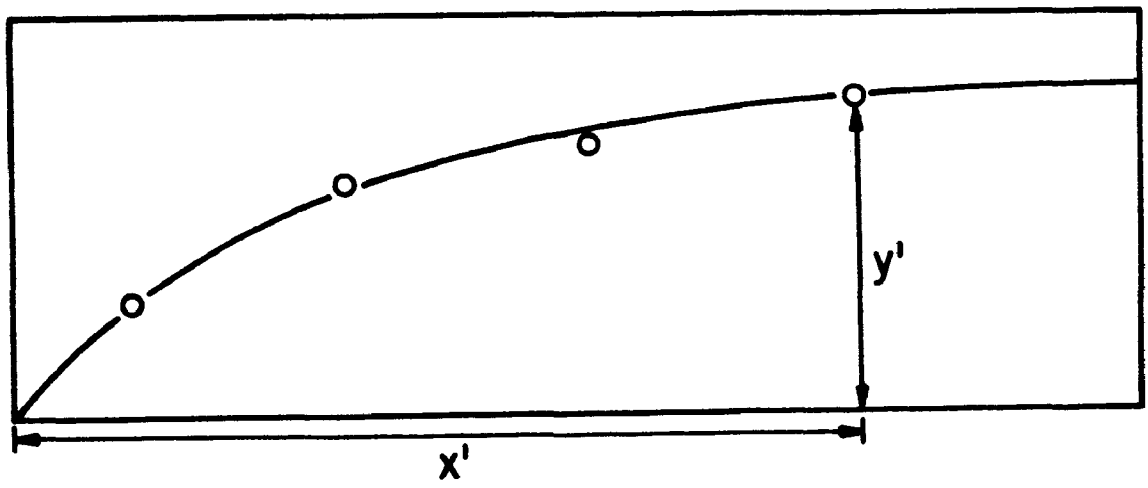

FIGURE 21 - REPRESENTATIVE PROFILE VIEW OF A JET'S TRAJECTORY

Jet Trajectories

Using the x'- and y'-coordinates, the jet trajectory of each run was plotted. Twenty-four runs were made. Table 3 gives the various combinations of densimetric Froude number, velocity ratio, and initial angle of discharge according to Fan's definitions. The angle at the end of the zone of flow establishment and the jet Reynolds number are also included, where the jet Reynolds number is defined as

$$R_e = \frac{U_o D_o}{\nu} \tag{88}$$

where R_e = jet Reynolds number

ν = kinematic viscosity of salt water

Table 4 gives the various combinations of densimetric Froude number, velocity ratio, and initial angle of discharge according to Abraham's definitions. Table 4 also includes the jet Reynolds number.

The difference between the two tables arises from the different definitions of the initial jet velocity. Fan defines U_o, the initial jet velocity at the end of the zone of flow establishment, as

$$U_o = u_o + U_a \cos \beta_o \tag{89}$$

whereas Abraham defines U_o as

$$U_o = u_o + U_a \cos \beta_o' \tag{90}$$

For both Fan's model and Abraham's model, the value of u_o is the same, but the addition of the vector component of the ambient velocity with two different initial angles give rise to two values for the component vector. The process of obtaining the value of β_o will be discussed in detail later, whereas β_o' is simply the horizontal angle that the discharge orifice makes with the ambient flow. By reviewing the initial conditions, Equations 42 and 52, this difference in the initial angle is illustrated.

Thus, using Equation 4, and knowing the value of the velocity ratio, k, the length of the zone of flow establishment, s_e', can be determined. This length is then measured along the jet axis. Once the end of the zone of flow establishment is determined, the x_e' and y_e' coordinates are determined. This is only necessary for the use of Fan's model, since

Abraham does not consider the zone of flow establishment. Once the end of the zone of flow establishment is determined, the initial angle of inclination, β_o, of the jet is measured. Hence, all of the unknown variables are known and the theoretical solution using Fan's and Abraham's model can be sought.

Only six runs will be discussed in the main text. However, the plots of the dilution, jet half-width, and trajectory for all 24 runs and for both models can be found in Appendix H. Tables 5 and 6 give the pertinent location, dilution, and jet half-width data for the six combinations discussed using Fan's model and Abraham's model, respectively.

Fitting of Data to Theoretical Curves

Trial computer solutions were made for the fitting of the data to Fan's model. Initial guesses of α and C_d were made based on experience. However, it was soon found that, for any value of C_d, the jet trajectory was under-predicted. The theoretical considerations concerning the behavior of C_d in the development of a positively buoyant jet apparently are not applicable when applied to the case of a negatively buoyant jet. The buoyancy forces that tend to retard the vertical momentum are apparently greater than the drag forces. Hence, in an effort to force the model to fit the data, the value of $C_d = 0.00$ was used for all runs. Hence, only an initial guess for α was needed.

Several trial computer solutions were made using different values of α. Theoretical values of the jet dilution and jet half-width were plotted on the same graph as the experimental data. Experimental values of jet dilution and jet half-width were both used to select an appropriate value of α which predicted the best fit. In most cases, a best

TABLE 5 - SUMMARY OF NEGATIVELY BUOYANT JET EXPERIMENTS IN A CROSS-FLOW FOR FAN'S MODEL

Run No.	β_o	F	k	β'_o	$\frac{s'_e}{D}$	$\frac{x'_e}{D}$	$\frac{y'_e}{D}$	$\frac{s}{D}$	$\frac{x}{D}$	$\frac{y}{D}$	$\frac{c_o}{c}$	$\frac{b}{D_o}$
13	90°	40.7	10.2	76.3	4.45	0.75	4.38	9.75	4.25	8.71	9.13	4.47
								15.75	9.25	12.05	14.60	4.15
								21.20	14.25	14.20	17.80	5.19
								31.56	24.25	16.72	30.97	6.42
								56.81	49.25	19.45	36.86	6.81
								112.50	104.88	19.86	62.34	9.61
								156.94	149.25	19.12	87.71	11.03
								207.02	199.25	18.09	87.04	11.68
10	90°	10.9	5.5	62.5	3.19	1.10	3.07	5.81	3.90	4.28	9.99	2.14
								11.38	8.90	6.60	11.59	3.24
								16.39	13.90	7.52	14.33	3.56
								21.52	18.90	5.98	17.56	2.95
								36.42	33.90	5.90	20.25	4.97
								41.62	38.90	4.56	35.37	5.35
								51.69	48.90	3.84	36.74	5.06
								76.88	73.90	1.96	40.70	4.11
33	60°	42.7	10.6	53.8	4.45	2.43	3.75	4.06	2.57	3.14	4.01	2.20
								10.42	7.57	6.97	7.43	3.58
								20.90	17.57	10.01	16.76	4.91
								31.22	27.57	11.94	25.46	4.96
								41.39	37.57	13.14	31.97	6.44
								51.39	47.57	12.33	35.13	7.23
								101.53	97.57	14.83	60.06	9.12
								201.58	197.57	11.57	77.11	13.50

TABLE 5 - Continued

Run No.	β_o	F	k	β'_o	$\frac{s'_e}{D}$	$\frac{x'_e}{D}$	$\frac{y'_e}{D}$	$\frac{s}{D}$	$\frac{x}{D}$	$\frac{y}{D}$	$\frac{c_o}{c}$	$\frac{b}{D_o}$
27	60°	11.3	5.7	48.8	3.19	1.94	2.57	3.97	3.06	2.43	4.34	1.68
								9.44	8.06	4.75	7.44	2.61
								19.58	18.06	5.93	11.65	3.24
								29.75	28.06	7.04	18.62	3.90
								39.86	38.06	6.00	21.28	4.48
								50.00	48.06	4.78	23.66	4.50
								75.49	73.06	0.00	45.05	5.26
22	45°	43.2	10.8	36.3	4.45	3.45	2.93	2.00	1.54	1.18	2.56	1.74
								7.68	6.55	3.95	4.11	2.57
								18.26	16.55	7.54	7.44	3.39
								28.58	26.55	10.08	12.25	4.52
								38.84	36.55	11.99	14.77	5.18
								48.86	46.55	13.41	19.58	5.63
								99.10	96.55	17.52	29.82	6.62
19	45°	11.7	5.9	31.8	3.19	2.68	1.81	2.58	2.32	1.18	3.67	1.72
								8.00	7.32	3.06	5.56	2.20
								18.05	17.32	4.08	10.12	3.15
								38.10	27.32	4.15	17.82	4.30
								48.21	47.32	3.69	25.08	5.40
								68.36	67.32	0.96	31.70	5.42

TABLE 6 - SUMMARY OF NEGATIVELY BUOYANT JET EXPERIMENTS IN A CROSS-FLOW FOR ABRAHAM'S MODEL

Run No.	β_o	F	k	$\frac{s'}{D}$	$\frac{x'}{D}$	$\frac{y'}{D}$	$\frac{c_o}{c}$	$\frac{b}{D_o}$
13	90°	40	10	14.20	5.00	13.15	9.13	4.47
				20.20	10.00	16.49	14.60	5.15
				25.65	15.00	18.64	17.86	5.19
				36.01	25.00	21.16	30.97	6.42
				61.26	50.00	23.89	36.86	6.81
				116.95	105.62	24.30	62.54	9.61
				161.39	150.00	23.56	87.71	11.04
				211.48	200.00	22.52	87.04	11.63
33	60°	42	10.5	8.50	5.00	6.89	4.01	2.20
				14.86	10.00	10.72	7.03	3.58
				25.35	20.00	13.76	16.76	4.91
				35.67	30.00	15.69	25.46	4.96
				45.83	40.00	16.89	31.97	6.44
				55.83	50.00	16.08	35.13	7.23
				105.97	100.00	18.58	60.06	9.13
				206.03	200.00	15.32	77.11	13.50
22	45°	42.8	10.7	6.45	4.99	4.10	2.56	1.70
				12.14	10.00	6.87	4.11	2.57
				22.72	20.00	10.46	7.44	3.39
				33.03	30.00	13.01	12.25	4.56
				43.29	40.00	14.92	14.77	5.18
				53.32	50.00	16.34	19.58	5.63
				103.56	100.00	20.45	29.82	6.63

TABLE 6 - Continued

Run No.	β_o	F	k	$\frac{s'}{D}$	$\frac{x'}{D}$	$\frac{y'}{D}$	$\frac{c_o}{c}$	$\frac{b}{D_o}$
10	90°	10	5	9.00	5.00	7.34	9.99	2.15
				14.56	10.00	9.66	11.59	3.24
				19.58	15.00	10.59	14.35	3.36
				24.71	20.00	9.04	17.56	2.95
				39.61	35.00	8.96	20.25	4.97
				44.81	40.00	7.62	35.37	5.35
				54.88	50.00	6.90	36.74	5.05
				80.06	75.00	5.01	40.70	4.11
27	60°	11	5.5	7.17	5.00	5.00	4.34	1.68
				12.64	10.00	7.32	7.44	2.61
				22.78	20.00	8.50	11.65	3.24
				32.94	30.00	9.61	18.62	3.90
				43.06	40.00	8.97	21.28	4.48
				53.19	50.00	7.35	23.68	4.50
				78.68	75.00	2.57	45.05	5.26
19	45°	11.4	5.7	5.77	5.00	2.99	3.67	1.72
				11.19	10.00	4.87	5.36	2.20
				21.24	20.00	5.89	10.12	3.15
				41.29	40.00	6.06	17.82	4.30
				51.40	50.00	5.50	25.08	5.40
				71.55	70.00	2.77	31.70	4.42

fit curve pertaining to a particular value of α was obvious. However, in several cases two or more values of α could fit the data, i.e., one value of α would cause the theoretical value of jet dilution to best fit the experimental data of dilution, and a different value of α would cause the theoretical value of jet half-width to best fit the experimental data of jet half-width. Since the equations of jet dilution and jet half-width are coupled, a technique using the squared difference between the theoretical and experimental data was used to select the best fit value of α. The squared difference between a theoretical point and an experimental point was calculated both for the dilution and jet half-width. Then all the squared differences for each value of α were summed. The value of α giving the smallest value of squared difference was used.

Figures 22, 23, 24, 25, 26, and 27 show the theoretical fit of Fan's model and the experimental results for six of the twenty-four combinations of k, F, and β_o' in question. Lines on the figures represent the theoretical values of jet dilution, jet half-width, and jet trajectory. A circle, o, represents an experimental value of dilution, and a triangle, Δ, represents an experimental value of jet half-width at a location s/D on the jet axis. On the trajectory curve, a circle, o, represents an experimental location (x/D, y/D) of its respective centerline dilution.

The fitting of the theoretical curves to experimental data for Abraham's model was much easier than the fitting of the data to Fan's model, since the entrainment coefficient for Abraham's model is assumed constant, i.e., it is not a function of k, F, and β_o'. Again,

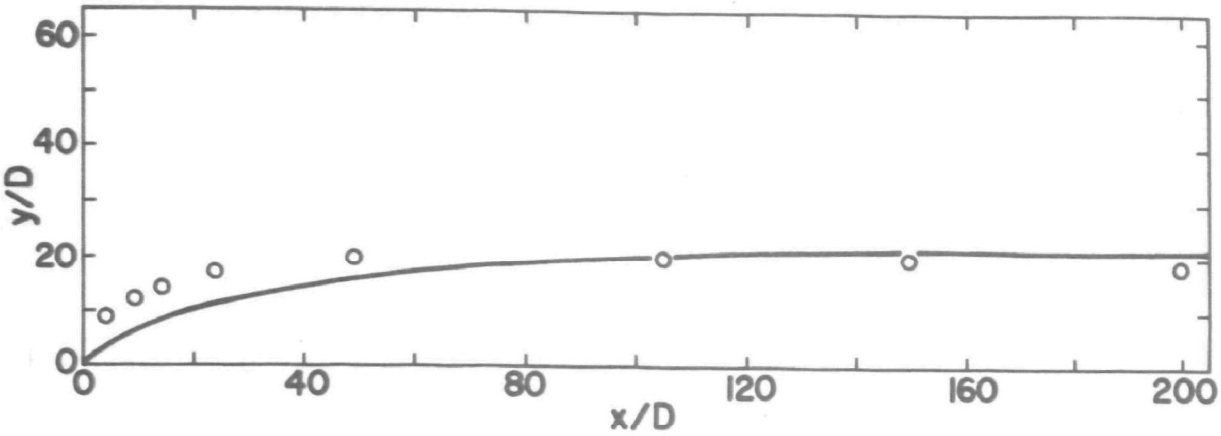

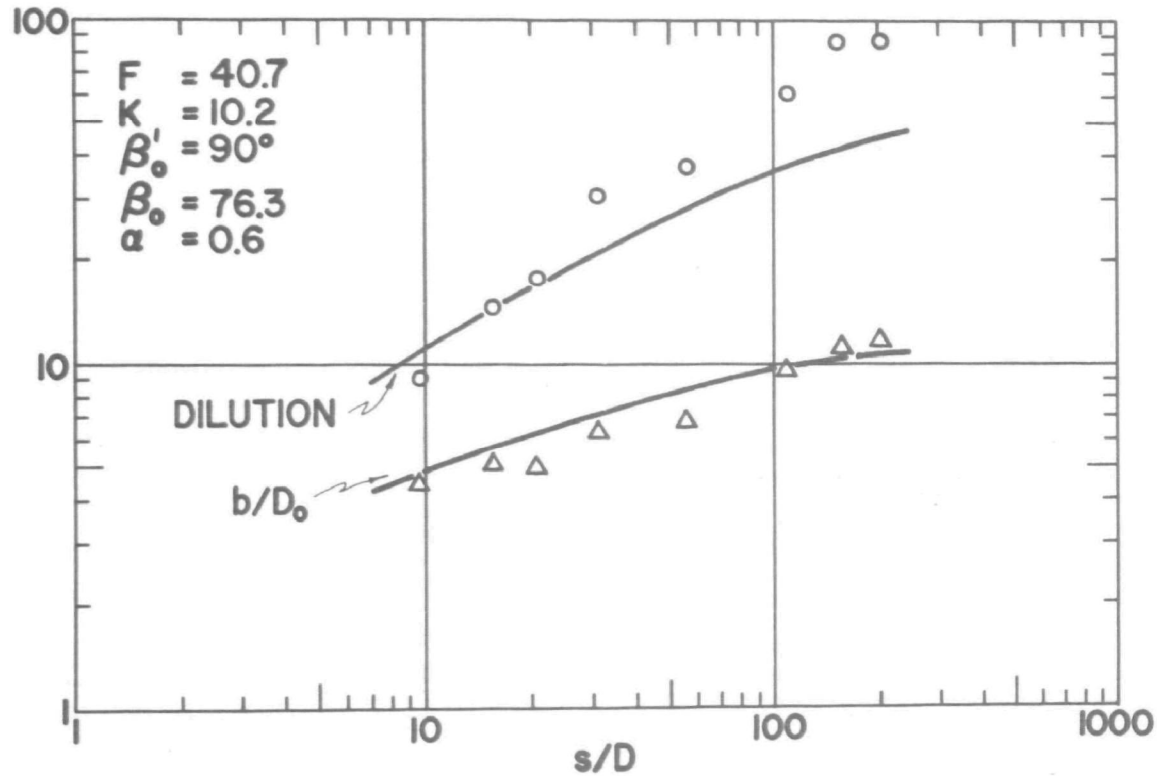

FIGURE 22 - OBSERVED VALUES AND THEORETICAL CURVES
PREDICTED BY FAN'S MODEL - RUN NO. 13

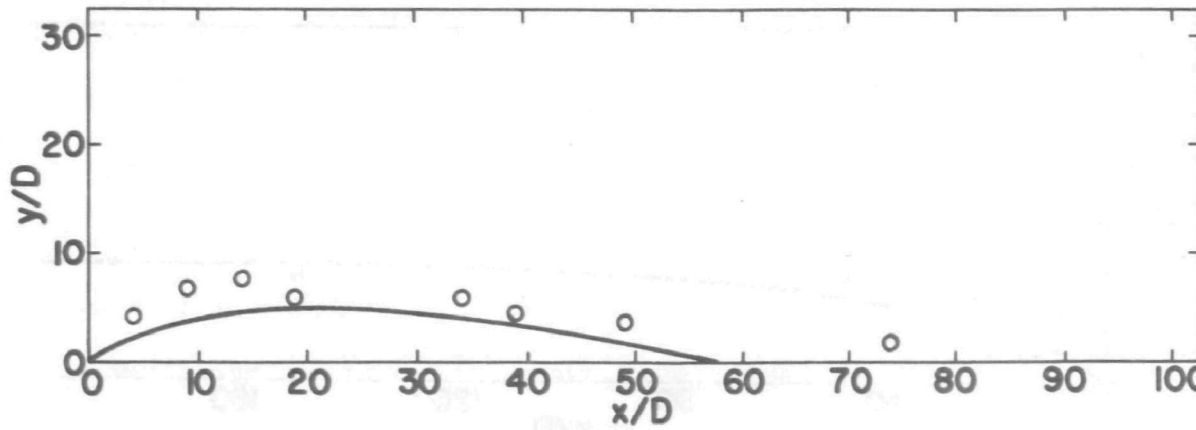

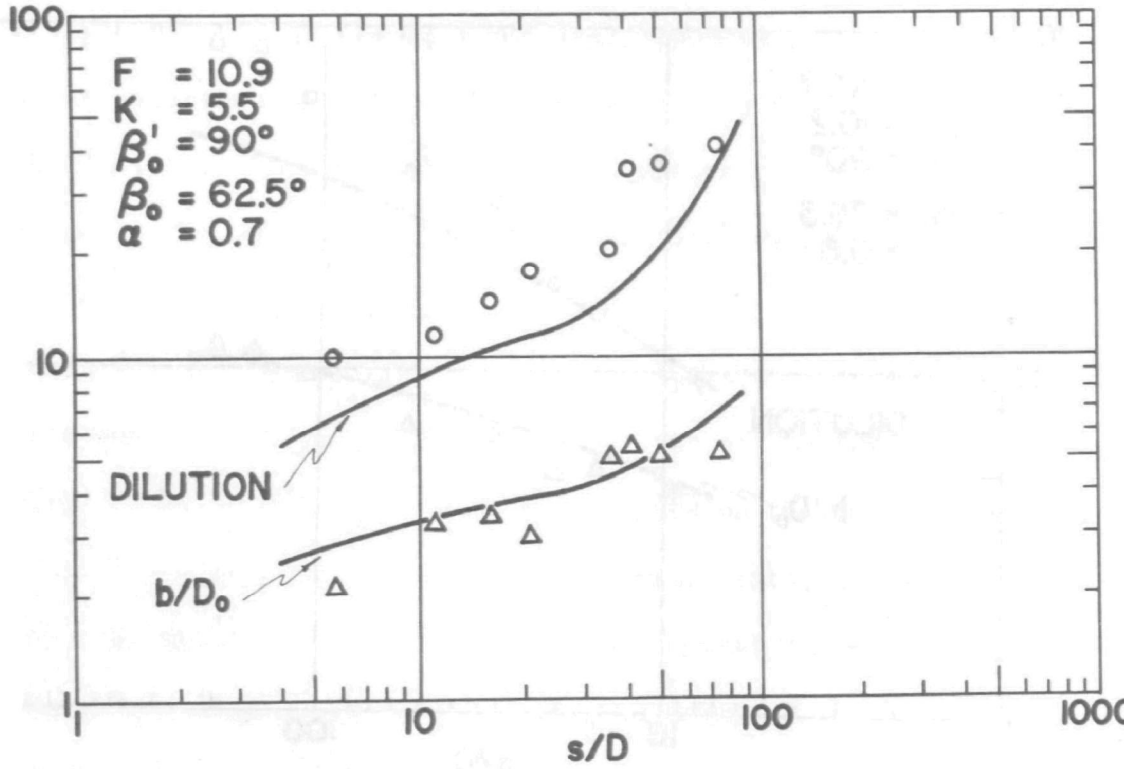

FIGURE 23 - OBSERVED VALUES AND THEORETICAL CURVES
PREDICTED BY FAN'S MODEL - RUN NO. 10

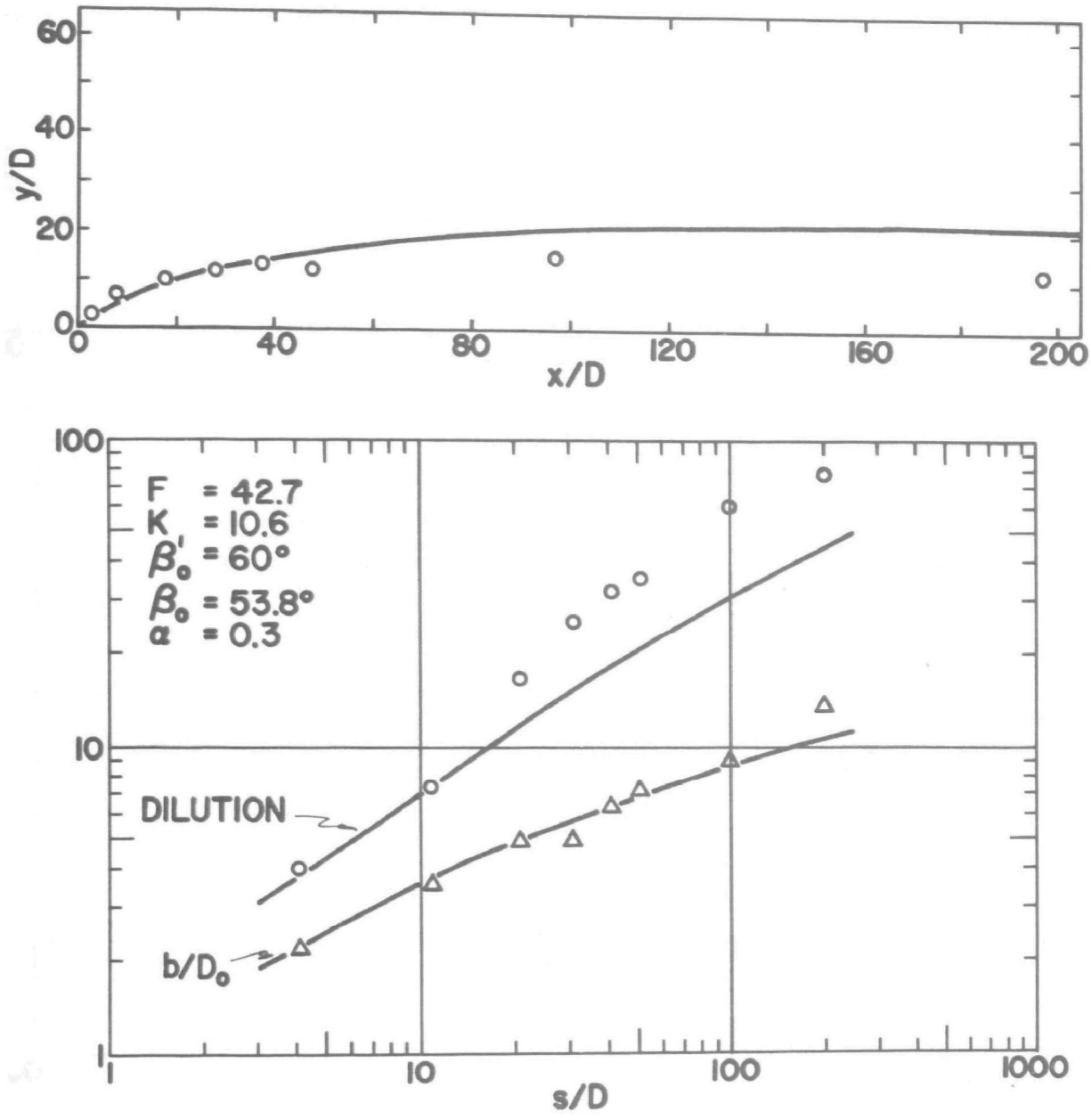

FIGURE 24 - OBSERVED VALUES AND THEORETICAL CURVES
PREDICTED BY FAN'S MODEL - RUN NO. 33

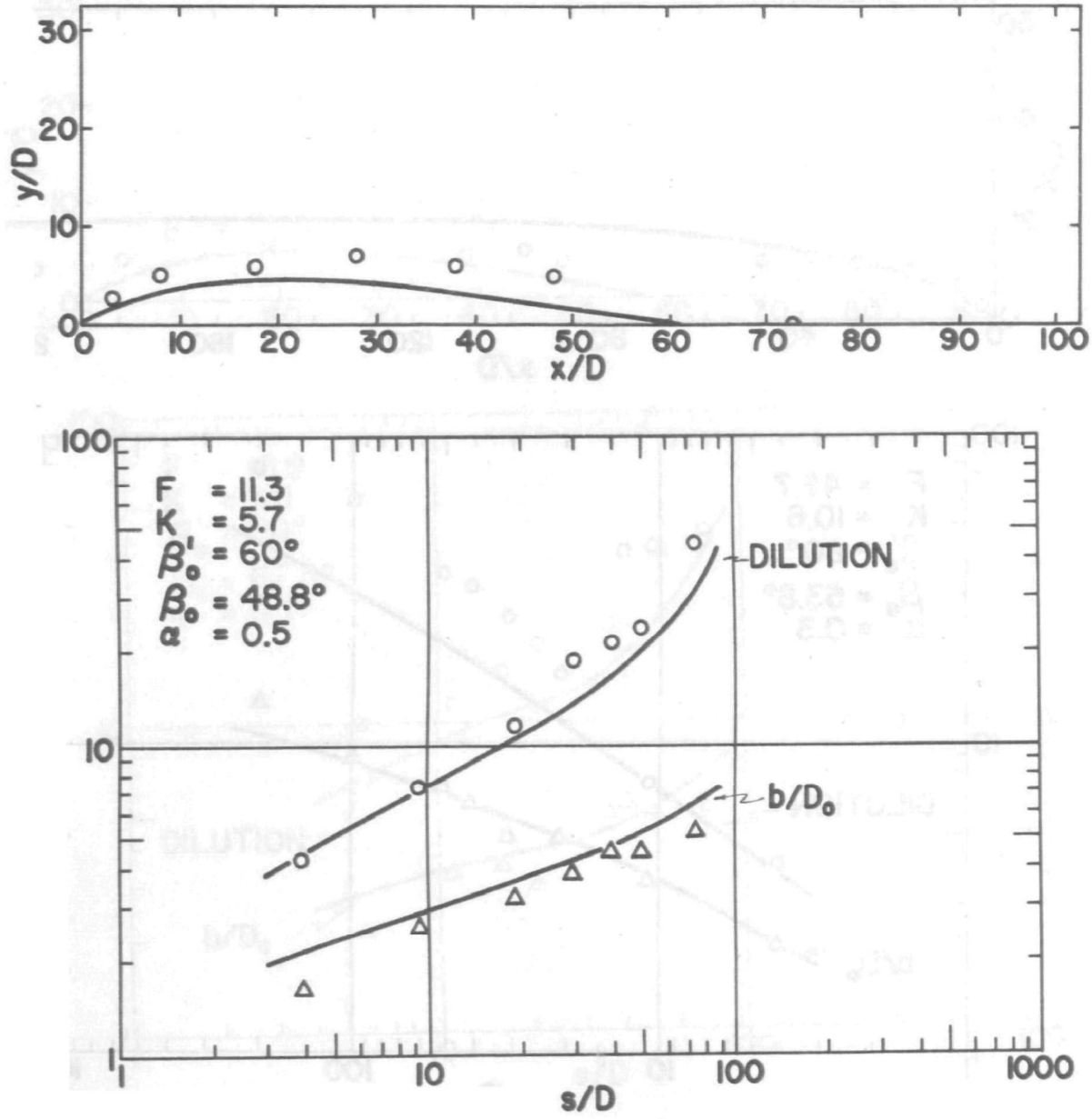

FIGURE 25 - OBSERVED VALUES AND THEORETICAL CURVE PREDICTED BY FAN'S MODEL - RUN NO. 27

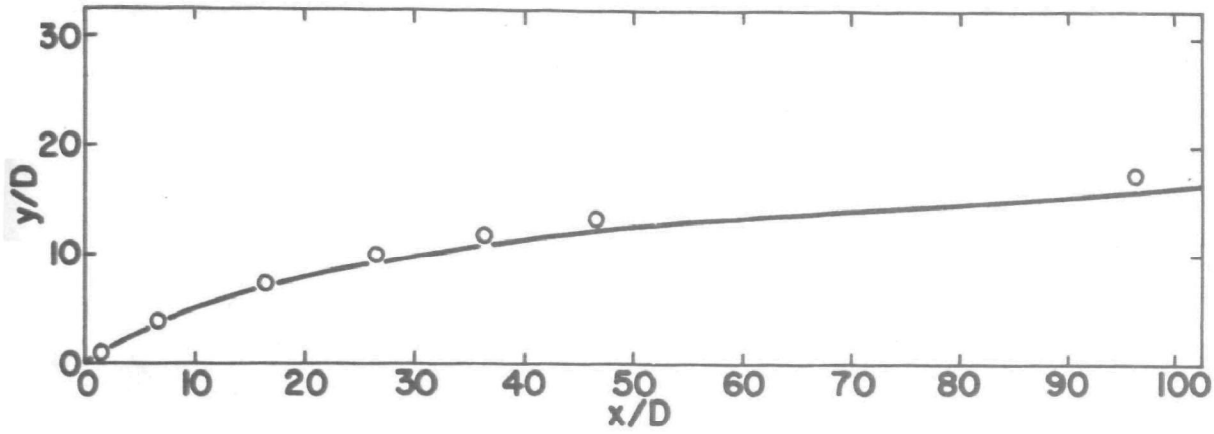

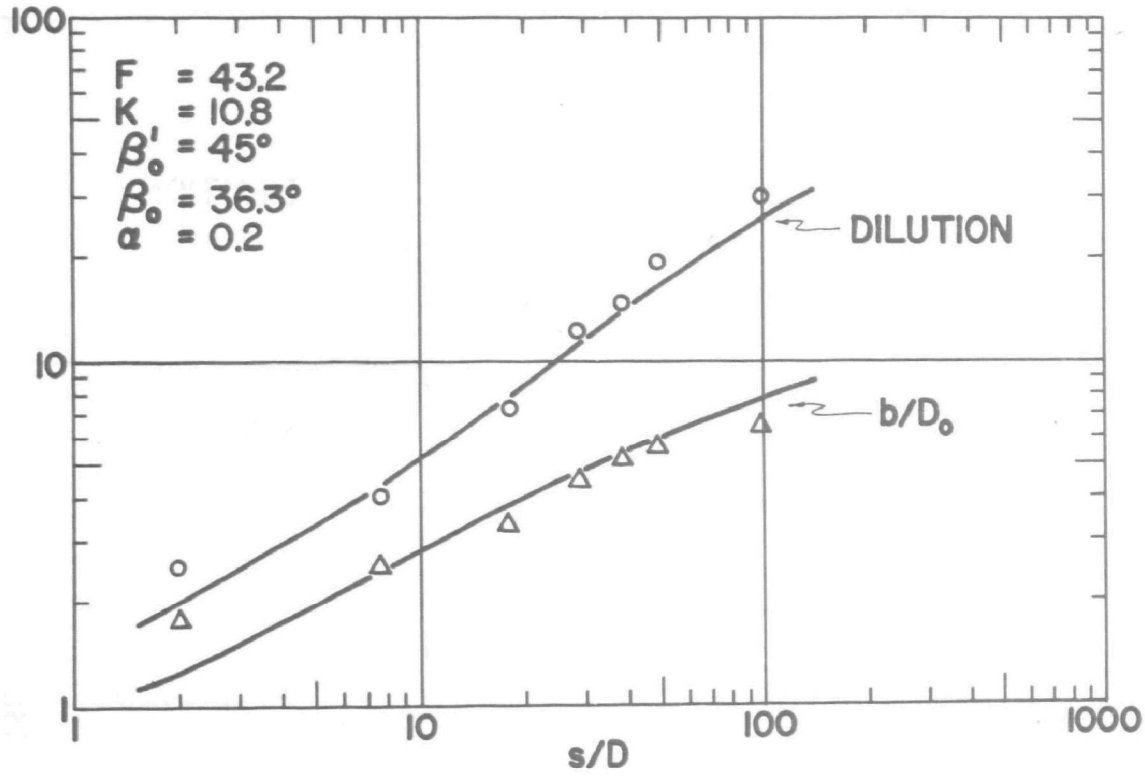

FIGURE 26 - OBSERVED VALUES AND THEORETICAL CURVES
PREDICTED BY FAN'S MODEL - RUN NO. 22

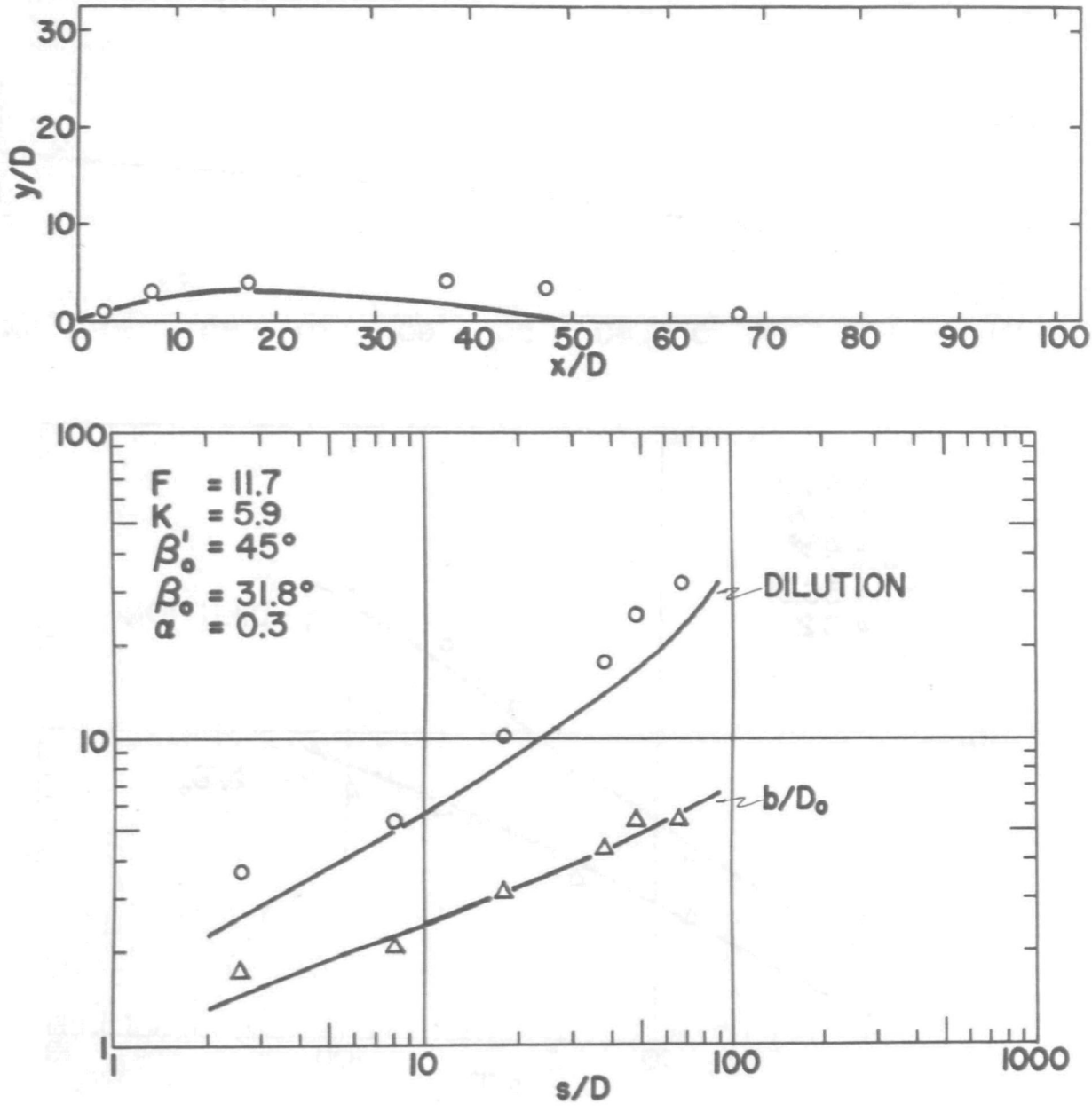

FIGURE 27 - OBSERVED VALUES AND THEORETICAL CURVES
PREDICTED BY FAN'S MODEL - RUN NO. 19

the value of the drag coefficient, C_d, was assumed equal to zero. For each run, only the values of the densimetric Froude number and velocity ratio are needed to obtain the theoretical results as outlined in Table 4.

Figures 28, 29, 30, 31, 32, and 33 show the theoretical values from Abraham's model and the experimental results for the six combinations under consideration. In addition, lines on the figures represent the theoretical values of jet dilution, jet half-width, and jet trajectory predicted using Abraham's model. A circle, o, represents an experimental value of dilution, and a triangle, Δ, represents an experimental value of jet half-width at some location s'/D on the jet axis. On the trajectory curve, a circle, o, represents an experimental location (x'/D, y'/D) of its respective centerline dilution. In addition, Figures 34, 35, 36, 37, 38, and 39 are photographs of the jet in actual laboratory conditions.

Discussion of Results - Fan's Model

For all angles of discharge (90°, 60°, and 45°), the best fit occurred at values of high densimetric Froude numbers and low velocity ratios, e.g., F = 46.9, k = 5.9, and β_o' = 90°. For the sake of discussion and comparison of the "goodness-of-fit" of the data to the theoretical model for the different combinations of F, k, and β_o', the value of U_o will be considered constant in determining the values of F and k as defined by Equation 9 and 11, respectively. At a high densimetric Froude number, e.g., F = 46.9, the difference between the initial density of the jet and the ambient density is very small.

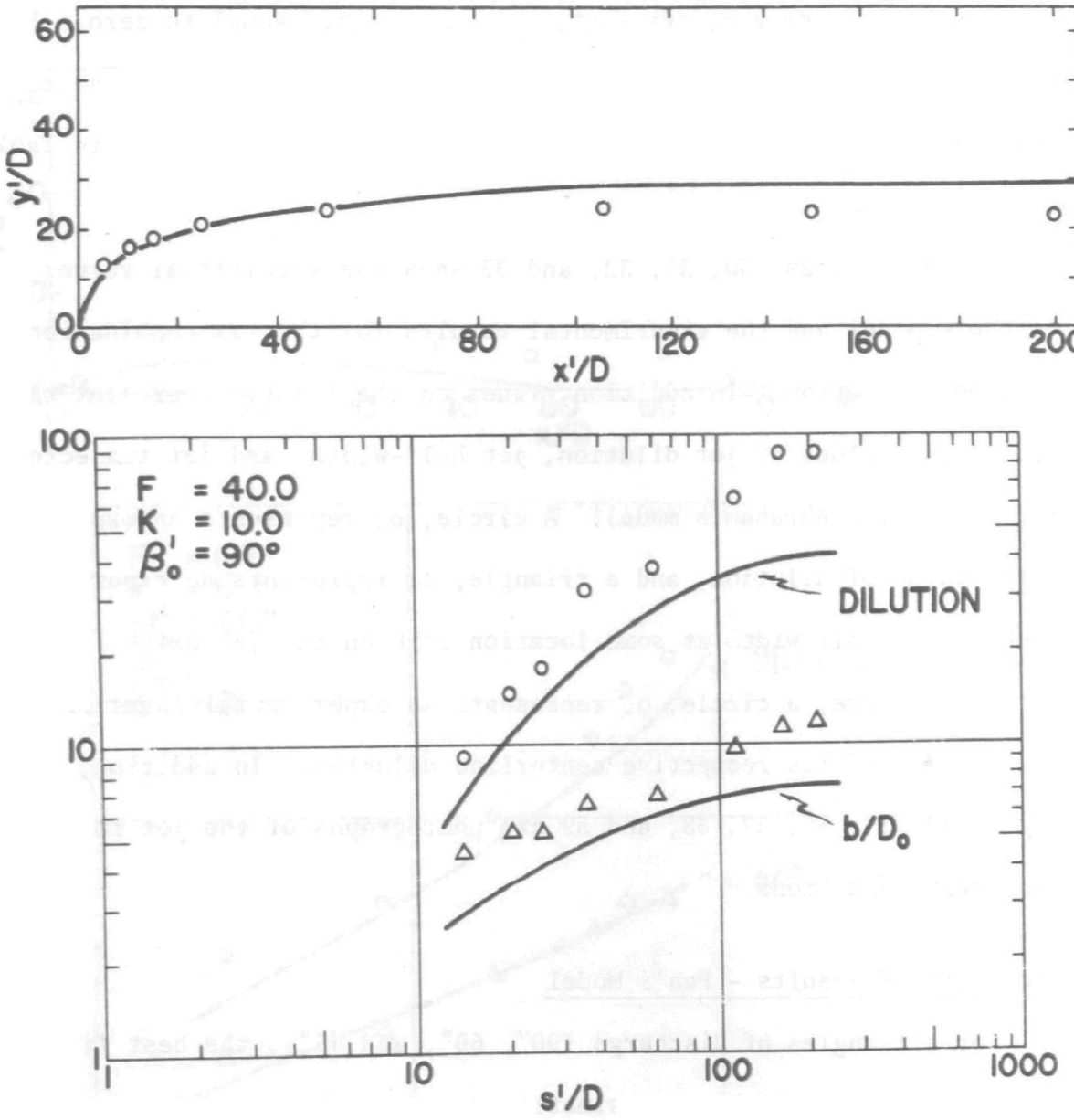

FIGURE 28 - OBSERVED VALUES AND THEORETICAL CURVES PREDICTED BY ABRAHAM'S MODEL - RUN NO. 13

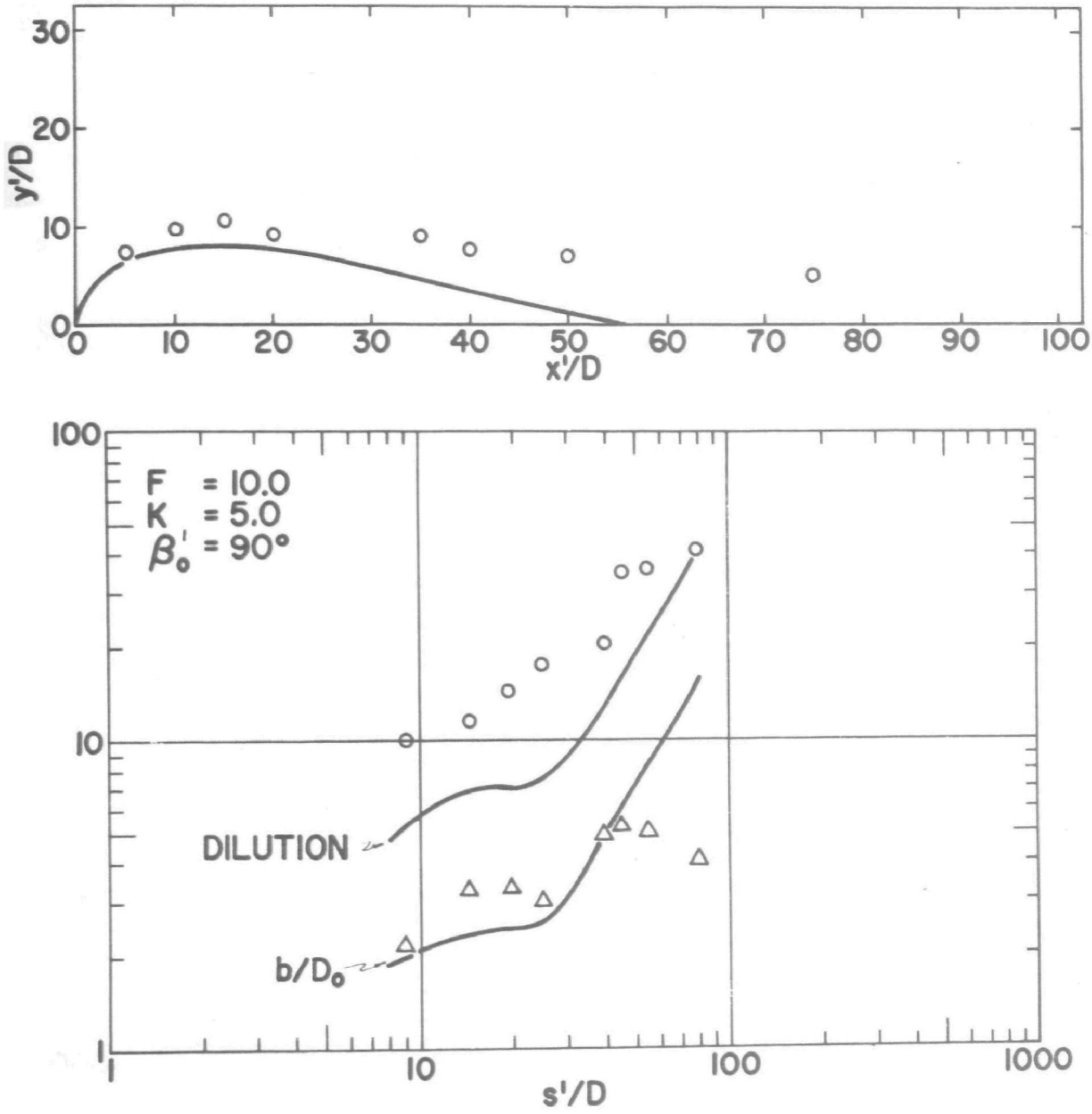

FIGURE 29 - OBSERVED VALUES AND THEORETICAL CURVES
PREDICTED BY ABRAHAM'S MODEL - RUN NO. 10

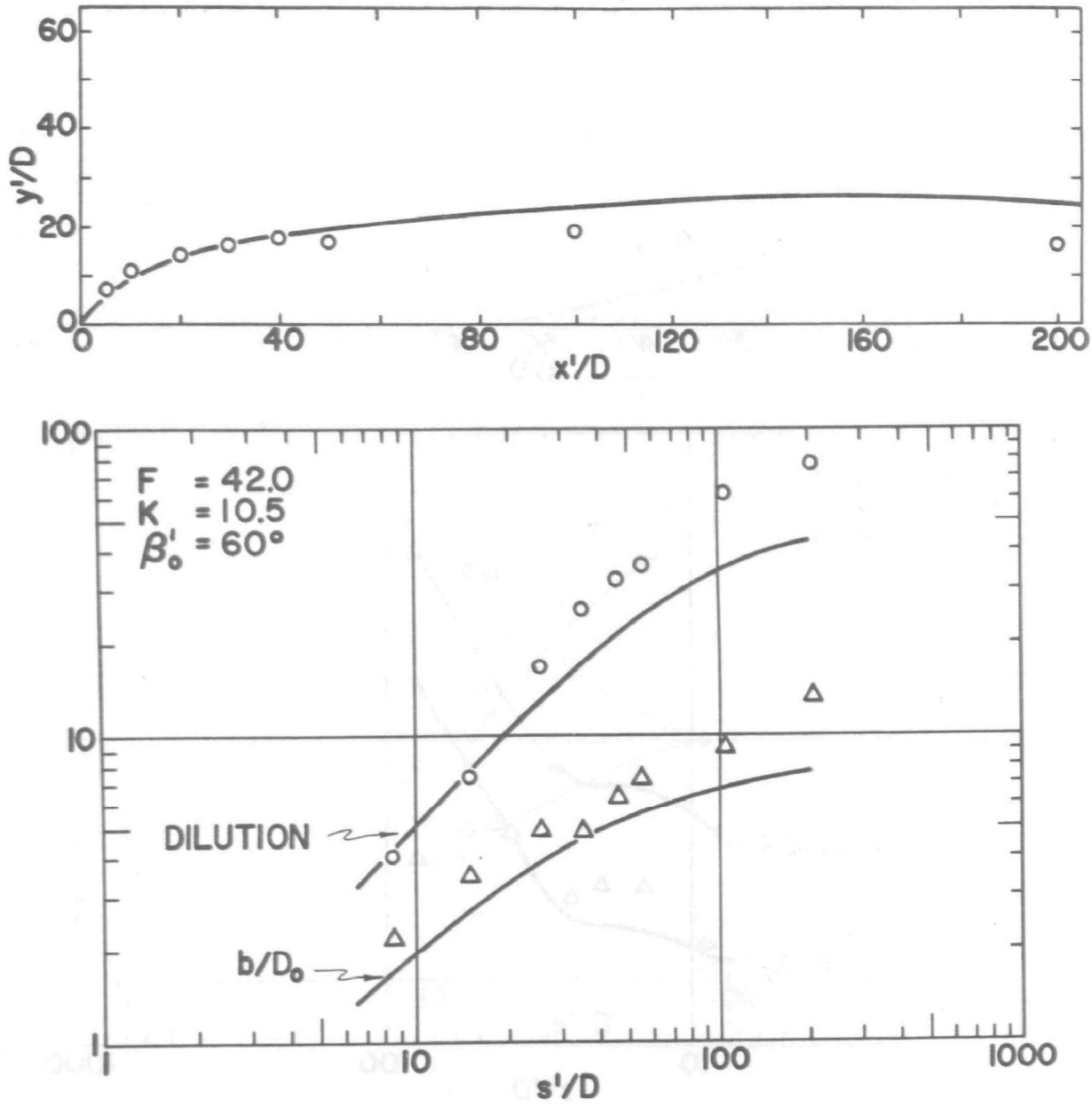

FIGURE 30 - OBSERVED VALUES AND THEORETICAL CURVES
PREDICTED BY ABRAHAM'S MODEL - RUN NO. 33

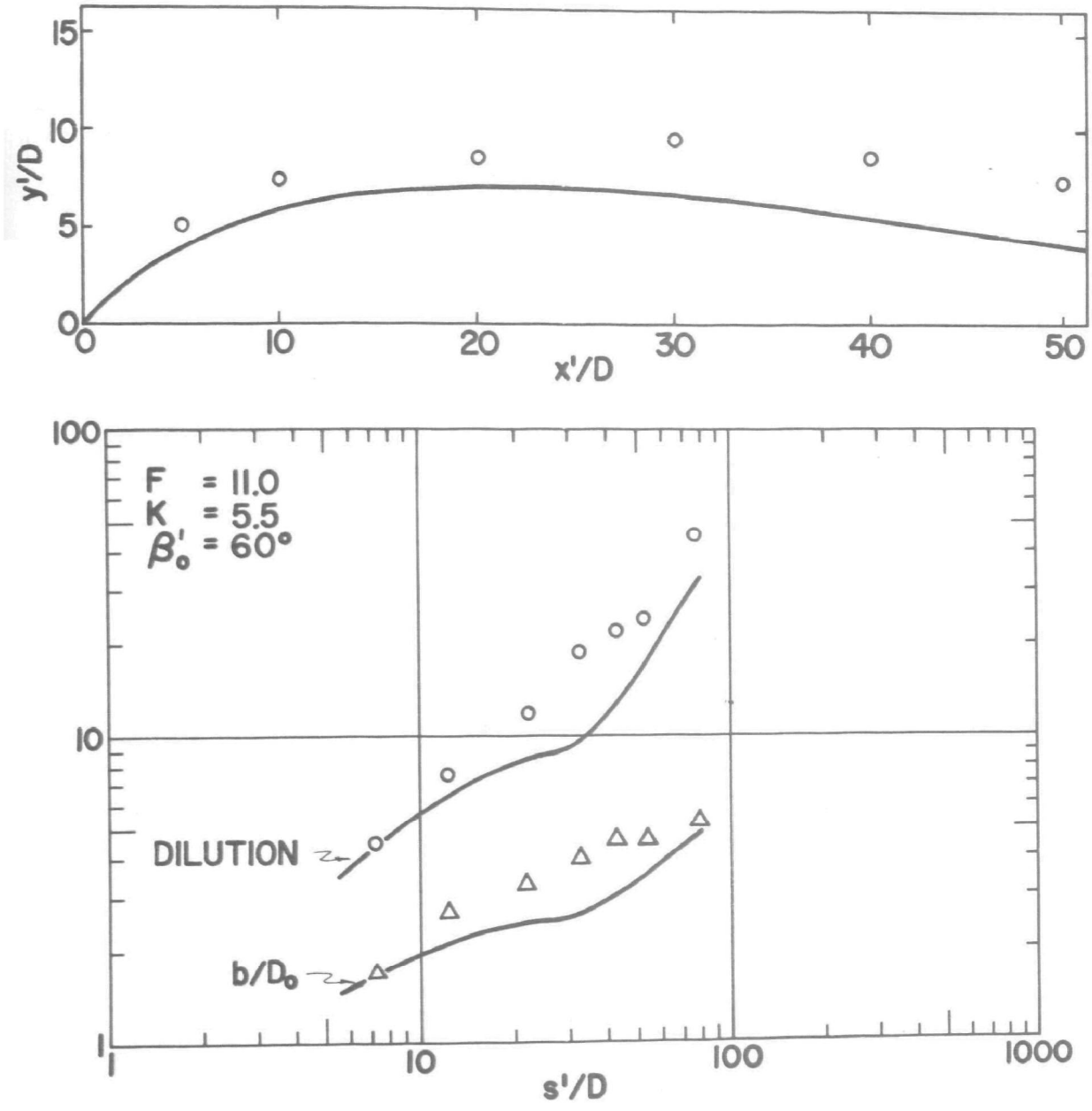

FIGURE 31 - OBSERVED VALUES AND THEORETICAL CURVES
PREDICTED BY ABRAHAM'S MODEL - RUN NO. 27

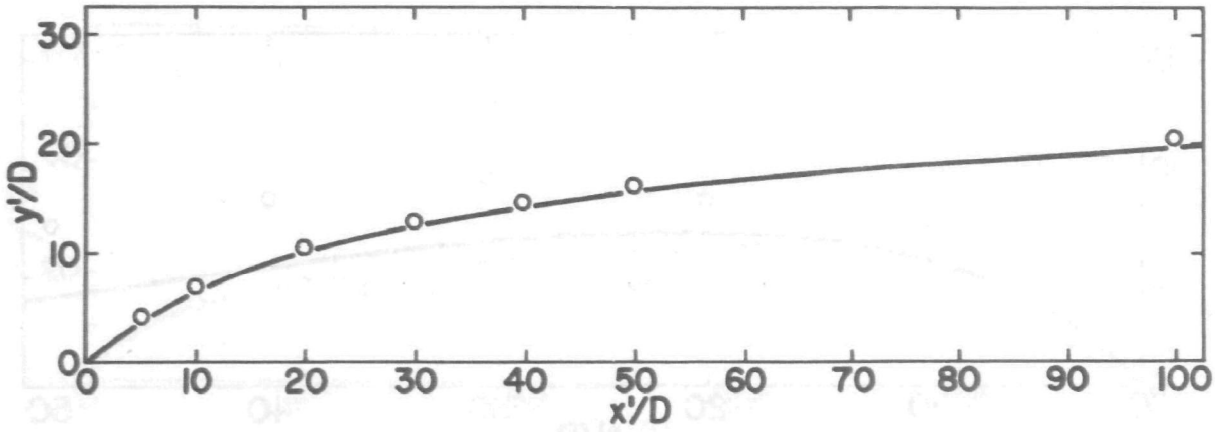

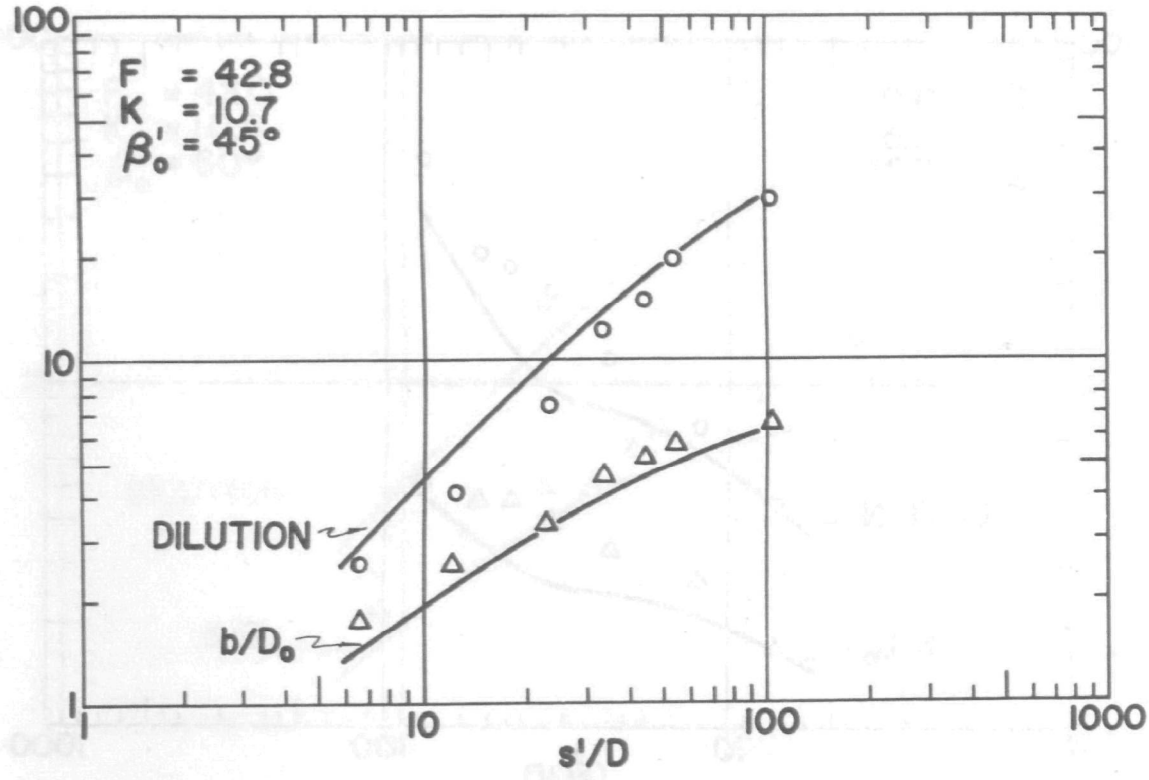

FIGURE 32 - OBSERVED VALUES AND THEORETICAL CURVES PREDICTED BY ABRAHAM'S MODEL - RUN NO. 22

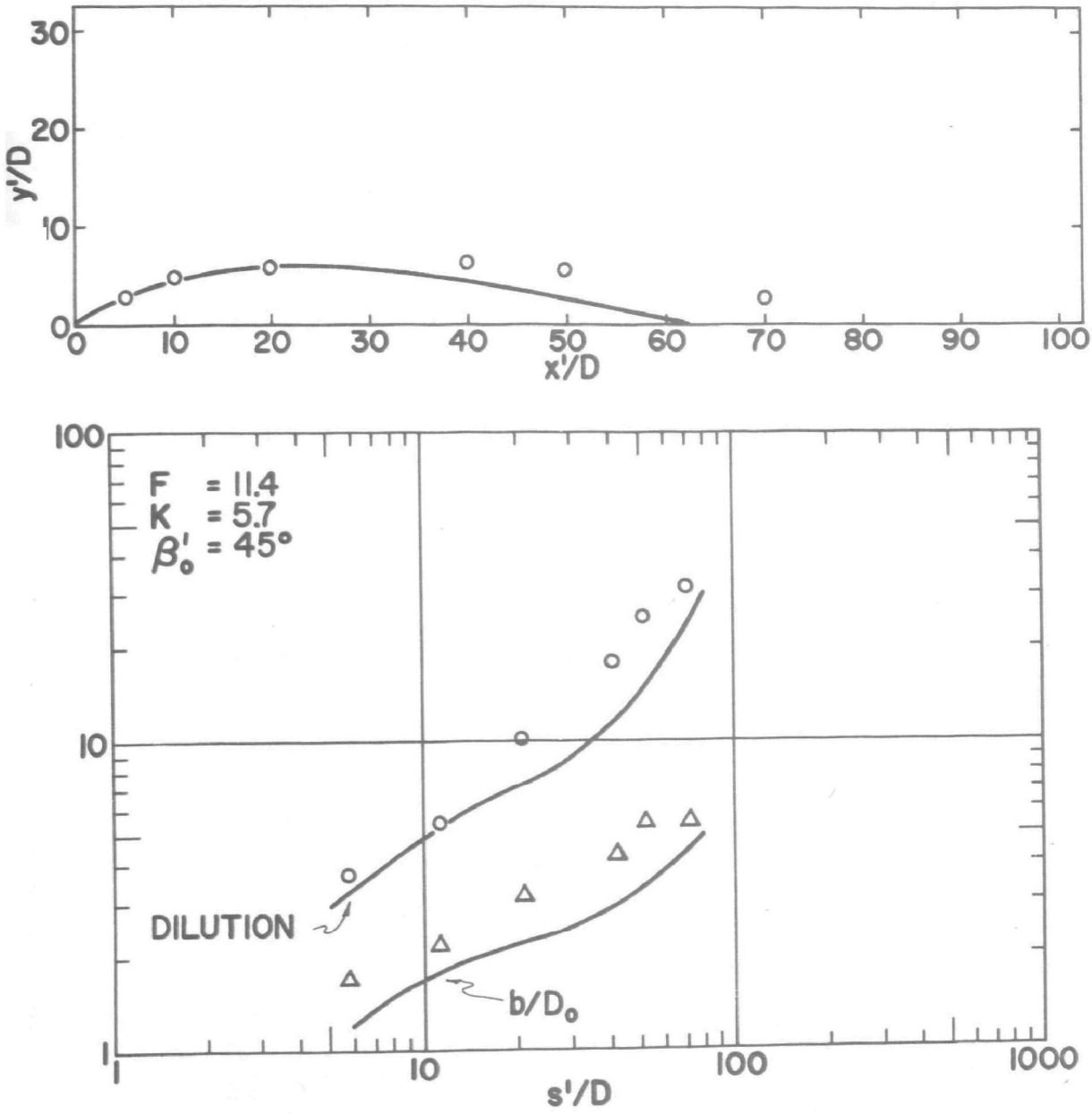

FIGURE 33 - OBSERVED VALUES AND THEORETICAL CURVES PREDICTED BY ABRAHAM'S MODEL - RUN NO. 19

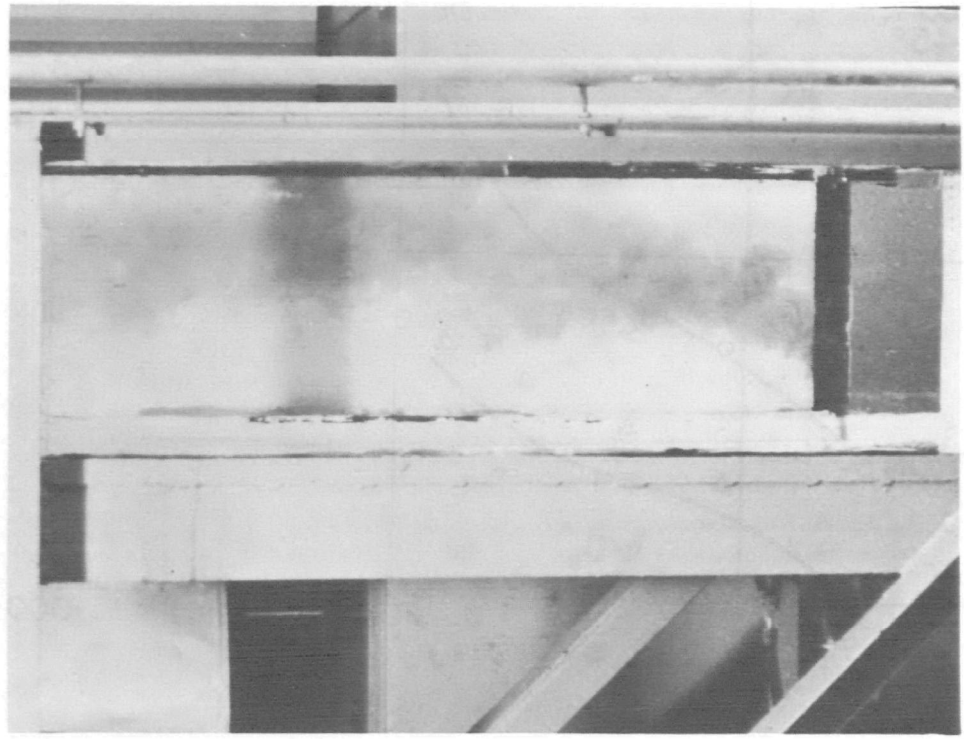

FIGURE 34 - PHOTOGRAPH OF NEGATIVELY BUOYANT JET FOR RUN NO. 13, $F \approx 40$, $k \approx 10$, $\beta_o' = 90°$

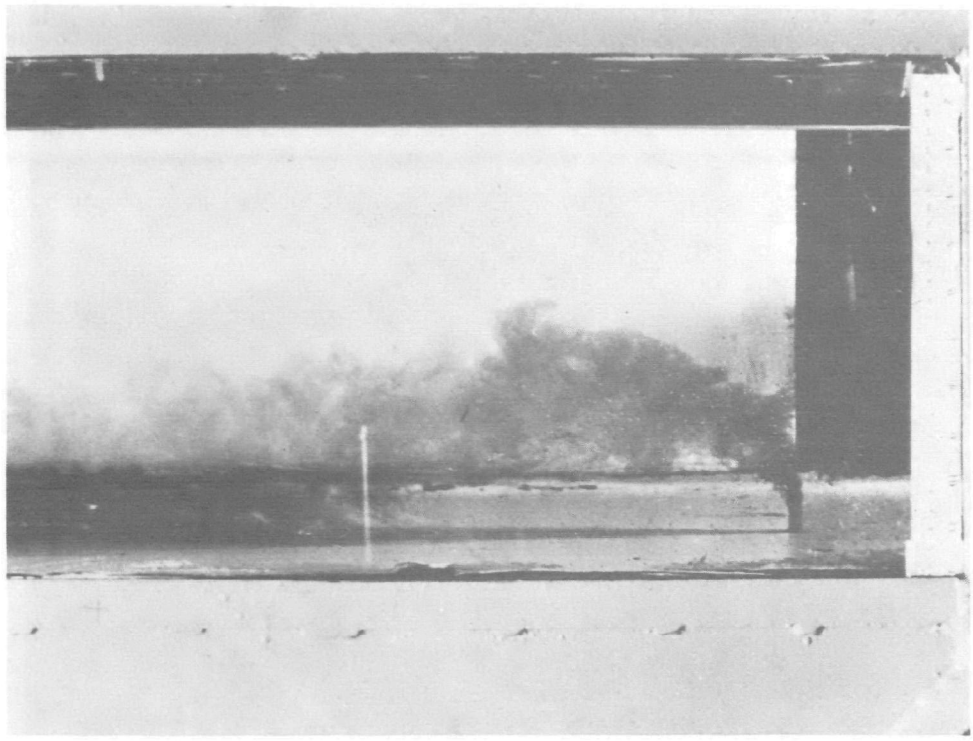

FIGURE 35 - PHOTOGRAPH OF NEGATIVELY BUOYANT JET FOR RUN NO. 10, $F \approx 10$, $k \approx 5$, $\beta_o' = 90°$

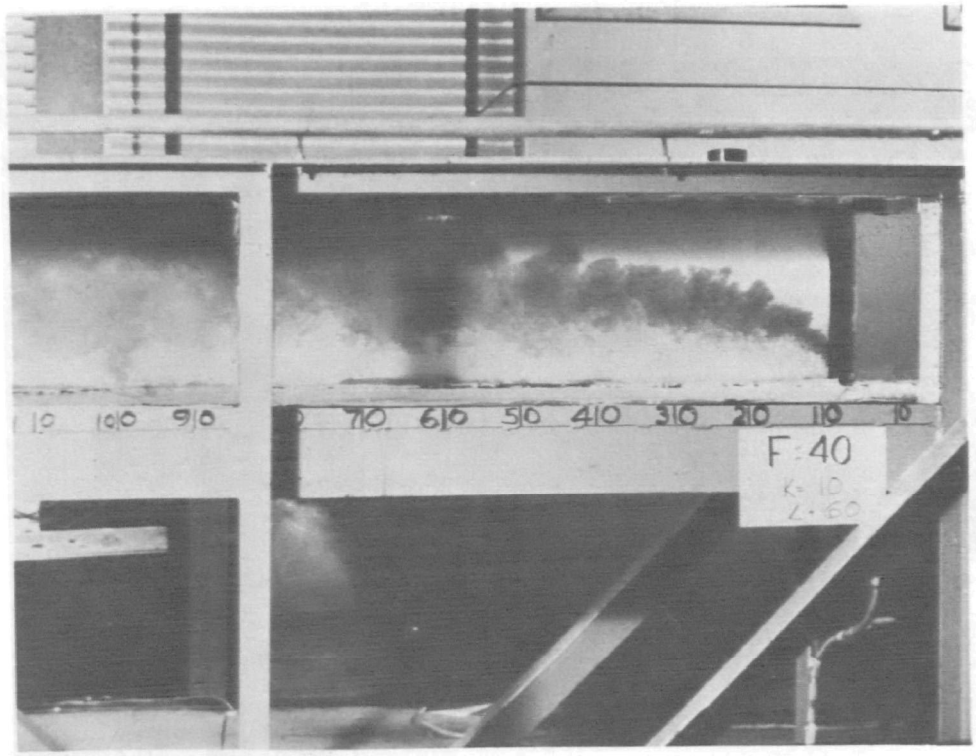

FIGURE 36 - PHOTOGRAPH OF NEGATIVELY BUOYANT JET
RUN NO. 33, $F \approx 40$, $k \approx 10$, $\beta'_o = 60°$

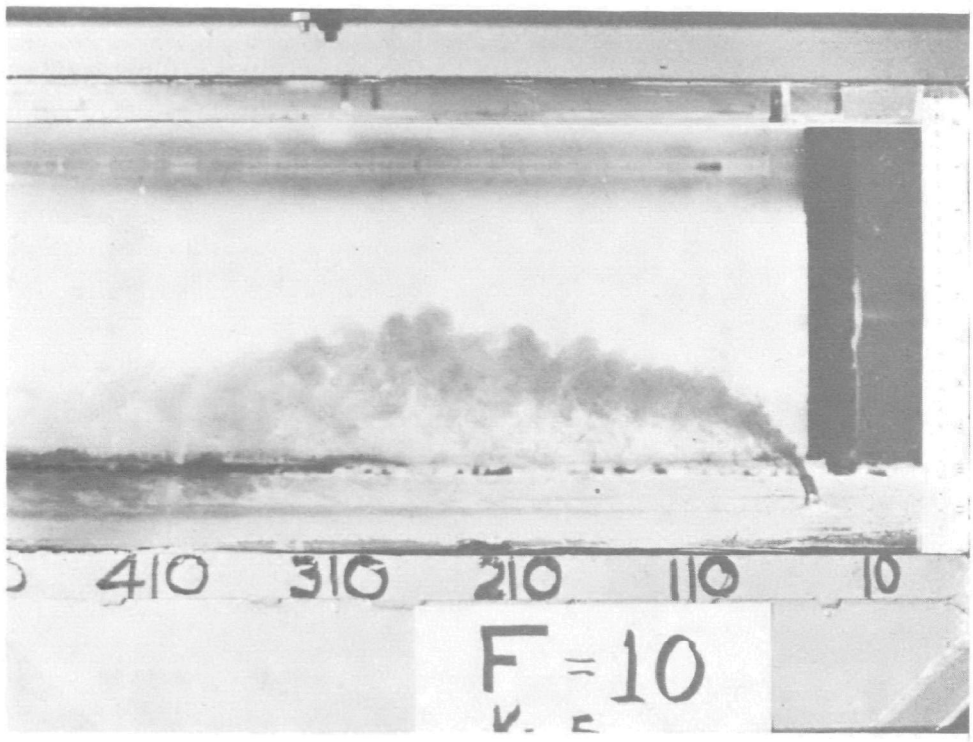

FIGURE 37 - PHOTOGRAPH OF NEGATIVELY BUOYANT JET FOR RUN NO. 27, F ≈ 10, k ≈ 5, $\beta_o' = 60°$

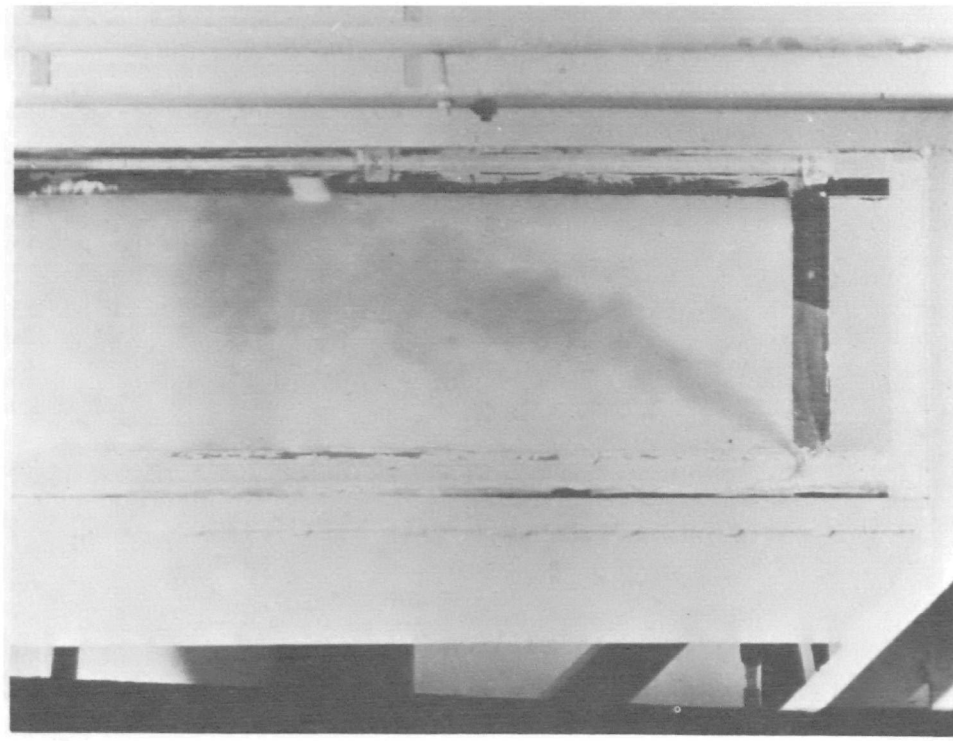

FIGURE 38 - PHOTOGRAPH OF NEGATIVELY BUOYANT JET FOR RUN NO. 22, $F \approx 40$, $k \approx 10$, $\beta_o' = 45°$

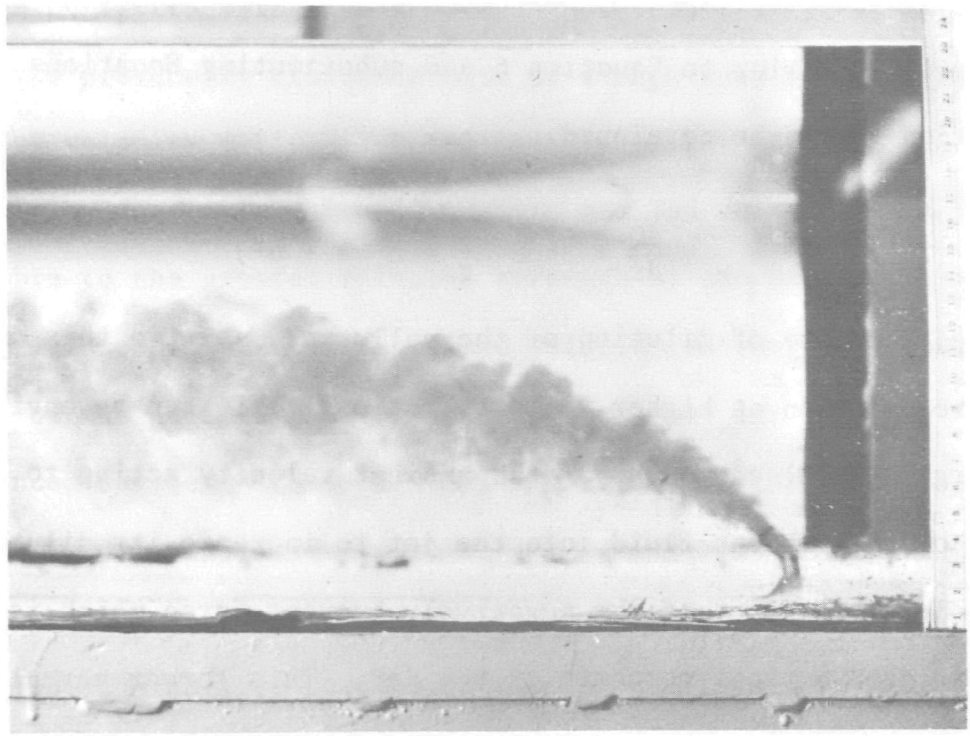

FIGURE 39 - PHOTOGRAPH OF NEGATIVELY BUOYANT JET FOR RUN NO. 19, $F \approx 10$, $k \approx 5$, $\beta_o' = 45°$

Consequently, the effect of the negatively buoyant force which tends to retard the vertical momentum is diminished. The relationship of the buoyancy parameter, f, in Equation 54 as a function of the densimetric Froude number is defined in Equation 50. In addition to the small density difference for high densimetric Froude numbers, at low velocity ratios, i.e., k = 5.9, the strength or relative velocity of the ambient fluid is greater. Considering the same value of U_o, at low velocity ratios the ambient velocity, U_a, is greater than at higher velocity ratios. Hence, the component of the jet velocity due to the ambient velocity will be a larger percentage of the jet velocity. Also, the normal component of the ambient velocity, $U_a \sin \theta$, will be larger. Referring to Equation 6 and substituting Equations 7 and 8, Equation 91 can be developed.

$$\frac{dQ}{ds} = 2\pi\alpha b(U_a^2 \sin^2 \theta + u^2)^{0.5} \tag{91}$$

Hence, the rate of dilution of the pollutant, salt in this case, will be greater than at higher velocity ratios. This can be envisioned as a larger normal component of the ambient velocity acting to entrain more of the ambient fluid into the jet to increase its dilution, thus reducing the effect of the negatively buoyant force which is acting to retard the vertical momentum of the jet. This larger normal component will necessarily increase the vorticity in the region of the jet, as outlined by Platten and Keffer (38); thus, it will increase the rate of dilution or mixing. The cross-flow component, $U_a \sin \theta$, decreases slowly relative to the growth in cross-sectional area. Hence, the cross-flow shearing force acts over an increasing jet circumference and

the rate of change of vortex inflow velocity would increase with distance as discussed by Platten and Keffer (38).

Also, the case of a high densimetric Froude number and low velocity ratio more nearly approximates Fan's basic assumptions as outlined in Chapter II. The radius of curvature for this combination of densimetric Froude number and velocity ratio is large. Hence, there will be no overlapping or interacting of the concentration profiles.

In addition, the cases of low densimetric Froude number, i.e., the density difference between the initial jet density and ambient density is large, and low velocity ratios, e.g., $F = 10.9$, $k = 5.5$, $\beta'_o = 90°$, can be fitted using Fan's model. However, the fit is not as good as for the previously discussed case of a high densimetric Froude number and low velocity ratio. Yet the ability to fit the data with the model for low densimetric Froude numbers and low velocity ratios is attributable to the greater relative strength of the ambient velocity where the normal component of the ambient velocity is large. Hence, the dilution of the pollutant occurs at a faster rate for the same reasons advanced earlier. Consequently, the effect of the negatively buoyant force is diminished.

Yet for the cases of low densimetric Froude numbers and high velocity ratios, the ability to predict the jet dilution, jet half-width, and jet trajectory is not very good. The cases of a low densimetric Froude number are the ones with a larger density difference. Hence, the negatively buoyant force tends to retard the vertical momentum and the advancement of the y-component of the jet axis to a greater degree than in the case of a high densimetric Froude number.

Once more, for high velocity ratios, the normal component of ambient velocity will be small compared to the jet velocity. Hence, the dilution capacity of the ambient stream is lessened. Consequently, the effect of the negatively buoyant force is not readily diminished. Also, the radius of curvature for this case is very small with the result being an overlapping and interacting of profiles which will inhibit the ability to adequately describe the concentration profiles.

Discussion of Results - Abraham's Model

The fitting of Abraham's model to the experimental results was much easier than for Fan's model, for reasons outlined earlier. The same type of situation was found for Abraham's model as for Fan's model. The cases of high densimetric Froude number and low velocity ratios, e.g., $F = 40.0$, $k = 10.0$, and $\beta_o' = 90°$, were fitted with the best results. All cases of high densimetric Froude number would fit the experimental data for all angles of discharge. This is due, in part, to the small density differences. The radius of curvature is very large, hence the dilution due to the action of the cylindrical thermal is more closely approximated. This is true for this case because the jet axis is nearly parallel to the direction of the ambient velocity. In addition, for low velocity ratios, the strength of the ambient velocity is greater than at high velocity ratios. Actually, for a high densimetric Froude number, the jet may be treated as a simple jet consisting of only momentum forces. The first term on the right-hand side of Equation 70 accounts for the region of the jet which is affected by its initial momentum.

In the cases of low densimetric Froude numbers and low velocity

ratios, e.g., F = 10.0, k = 5.0, and β'_o = 90°, Abraham's model begins to deviate from the experimental data after the jet reaches its maximum height. Apparently, in the initial reaches where the jet behaves like a momentum jet, the model will predict the jet dilution and jet trajectory satisfactorily. However, after the jet reaches its maximum height and is deflected towards the discharge level, the predicted data begin to deviate from the experimental data. Similarly, as discussed above, the assumption was made that the direction of flow is parallel to the jet axis at distances far downstream. This assumption is violated. However, at a distance far downstream, the confidence with which the centerline dilutions are measured and reported is open to question, due to techniques of measuring the concentration profiles. In addition, the jet dilution is under-predicted. As a result, the model will under-predict the jet trajectory due to the larger negatively buoyant force which will hinder the jet from increasing its y-component.

In the cases of low densimetric Froude numbers and high velocity ratios, e.g., F = 10.0, k = 20.0, and β'_o = 90°, the fit of Abraham's model to the experimental data is poor. Due to the large density difference, the vertical momentum is retarded to such an extent that the jet trajectory is grossly under-predicted. The assumption that the jet centerline is parallel to the direction of flow at distances far downstream is flagrantly violated as indicated in the example cited.

Hence, when the density differences are small and the strength of the ambient velocity is large with respect to the jet velocity, Abraham's model can be used to predict the jet dilution, jet half-width,

and jet trajectory. For the cases of a low densimetric Froude number and high velocity ratio, Abraham's model should not be used.

CHAPTER VI
VIII
SUMMARY AND CONCLUSIONS

Introduction

Two existing jet models have been analyzed to determine the feasibility of their use to predict the dilution, jet half-width, and jet trajectory of a negatively buoyant jet. An equation has been developed to predict the coefficient of entrainment, α, used in Fan's model as a function of the jet densimetric Froude number, velocity ratio, and initial angle of discharge. The limits of application, sources of errors, and recommendations for further research are found in the discussion that follows.

Fan's Model

Fan's model (3) was developed to predict the dilution and buoyant jet trajectory in a cross-stream with a uniform velocity. An integral approach was used to develop equations of (a) continuity, (b) momentum, (c) conservation of tracer and density deficiency, and (d) two geometric equations. The same approach could be modified to predict the behavior of a negatively buoyant jet in a cross-stream. The main difference would be in the derivation of the y-momentum equation where the direction of the buoyancy term is simply reversed (i.e., given a negative sign) in order for the analogy of a negatively buoyant jet to be appropriate.

Twenty-four experiments were completed in the laboratory flume at Vanderbilt University. Eight combinations of densimetric Froude number

and velocity ratio were utilized for each angle of discharge, i.e., 90°, 60°, and 45°. The data was analyzed using the seven equations developed in the integral approach. Values were determined for α, the coefficient of entrainment, and C_d, the reduced drag coefficient, by trial and error fitting of the experimental data to the theoretical solutions. The value of the drag coefficient, C_d, was assumed to be zero because, for any value of C_d, the jet trajectory was under-predicted. Fan (3) and Motz and Benedict (25) stated that the value of C_d was predominately used in determining the best fit for the jet trajectory and played an insignificant role in its effect on the dilution of the salt water tracer along the jet axis. Hence, only values of α were obtained from the fitting of the experimental dilution and jet half-width data along the jet axis to theoretical dilution and jet half-width data.

In all cases (90°, 60°, and 45°), the best fit of experimental and predicted data occurred at values of high densimetric Froude numbers and low velocity ratios. At high densimetric Froude numbers, the effect of the density difference was small. In addition, at low velocity ratios, the momentum and velocity of the ambient fluid is greater. Hence, dilution of the salt water is attained at a faster rate. Consequently, the sinking of the jet after attaining its maximum height is much less for jets with low velocity ratios compared to jets with a high velocity ratio. In addition, for jets with small densimetric Froude numbers (large density differences) and small velocity ratios, the prediction for the dilution and the jet trajectory was also better than for the same densimetric Froude number and high velocity ratios.

This is due to the higher relative effect of the ambient velocity. However, due to the higher density differences for low values of densimetric Froude number, sinking of the jet after the jet reaches its maximum height is more pronounced than for jets investigated with high values of densimetric Froude number. For jets with small densimetric Froude numbers, there is an inflection in both the theoretical dilution and jet half-width curves. By comparing the jet trajectory curve and the dilution curve, this inflection occurs at the point where the jet has reached its maximum height. Consequently, it is at the same point along the jet axis that the angle, θ, changes from a positive value to a negative value.

In most cases, Fan's model can be used to predict the dilution and jet trajectory. One of the basic assumptions for the development of the equations was that the radius of curvature was large. However, for a negatively buoyant jet with a low densimetric Froude number, this is not the case. The radius of curvature of the jet axis is small for low values of densimetric Froude number due to the greater density differences after the maximum height has been reached, which causes a more rapid downward deflection and sinking of the jet axis than for jets with high values of densimetric Froude number. In addition, accuracy in measuring the real profile may be limited due to the interacting or overlapping of sections of profiles along the jet axis. Nevertheless, if a value of α is known for some combination of densimetric Froude number, velocity ratio, and initial angle of discharge, Fan's model can be used to predict the dilution and jet trajectory. A mathematical expression for obtaining α as a function of F, k, and β_o'

will be evaluated later.

Abraham's Model

Abraham's model is a modification of Fan's model. Abraham considers the coefficient of entrainment constant, not a function of the densimetric Froude number, velocity ratio, or initial angle of discharge. Abraham considered the equation of continuity to consist of two terms, a term related to a simple jet in a region near the discharge point and a term related to a cylindrical thermal for a region at some distance downstream from the discharge point. In addition, the equation governing the momentum in the x-direction was different from that used in Fan's model due to the above consideration. Moreover, Abraham does not consider a zone of flow establishment in the development of his model.

The use of Abraham's model has one advantage over Fan's model in that the coefficients of entrainment are set a priori. Hence, the prediction of the dilution, jet half-width, and jet trajectory curves rely only on a knowledge of the densimetric Froude number, velocity ratio, and initial angle of discharge. In this study, Abraham's model was used to predict dilution, jet half-width, and trajectory curves for the experimental conditions. For values of high densimetric Froude number and low velocity ratios, the fitting of the jet trajectory curves was excellent.

Albertson, et al. (10), developed two separate equations to predict the dilution of a simple momentum jet. One predicted the dilution (volumetric flux ratio) in the zone of flow establishment while the

other predicted the dilution in sections beyond the zone of flow establishment. Abraham used a relationship developed by Albertson to express the dilution of the jet tracer near the discharge when, in reality, the equation can actually be used only to describe the dilution in the region of established flow. Hence, the prediction of the dilution in the region of zone of flow establishment is not valid, but this does not preclude the use of the model to predict dilution at cross-sections beyond the zone of flow establishment.

In the case of a high densimetric Froude number and low velocity ratio, the jet is approaching the case of a simple jet. The case of a high densimetric Froude number and low velocity ratio approaches the case for which Abraham's assumptions are valid. Basically, the region near the nozzle is a momentum (simple) jet, and in the region where the cylindrical thermal approximation is valid, the predominant direction of flow of the jet is parallel to the direction of flow of the flowing ambient stream. Hence, for these cases, Abraham's model fit the experimental data exceptionally well. However, for the cases with low values of densimetric Froude number and high velocity ratios, the fit of the trajectory curve was not as good as discussed above. In all cases the predicted height of rise of the jet was underestimated with respect to the actual height of rise observed in the experiments. The assumption that at some distance downstream from the discharge point the direction of flow is parallel to the direction of flow of the ambient stream is violated. Hence, the theoretical prediction of the jet trajectory after the deflection in a downward direction is not valid.

Angle at the End of the Zone of Flow Establishment

One of the more important parameters in the utilization of Fan's model was the reduced angle of inclination or angle at the end of flow establishment, β_o. There was no data existing for a priori prediction of β_o for a negatively buoyant jet. However, in the region in which this initial deflection occurs, Abraham considered the jet to act as a simple jet since the initial momentum forces are greater than the buoyancy forces. With this in mind, data for the reduced angle of inclination of a simple jet in a cross-flow does exist. Fan (3) presented results from Gördier (15), Jordinson (16), and Keffer and Baines (17) in his study of a round, positively-buoyant jet in a cross-flow. For the above studies the angle of discharge was 90°. Fan used Equation 92 to predict the reduced angle of inclination at the end of the zone of flow establishment as

$$\frac{\beta_o}{\beta_o'} = 90° - 110/k \qquad (92)$$

Motz and Benedict (25) presented results obtained for β_o/β_o' in a study of a heated surface jet into a cross-flow. In the present study, the reduced angle of inclination was obtained as discussed earlier. Figure 40 represents the data found in Fan's (3), Motz and Benedict's (25) and the present study of the angle at the end of the zone of flow establishment versus the inverse of the velocity ratio, 1/k. The value of β_o/β_o' seems to decrease with an increase in 1/k. With an increase in 1/k, the relative value of the ambient velocity is higher. Consequently, the deflection of the jet will be more due to the increased amount of entrained ambient momentum in the x-direction.

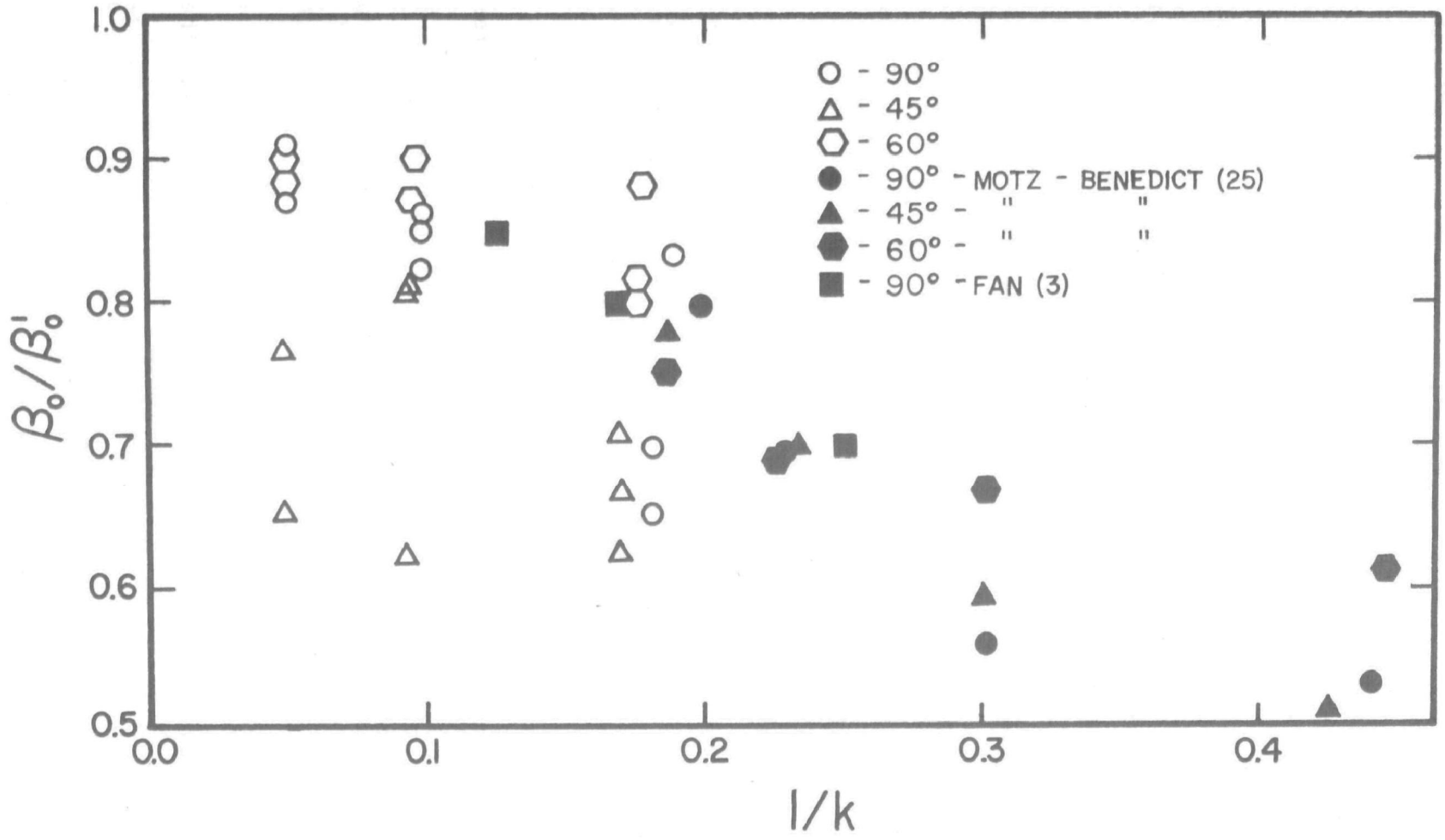

FIGURE 40 - INVERSE VELOCITY RATIO, 1/k, VERSUS β_o/β'_o

However, there is quite a bit of scatter in the data, particularly for the 45° jet. For the 60° and 90° jets at low 1/k values, the values of β_o/β_o' are clustered closely around values of $\beta_o/\beta_o' = .89$ for 1/k ~ 20 and $\beta_o/\beta_o' = .845$ for 1/k ~ 10. However, the rest of the data exhibits a high degree of scatter. Hence, no statement can be made for a general predictive equation relating the value of the angle at the end of zone of flow establishment as a function of the inverse of the velocity ratio, 1/k.

Coefficient of Entrainment

The most important parameter for the prediction of the dilution, jet half-width, and jet trajectory curves is the coefficient of entrainment, regardless of whether it is a positively or negatively buoyant jet. In Fan's model the coefficient of entrainment is constant for a given combination of initial angle of discharge, densimetric Froude number, and velocity ratio.

Fan (3) presents data for the prediction of the coefficient of entrainment, α, for a positively buoyant jet. The present study presents data for an a priori prediction of α for a negatively buoyant jet. The values of α were obtained for the 24 combinations of densimetric Froude number, velocity ratio, and initial angle of discharge. Figure 41 shows the relationship between the values of α for the various combinations. A multiple linear regression analysis was performed on the data. The basic equation related α as a function of Log F, Log (k), and sin (β_o'). Equation 93 was developed and the correlation coefficient was 0.91.

$$\alpha = -0.107 + 0.104 \text{ Log}(F) - 0.553 \text{ Log}(k) + 1.05 \sin(\beta_o') \qquad (93)$$

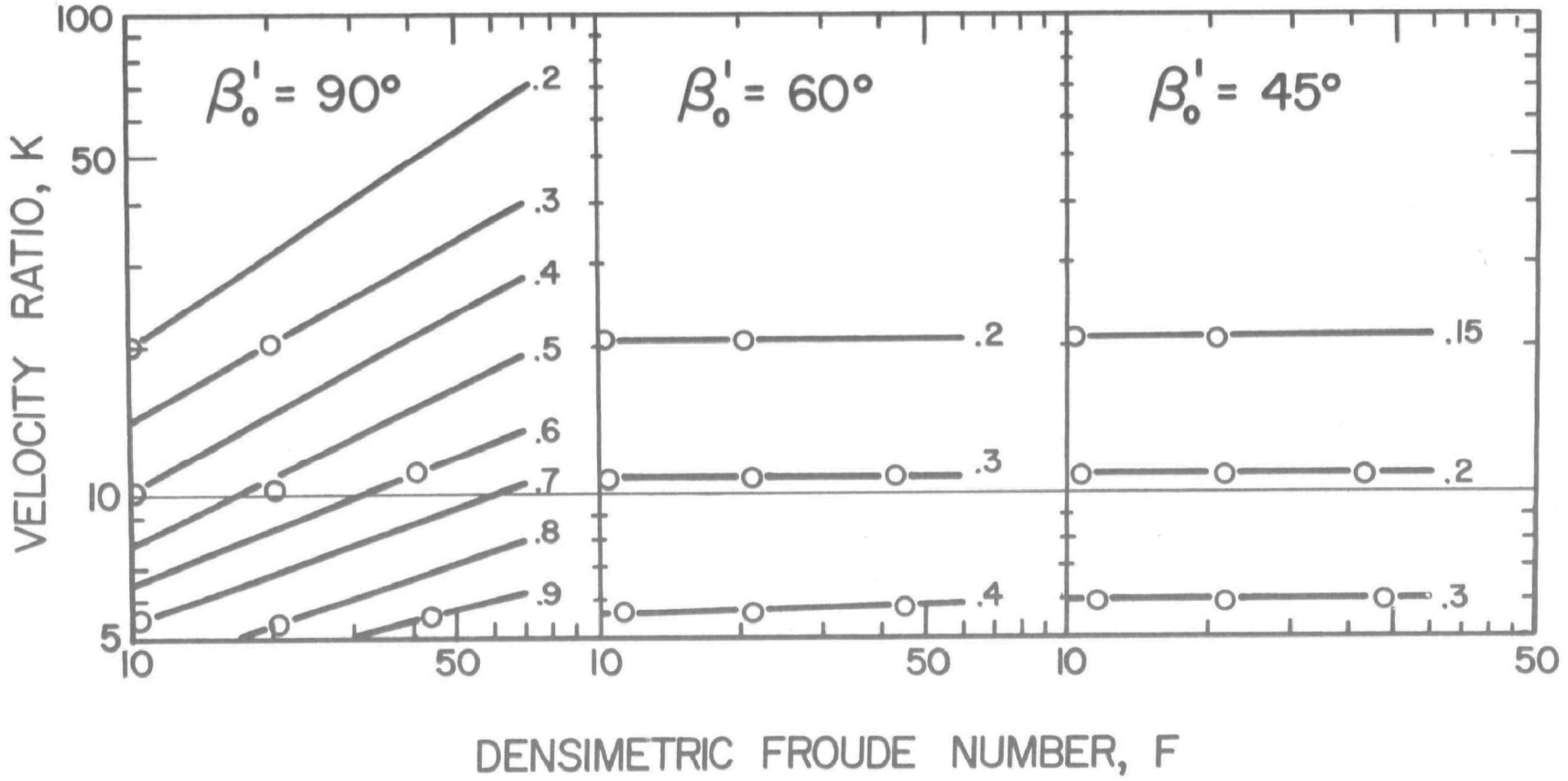

FIGURE 41 - VALUES OF α FOR EXPERIMENTAL COMBINATIONS OF F, k, and β_o'

A test of significance of the correlation coefficient shows that, with the null hypothesis, there is no relationship between the variables which can be rejected at the 1% level. Hence, Equation 92 will give a value of α for any combination of densimetric Froude number, velocity ratio, and initial angle of discharge within the ranges of these parameters used in this study.

The values of α ranged from 0.15 to 0.9. The value of $\alpha = 0.15$ was found for the combination of $F \sim 10$, $k \sim 20$, and $\beta_o' = 45°$, and the value of $\alpha = 0.9$ was found for the combination of $F \sim 40$, $k \sim 5$, and $\beta_o' = 90°$. The value of α decreases as the case of a coflowing stream is approached.

Due to geometric limitation, the degree that ambient fluid is entrained is less for discharge of 45° than for a discharge of 90°. Hence, as β_o' is decreased the volume of ambient fluid available for in-flow and dilution of the jet on the side of the jet near the boundary is decreased. Motz and Benedict (25) obtained similar results for a heated surface jet. When the discharge angle was changed from 90° to 45°, the value of the entrainment coefficient was changed from 0.4 to 0.2. Equation 92 will predict a decrease in α for a decrease in the initial angle of discharge. Also, the value of α tends to decrease as the velocity ratio increases. As the velocity ratio increases, the effect of the ambient current decreases (i.e., the dilution caused by the ambient current is less). Consequently, the values of the entrainment coefficient are less. One would expect lower values of α for this situation, since the jet is approaching the case of a simple jet issuing into a stagnant environment with $\alpha = 0.057$.

Jet Reynolds Number

Values of the jet Reynolds number as defined by Equation 87 for the cases presently under study are listed in Tables 3 and 4. The values range from 1000 to 5000. Rawn, Bowerman, and Brooks (35) stated that, for R_e > 2,000, the jet flow will usually be turbulent, but turbulence is probably not fully developed until R_e reaches 10,000 or 20,000. Frankel and Cummings (36) stated that, for a fully turbulent jet, the Reynolds number is sufficiently large to have no appreciable influence on the dilution. Rouse (37) noted that, for low Reynolds numbers, the expansion in a lateral direction will be due solely to mixing caused by molecular diffusion, i.e., viscous shear. However, at high Reynolds numbers, eddies will be generated in the zone of maximum instability, and the expansion process will occur much more rapidly. The eddies forming in this region will not only produce the deceleration and acceleration of the respective zones, but will themselves penetrate farther and farther into each zone. Burdick (31) concluded that, as long as the jet could be considered turbulent, the Reynolds number could be neglected as a significant parameter.

The runs with jet Reynolds numbers greater than 2000 had the best agreement of predicted data to experimental data. For experimental runs with jet Reynolds numbers less than 2000, the rate of decay of the potential core will be less than for the fully turbulent case. Hence, the length of the potential core will be longer. Consideration of the longer length of the potential core would cause the experimental values of the y-coordinate to be decreased. This would imply a better fit of the jet trajectory since the jet trajectory was under-predicted using

the previously determined values of the y-coordinate. Yet this effect may be offset by the possibility of a smaller reduced angle of inclination, β_o, for a longer potential core. A smaller β_o would imply a smaller initial vertical momentum component which would tend to reduce the height of rise of the jet and to again cause under-pediction of the jet axis. In addition, there will be less dilution in the cases of jet Reynolds numbers less than 2000 due to the decreased turbulence. Consequently, values of α for the experimental runs with $R_e > 2000$ may be too low in considering application to a fully turbulent jet. Hence, α should be higher to reflect the increased dilution due to turbulent flow conditions. A higher α would also imply a better fit of the trajectory data. Hence, the difficulty of fitting the trajectory data could possibly have been due to violation of the model assumption of fully turbulent flow.

The reasons for the low jet Reynolds number are twofold. The maximum flow in the laboratory flume was restricted and the size of the flume was also restricted. Hence, in some cases the jet velocity had to be so low to meet the above restrictions that the criterion that the jet Reynolds number be greater than 2,000 had to be violated.

IX

LIST OF REFERENCES

1. Water Resources Council, "The Nation's Water Resources," Washington, D. C., 1968.

2. Brooks, N., and Koh, R., "Discharge of Sewage Effluents from a Line Source into a Stratified Ocean," International Association for Hydraulic Research, XIth Congress, Leningrad, September, 1965, pp. 1-8.

3. Fan, L. N., "Turbulent Buoyant Jets into Stratified or Flowing Ambient Fluids," Technical Report No. KH-R-15, W. M. Keck Laboratory of Hydraulics and Water Resources, California Institute of Technology, Pasadena, California, June, 1967.

4. Cederwall, K., "Jet Diffusion: Review of Model Testing and Comparison with Theory," Hydraulics Division, Chalmers Institute of Technology, Göteborg, Sweden, February, 1967.

5. Cederwall, K., "Hydraulics of Marine Waste Water Disposal," Report No. 42, Hydraulic Division, Chalmers Institute of Technology, Göteborg, Sweden, January, 1968.

6. Abraham, G., "The Flow of Round Jets Issuing Vertically into Ambient Fluid Flowing in a Horizontal Direction," Proceedings of the 5th International Water Pollution Research Conference, San Francisco, July-August, 1970, pp. III 15/1 - III 15/7.

7. Cederwall, K., and Brooks, N., "A Buoyant Slot Jet into a Stagnant or Flowing Environment," Report No. KH-R-25, W. M. Keck Laboratory of Hydraulics and Water Resources, California Institute of Technology, Pasadena, California, March, 1971.

8. Abraham, G., "Jets with Negative Buoyancy in Homogeneous Fluid," Journal of Hydraulic Research, Vol. 5, No. 4, 1967, pp. 235-248.

9. Turner, J. S., "Jets and Plumes with Negative or Reversing Buoyancy," Journal of Fluid Mechanics, Vol. 26, Part 4, 1966, pp. 779-792.

10. Albertson, M. L., Dai, Y. B., Jensen, R. A., and Rouse, H., "Diffusion of Submerged Jets," Transactions, American Society of Civil Engineers, Vol. 115, 1950, pp. 639-697.

11. Morton, B. R., "Forced Plumes," Journal of Fluid Mechanics, Vol. 5, Part I, 1959, pp. 151-163.

12. Parker, F. L., and Krenkel, P. A., "Thermal Pollution: Status of the Art," Report No. 3, National Center for Research and Training in the Hydrologic and Hydraulic Aspects of Water Pollution Control, Vanderbilt University, Nashville, Tennessee, December, 1969.

13. Morton, B. R., Taylor, G. I., and Turner, J. S., "Turbulent Gravitational Convection from Maintained and Instantaneous Sources," Proceedings, Royal Society of London, Vol. 234A, No. 1196, January, 1956, pp. 1-23.

14. Morton, B. R., "On a Momentum-Mass Flux Diagram for Turbulent Jets, Plumes, and Wakes," Journal of Fluid Mechanics, Vol. 10, 1961, pp. 101-112.

15. Gördier, R. L., "Studies on Fluid Jets Discharging Normally Into Moving Liquid," Technical Report No. 28, Series B, St. Anthony Falls Hydraulic Laboratory, University of Minnesota, Minneapolis, Minnesota, August, 1959.

16. Jordinson, R., "Flow in a Jet Directed Normal to the Wind," Aero. Research Council, Report and Memo No. 3074, 1956.

17. Keffer, J. F., and Baines, W. D., "The Round Turbulent Jet in a Cross-Wind," Journal of Fluid Mechanics, Vol. 15, 1963, pp. 481-496.

18. Pratte, B. D., and Baines, W. D., "Profiles of the Round Turbulent Jet in a Cross Flow," Journal of the Hydraulics Division, American Society of Civil Engineers, Vol. 92, No. HY6, Proc. Paper 5556, November, 1967, pp. 53-64.

19. Tollmien, W., "Strahlverbreiterung," Zeitschr. Angew. Math. und Mech., 1926, pp. 468-478.

20. Schmidt, W., "Turbulente Ausbreitung eines Stromes Erhitzter Luft," Zeitschr. Angew. Math. und Mech., Vol. 21, 1941, pp. 265-278, pp. 351-363.

21. Abraham, G., "Entrainment Principle and Its Restriction to Solve Problems of Jets," Journal of Hydraulic Research, Vol. 3, No. 2, 1965, pp. 1-23.

22. Fan, L. N., and Brooks, N. H., Discussion of "Horizontal Jets in a Stratified Fluid of Other Density," by G. Abraham, Journal of the Hydraulics Division, American Society of Civil Engineers, HY2, March, 1966, pp. 423-429.

23. Abraham, G., "Horizontal Jets in a Stagnant Fluid of Other Density," Journal of the Hydraulics Division, American Society of Civil Engineers, HY4, July, 1965, pp. 139-154.

24. Rouse, H., Yih, C. S., and Humphreys, H. W., "Gravitational Convection from a Boundary Source," Tellus, Vol. 4, 1952, pp. 201-210.

25. Motz, L. H., and Benedict, B. A., "Heated Surface Jet Discharged into a Flowing Ambient Stream," Report No. 4, National Center for Research and Training in the Hydrologic and Hydraulic Aspects of Water Pollution Control, Vanderbilt University, August, 1970.

26. Richards, J. M., "Experiments on the Motion of Isolated Cylindrical Thermals Through Unstratified Surroundings," International Journal of Air and Water Pollution, Vol. 7, 1963, pp. 17-34.

27. Bosanquet, C. H., Horn, G., and Thring, M. W., "The Effect of Density Differences on the Path of Jets," Journal of Fluid Mechanics, Vol. 5, Part I, January, 1959, pp. 340-352.

28. Fan, L. N., and Brooks, N. H., "Dilution of Waste Gas Discharge from Campus Buildings," Technical Memorandum 68-1, W. M. Keck Laboratory of Hydraulics and Water Resources, California Institute of Technology, Pasadena, California, January, 1968.

29. Priestley, C. H. B., and Ball, F. K., "Continuous Convection from an Isolated Source of Heat," Quarterly Journal of the Royal Meteorological Society of London, England, Vol. 81, 1955.

30. Krenkel, P. A., and Orlob, G. T., "Turbulent Diffusion and the Reaeration Coefficient," Journal of the Sanitary Engineering Division, American Society of Civil Engineers, Vol. 88, SA2, March, 1962.

31. Burdick, J. C., and Krenkel, P. A., "Jet Diffusion Under Stratified Flow Conditions," Technical Report No. 11, Environmental and Water Resources Engineering, Vanderbilt University, 1967.

32. Krenkel, P. A., "Turbulent Diffusion and Kinectics of Oxygen Absorption," Ph.D. Dissertation, University of California, Berkeley, California, 1960.

33. Clements, W. C., "Pulse Testing for Dynamic Analysis. Part I. An Investigation of Computational Methods and Difficulties in Pulse Testing. Part II. Application of Pulse Testing to Flow and Extraction Dynamics," Ph.D. Dissertation, Vanderbilt University, Nashville, Tennessee, June, 1963, pp. 91-93.

34. Clements, W. C., "Electrical Conductivity Monitor," Instruments and Control Systems, Vol. 41, November, 1968, pp. 97-98.

35. Rawn, A. M., Bowerman, R. F., and Brooks, N. H., "Diffusers for Disposal of Sewage in Sea Water," Journal of the Sanitary Engineering Division, American Society of Civil Engineers, Vol. 86, March, 1960.

36. Frankel, R. M., and Cumming, J. D., "Turbulent Mixing Phenomena of Ocean Outfalls," Journal of the Sanitary Engineering Division, American Society of Civil Engineers, Vol. 91, April, 1965.

37. Rouse, H., Engineering Hydraulics, Wiley and Sons, Inc., New York, 1950.

38. Platten, J. L., and Keffer, J. F., "Entrainment in Deflected Axisymmetric Jets at Various Angles to the Stream," Technical Publication No. 6808, Department of Mechanical Engineering, University of Toronto, June, 1968.

39. Larsen, J., and Hecker, G. E., "Design of Submerged Diffusers and Jet Interaction," Preprint No. 1614, presented at the American Society of Civil Engineers National Water Resources Engineering Meeting, Atlanta, Georgia, January, 1972.

40. Holly, F. M., and Grace, J. L., "Model Study of a Dense Fluid in a Flowing Fluid," Preprint No. 1587, presented at the American Society of Civil Engineers National Water Resources Engineering Meeting, Atlanta, Georgia, January, 1972.

41. Perry's Chemical Engineers' Handbook, Fourth Edition, McGraw-Hill, New York, New York, 1969.

42. Briggs, G. A., "Plume Rise," AEC Critical Review Series, No. 26, 1969.

GLOSSARY

LIST OF NOTATIONS

X

LIST OF NOTATIONS

A - Jet cross-section normal to jet axis, L^2

b - Local characteristic length of half-width of the jet, L

b_o - Jet half-width at the end of the zone of flow establishment, L

B_{th} - Radius of thermal, L

c - Concentration at the jet axis

c* - Local concentration value

c_o - Initial concentration at the end of the zone of flow establishment, i.e., at 0

CI - Δy, the incremental distance between each $y'_{j,k}$,L

C_d - Drag coefficient for Fan's model

C'_d - Reduced drag coefficient for Fan's Model

C_{da} - Drag coefficient for Abraham's model

$\bar{c}_{j,k}$ - Local concentration at location (j,k)

$\bar{c}_k$ - Mean value of the concentration profile

D_o - Diameter of jet at orifice and orifice diameter, L

E_i - Constant supply voltage

E_o - Internal voltage of conductivity monitor

f - Buoyancy parameter

F - Densimetric jet Froude number

F_D - Drag force per unit length, L^3T^{-2}

g - Gravitational acceleration, LT^{-2}

G - Conductivity of salt solution

h - Dimensionless horizontal or x-momentum flux parameter

H_w - Head of water above apex of notch, L

i - Vector in the direction tangent to the jet axis or index number of time period

j - Vector perpendicular to the jet axis or index number denoting a given location in a cross-section, k

k - Velocity ratio or index number denoting a given cross-section

k' - $k + \cos \theta_o$

m - Momentum flux parameter

$\bar{m}_{j,k}$ - Time-averaged millivolt output at location j in cross-section, k

$m_{i,j,k}$ - Millivolt output at location (j,k) over time increment Δt_i

n - Number of time increments

N - Number of j location in a given cross-section, k

O - Origin of the coordinate system (x,y), beginning of the zone of flow establishment

O' - Origin of the coordinate system (x',y'), beginning at the point of jet discharge

Q - Volumetric flux, L^3T^{-1}

Q_a - Flow in laboratory flume, L^3T^{-1}

Q_o - Initial volume flux at the nozzle, L^3T^{-1}

r - Radial distance measured from the jet axis, L

R_e - Initial jet Reynolds number

s - Distance along the jet axis from the zone of flow establishment, L

s' - Distance along the jet axis from the jet discharge point, L

s'_e - Jet axis length of the zone of flow establishment, L

S_t - Dilution ratio at terminal height of rise, y_t

Δt_i - Time period used in time-averaging, T

u - Jet velocity at the centerline of the jet, LT^{-1}

u_o - Jet discharge velocity at orifice, LT^{-1}

u^* - Jet velocity at a local point, LT^{-1}

U_a - Ambient uniform velocity, LT^{-1}

U_o - Initial jet discharge velocity, LT^{-1}

v - Dimensionless vertical or y-momentum flux parameter

V_q - Quantity of fluid contained in a thermal jet per unit of length, L^2

x - Horizontal coordinate measured from the end of the zone of flow establishment, L

x' - Coordinate axis in horizontal direction on the same plane as jet axis with origin at O', L

x'_e - Horizontal distance from jet discharge point to the end of the zone of flow establishment, L

y - Vertical coordinate measured from the end of the zone of flow establishment, L

y' - Coordinate axis in vertical direction, with origin at O', L

y'_e - Vertical distance from the jet discharge point to the end of the zone of flow establishment, L

y'_k - y-location of the mean value of the concentration profile, L

$y'_{j,k}$ - Vertical distance of local point at location (j,k) from jet discharge point, L

y_t - Mean vertical height of rise of the plume, L

α - Coefficient of entrainment

α_{mom} - Coefficient of entrainment for jets primarily influenced by initial momentum

α_{th} - Coefficient of entrainment for thermal moving through a stagnant ambient fluid

ξ - Dimensionless vertical distance (y)

ξ' - Dimensionless vertical distance (y')

η - Dimensionless horizontal distance (x)

η' - Dimensionless horizontal distance (x')

ζ - Dimensionless distance along s-axis (s)

ζ' - Dimensionless distance along s-axis (s')

β_o - Initial angle of inclination at the end of the zone of flow establishment, degrees

β'_o - Initial angle of inclination at jet discharge point, degrees

θ - Angle of inclination of the jet axis (with respect to the x-axis), degrees

θ_o - Initial angle of inclination (with respect to x-axis) (θ_o = β_o for Fan's model and $\theta_o = \beta'_o$ for Abraham's model), degrees

μ - Volumetric flux parameter

ν - Kinematic viscosity, L^2T^{-1}

ρ_a - Density of the ambient fluid, FT^2L^{-4}

ρ_o - Reference density taken as $\rho_a(0)$, FT^2L^{-4}

ρ_1 - Initial jet density, FT^2L^{-4}

ρ^* - Local density within a jet, FT^2L^{-4}

ϕ - Angular coordinate on a cross-section normal to jet axis, degrees

σ_k - Standard deviation at cross-section k, L

Δh - Plume rise above top of stack

XI

APPENDIX A

SALINITY-DENSITY RELATIONSHIP

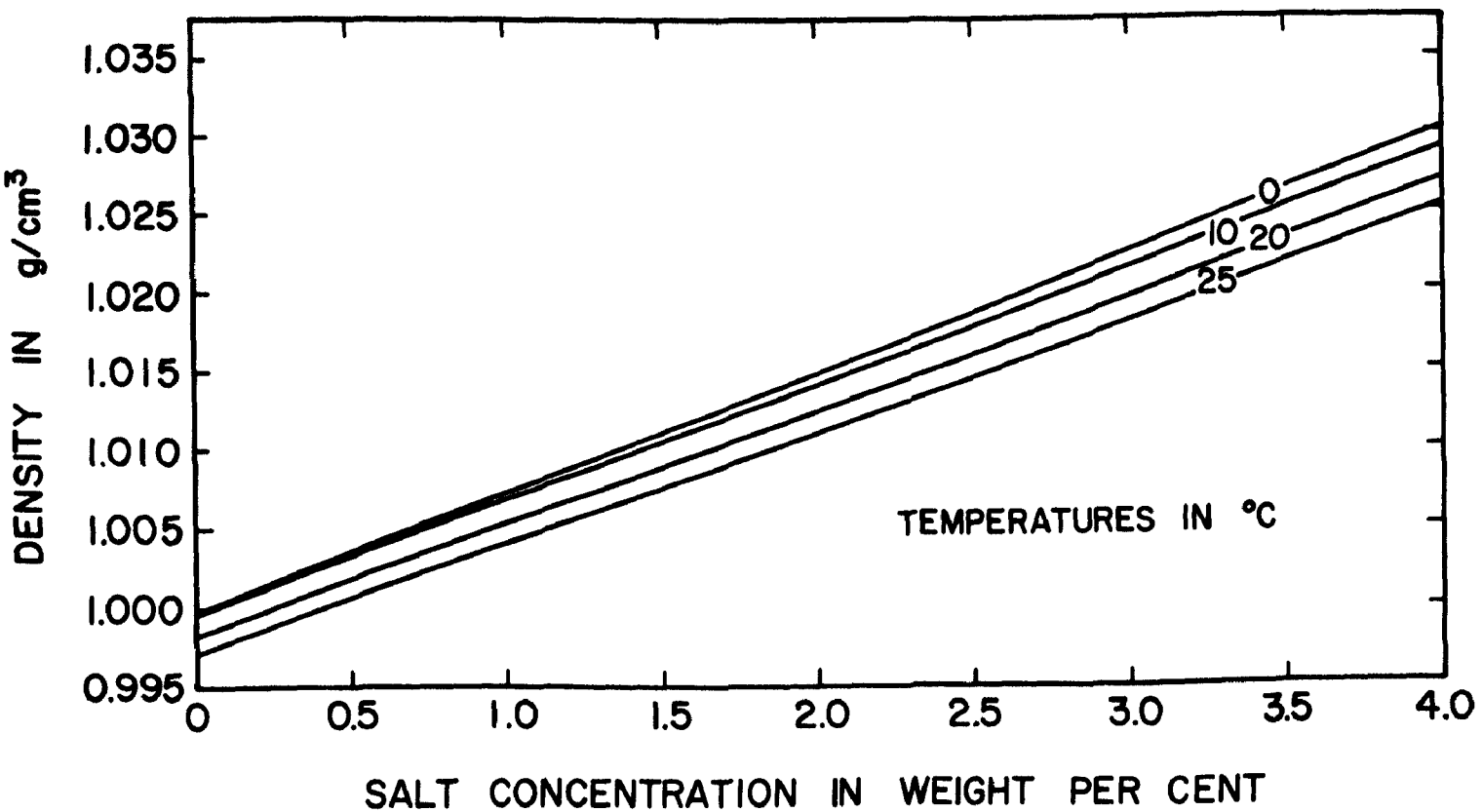

FIGURE 42 - DENSITY OF SALT WATER AS A FUNCTION OF SALT CONCENTRATION AND TEMPERATURE (PERRY'S CHEMICAL ENGINEERS HANDBOOK, REF. 41)

APPENDIX B

COMPUTER PROGRAM - FAN'S MODEL

```
C****THIS PROGRAM CONTAINS THE MAIN PROGRAM, AND
C     TWO SUBROUTINES NEEDED TO PROVIDE INPUT AND
C     OUTPUT CONTROL TO SOLVE THE FIVE EQUATIONS IN
C     FANS MODEL.  THE MAIN PROGRAM CONTAINS THE
C     NECESSARY INPUT INFORMATION WHILE SUBROUTINE FCT HAS
C     THE EQUATIONS FOR INTEGRATION AND SUBROUTINE OUTP
C     PROVIDES THE NECESSARY OUTPUT CONTROL.  THE OUTPUT
C     VARIOUS DISTANCES ARE IN TERMS OF DIAMETERS.  THE
C     OTHER OUTPUT VALUES ARE SELF-EXPLANATORY.
C     IN ADDITION, SUBROUTINE DRKGS MUST ALSO BE USED AS
C     OUTLINED IN THE MAIN PROGRAM.
C*********************************************************
      IMPLICIT REAL*8(A-Z)
      INTEGER NDIM,IHLF,I,NDATA,MI
      REAL OUTP,FCT
      REAL*8 AUX(8,5),Y(5),DERY(5),PRMT(5),SDATA(25),
     &BDATA(25),XDATA(25),YDATA(25),CONC1(25),VAR(20)
      COMMON /INPUT/ K,BETA1,BOUPAR,CD,KK,BO,DIAM,ALPHA
      EXTERNAL FCT, OUTP
      DATA DERY/5*.2D0/
      DO 978 MI = 1,10
C******INPUT THE VALUE OF INDEX************************
C******INDEX = 1  ALLOWS ONE TO INPUT EXPERIMENTAL DATA
C******AND THEN MAKE AN INITIAL GUESS AT A VALUE OF
C******ALPHA.  IF ANOTHER VALUE OF ALPHA IS DESIRED
C******AFTER THE INITIAL GUESS SIMPLY FOLLOW THE
C******INITIAL DATA FOR INDEX=1 WITH A CARD WITH INDEX=2
C****** AND THEN ANOTHER CARD WITH THE SECOND GUESS AT
C******ALPHA.  THIS MAY BE DONE FOR AS MANY TIMES AS
C******DESIRED UP TO 10.  IF YOU DESIRE THE CALCULATION
C******TO STOP.  INSERT A CARD WITH INDEX = 3.
C
C
      READ(5,974)INDEX
      IF(INDEX .EQ. 2)GO TO 975
      IF(INDEX .EQ. 3)GO TO 976
C**TITLE OF PROJECT OR RUN UNDER INVESTIGATION**********
      READ(5,804)(VAR(I),I=1,20)
C******INPUT INITIAL JET LOCATION, JET TERMINAL DISTANCE,
C*******INCREMENTAL DISTANCE, AND ALLOWABLE ERROR
      READ(5,800)(PRMT(I),I=1,4)
C******PARAMETERS NECESSARY FOR OPERATION
C******
C       1  FROUDE  NUMBER
C       2  ALPHA-COEFFICIENT OF ENTRAINMENT
C       3  K-VELOCITY RATIO
C       4  BETAI-INITIAL ANGLE OF DISCHARGE-DEGREES
C       5  CD-DRAG COEFFICIENT
      READ(5,879)FROUDE,ALPHA,K,BETAI,CD
C****INPUT INITIAL CONDITIONS*****************************
```

```
C      1. Y(1)=1.0
C      2. Y(2)=1.0
C      3. Y(3)= ANYTHING--NEVER USED
C      4. Y(4)=0.0
C      5. Y(5)=0.0
       READ(5,801)(Y(I),I=1,5)
       READ(5,802) NDIM
C****INPUT REDUCED ANGLE OF INCLINATION AT END OF ZONE
C***        OF FLOW ESTABLISHMENT
       READ(5,973)BETA1
       BETA1 = BETA1/57.29578
C
C*************************************************************
C
C      INPUT THE NUMBER OF CROSS-SECTIONS ALONG THE
C      JET AXIS (NDATA), THE DIAMETER OF THE JET
C      (DIAM) FOR THIS PARTICULAR RUN.
C      INPUT THE X-DISTANCE,Y-DISTANCE, S-DISTANCE,
C      CONCENTRATION RATIO, AND JET HALF-WIDTH DATA FOR A
C      PARTICULAR CROSS-SECTION DOWNSTREAM.
C
C
C*************************************************************
       READ(5,970)NDATA,DIAM,(XDATA(I),YDATA(I),SDATA(I),
      &CONC1(I),BDATA(I),I=1,NDATA)
       GO TO 953
  975  READ(5,973)ALPHA
  953  CONTINUE
       CORR = Y(2)
       Y(2)=CORR*DCOS(BETA1)
       Y(3)=CORR*DSIN(BETA1)
       KK=K+DCOS(BETA1)
       BOUPAR=-(((K/KK)**2.5)/((DSQRT(2.D0))*ALPHA))/FROUDE**
      $2
C****WRITE THE WORKING PARAMETERS***********
       WRITE(6,905)
       WRITE(6,804)(VAR(I),I=1,20)
       WRITE(6,900)FROUDE,K,ALPHA,BOUPAR,CD,BETAI
       IF(INDEX .GT. 1)GO TO 977
       BETA5=BETA1*57.29578
       WRITE(6,910)BETA5
       WRITE(6,911)DIAM
       BO = DIAM*(DSQRT(K/(2.D0*KK)))
       WRITE(6,969)K,KK,BO
       WRITE(6,905)
       WRITE(6,968)
  968  FORMAT(1X,'EXPERIMENTAL',T16,'EXPERIMENTAL',T32,
      &'EXPERIMENTAL',T45,'EXPERIMENTAL',T59,'EXPERI
      &MENTAL'/T6,'JET',T16,'CONCENTRATION',T36,'JET',T46
      &,'X-DISTANCE',T60,'Y-DISTANCE'/T5,'AXIS',T33,'HA
```

```
     &LF-WIDTH'/T6,'S/D',T36,'B/D',T49,'X/D',T62,'Y/D
     &'//)
      DO 20 I=1,NDATA
      SDATA(I) = SDATA(I)/DIAM
      XDATA(I) = XDATA(I)/DIAM
      YDATA(I) = YDATA(I)/DIAM
      BDATA(I) = BDATA(I)*DSQRT(2.D0)/DIAM
      CONC1(I) = 1.D0/(CONC1(I)*.01D0)
      WRITE(6,966)SDATA(I),CONC1(I),BDATA(I),XDATA(I),YDATA(
     $I)
   20 CONTINUE
  977 WRITE(6,904)
      CALL DRKGS(PRMT,Y,DERY,NDIM,IHLF,FCT,OUTP,AUX)
      Y(1)=1.0
      Y(2)=1.0
      Y(4)=0.0
      Y(5)=0.0
  978 CONTINUE
      IF(IHLF.EQ.11)GO TO11
      IF(IHLF.EQ.12)GO TO12
      WRITE(6,901)IHLF
   11 WRITE(6,902)IHLF
   12 WRITE(6,903)IHLF
      STOP
  800 FORMAT(3F10.1,D10.4)
  801 FORMAT(5F5.1)
  802 FORMAT(I1)
  804 FORMAT(20A4)
  879 FORMAT(F10.5,F5.2,3F5.1)
  900 FORMAT(///T28,'FAN''S MODEL'//'DENSIMETRIC FROUDE NO.'
     $,T33,'=',T37
     &,F6.3/'VELOCITY RATIO',T33,'=',T39,F4.1/'ENTRAINMENT C
     $OEFFICIENT (
     &ALPHA)',T33,'=',T38,F5.3/'BUOYANCY PARAMETER',T33,'=',
     $T35,F8.5/'DR
     &AG COEFFICIENT',T33,'=',T38,F5.2/'INITIAL ANGLE OF DIS
     $CHARGE',T33,
     &'=',T39,F3.0//)
  901 FORMAT(/'****ERROR---SIGN(PRMT(3)).NE.SIGN(PRMT(
     &2)-PRMT(1)).'/'IHLF = ',I2,')'/)
  902 FORMAT(/'****ERROR---INITIAL INCREMENT BISECTED
     &MORE THAN 10 TIMES'/'(IHLF = ',I2,')'/)
  903 FORMAT(/'****ERROR---PRMT(3) = 0'/'(IHLF = ',I2,')'/)
  904 FORMAT(T8,'JET',T18,'VOLUMETRIC',T32,'CONCENTRATION',
     &T49,'MOMENTUM',T65,'VELOCITY',T83,'JET',T99,'X',T114,
     &'Y',T126,'BETA'/T7,'AXIS',T20,'FLUX',T51,'FLUX',T66,
     &'RATIO',T79,'HALF-WIDTH',T95,'DISTANCE',T110,'DISTA
     &NCE'//T8,'S/D',T65,'UJ/UO',T83,'B/D',T98,'X/D',T113,
     &'Y/D',T124,'DEGREES'//)
  905 FORMAT(1H1)
```

```
  910 FORMAT(/'BETA5 = ',F5.2/)
  911 FORMAT(/'DIAM = ',F5.2)
  966 FORMAT(T5,F8.4,T20,F8.4,T34,F8.4,T47,F8.4,T60,F8.4)
  969 FORMAT(T21,'K',T26,'=',T30,F8.5/T21,'K''',T26,'=',T
     &30,F8.5/T21,'BO',T26,'=',T30,F8.5)
  970 FORMAT(I2,F3.2/(5F10.5))
  973 FORMAT(F10.5)
  974 FORMAT(1I1)
  976 END
C
C
C*****SUBROUTINE FCT(X,Y,DERY)
C     CONTAINS THE DIFFERENTIAL EQUATIONS THAT ARE
C     TO BE INTEGRATED AND ARE LISTED AS DERY(I).
C
C
      SUBROUTINE FCT(X,Y,DERY)
      IMPLICIT REAL*8(A-Z)
      REAL*8    Y(5), DERY(5)
      COMMON /INPUT/ K,BETA1,BOUPAR,CD,KK,BO,DIAM,ALPHA
      M=DSQRT(Y(2)**2+Y(3)**2)
      BETA=DATAN(Y(3)/Y(2))
      IF(BETA)1,2,2
    1 IF(CD)2,2,3
    3 CD = -CD
      PRINT 901, CD
    2 CONTINUE
      SS=DSIN(BETA)**2
      SSS=DSIN(BETA)**3
      CS=DCOS(BETA)
      KKK=KK*KK
      USM=Y(1)/DSQRT(M)
      MU=M/Y(1)
      UM=Y(1)/M
      CHI=DSQRT(SS+(KK*MU-2.DO*CS)**2)
      DERY(1)=(USM*CHI)/KK
      DERY(2)=(USM/KKK)*(2.DO*CHI+CD*SSS)
      DERY(3)=BOUPAR*UM-(CD*USM*SS*CS/KKK)
      DERY(4)=CS
      DERY(5)=DSIN(BETA)
  901 FORMAT(1X,F5.2)
      RETURN
      END
C
C
C*****SUBROUTINE OUTP(X,Y,DERY,IHLF,NDIM,PRMT)
C
C
      SUBROUTINE OUTP(X,Y,DERY,IHLF,NDIM,PRMT)
      IMPLICIT REAL*8(A-Z)
```

```
      INTEGER NDIM, IHLF
      REAL*8    Y(5), DERY(5), PRMT(5)
      COMMON /INPUT/ K,BETA1,BOUPAR,CD,KK,BO,DIAM,ALPHA
      IF(DABS((X*10.D0)-IDINT((X+1D-6)*10.D0)) .GT.
     & .001D0)RETURN
      IF(X .LT. 1.0D0) GO TO 10
      IF(DABS(X-IDINT(X+1D-6)).GT..001D0)RETURN
      IF(X .LT. 40.01)GO TO 10
      IF(DABS((X/10.D0)-IDINT((X+1D-6)/10.D0)) . GT.
     & .001)RETURN
   10 CONC = 1.D0/Y(1)
      M=DSQRT(Y(2)**2+Y(3)**2)
      R=DSQRT(Y(1)*Y(1)/M)
      BETA = (DATAN(Y(3)/Y(2)))
      R=R*BO/DIAM
      URATIO = (Y(1)*KK*BO**2/R**2)-DCOS(BETA)
      BETA = BETA*57.2957B
      XX=X*BO/(DIAM*2.D0*ALPHA)
      XXXX=Y(4)*BO/(DIAM*2.D0*ALPHA)
      YYYY=Y(5)*BO/(DIAM*2.D0*ALPHA)
      WRITE(6,901)XX,Y(1),CONC,M,URATIO,R,XXXX,YYYY,BETA
  901 FORMAT(1X,9(F10.5,5X))
      RETURN
      END
```

APPENDIX C

COMPUTER PROGRAM - ABRAHAM'S MODEL

```
C****THIS PROGRAM CONTAINS THE MAIN PROGRAM, AND
C     TWO SUBROUTINES NEEDED TO PROVIDE INPUT AND
C     OUTPUT CONTROL TO SOLVE THE FIVE EQUATIONS IN ABRA-
C     HAMS MODEL.  THE MAIN PROGRAM CONTAINS THE
C     NECESSARY INPUT INFORMATION WHILE SUBROUTINE FCT HAS
C     THE EQUATIONS FOR INTEGRATION AND SUBROUTINE OUTP
C     PROVIDES THE NECESSARY OUTPUT CONTROL.  THE OUTPUT
C     VARIOUS DISTANCES ARE IN TERMS OF DIAMETERS.  THE
C     OTHER OUTPUT VALUES ARE SELF-EXPLANATORY.
C     IN ADDITION, SUBROUTINE DRKGS MUST ALSO BE USED AS
C     OUTLINED IN THE MAIN PROGRAM.
C*****************************************************
      IMPLICIT REAL*8(A-Z)
      INTEGER NDIM,IHLF,I,NDATA,NTIMES
      REAL OUTP,FCT
      REAL*8 AUX(8,5),Y(5),DERY(5),PRMT(5),SDATA(25),
     &BDATA(25),XDATA(25),YDATA(25),CONC1(25),VAR(20)
      COMMON /INPUT/ K,KK,BOUPAR,CD,AMOM,ATHERM,BO,DIAM
      EXTERNAL FCT, OUTP
      DATA DERY/5*.2D0/
C**TITLE OF PROJECT OR RUN UNDER INVESTIGATION**********
      READ(5,804)(VAR(I),I=1,20)
C******INPUT INITIAL JET LOCATION, JET TERMINAL DISTANCE,
C*******INCREMENTAL DISTANCE, AND ALLOWABLE ERROR
      READ(5,800)(PRMT(I),I=1,4)
C******PARAMETERS NECESSARY FOR OPERATION
C******
C       1  FROUDE  NUMBER
C       2  K-VELOCITY RATIO
C       3  BETAI-INITIAL ANGLE OF DISCHARGE-DEGREES
      READ(5,803)FROUDE,K,BETAI
      PI=3.14159265358979320
C***  THE VALUES OF THE ENTRAINMENT COEFFICIENT
C***  AND DRAG COEFFICIENT ARE CONSTANT FOR ABRAHAM'S
C***  MODEL.  HENCE THE VALUES CAN BE IDENTIFIED
C***  FOR ALL COMBINATIONS WITHIN THE
C***  COMPUTER PROGRAM.
      AMOM=0.057D0
      ATHERM=0.5D0
      CD=0.0
C****INPUT INITIAL CONDITIONS*****************************
C     1. Y(1)=1.0
C     2. Y(2)=1.0
C     3. Y(3)= ANYTHING--NEVER USED
C     4. Y(4)=0.0
C     5. Y(5)=0.0
      READ(5,801)(Y(I),I=1,5)
      READ(5,802) NDIM
      BETAI = BETAI/57.29578
C***
```

```
C***
C***   IT IS NECESSARY TO INPUT THE VALUES OF THE
C***   RESPECTIVE LENGTHS FOR THE ZONE OF
C***   FLOW ESTABLISHMENT, I.E. XESTAB= THE X
C***   DISTANCE WITHIN THE ZONE OF LOW ESTABLISHMENT
C***   YESTAB= THE Y DISTANCE WITHIN THE ZONE OF FLOW
C***   ESTABLISHMENT, AND SESTAB= THE S DISTANCE
C***   WITHIN THE ZONE OF FLOW ESTABLISHMENT.  THE
C***   VALUES OF XDATA(I), YDATA(I), AND SDATA(I) THAT
C***   FOLLOW MUST HAVE THESE VALUES OF XESTAB,YESTAB,
C***   AND SESTAB ADDED SO THAT THE DISTANCES WILL BE WITH
C***   RESPECT TO THE DISCHARGE POINT.
C***
C***
      READ(5,803)XESTAB,YESTAB,SESTAB
C
C*************************************************************
C
C     INPUT THE NUMBER OF CROSS-SECTIONS ALONG THE
C     JET AXIS (NDATA), THE DIAMETER OF THE JET
C     (DIAM) FOR THIS PARTICULAR RUN.
C     INPUT THE X-DISTANCE,Y-DISTANCE, S-DISTANCE,
C     CONCENTRATION RATIO, AND JET HALF-WIDTH DATA FOR A
C     PARTICULAR CROSS-SECTION DOWNSTREAM.
C
C
C*************************************************************
      READ(5,970)NDATA,DIAM,(XDATA(I),YDATA(I),SDATA(I),
     &CONC1(I),BDATA(I),I=1,NDATA)
      CORR = Y(2)
      Y(2)=CORR*DCOS(BETAI)
      Y(3)=CORR*DSIN(BETAI)
      KK=K+DCOS(BETAI)
      BOUPAR=-K**2/(2.D0*KK**2*FROUDE**2)
      BETAI=BETAI*57.29578
      WRITE(6,905)
C****WRITE THE WORKING PARAMETERS************
      WRITE(6,804)(VAR(I),I=1,20)
      WRITE(6,900)FROUDE,K,AMOM,ATHERM,BOUPAR,CD,BETAI
      CD=CD*DSQRT(2.D0)/PI
      WRITE(6,911)DIAM
      BO = DIAM/2.D0
      WRITE(6,969)K,KK,BO
      WRITE(6,968)
      DO 20 I=1,NDATA
      SDATA(I) =(SDATA(I)+SESTAB)/DIAM
      XDATA(I) =(XDATA(I)+XESTAB)/DIAM
      YDATA(I) =(YDATA(I)+YESTAB)/DIAM
      BDATA(I) = BDATA(I)*DSQRT(2.D0)/DIAM
      CONS1(I) = 1.D0/(CONC1(I)*.01D0)
```

```
      WRITE(6,966)SDATA(I),CONC1(I),BDATA(I),XDATA(I),YDATA(
     $I)
   20 CONTINUE
      WRITE(6,904)
      CALL DRKGS(PRMT,Y,DERY,NDIM,IHLF,FCT,OUTP,AUX)
      IF(IHLF.EQ.11)GO TO11
      IF(IHLF.EQ.12)GO TO12
      WRITE(6,901)IHLF
   11 WRITE(6,902)IHLF
   12 WRITE(6,903)IHLF
      STOP
  800 FORMAT(3F10.1,D10.4)
  801 FORMAT(5F5.1)
  802 FORMAT(I1)
  803 FORMAT(3F10.5)
  804 FORMAT(20A4)
  900 FORMAT(///T26,'ABRAHAM''S MODEL'//'DENSIMETRIC',
     &' FROUDE NO.',T33,'=',T37,F6.3/'VELOCITY RATIO'
     &,T33,'=',T39,F4.1/'MOMENTUM COEFFICIENT'/
     &'OF ENTRAINMENT',T33,'=',T38,F5.3/'CYCLINDRICAL',
     &' THERMAL'/'COEFFICIENT OF ENTRAINMENT',T33,'=',
     &T38,F5.3/'BOUYANCY PARAMETER',T33,'=',T35,F8.5/
     &'DRAG COEFFICIENT',T33,'=',T38,F5.2/'INITIAL ANGLE',
     &' OF DISCHARGE',T33,'=',T40,F3.0)
  901 FORMAT(/'****ERROR---SIGN(PRMT(3)).NE.SIGN(PRMT(
     &2)-PRMT(1)).'/'IHLF = ',I2,')'/)
  902 FORMAT(/'****ERROR---INITIAL INCREMENT BISECTED
     &MORE THAN 10 TIMES'/'(IHLF = ',I2,')'/)
  903 FORMAT(/'****ERROR---PRMT(3) = 0'/'(IHLF = ',I2,')'/)
  904 FORMAT(///' JET  VOLUMETRIC CONCEN- MOMENTUM',
     &'    JET',T46,'X',T56,'Y',T66,'BETA'/' AXIS',
     &T10,'FLUX',T18,'TRATION',T28,'FLUX',T36,'HALF',
     &T43,'DISTANCE  DISTANCE    DEGREES'/T36,'WIDTH'
     &/'  S/D',T11,'U',T29,'M',T37,'B/D',T45,'X/D',
     &T56,'Y/D'///)
  905 FORMAT(1H1)
  911 FORMAT(/'DIAM = ',F5.2)
  966 FORMAT(T5,F8.4,T20,F8.4,T34,F8.4,T47,F8.4,T60,F8.4)
  968 FORMAT(1X,'EXPERIMENTAL',T16,'EXPERIMENTAL',T32,
     &'EXPERIMENTAL',T45,'EXPERIMENTAL',T59,'EXPERIMENTAL'
     &/T6,'JET',T16,'CONCENTRATION',T36,'JET',T46,
     &'X-DISTANCE',T60,'Y-DISTANCE'/T5,'AXIS',T33,
     &'HALF-WIDTH'/T6,'S/D',T36,'B/D',T49,'X/D',T62,
     &'Y/D'//)
  969 FORMAT(T21,'K',T26,'=',T30,F8.5/T21,'K''',
     &T26,'=',T30,F8.5/T21,'B0',T26,'=',T30,F8.5)
  970 FORMAT(I2,F3.2/(5F10.5))
      END
C
C
```

```
C*****SUBROUTINE FCT(X,Y,DERY)
C      CONTAINS THE DIFFERENTIAL EQUATIONS THAT ARE
C      TO BE INTEGRATED AND ARE LISTED AS DERY(I).
C
C
       SUBROUTINE FCT(X,Y,DERY)
       IMPLICIT REAL*8(A-Z)
       REAL*8     Y(5), DERY(5)
       COMMON /INPUT/ K,KK,BOUPAR,CD,AMOM,ATHERM,BO,DIAM
       M=DSQRT(Y(2)**2+Y(3)**2)
       BETA=DATAN(Y(3)/Y(2))
       IF(BETA)1,2,2
     1 IF(ATHERM)2,2,3
     3 CD = -CD
       ATHERM=-ATHERM
       WRITE(6,901) CD,ATHERM
     2 CONTINUE
       S=DSIN(BETA)
       SS=DSIN(BETA)**2
       SSS=DSIN(BETA)**3
       CS=DCOS(BETA)
       KKK=KK*KK
       USM=Y(1)/DSQRT(M)
       MU=M/Y(1)
       UM=Y(1)/M
       DERY(1)=4.D0*(AMOM*DSQRT(M)-(USM/KK)*(2.D0*AMOM*CS-ATH
      $ERM*S*CS))
       DERY(2)=(4.D0*USM/KKK)*(2.D0*AMOM*(KK*MU-2.D0*CS)
      &+2.D0*ATHERM*S*CS+CD*SSS)
       DERY(3)=4.D0*(BOUPAR*UM-(CD*USM*SS*CS/KKK))
       DERY(4)=CS
       DERY(5)=S
  901  FORMAT(1X,F5.2,7X,F5.2)
       RETURN
       END
C
C
C*****SUBROUTINE OUTP(X,Y,DERY,IHLF,NDIM,PRMT)
C
C
       SUBROUTINE OUTP(X,Y,DERY,IHLF,NDIM,PRMT)
       IMPLICIT REAL*8(A-Z)
       INTEGER NDIM, IHLF
       REAL*8     Y(5), DERY(5), PRMT(5)
       COMMON"/INPUT/ K,KK,BOUPAR,CD,AMOM,ATHERM,BO,DIAM
       IF(DABS((X*10.D0)-IDINT((X+1D-6)*10.D0)) .GT.
      & .001D0)RETURN
       IF(X .LT. 1.0D0) GO TO 10
       IF(DABS(X-IDINT(X+1D-6)).GT..001D0)RETURN
       IF(X .LT. 40.01)GO TO 10
```

```
      IF(DABS((X/10.D0)-IDINT((X+1D-6)/10.D0)) . GT.
     & .001)RETURN
   10 CONC = 1.D0/Y(1)
      M=DSQRT(Y(2)**2+Y(3)**2)
      R=DSQRT(Y(1)*Y(1)/M)
      BETA = (DATAN(Y(3)/Y(2)))*57.29578
      R=R*B0/DIAM
      XX=X
      XXXX=Y(4)
      YYYY=Y(5)
      WRITE(6,901)XX,Y(1),CONC,M,R,XXXX,YYYY,BETA
  901 FORMAT(1X,F6.2,T8,F7.2,T18,F7.5,T27,F7.2,T36,
     &F6.2,T44,F7.2,T52,F8.2,T65,F6.2)
      RETURN
      END
```

APPENDIX D

COMPUTER PROGRAM - DRKGS

```
C
C
C   THIS IS A SCIENTIFIC LIBRARY PROGRAM TO INTEGRATE A
C   SYSTEM OF SIMULTANEOUS ORDINARY DIFFERENTIAL
C   EQUATIONS USING A FOURTH-ORDER RUNGE-KUTTA TECHNIQUE.
C   THIS PROGRAM IS AVAILABLE A MOST COMPUTER CENTERS.
C   THE INPUT VARIABLES ARE EXPLAINED IN THE PROGRAMS
C   FAN AND/OR ABRAHAM.

C
C
C
      SUBROUTINE DRKGS(PRMT,Y,DERY,NDIM,IHLF,FCT,OUTP,AUX)
      DIMENSION Y(1),DERY(1),AUX(8,1),A(4),B(4),C(4),PRMT(1)
      DOUBLE PRECISION PRMT,Y,DERY,AUX,A,B,C,X,XEND,H,AJ,BJ,
     $CJ,R1,R2,
     1DELT
      DO 1 I=1,NDIM
    1 AUX(8,I)=.06666666666666667D0*DERY(I)
      X=PRMT(1)
      XEND=PRMT(2)
      H=PRMT(3)
      PRMT(5)=0.D0
      CALL FCT(X,Y,DERY)
C
C     ERROR TEST
      IF(H*(XEND-X))38,37,2
C
C     PREPARATIONS FOR RUNGE-KUTTA METHOD
    2 A(1)=.5D0
      A(2)=.29289321881345248D0
      A(3)=1.7071067811865475D0
      A(4)=.16666666666666667D0
      B(1)=2.D0
      B(2)=1.D0
      B(3)=1.D0
      B(4)=2.D0
      C(1)=.5D0
      C(2)=.29289321881345248D0
      C(3)=1.7071067811865475D0
      C(4)=.5D0
C
C     PREPARATIONS OF FIRST RUNGE-KUTTA STEP
      DO 3 I=1,NDIM
      AUX(1,I)=Y(I)
      AUX(2,I)=DERY(I)
      AUX(3,I)=0.D0
    3 AUX(6,I)=0.D0
      IREC=0
      H=H+H
      IHLF=-1
```

```
      ISTEP=0
      IEND=0
C
C
C     START OF A RUNGE-KUTTA STEP
    4 IF((X+H-XEND)*H) 7,6,5
    5 H=XEND-X
    6 IEND=1
C
C     RECORDING OF INITIAL VALUES OF THIS STEP
    7 CALL OUTP(X,Y,DERY,IREC,NDIM,PRMT)
      IF(PRMT(5))40,8,40
    8 ITEST=0
    9 ISTEP=ISTEP+1
C
C
C     START OF INNERMOST RUNGE-KUTTA LOOP
      J=1
   10 AJ=A(J)
      BJ=B(J)
      CJ=C(J)
      DO 11 I=1,NDIM
      R1=H*DERY(I)
      R2=AJ*(R1-BJ*AUX(6,I))
      Y(I)=Y(I)+R2
      R2=R2+R2+R2
   11 AUX(6,I)=AUX(6,I)+R2-CJ*R1
      IF(J-4)12,15,15
   12 J=J+1
      IF(J-3)13,14,13
   13 X=X+.5D0*H
   14 CALL FCT(X,Y,DERY)
      GOTO 10
C     END OF INNERMOST RUNGE-KUTTA LOOP
C
C     TEST OF ACCURACY
   15 IF(ITEST)16,16,20
C
C     IN CASE ITEST=0 THERE IS NO POSSIBILITY FOR TESTING OF
C     ACCURACY
   16 DO 17 I=1,NDIM
   17 AUX(4,I)=Y(I)
      ITEST=1
      ISTEP=ISTEP+ISTEP-2
   18 IHLF=IHLF+1
      X=X-H
      H=.5D0*H
      DO 19 I=1,NDIM
      Y(I)=AUX(1,I)
      DERY(I)=AUX(2,I)
```

```
   19 AUX(6,I)=AUX(3,I)
      GOTO 9
C
C     IN CASE ITEST=1 TESTING OF ACCURACY IS POSSIBLE
   20 IMOD=ISTEP/2
      IF(ISTEP-IMOD-IMOD)21,23,21
   21 CALL FCT(X,Y,DERY)
      DO 22 I=1,NDIM
      AUX(5,I)=Y(I)
   22 AUX(7,I)=DERY(I)
      GOTO 9
C
C     COMPUTATION OF TEST VALUE DELT
   23 DELT=0.D0
      DO 24 I=1,NDIM
   24 DELT=DELT+AUX(8,I)*DABS(AUX(4,I)-Y(I))
      IF(DELT-PRMT(4))28,28,25
C
C     ERROR IS TOO GREAT
   25 IF(IHLF-10)26,36,36
   26 DO 27 I=1,NDIM
   27 AUX(4,I)=AUX(5,I)
      ISTEP=ISTEP+ISTEP-4
      X=X-H
      IEND=0
      GOTO 18
C
C     RESULT VALUES ARE GOOD
   28 CALL FCT(X,Y,DERY)
      DO 29 I=1,NDIM
      AUX(1,I)=Y(I)
      AUX(2,I)=DERY(I)
      AUX(3,I)=AUX(6,I)
      Y(I)=AUX(5,I)
   29 DERY(I)=AUX(7,I)
      CALL OUTP(X-H,Y,DERY,IHLF,NDIM,PRMT)
      IF(PRMT(5))40,30,40
   30 DO 31 I=1,NDIM
      Y(I)=AUX(1,I)
   31 DERY(I)=AUX(2,I)
      IREC=IHLF
      IF(IEND)32,32,39
C
C     INCREMENT GETS DOUBLED
   32 IHLF=IHLF-1
      ISTEP=ISTEP/2
      H=H+H
      IF(IHLF)4,33,33
   33 IMOD=ISTEP/2
      IF(ISTEP-IMOD-IMOD)4,34,4
```

```
   34 IF(DELT-.02D0*PRMT(4))35,35,4
   35 IHLF=IHLF-1
      ISTEP=ISTEP/2
      H=H+H
      GOTO 4
C
C
C     RETURNS TO CALLING PROGRAM
   36 IHLF=11
      CALL FCT(X,Y,DERY)
      GOTO 39
   37 IHLF=12
      GOTO 39
   38 IHLF=13
   39 CALL OUTP(X,Y,DERY,IHLF,NDIM,PRMT)
   40 RETURN
      END
```

APPENDIX E

CALIBRATION OF 0.5 gpm ROTAMETER

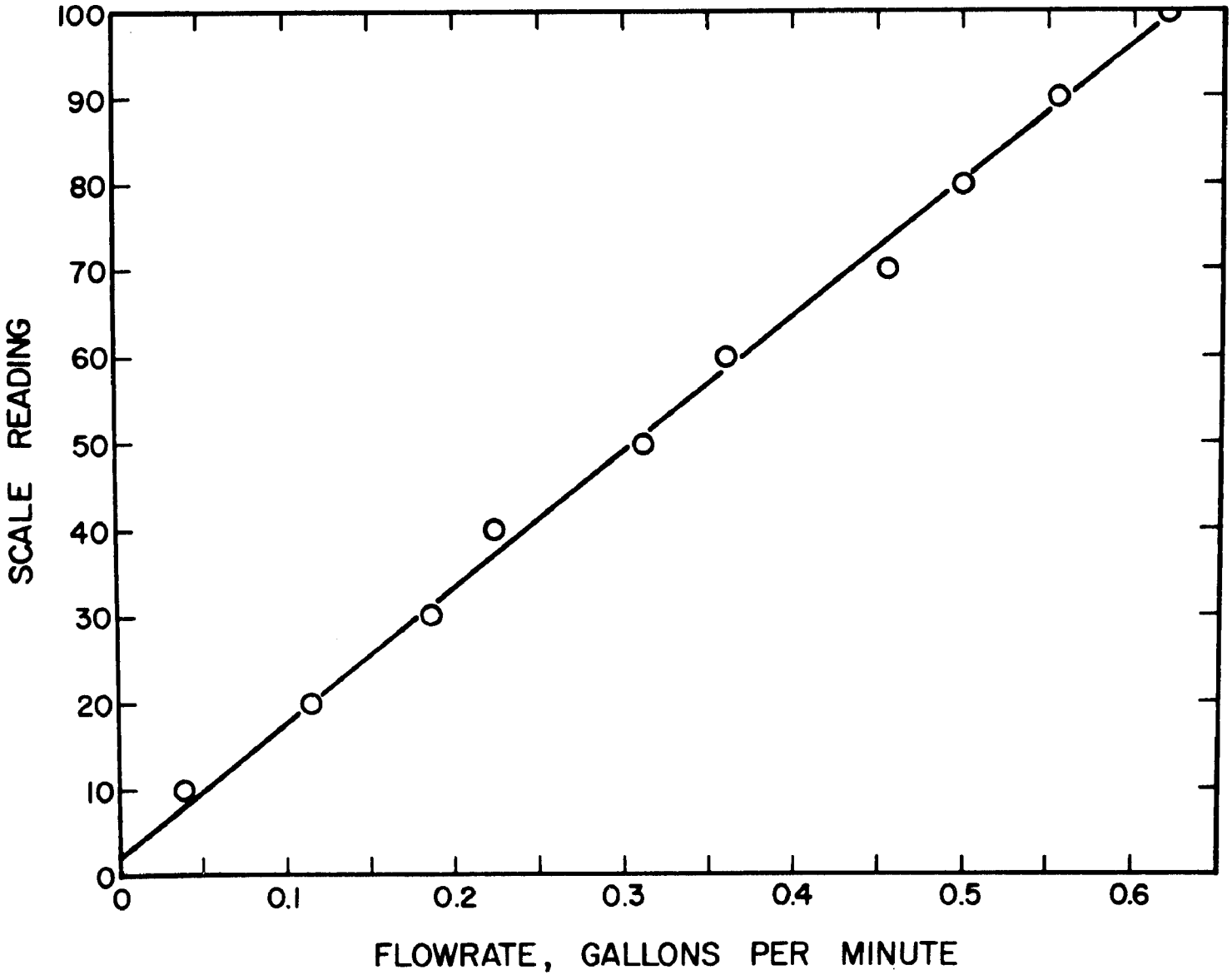

FIGURE 43 - CALIBRATION OF 0.5 gpm ROTAMETER

APPENDIX F

CALIBRATION OF 60° V-NOTCH WEIR

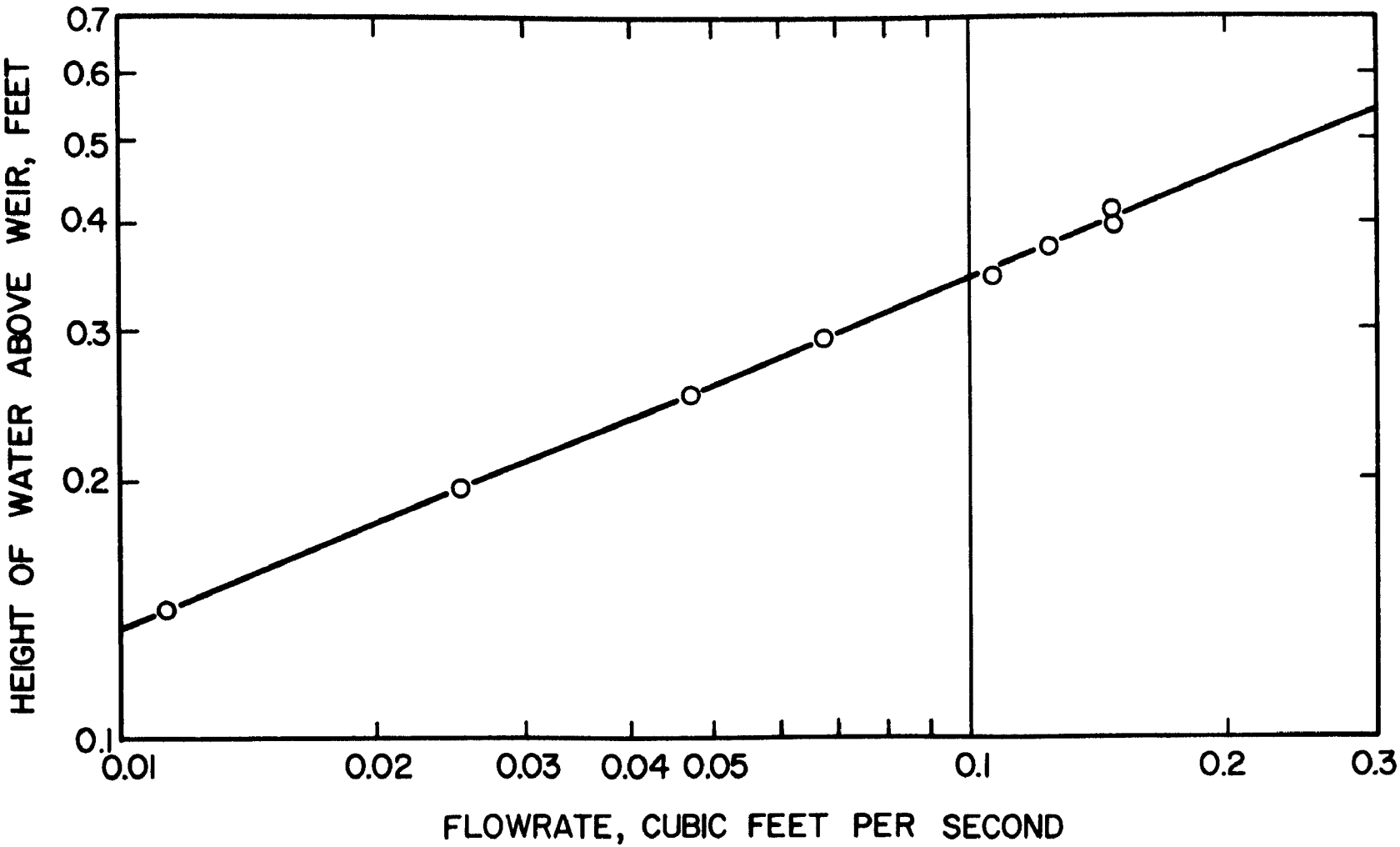

FIGURE 44 - CALIBRATION OF 60° V-NOTCH WEIR

APPENDIX G

COMPUTER PROGRAM - ANALYSIS

```
C
C COMPUTER PROGRAM TO CONVERT RAW LABORATORY DATA
C TO JET AXIS DATA.
C
C
      REAL M(100)
      DIMENSION C(100),S(100),D(100),X3(100),CXD(100),CXDSQ(
     $100),C1(100
     &),CALC2(100),XDIST(25),DIF2(100),YMEAN1(25),CONMAX(25)
     $,STDEV1(25)
C     YCEPT AND SLOPE ARE THE PERTINENT PARAMETERS TO
C     DEFINE THE CALIBRATION CURVE.  YCEPT AND SLOPE ARE
C     DIFFERENT FOR EACH RUN.  THE CALIBRATION CURVE IS A
C     LINEAR EXPRESSION WHICH RELATES THE MILLIVOLT OUTPUT
C     TO THE CONCENTRATION OF SALT.
C
      READ(5,950)YCEPT,SLOPE
C     IRUNNO = THE EXPERIMENTAL RUN NO.
C     PGTW   = IS THE RELATIVE DEPTH OF THE MEASURING DEVICE
C              TO TOP OF THE WATER
C     PGBW   = IS THE RELATIVE DEPTH OF THE MEASURING
C              DEVICE TO THE BOTTOM OF THE WATER OR THE
C              BOTTOM OF THE LABORATORY FLUME
C     PROBTW = IS THE RELATIVE LOCATION OF THE CONDUCTIVITY
C              PROBE WITH RESPECT TO THE MEASURING DEVICE
C              AND TOP OF THE WATER
C     ELEJET = THE HEIGHT OF THE JET DISCHARGE POINT FROM
C              BOTTOM OF THE FLUME
C     THE ABOVE VARIABLES ARE NEEDED TO TRANSFORM THE
C     LABORATORY DATA OF THE MEASURED DEPTHS TO ACTUAL
C     DEPTHS WITH RESPECT TO THE JET DISCHARGE POINT.
      READ(5,903)IRUNNO,PGTW,PGBW,PROBTW,ELEJET
      READ(5,920)FROUDE
C     FROUDE = DENSIMETRIC FROUDE NUMBER FOR THIS EXPERI-
C              MENTAL RUN
      WRITE(6,802)IRUNNO
      DEPTH =PGTW-PGBW
      DEPINC = PGTW-PROBTW
      ELEINC = ELEJET - PGBW
      WRITE(6,907)PGTW,PGBW,PROBTW,DEPTH,DEPINC,ELEINC
C     N = THE NUMBER OF CROSS-SECTIONS ALONG THE JET AXIS
C     X1= THE RELATIVE LOCATION OF THE JET DISCHARGE POINT
C         IN THE X-DIRECTION.  THIS VALUE MAYBE ZERO OR
C         SOME OTHER RELATIVE X VALUE
C     DIAM = THE JET DIAMETER
      READ(5,900)N,X1,DIAM
      READ(5,912)AK,BETA
C     AK = THE VELOCITY RATIO FOR THIS EXPERIMENTAL RUN
C     BETA = THE INITIAL ANGLE OF DISCHARGE
      WRITE(6,801)N,X1,DIAM
```

```
      DO 10 J=1,N
C     N1 = NUMBER OF Y LOCATIONS ON THE CROSS-SECTION OF THE
C         JET AXIS THAT WERE MEASURED
C     X = THE RELATIVE X LOCATION OF THE CROSS-SECTION WITH
C         RESPECT TO THE JET DISCHARGE POINT.
C     CI = THE DELTA Y VALUE OR THE INCREMENTAL Y DISTANCE
C          ALONG THE CROSS-SECTION
C     M(I) = THE AVERAGE MILLIVOLT OUPUT AT THIS PARTICULAR
C            Y LOCATION
C     D(I) = THE RELATIVE Y LOCATION AT WHICH THE MILLIVOLT
C        READINGS WERE TAKEN
      READ(5,910)N1,X,CI,(M(I),D(I),I=1,N1)
      CI=CI*30.48
      SQ2PI = 2.506628274631
      DIF22 = 0.0
      CNSUM1  = 0.0
      CNSUM2  = 0.0
      FREQ = 0.0
      X2=(X-X1)/DIAM
      XDIST(J)=X2*DIAM
      WRITE(6,901)J,X,X2
      WRITE(6,902)
C
C
C   CALCULATES THE MEAN Y-DISTANCE, THE STANDARD DEVIA-
C   TION, AND VARIANCE OF THE PARTICULAR CROSS-SECTION
C
C
      DO 20 I=1,N1
      D(I)=D(I)-PGBW+DEPINC-ELEINC
      D(I) = D(I)*30.48
      C(I)=YCEPT  + SLOPE*M(I)
      IF(C(I) .GT. 0.000000)GO TO 21
      C(I) = 0.00000000
      S(I) = 10000000.00
      GO TO 22
   21 S(I)=1./C(I)
   22 C1(I) = C(I)*100.00
      FREQ = FREQ + C1(I)
      CXD(I) = C1(I) * D(I)
      CXDSQ(I) = CXD(I) * D(I)
      CNSUM1  = CNSUM1  + CXD(I)
      CNSUM2   = CNSUM2  + CXDSQ(I)
   20 CONTINUE
      YMEAN = CNSUM1/FREQ
      STD = SQRT((CNSUM2  - ((CNSUM1**2)/FREQ))/FREQ)
      YMEAN1(J)=YMEAN
      STDEV1(J)=STD
C
C
```

```
C    CALCULATES THE CONCENTRATION AT THE MEAN Y-DISTANCE
C
C
      CONMAX(J)=(FREQ*CI)/(STD*SQ2PI)
      VAR = STD**2
      DO 40 I =1,N1
      WRITE(6,800)M(I),S(I),D(I),C(I),C1(I)
   40 CONTINUE
      WRITE(6,811)FREQ
      WRITE(6,812)YMEAN,STD,VAR
      WRITE(6,814)
C
C
C    CALCULATES THE GAUSSIAN DISTRIBUTIONS USING THE ABOVE
C    INFORMATION AND THE COMPARES THE CALCULATED VALUE
C    WITH THE OBSERVED VALUE AND CALCULATES THE
C    SQUARED DIFFERENCE.
      DO 60 I = 1,N1
      X3(I) = D(I) -YMEAN
      CALC2(I) = ((FREQ*CI)/(STD*SQ2PI))*EXP(-(X3(I)**2)/(2.
     $*STD**2))
      DIF2(I) = (C1(I) - CALC2(I))**2
      DIF22 = DIF22 + DIF2(I)
      WRITE(6,813)D(I),X3(I),C1(I),CALC2(I),DIF2(I)
   60 CONTINUE
      WRITE(6,815)DIF22
      NPTS = N1
      XMAX = 60.00
C
C
C     XMAX IS A SCALING FACTOR FOR THE PLOT IN SUB-
C     ROUTINE PLOT2D.IT SHOULD HOWEVER BE SOME
C     INTEGER VALUE OF 12 SINCE 120 COLUMNS ARE
C     USED IN THE OUTPUT
      WRITE(6,957)IRUNNO,FROUDE,AK,XDIST(J)
      CALL PLOT2D(NPTS,XMAX,D,C1,CALC2)
   10 CONTINUE
      WRITE(6,958)
C    WRITES OUT THE PERTINENT INFORMATION FOR EACH
C    CROSS-SECTION, X-DISTANCE, MEAN Y-DISTANCE, MAXI-
C    MUM CONCENTRATION, AND THE STANDARD DEVIATION
      DO 313 J=1,N
      WRITE(6,959)XDIST(J),YMEAN1(J),CONMAX(J),STDEV1(J)
  313 CONTINUE
  800 FORMAT(1X,F7.2,T13,F11.2,T29,F6.3,T43,F8.6,T58,F11.7)
  801 FORMAT(T11,'NO. OF OBSERVATIONS',T33,'=',T36,I2/T11,'O
     $FFSET DISTAN
     &CE',T33,'=',T36,F5.2,' CENTIMETERS'/T11,'DIAMETER OF J
     $ET',T33,'=',
     &T36,F5.2,' CENTIMETERS'///)
```

```
802 FORMAT(1H1/////T33,'RUN NO. ',I2///)
811 FORMAT(T58,'-----------'/T46,'SUMMATION = ',F11.7)
812 FORMAT(T26,'Y-MEAN',T48,'=',T52,F8.4/T26,'STANDARD DEV
   $IATION',T48
   &,'=',T54,F8.6/T26,'VARIANCE',T48,'=',T54,F8.6)
813 FORMAT(T9,F6.3,T23,F6.3,T35,F11.7,T49,F11.7,T73,F11.7)
814 FORMAT(1H3T9,'OBSERVED',T22,'DISTANCE',T37,'OBSERVED',
   $T51,'CALCULA
   &TED',T72,'DIFFERENCE'/T11,'DEPTH',T24,'FROM',
   &T34,'CONCENTRATION',T53,'SQUARED'/T11,'(CM)',T24,
   &'MEAN',T38,'X100',T54,'X100',T72,'FOR NORMAL'/
   &T24,'(CM)',T51,'NORMAL CURVE',T75,'CURVE')
815 FORMAT(T73,'---------------'/T60,'SUMMATION = ',
   &T76,F11.7)
900 FORMAT(I5,F5.2,F5.3)
901 FORMAT(1H1/////T26,'CROSS-SECTION NO. ',I2//T4,'DISTAN
   $CE FROM DISC
   &HARGE POINT ',T45,'=',T48,F6.2,' CENTIMETERS'/T4,'X/D
   $(NO. OF JET
   &DIAMETERS DOWNSTREAM)',T45,'=',T48,F6.2)
902 FORMAT(T27,'Y-DISTANCE'/T28,'FROM JET'/1X,'MILLIVOLT',
   $T14,'DILUTIO
   &N',T28,'DISCHARGE',T41,'CONCENTRATION',T58,'CONCENTRAT
   $ION'
   &/T30,'POINT',T62,'X100'/T30,'(CM)')
903 FORMAT(I2,4F5.3)
907 FORMAT(T7,'POINT GAGE TOP OF WATER',T35,'=',T39,F5.3,T
   $47,'FEET'/T7
   &,'POINT GAGE BOTTOM OF WATER',T35,'=',T39,F5.3,T47,'FE
   $ET'/T7,'PROB
   &E TOP OF WATER',T35,'=',T39,F5.3,T47,'FEET'/T7,'DEPTH
   $OF WATER',T3
   &5,'=',T39,F5.3,T47,'FEET'/T7,'DEPTH INCREMENT',T35,'='
   $,T39,F5.3,T4
   &7,'FEET'/T7,'LOCATION OF JET ABOVE'/T7,'BOTTOM OF FLUM
   $E',T35,'=',T
   &39,F5.3,T47,'FEET'///)
910 FORMAT(I5,F5.2,F5.3/(6F10.2))
912 FORMAT(2F5.2)
920 FORMAT(F5.2)
950 FORMAT(2F15.9)
957 FORMAT(1H1T53,'RUN NO. = ',T64,I2//T50,'FROUDE NO. = '
   $,T64,F5.2//T
   &50,'VELOCITY'/T52,'RATIO(K) = ',T64,F5.2//T50,'X-DISTA
   $NCE =',T63,F
   &8.4,T72,'CENTIMETERS'////)
958 FORMAT(1H1T3,'X-DISTANCE',T20,'Y-DISTANCE',T41,'MAXIMU
   $M',T54,'STAN
   &DARD'/T39,'CALCULATED',T54,'DEVIATION'/
   &T38,'CONCENTRATION'/T2,'(CENTIMETERS)',T21,'(MEAN DIST
   $.)'/
```

```
     &T20,'(CENTIMETERS)'//)
 959 FORMAT(T5,F8.4,T22,F7.3,T41,F9.5,T56,F7.4)
     END
C
C
C
C    PLOTS THE OBSERVED AND CALCULATED VALUES ON THE SAME
C    PLOT
C
C
     SUBROUTINE PLOT2D(NPTS,XMAX,D,C1,CALC2)
     INTEGER BLANK/' '/,O/'O'/,G/'G'/
     INTEGER BAR/'['/,MINUS/'-'/
     DIMENSION D(100),C1(100),CALC2(100),LINE(121),XTEMP(13
    $)
     DELTY = D(1)-D(2)
     DO 100 I=1,NPTS
     DO 101 J=1,121
 101 LINE(J)=BLANK
     IF(ABS(D(I)) .GT. DELTY/2.)GO TO 200
     DO 102 K=1,121
 102 LINE(K)=MINUS
 200 DO 104 J=1,121,10
 104 LINE(J)=BAR
     N=((CALC2(I)*120.)/XMAX)+1.5
     LINE(N)=G
     N=((C1(I)*120.)/XMAX)+1.5
     LINE(N)=O
 100 WRITE(6,900)D(I),LINE
     X=0.0
     DELTX=XMAX/12.
     DO 103 J=1,13
     XTEMP(J)=X
 103 X=X+DELTX
     WRITE(6,901)XTEMP
 900 FORMAT(1X,F9.4,2X,121A1)
 901 FORMAT(12X,13('[',9X)/T11,13(F6.2,4X))
     RETURN
     END
```

APPENDIX H

OBSERVED VALUES AND THEORETICAL CURVES PREDICTED BY FAN'S AND ABRAHAM'S MODEL

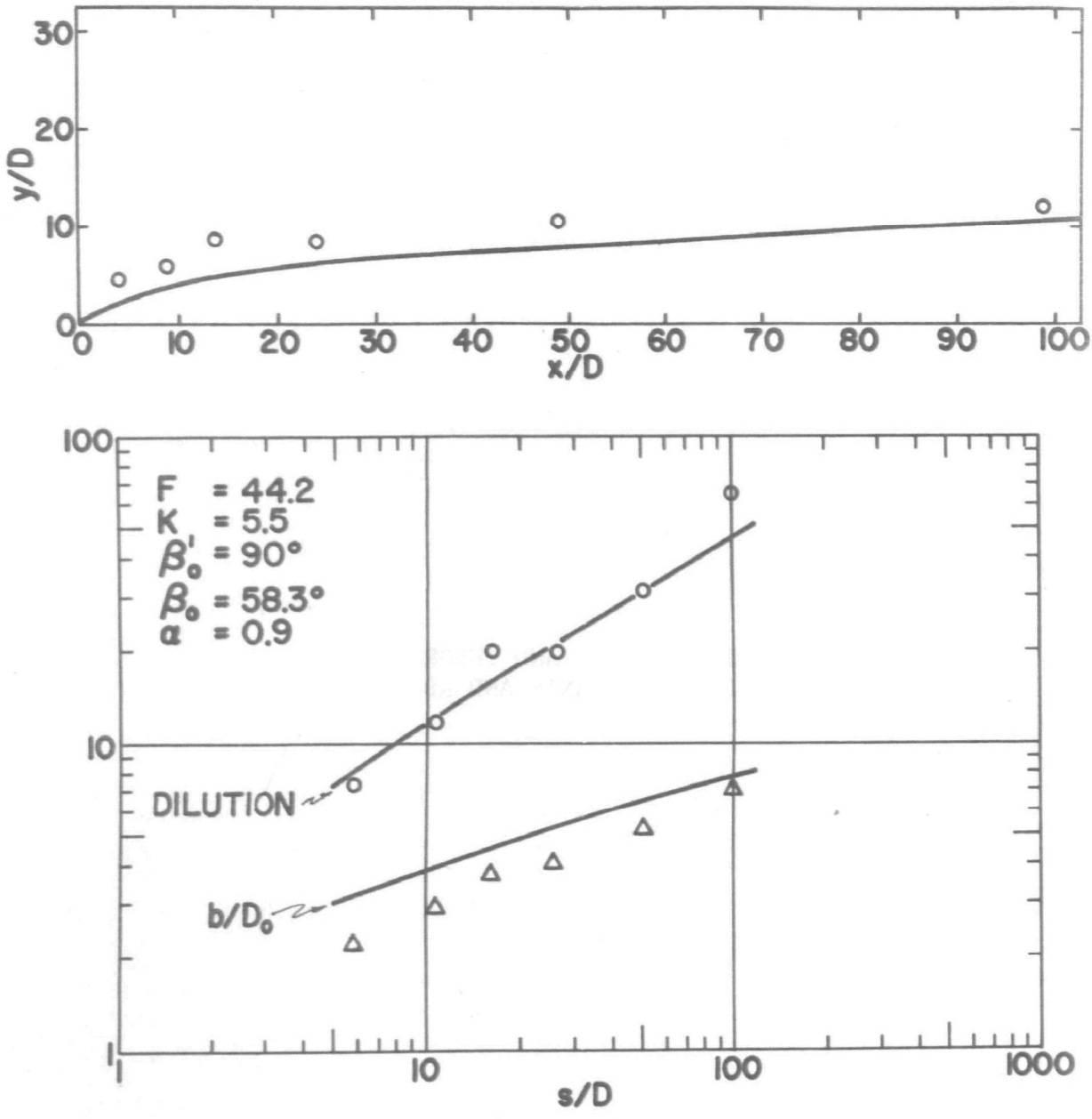

FIGURE 45 - OBSERVED VALUES AND THEORETICAL CURVES PREDICTED BY FAN'S MODEL - RUN NO. 18

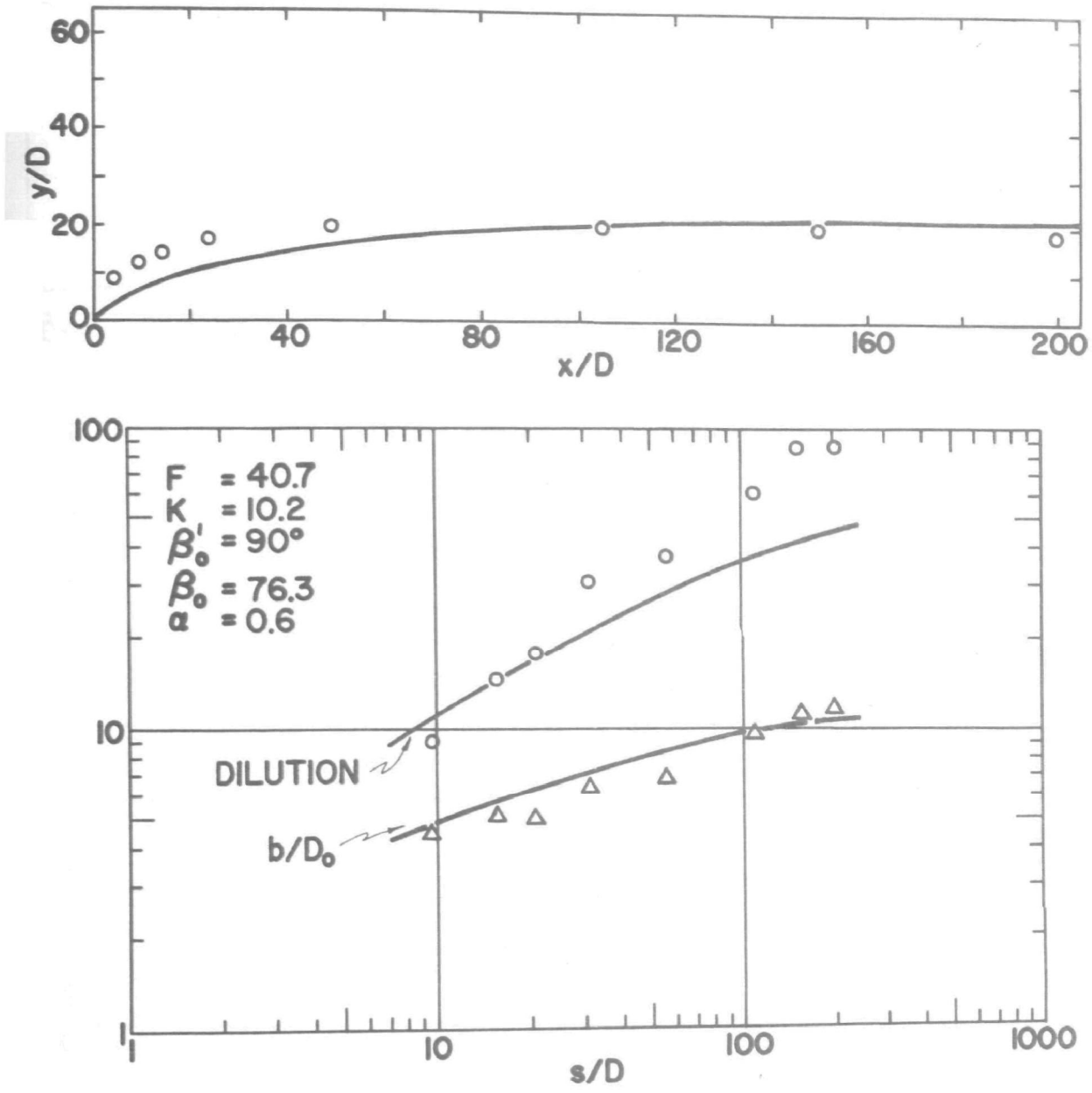

FIGURE 46 - OBSERVED VALUES AND THEORETICAL CURVES
PREDICTED BY FAN'S MODEL - RUN NO. 13

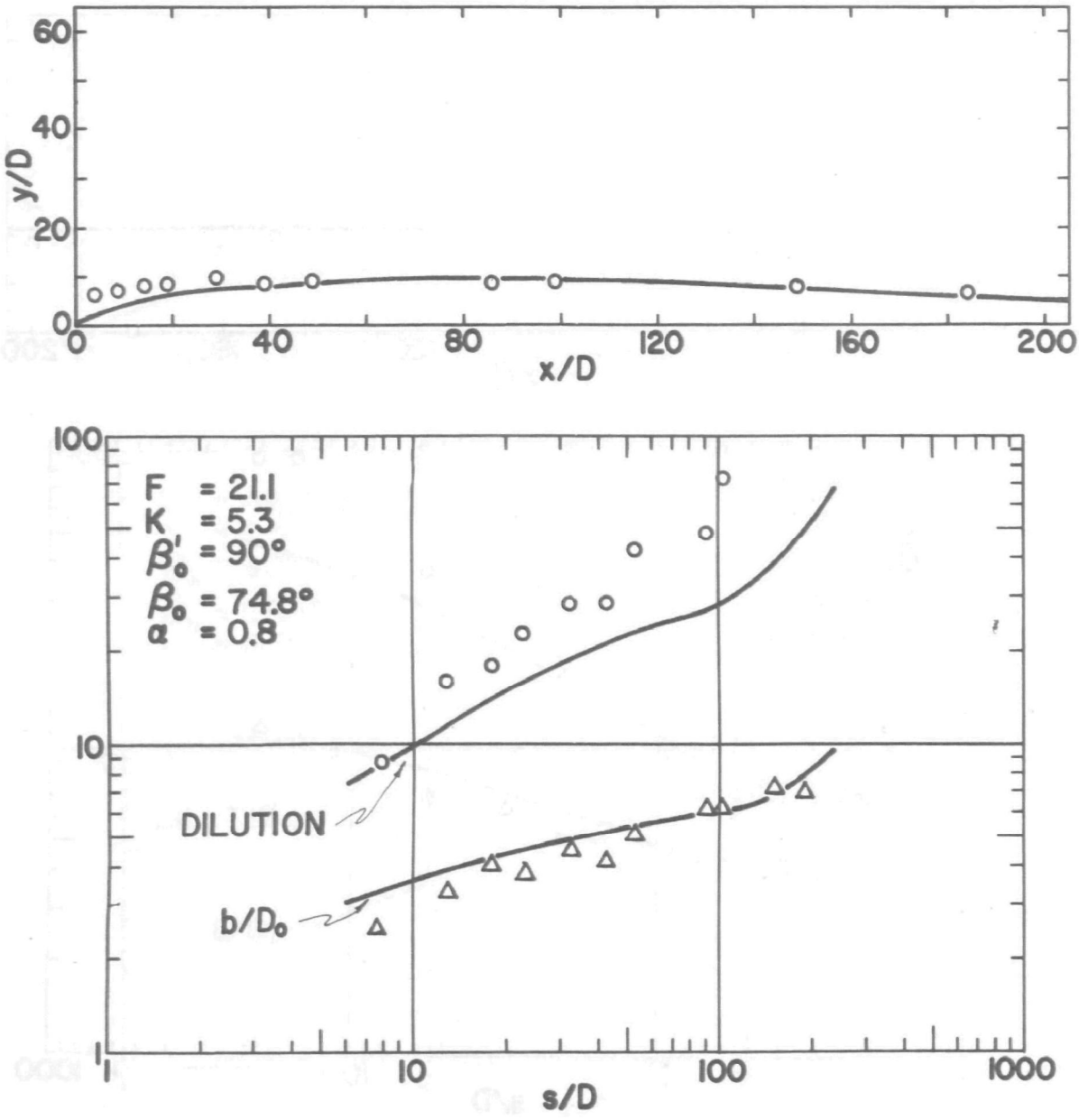

FIGURE 47 - OBSERVED VALUES AND THEORETICAL CURVES
PREDICTED BY FAN'S MODEL - RUN NO. 12

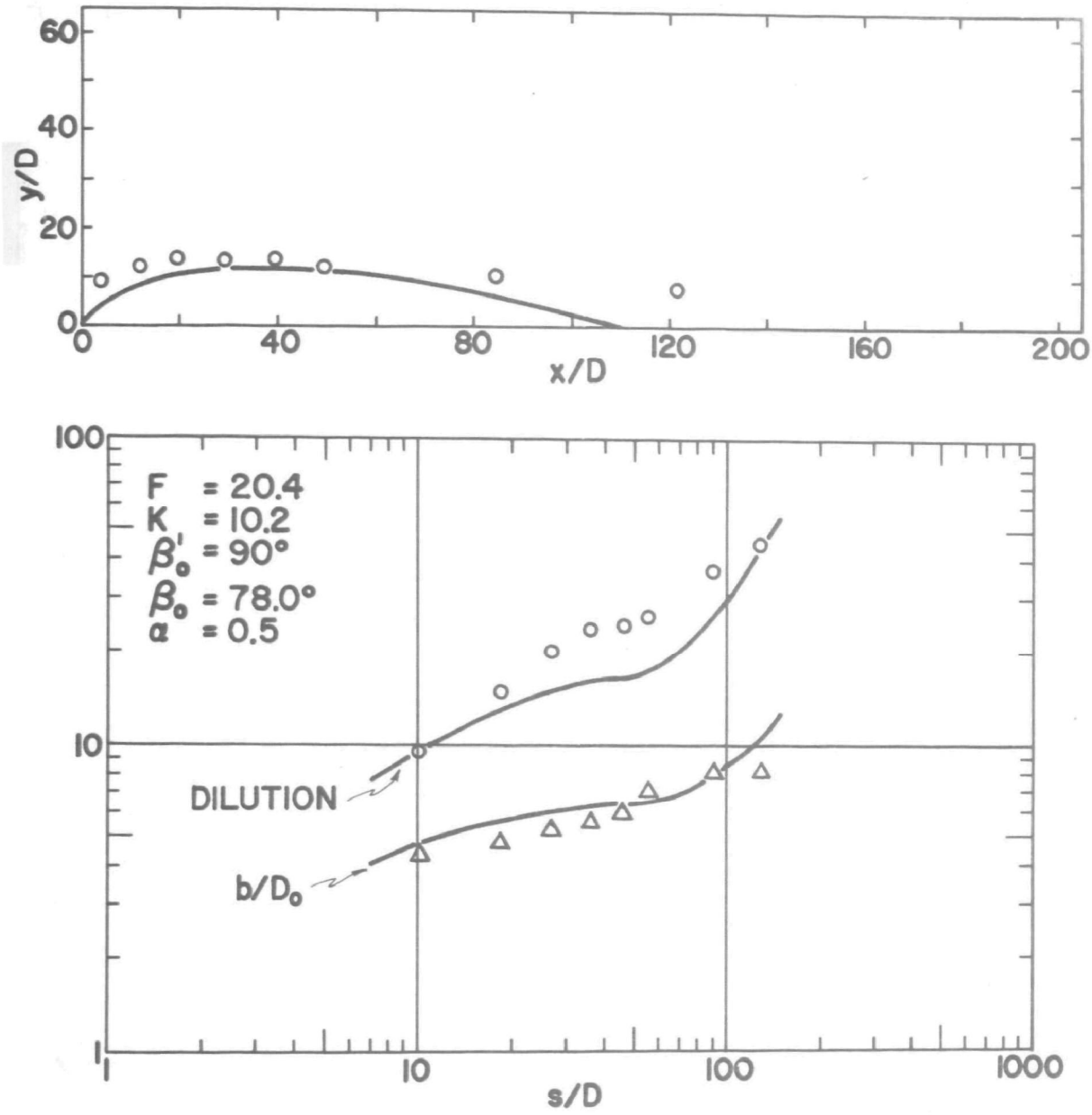

FIGURE 48 - OBSERVED VALUES AND THEORETICAL CURVES
PREDICTED BY FAN'S MODEL - RUN NO. 11

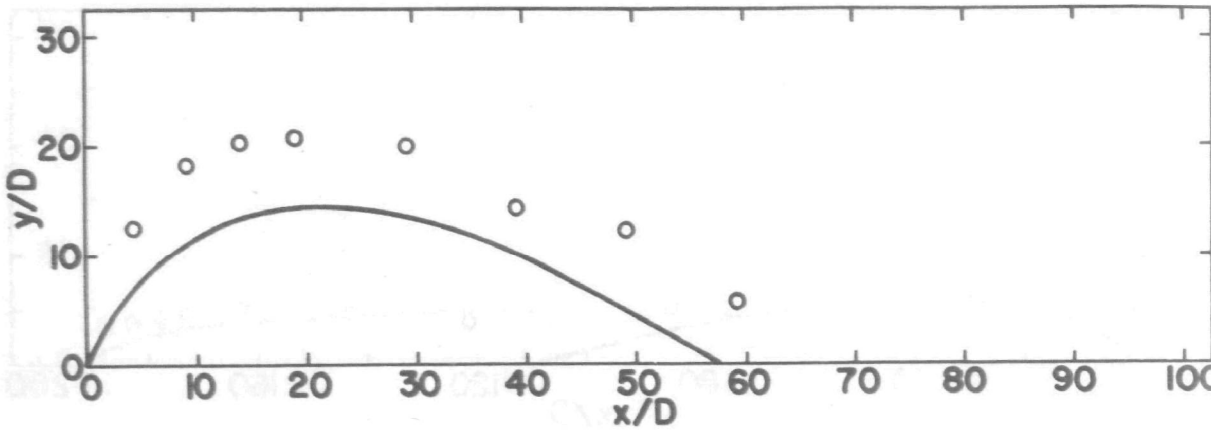

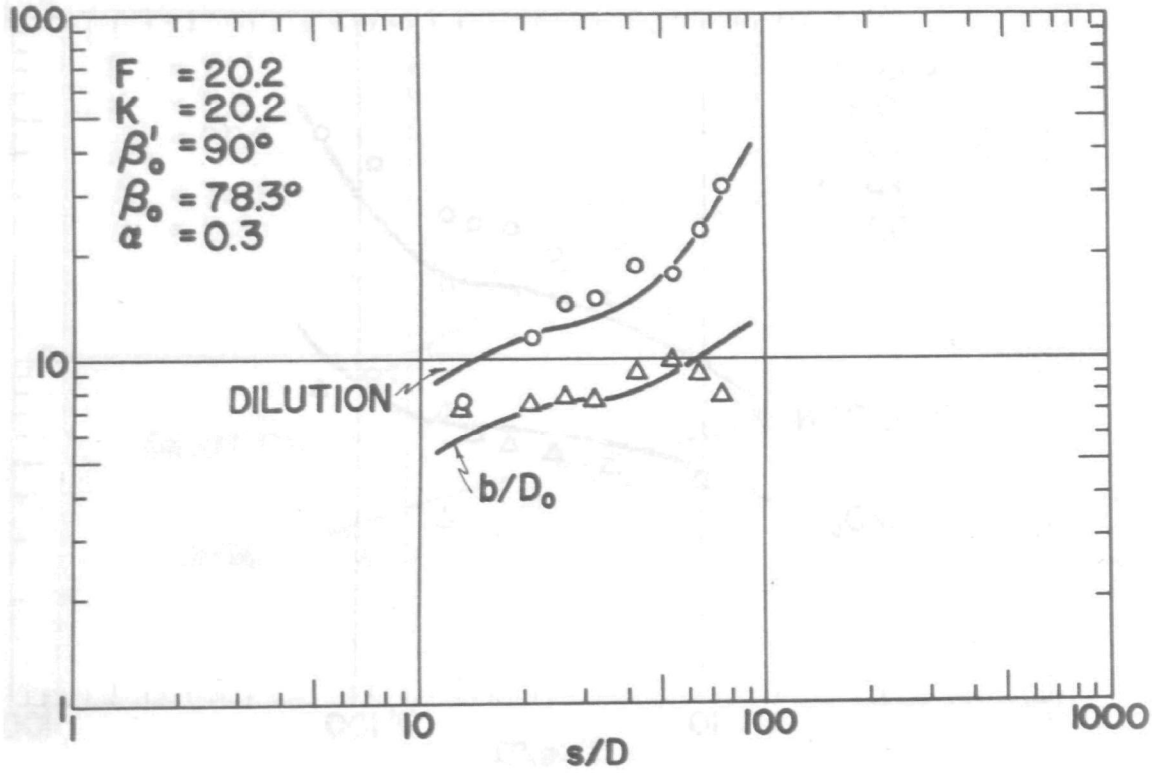

FIGURE 49 - OBSERVED VALUES AND THEORETICAL CURVES
PREDICTED BY FAN'S MODEL - RUN NO. 16

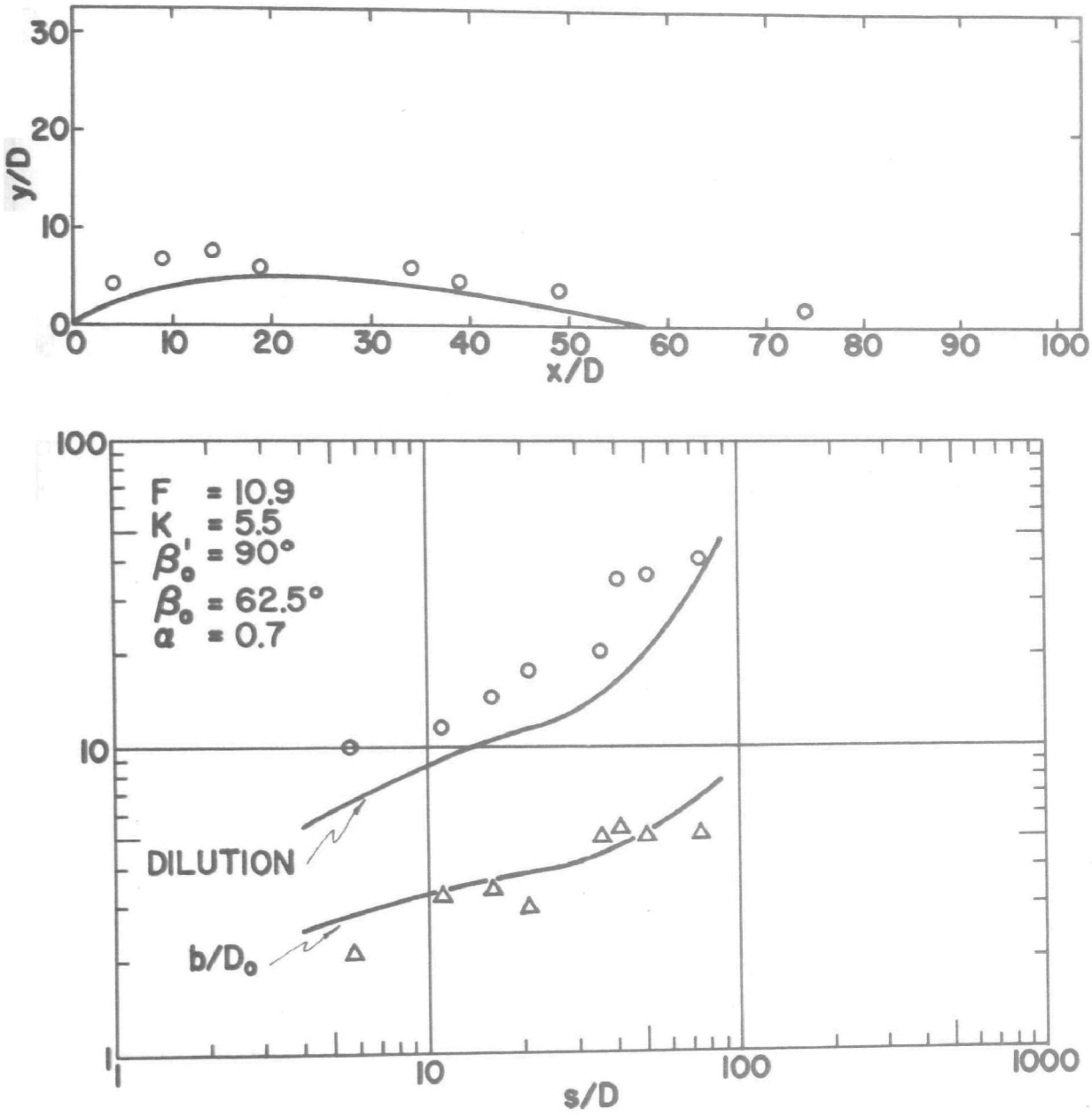

FIGURE 50 - OBSERVED VALUES AND THEORETICAL CURVES PREDICTED BY FAN'S MODEL - RUN NO. 10

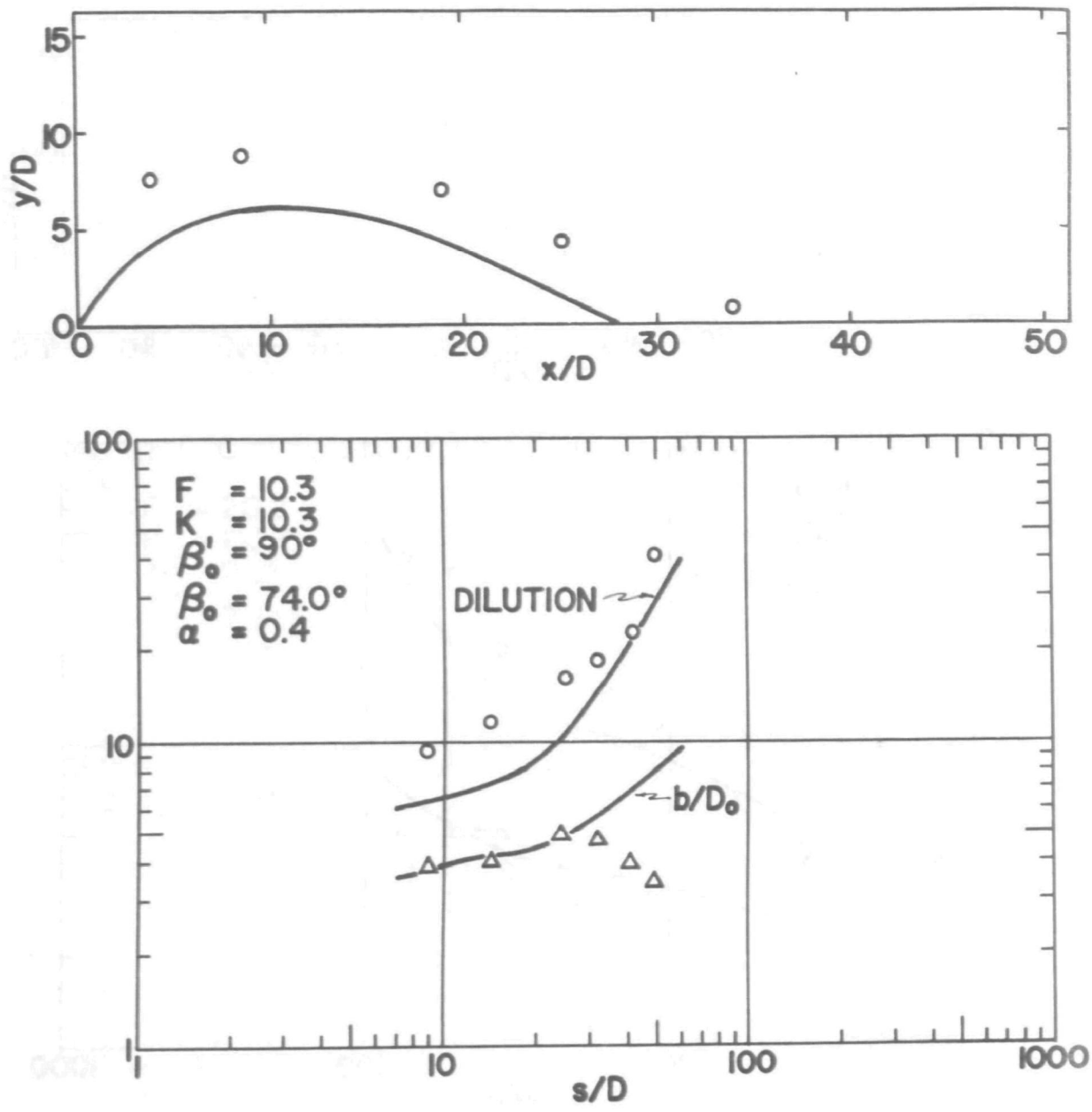

FIGURE 51 - OBSERVED VALUES AND THEORETICAL CURVES
PREDICTED BY FAN'S MODEL - RUN NO. 9

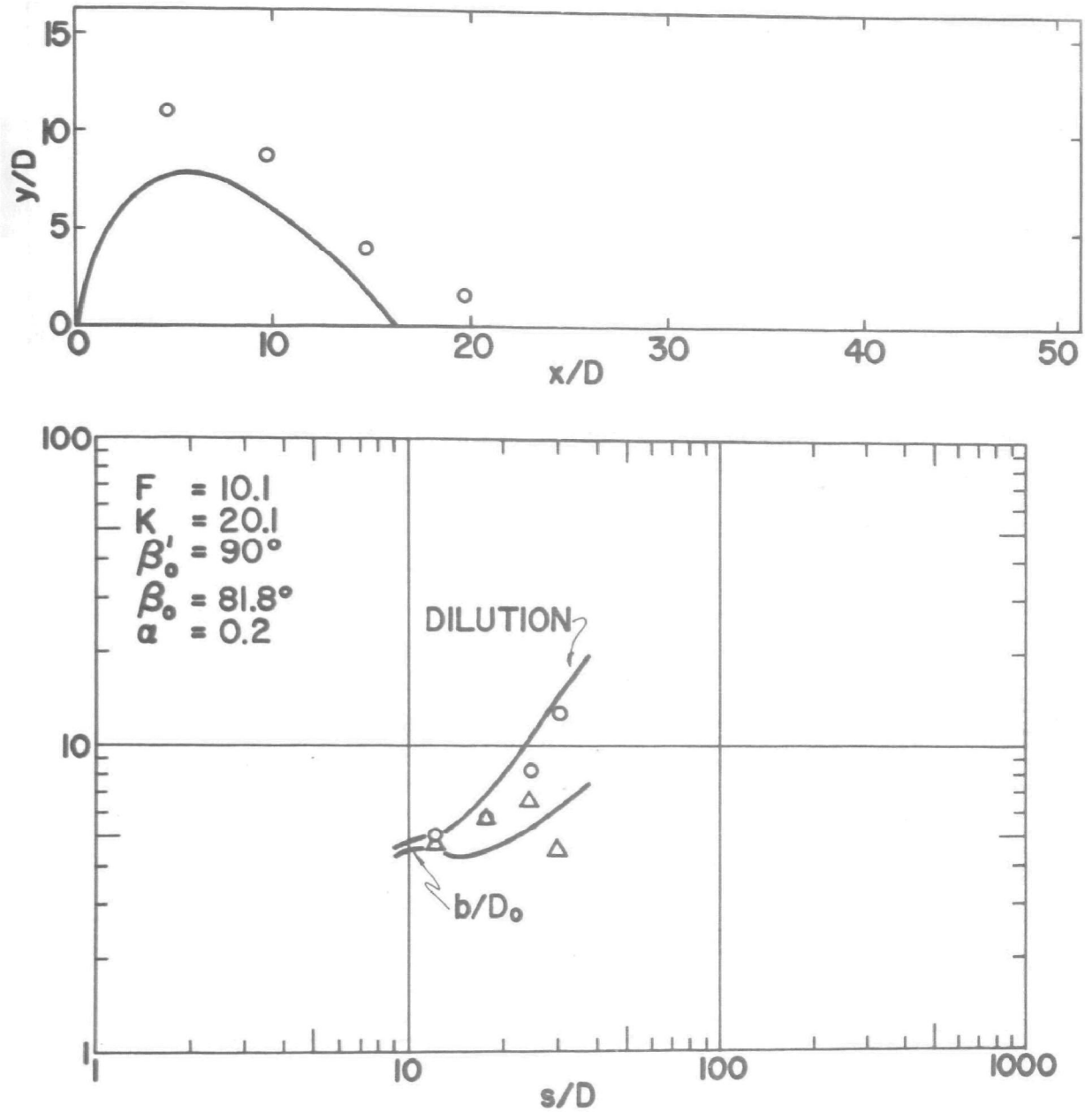

FIGURE 52 - OBSERVED VALUES AND THEORETICAL CURVES PREDICTED BY FAN'S MODEL - RUN NO. 15

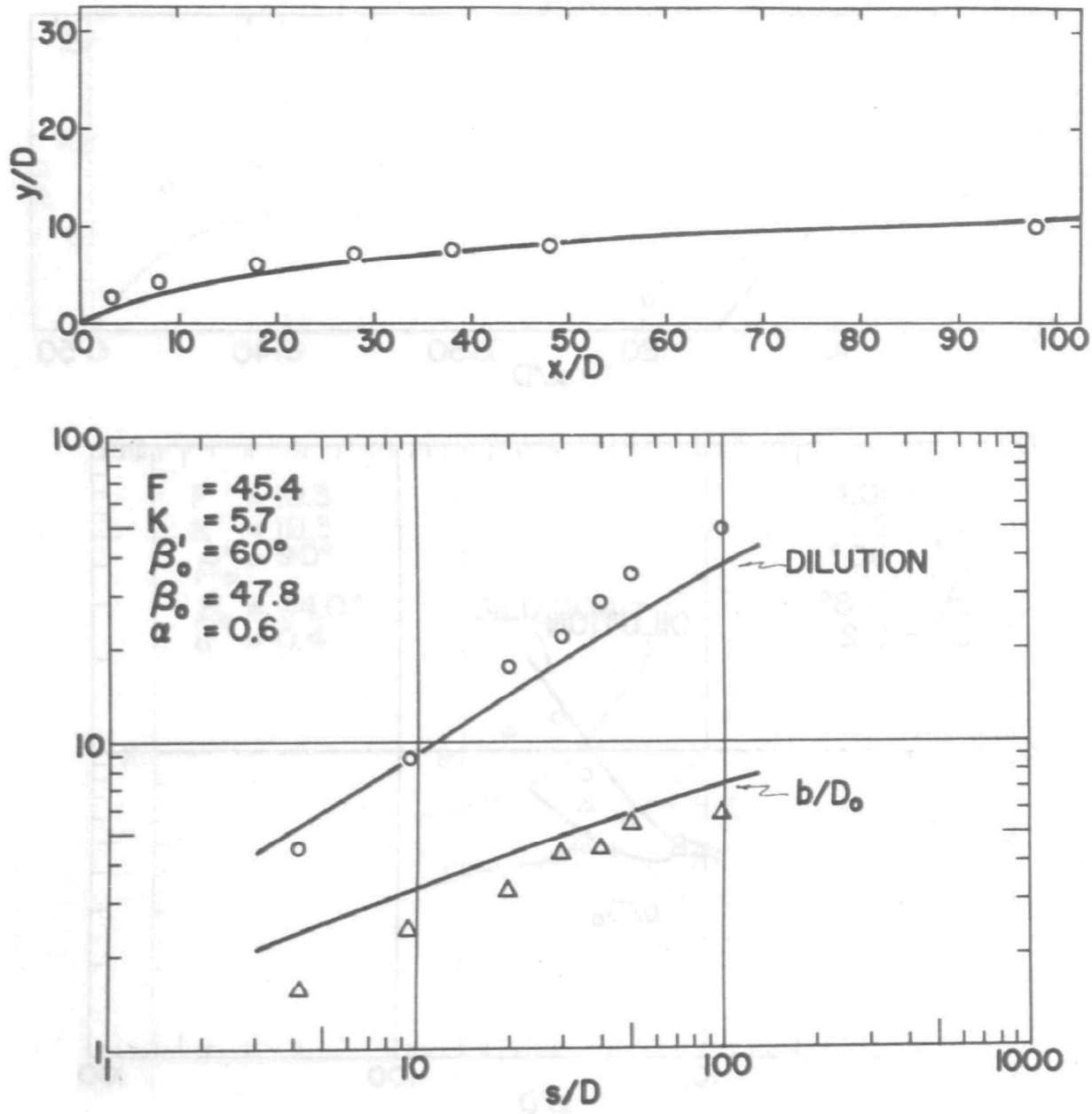

FIGURE 53 - OBSERVED VALUES AND THEORETICAL CURVES PREDICTED BY FAN'S MODEL - RUN NO. 34

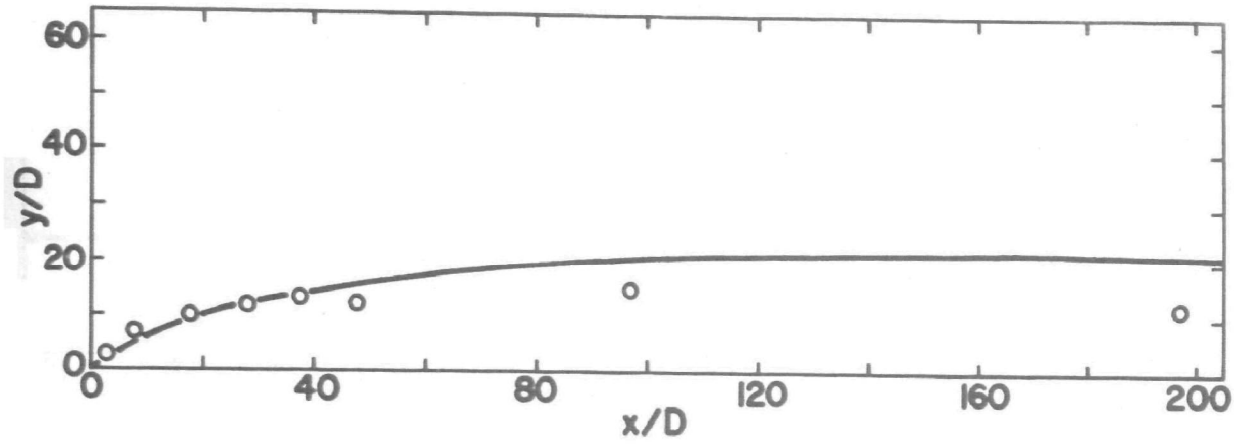

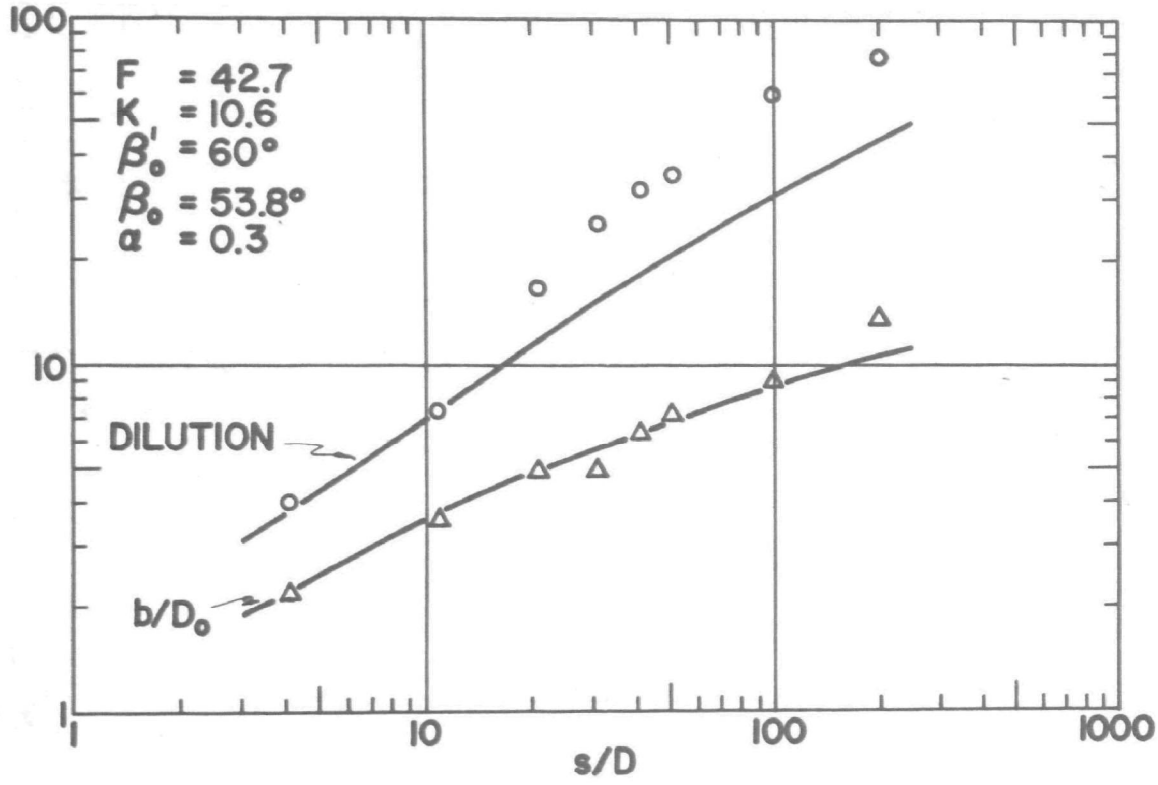

FIGURE 54 - OBSERVED VALUES AND THEORETICAL CURVES
PREDICTED BY FAN'S MODEL - RUN NO. 33

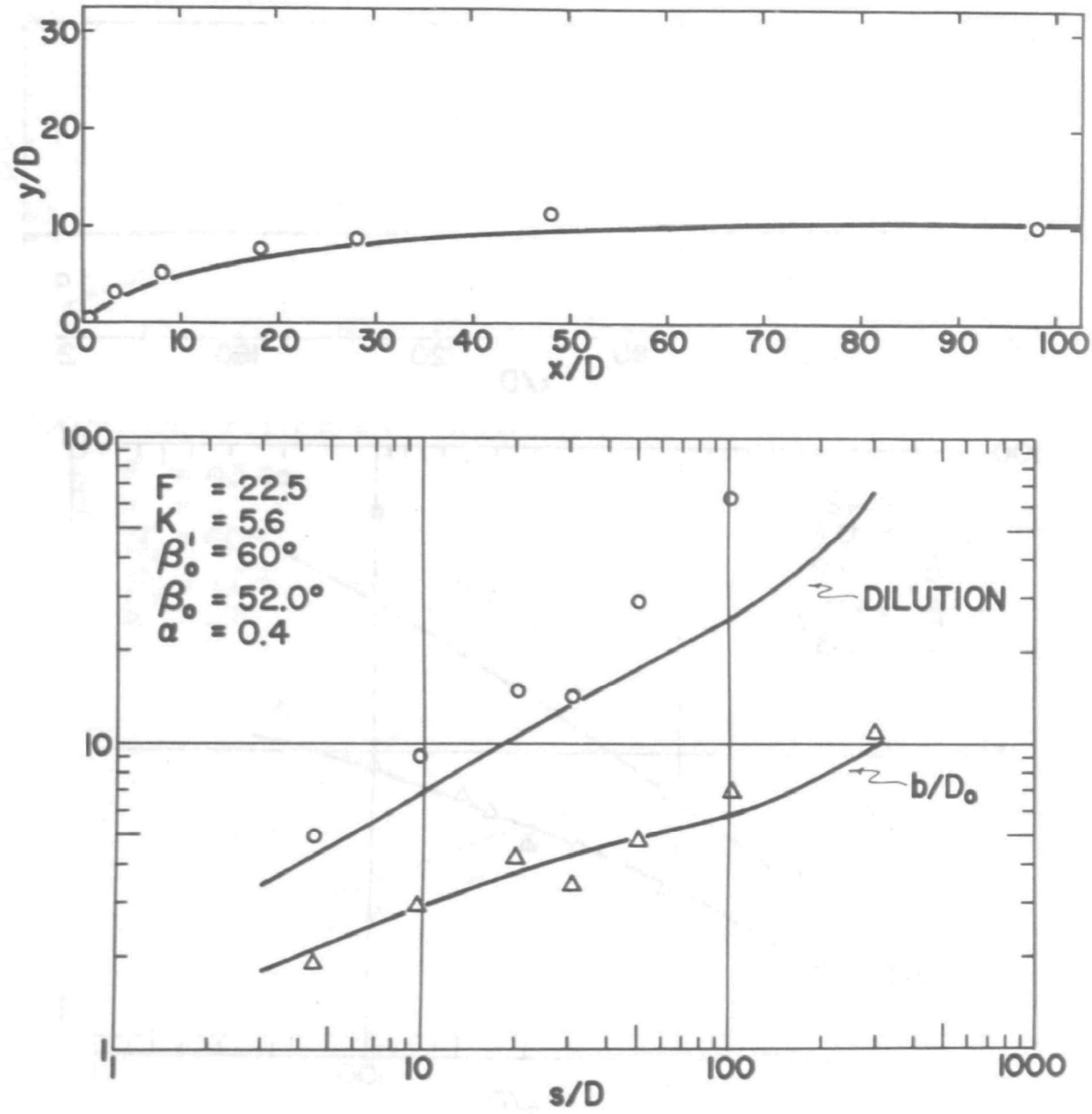

FIGURE 55 - OBSERVED VALUES AND THEORETICAL CURVES PREDICTED BY FAN'S MODEL - RUN NO. 32

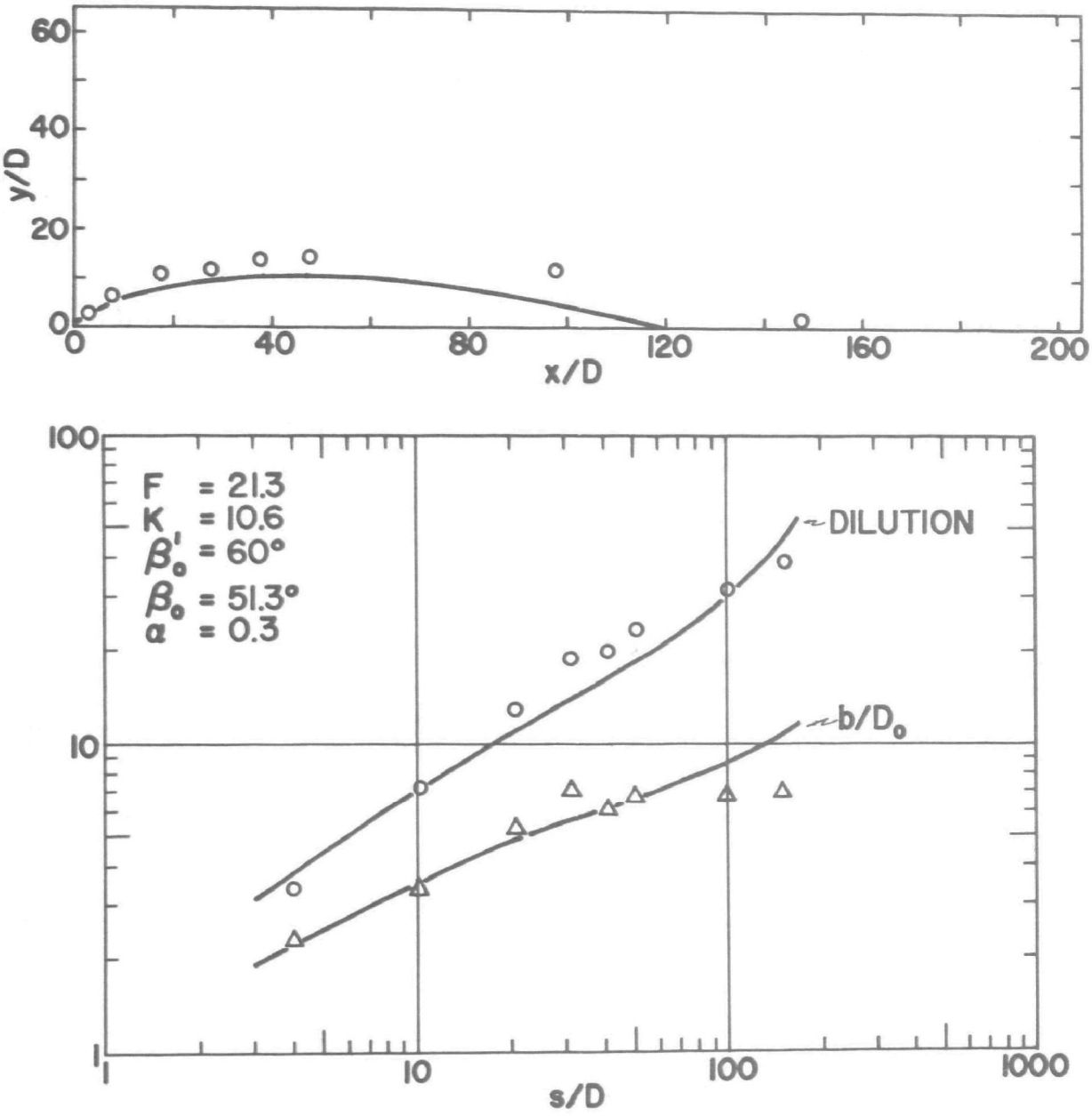

FIGURE 56 - OBSERVED VALUES AND THEORETICAL CURVES
PREDICTED BY FAN'S MODEL - RUN NO. 28

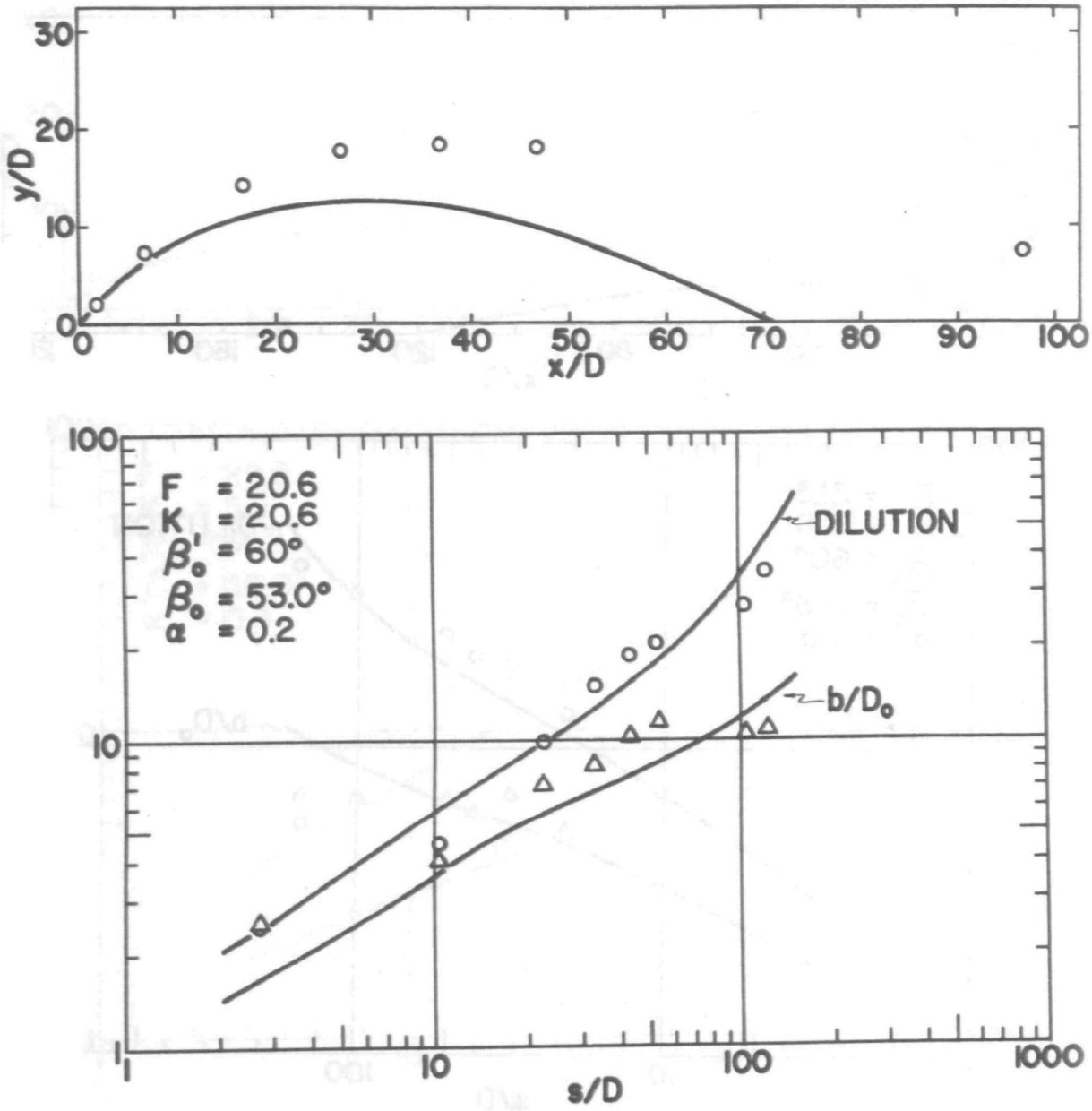

FIGURE 57 - OBSERVED VALUES AND THEORETICAL CURVES PREDICTED BY FAN'S MODEL - RUN NO. 30

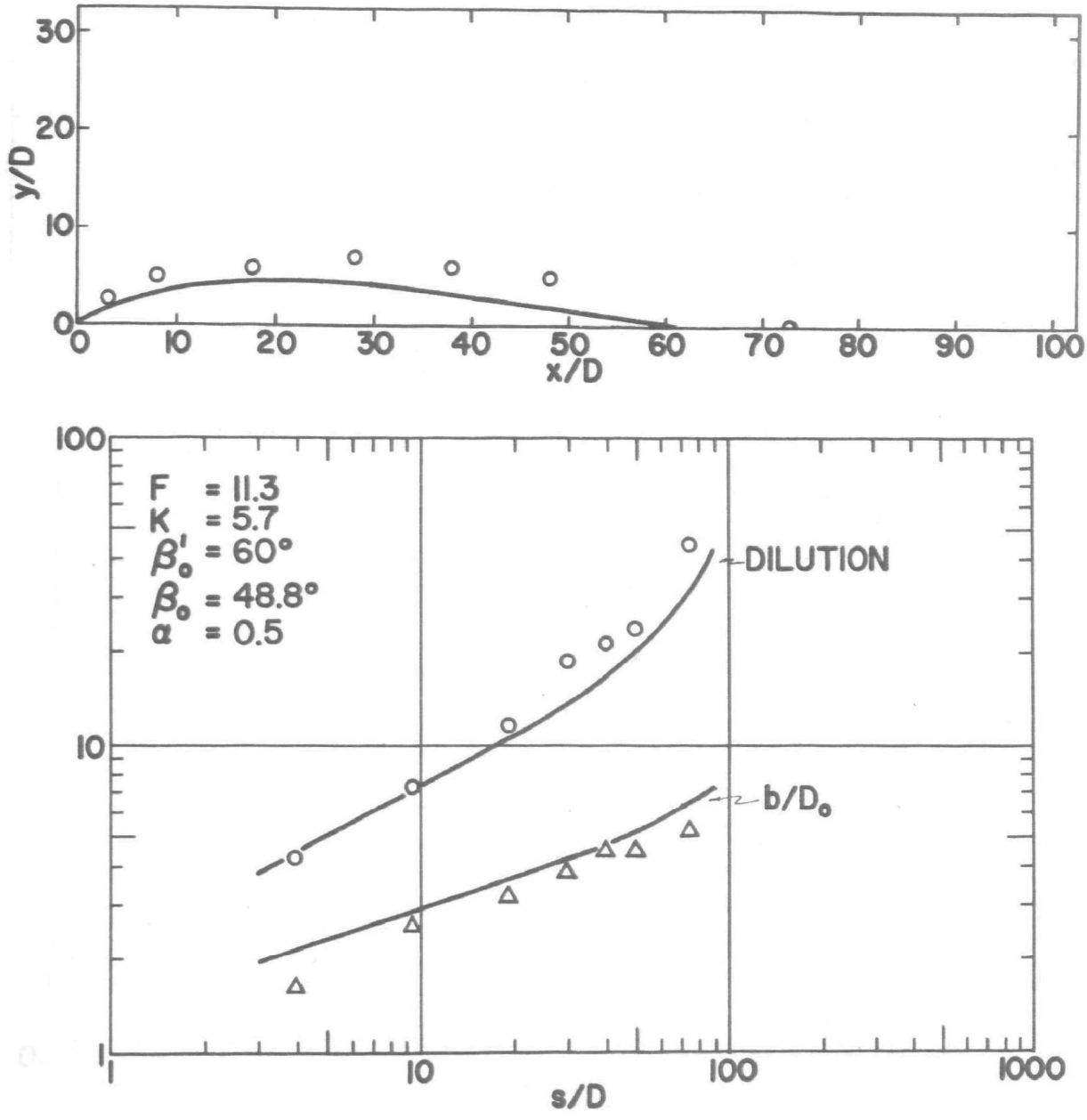

FIGURE 58 - OBSERVED VALUES AND THEORETICAL CURVES PREDICTED BY FAN'S MODEL - RUN NO. 27

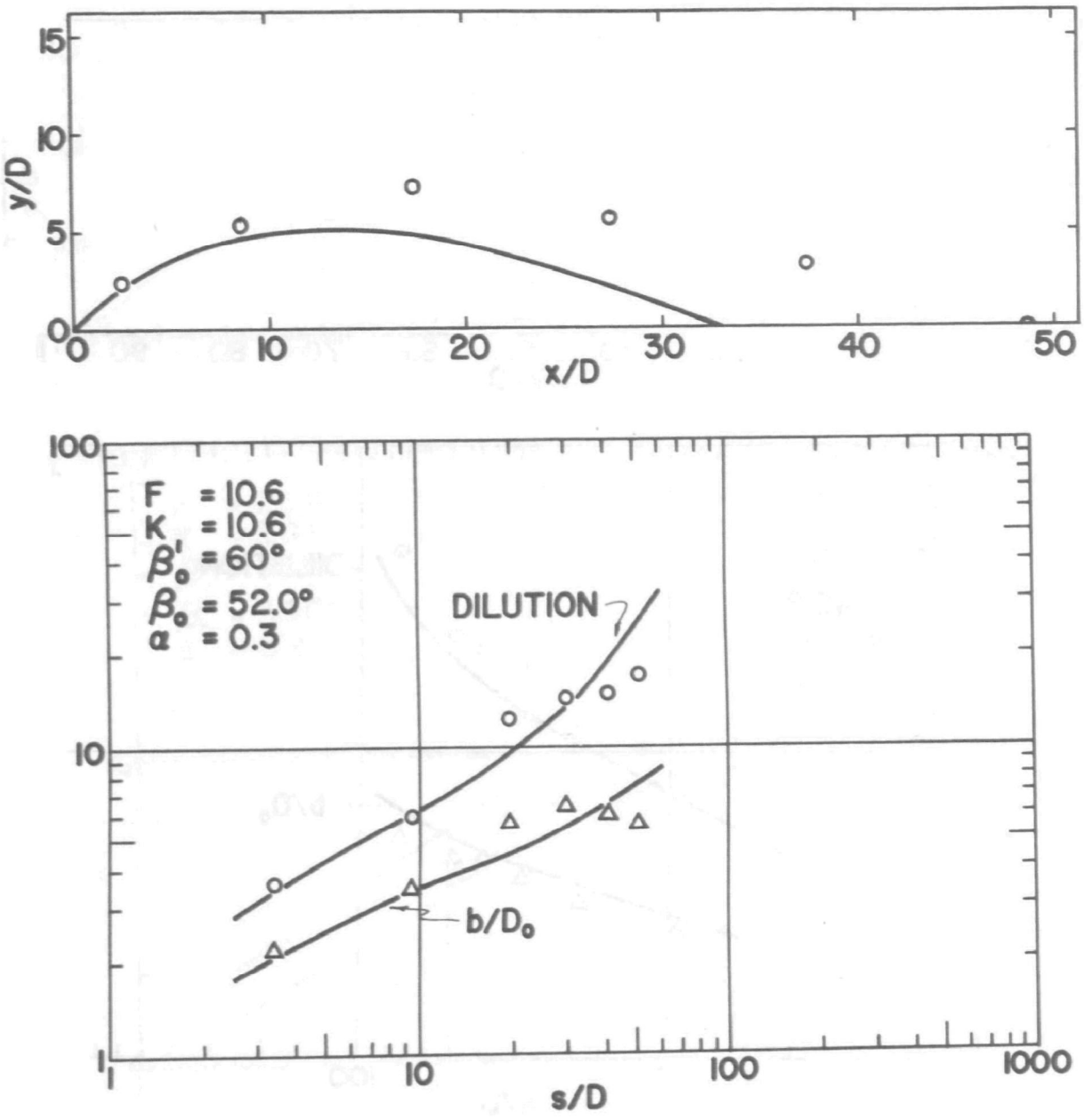

FIGURE 59 - OBSERVED VALUES AND THEORETICAL CURVES PREDICTED BY FAN'S MODEL - RUN NO. 29

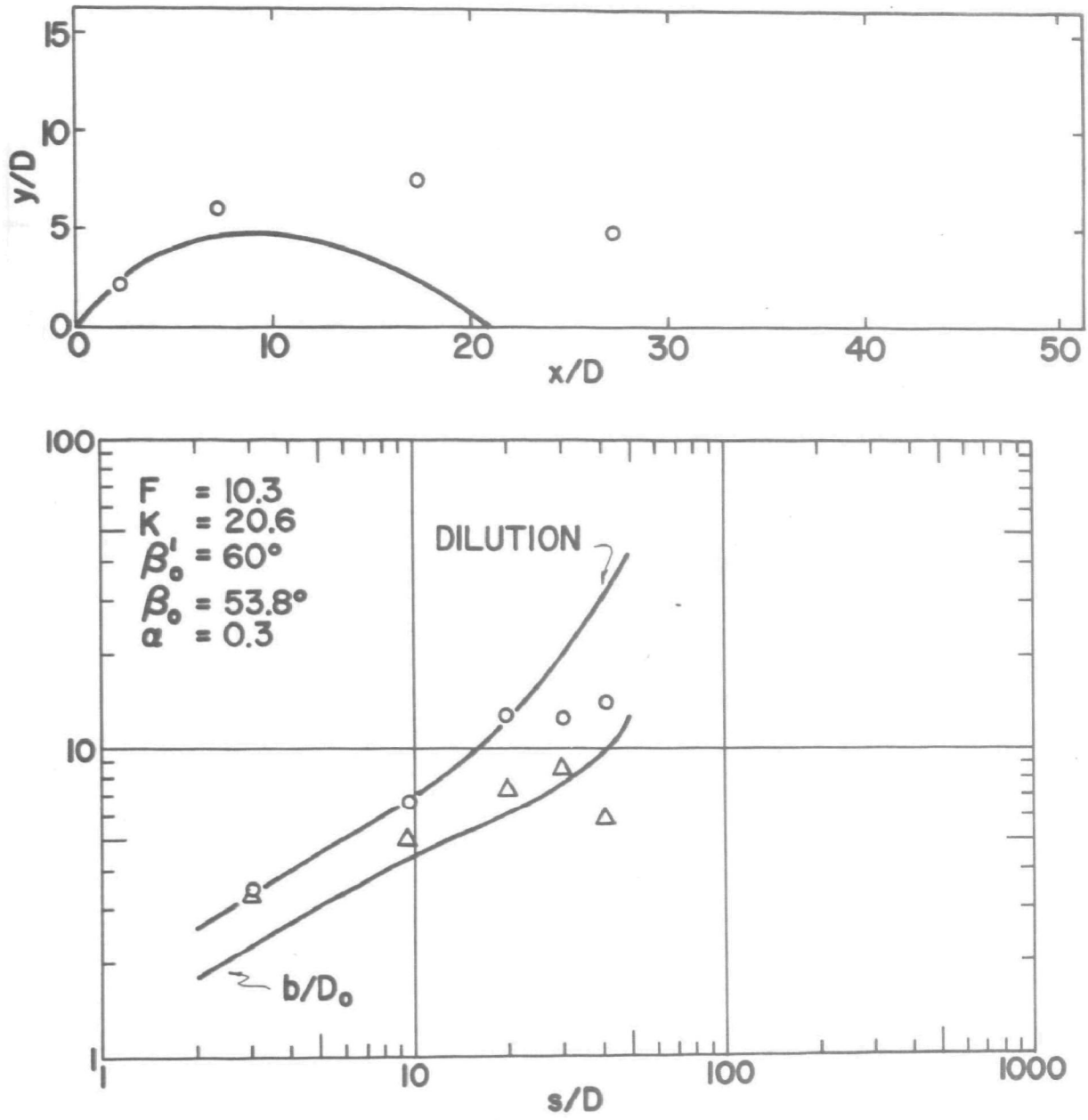

FIGURE 60 - OBSERVED VALUES AND THEORETICAL CURVES
PREDICTED BY FAN'S MODEL - RUN NO. 31

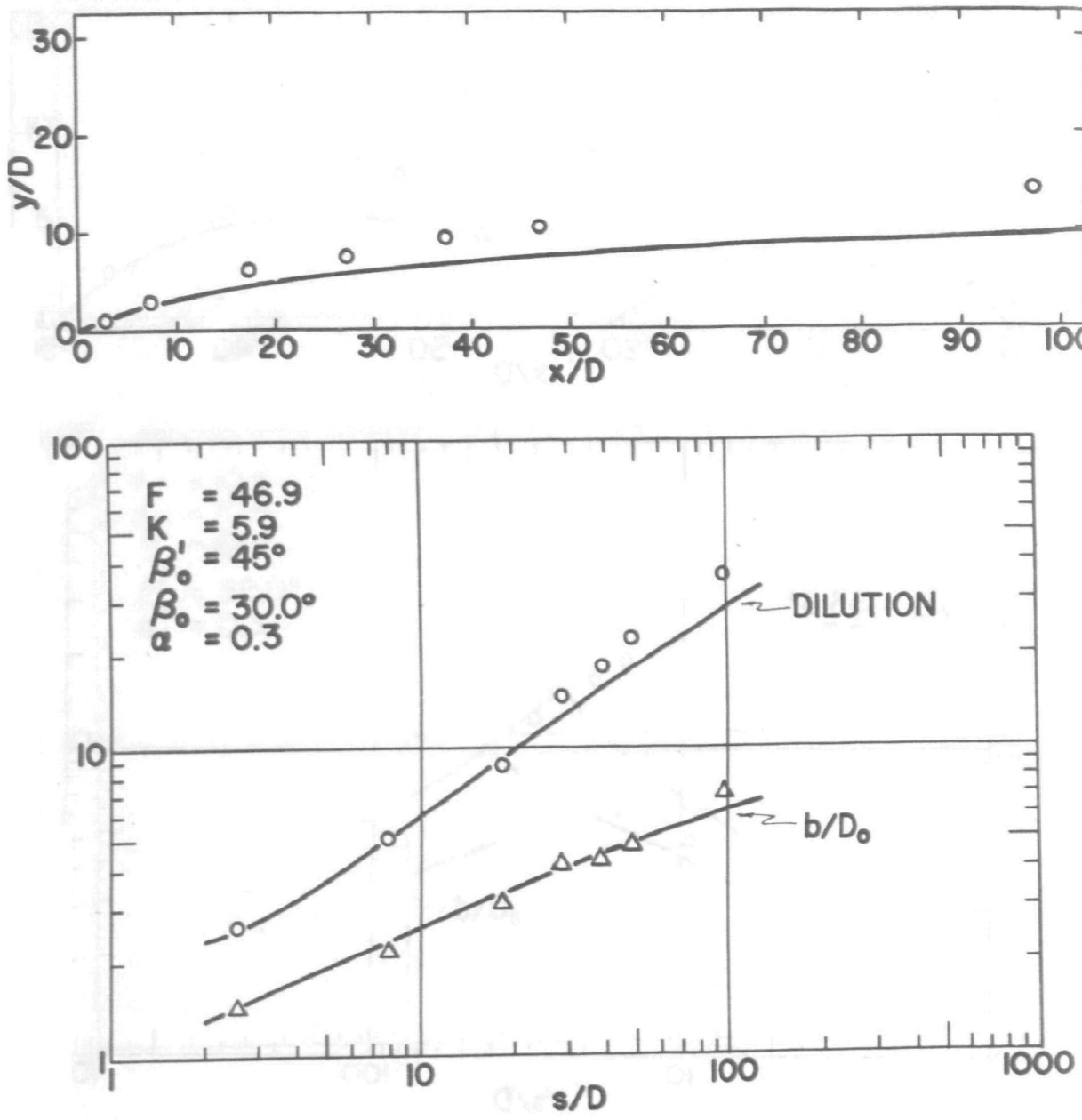

FIGURE 61 - OBSERVED VALUES AND THEORETICAL CURVES PREDICTED BY FAN'S MODEL - RUN NO. 26

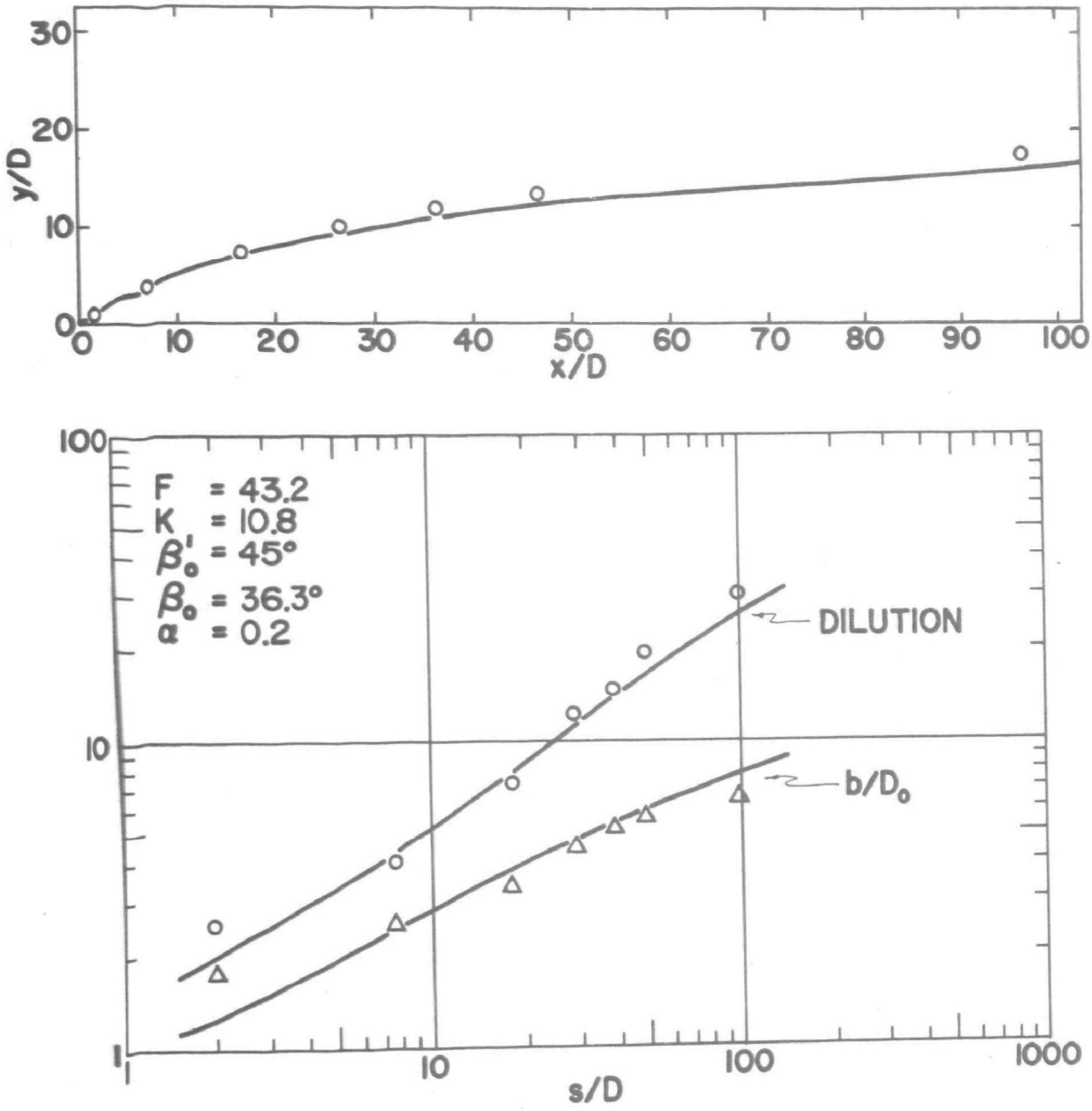

FIGURE 62 - OBSERVED VALUES AND THEORETICAL CURVES
PREDICTED BY FAN'S MODEL - RUN NO. 22

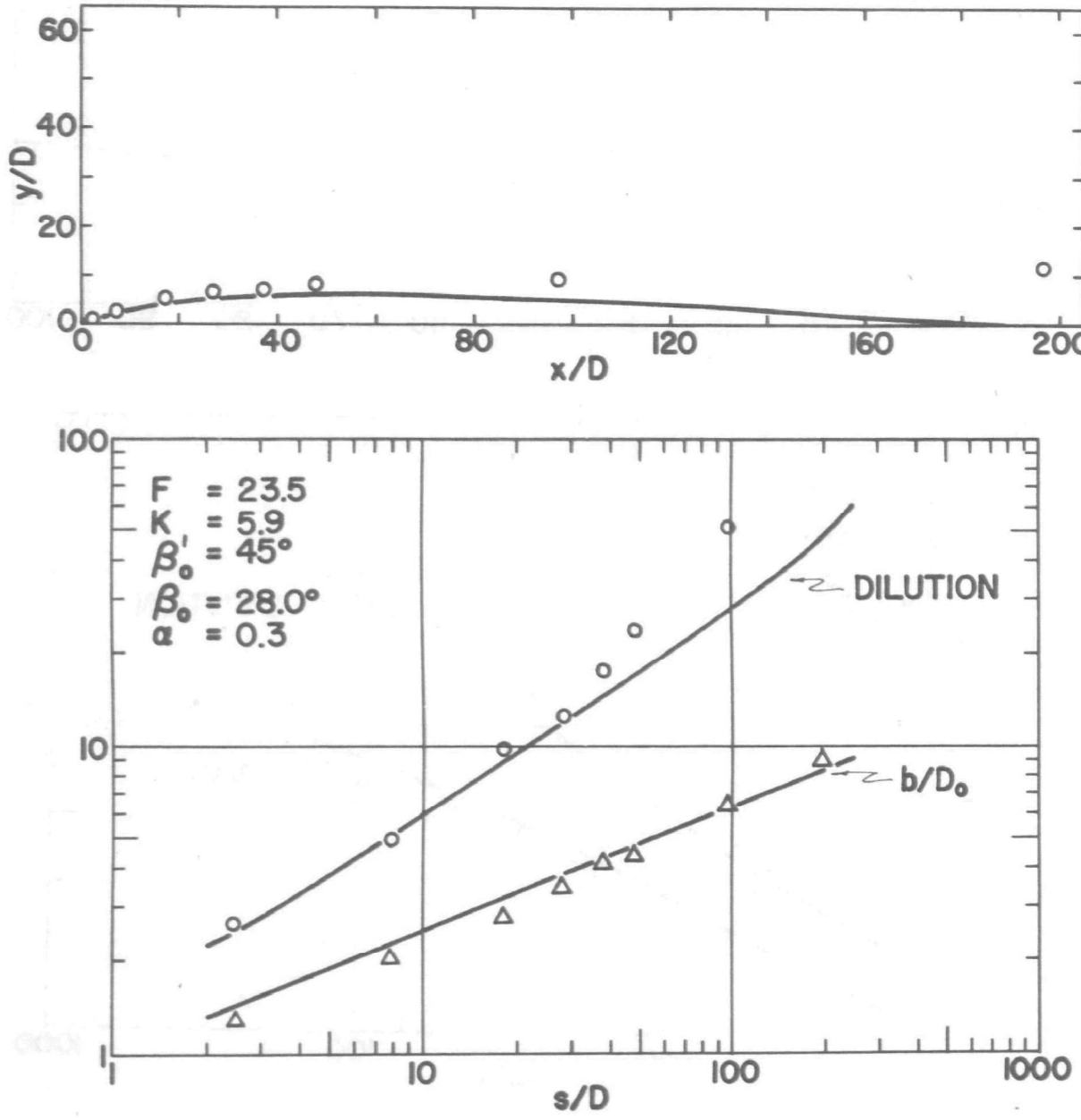

FIGURE 63 - OBSERVED VALUES AND THEORETICAL CURVES PREDICTED BY FAN'S MODEL - RUN NO. 21

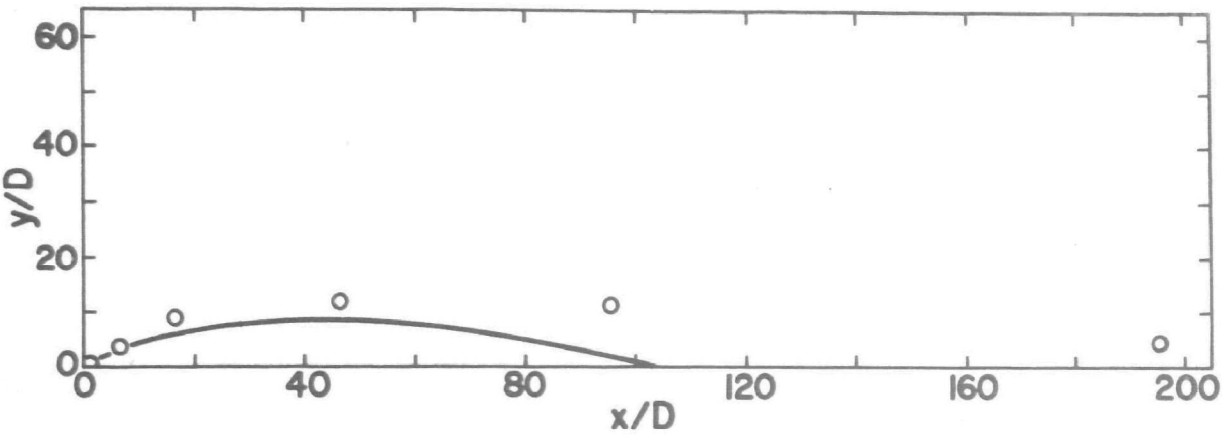

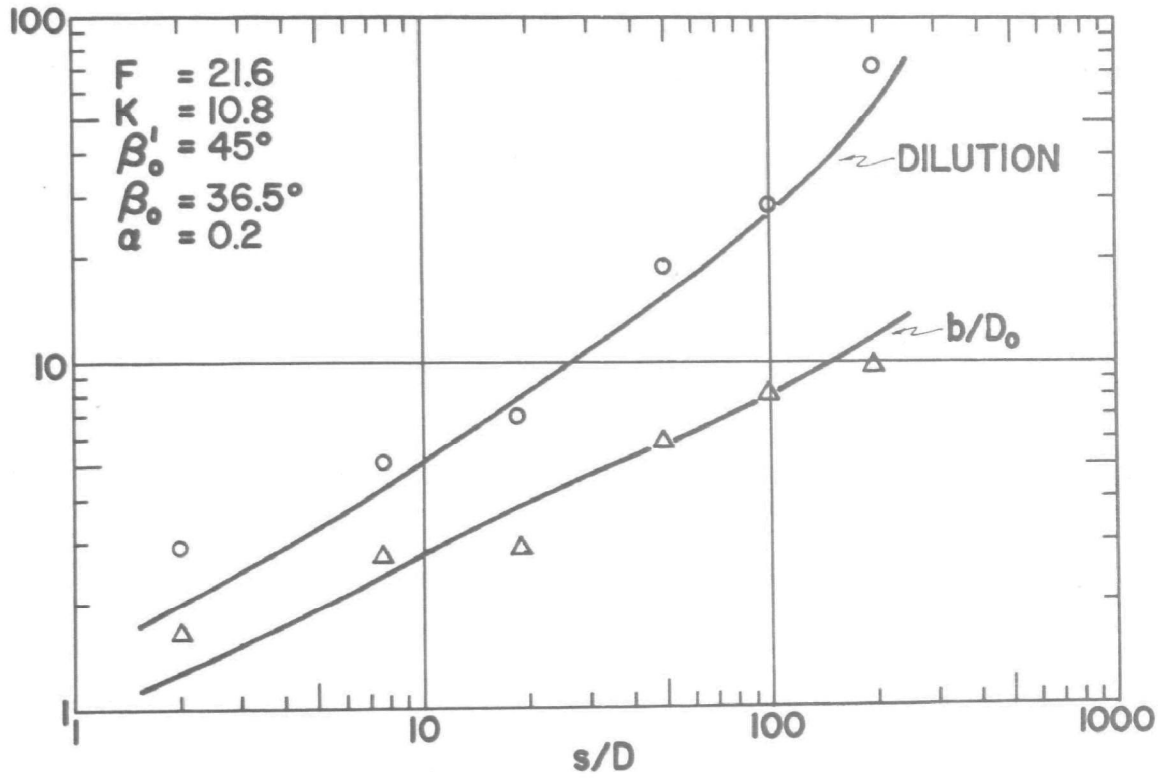

FIGURE 64 - OBSERVED VALUES AND THEORETICAL CURVES
PREDICTED BY FAN'S MODEL - RUN NO. 20

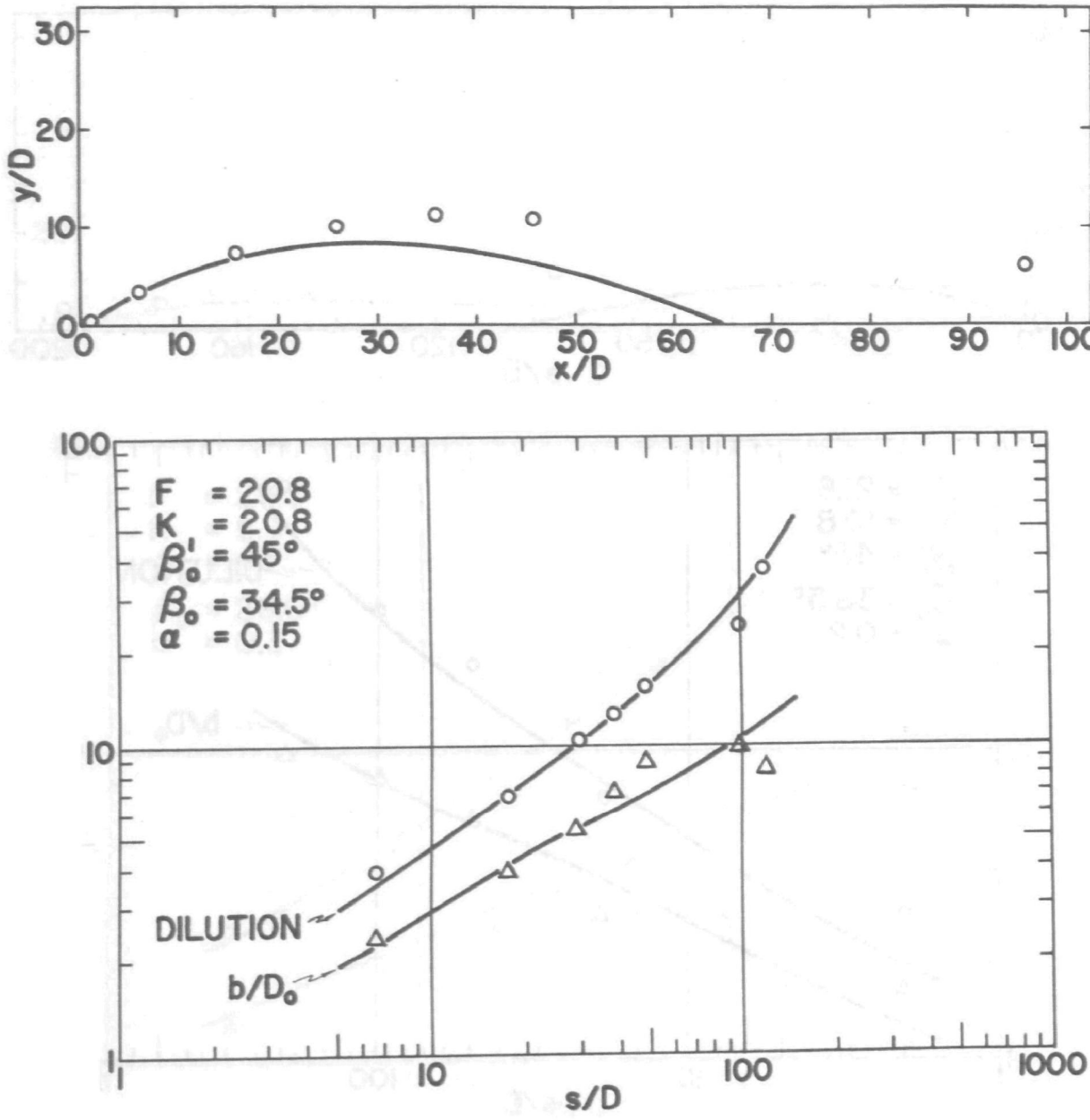

FIGURE 65 - OBSERVED VALUES AND THEORETICAL CURVES PREDICTED BY FAN'S MODEL - RUN NO. 24

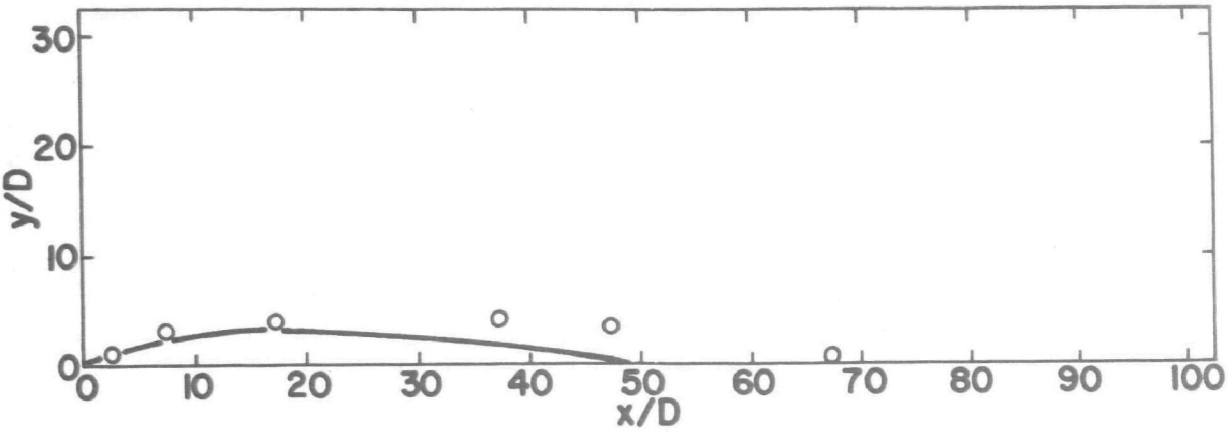

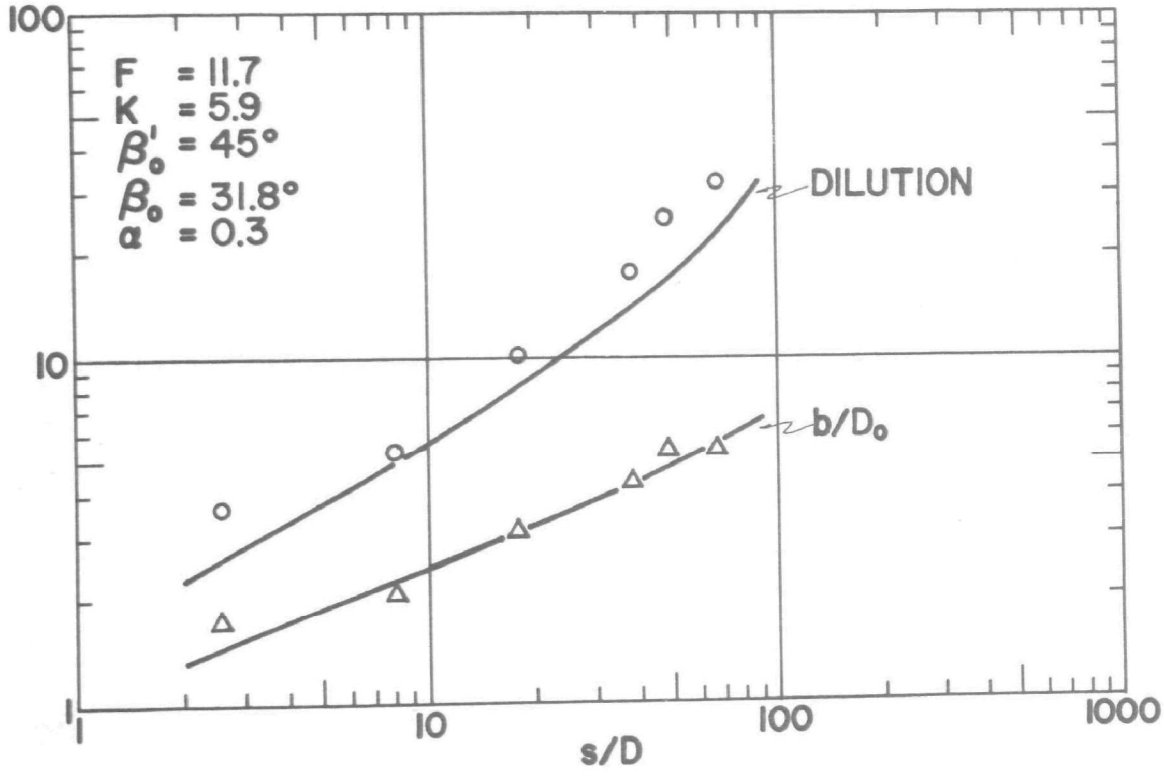

FIGURE 66 - OBSERVED VALUES AND THEORETICAL CURVES
PREDICTED BY FAN'S MODEL - RUN NO. 19

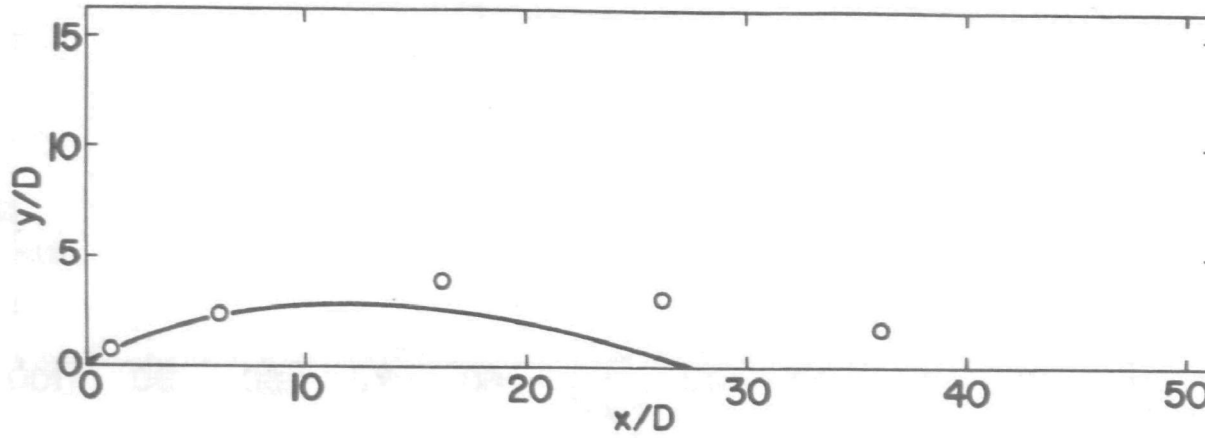

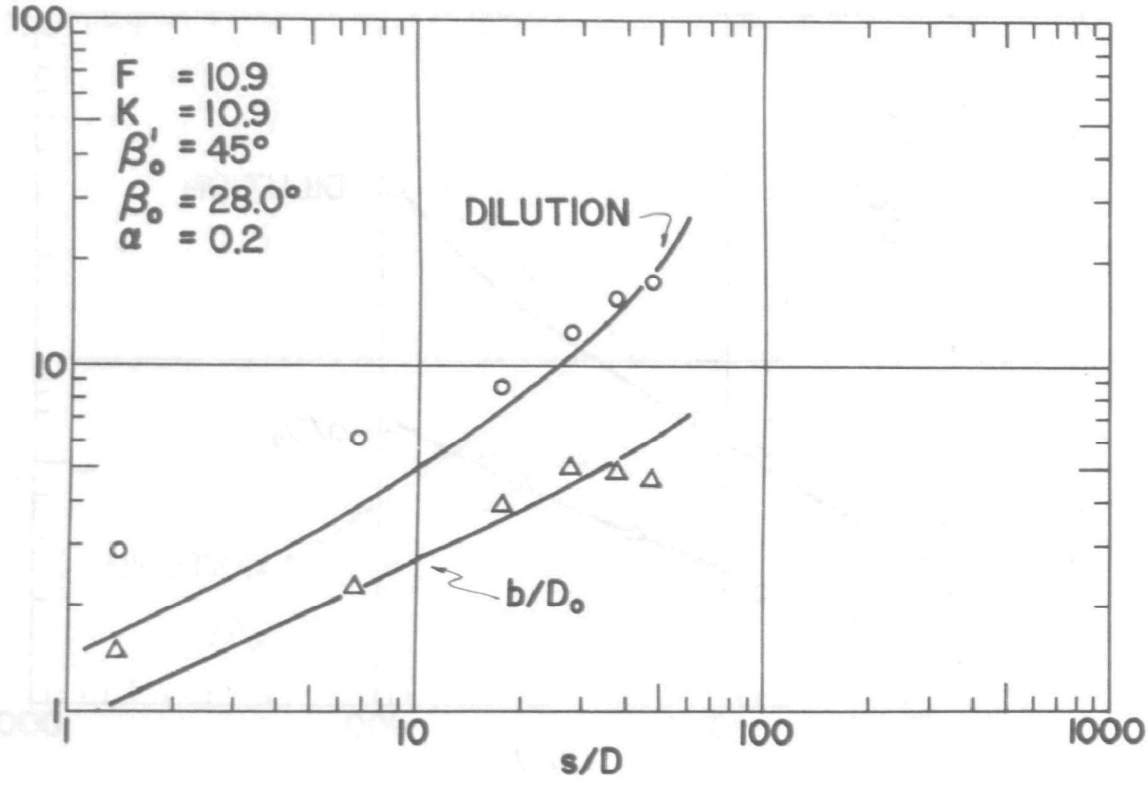

FIGURE 67 - OBSERVED VALUES AND THEORETICAL CURVES
PREDICTED BY FAN'S MODEL - RUN NO. 23

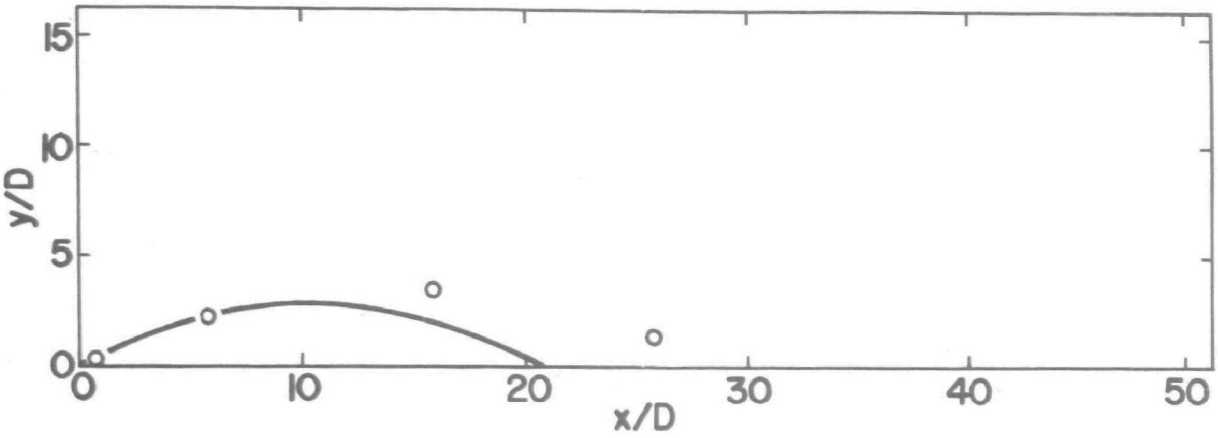

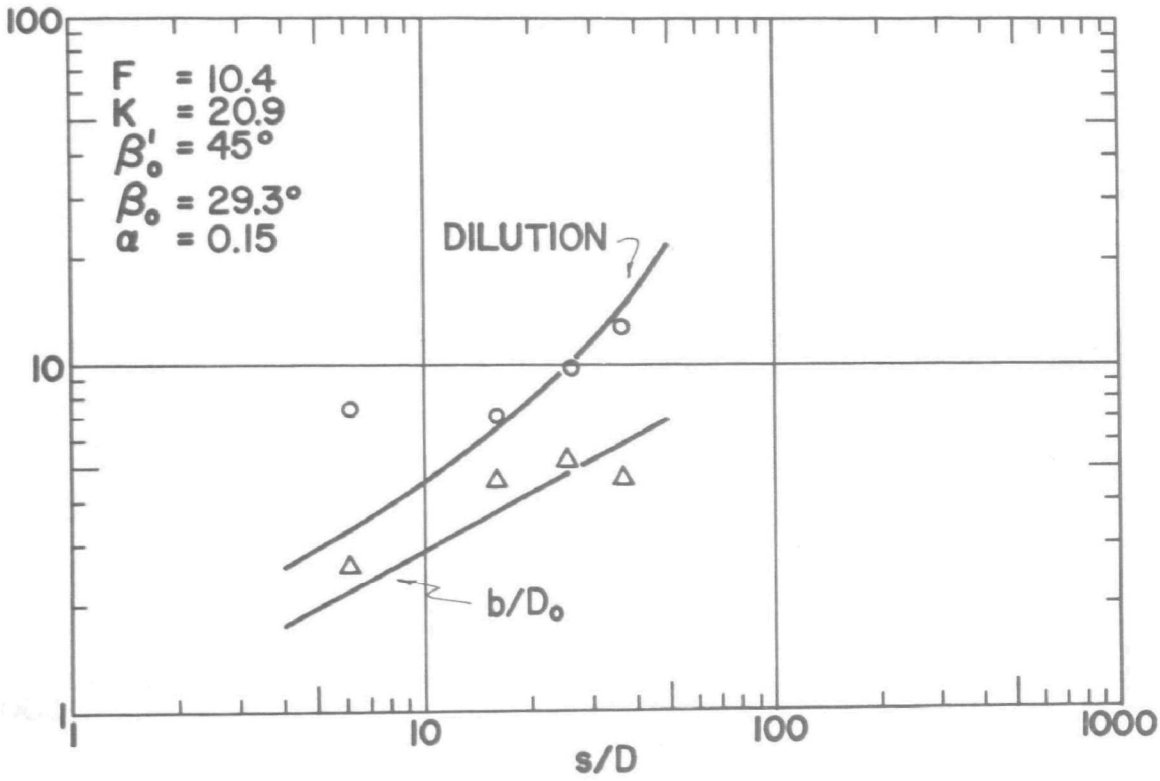

FIGURE 68 - OBSERVED VALUES AND THEORETICAL CURVES
PREDICTED BY FAN'S MODEL - RUN NO. 25

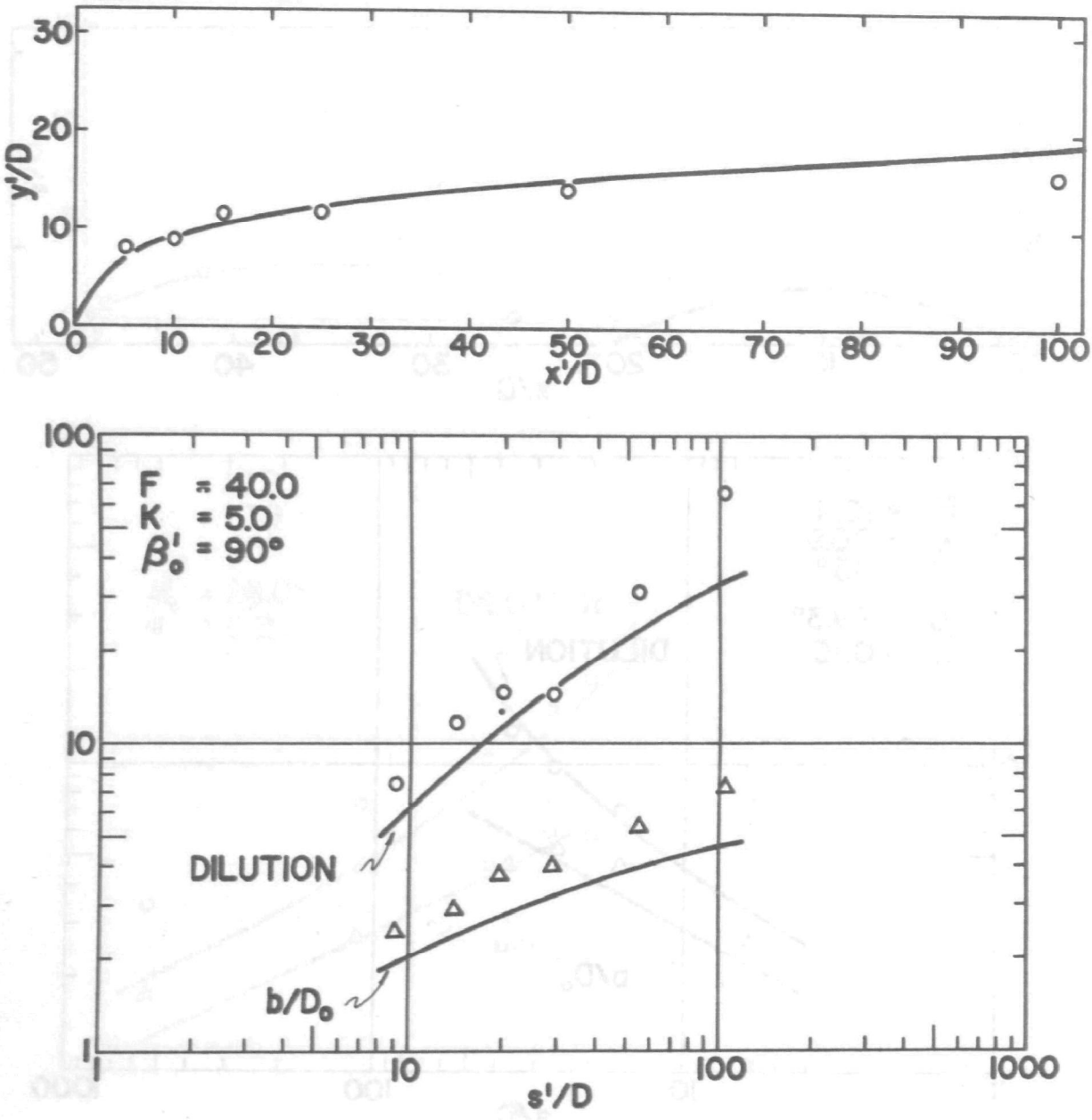

FIGURE 69 - OBSERVED VALUES AND THEORETICAL CURVES
PREDICTED BY ABRAHAM'S MODEL - RUN NO. 18

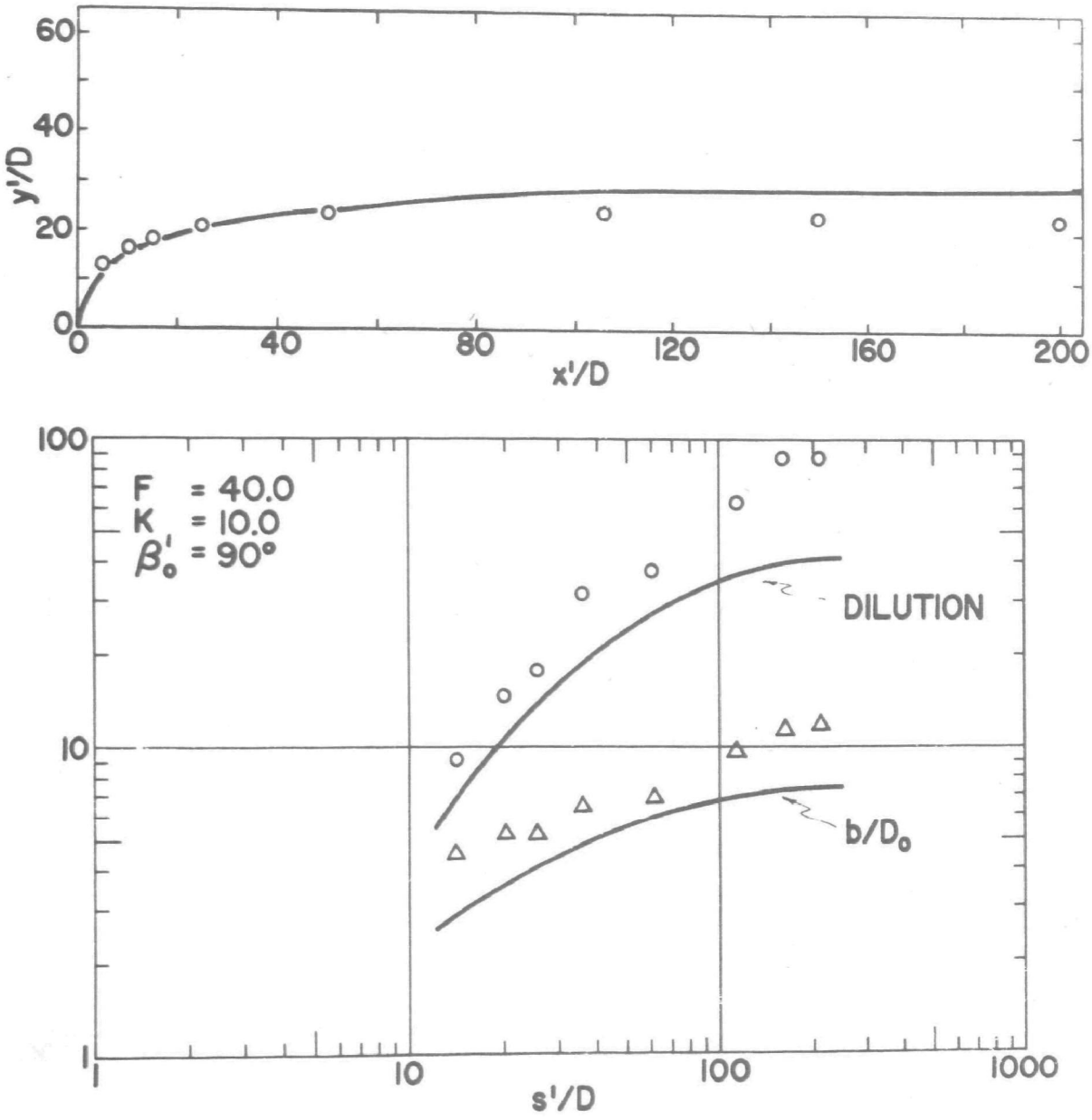

FIGURE 70 - OBSERVED VALUES AND THEORETICAL CURVES
PREDICTED BY ABRAHAM'S MODEL - RUN NO. 13

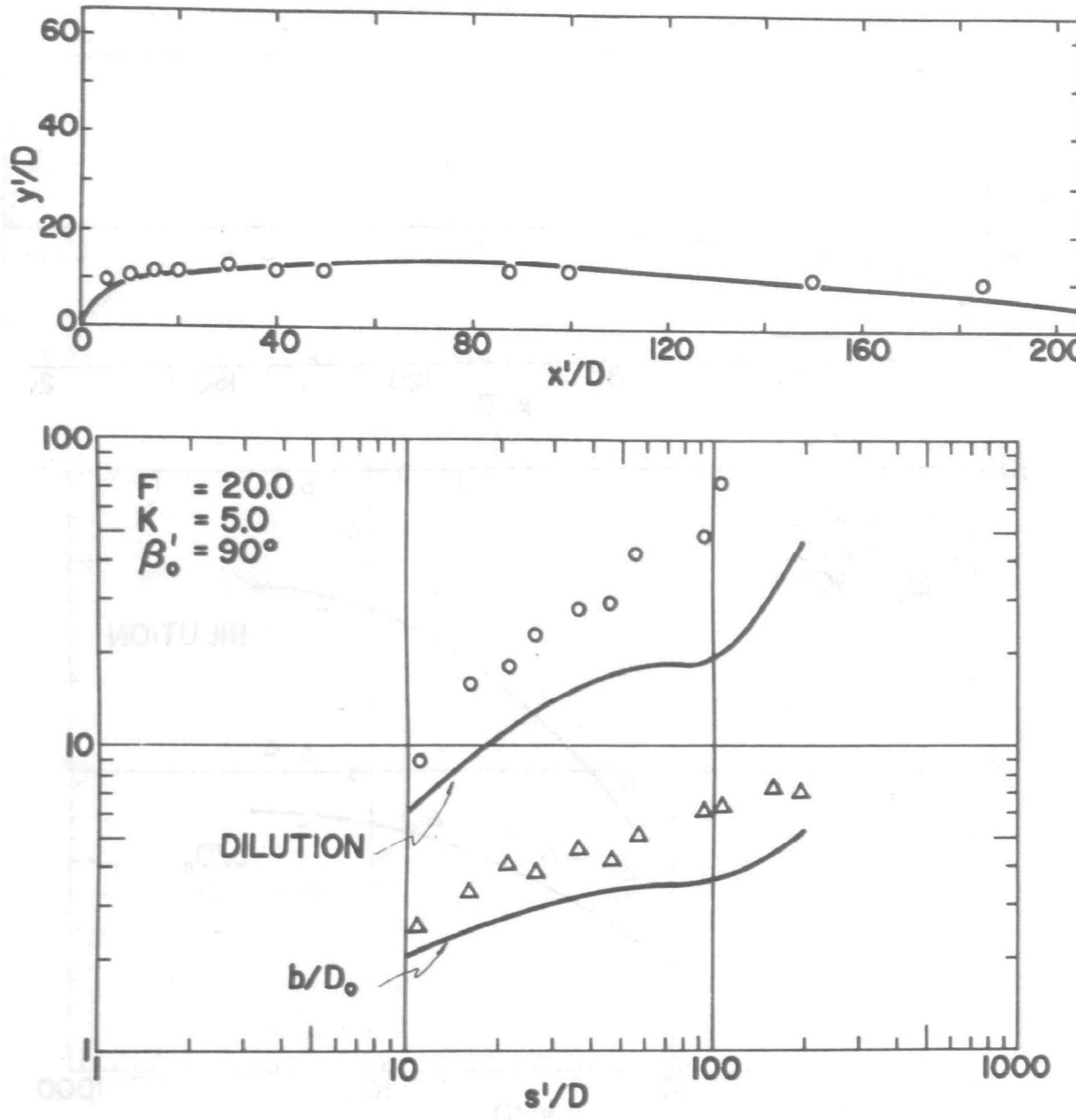

FIGURE 71 - OBSERVED VALUES AND THEORETICAL CURVES
PREDICTED BY ABRAHAM'S MODEL - RUN NO. 12

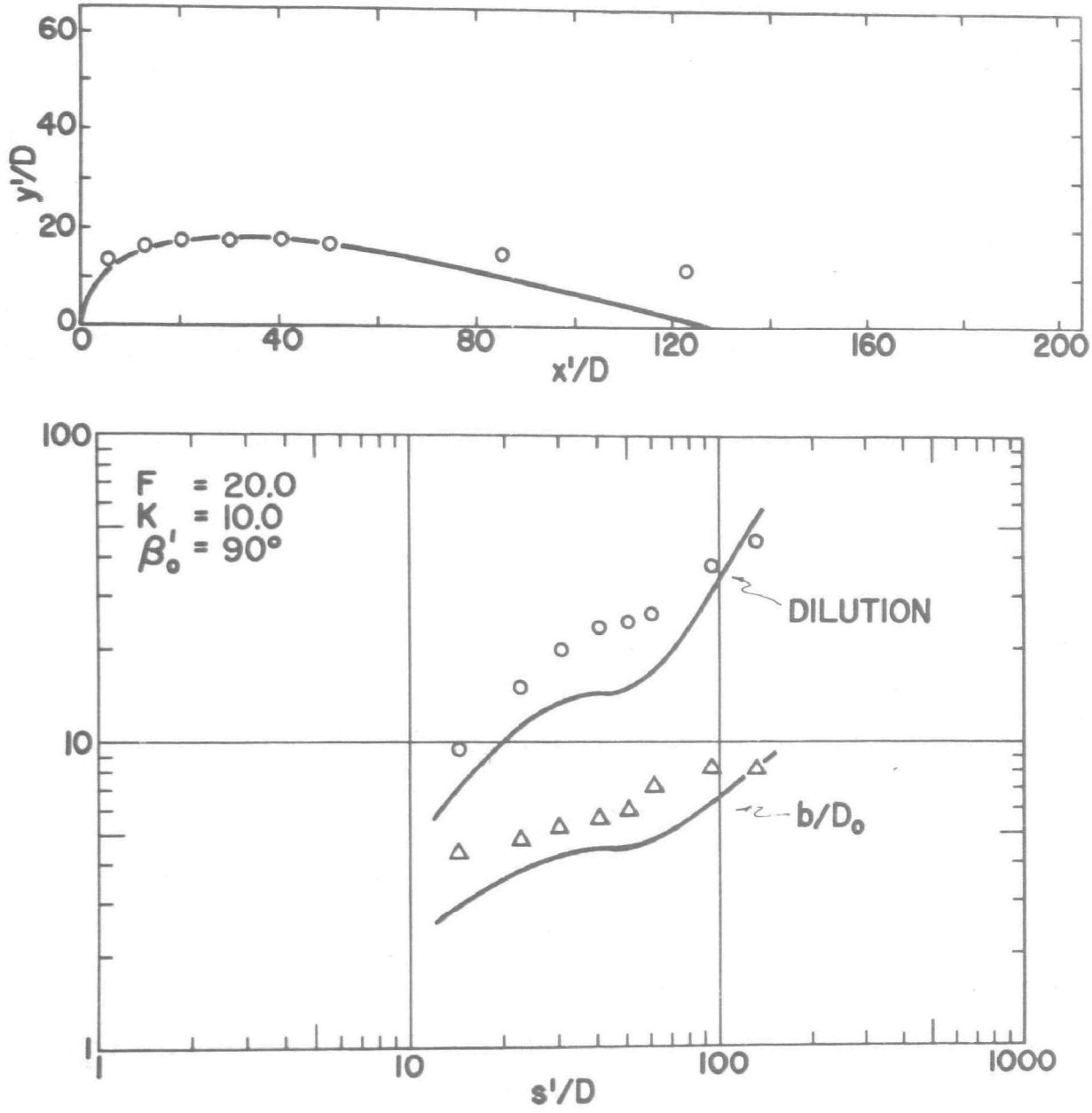

FIGURE 72 - OBSERVED VALUES AND THEORETICAL CURVES
PREDICTED BY ABRAHAM'S MODEL - RUN NO. 11

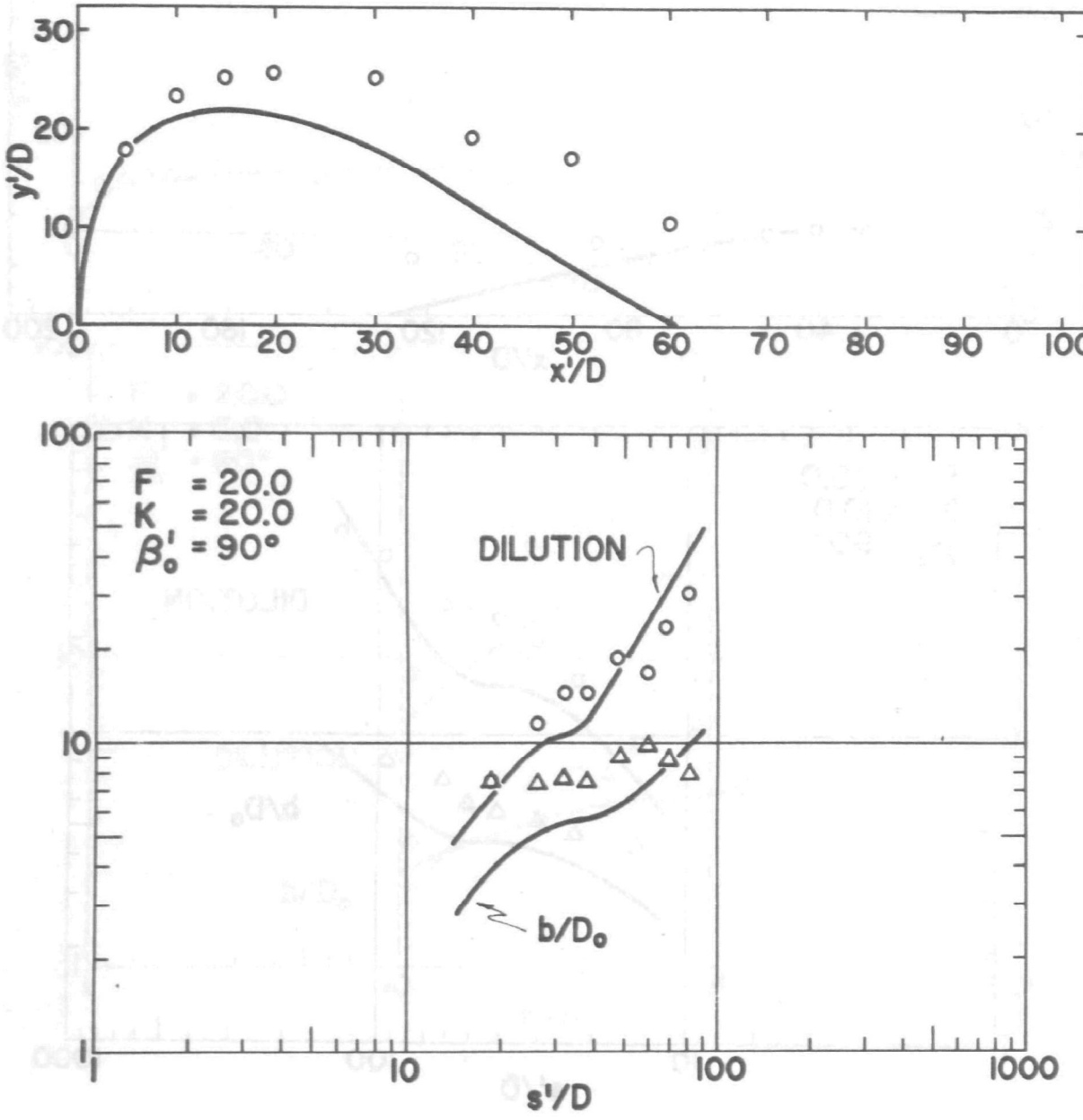

FIGURE 73 - OBSERVED VALUES AND THEORETICAL CURVES
PREDICTED BY ABRAHAM'S MODEL - RUN NO. 16

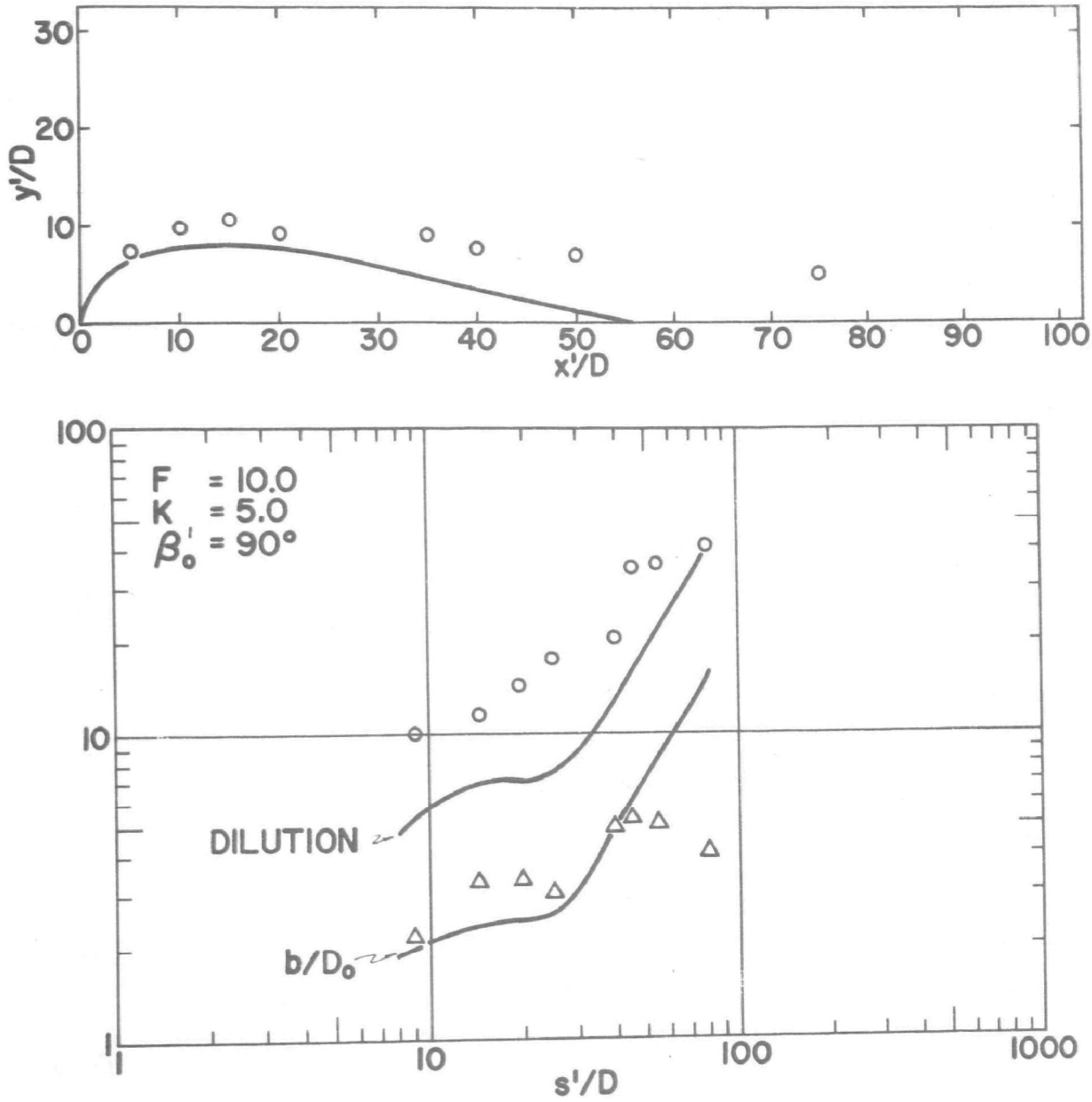

FIGURE 74 - OBSERVED VALUES AND THEORETICAL CURVES PREDICTED BY ABRAHAM'S MODEL - RUN NO. 10

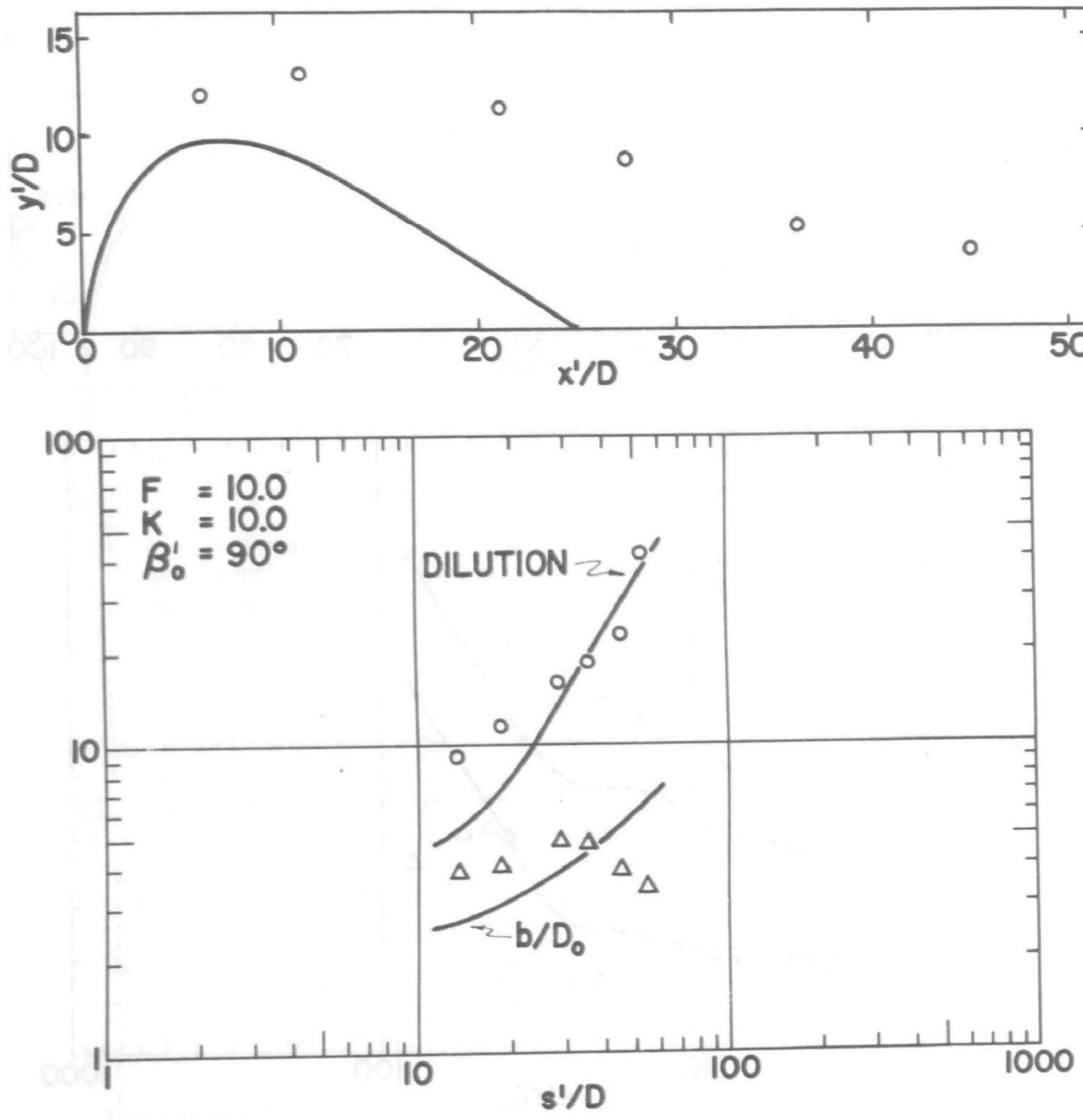

FIGURE 75 - OBSERVED VALUES AND THEORETICAL CURVES PREDICTED BY ABRAHAM'S MODEL - RUN NO. 9

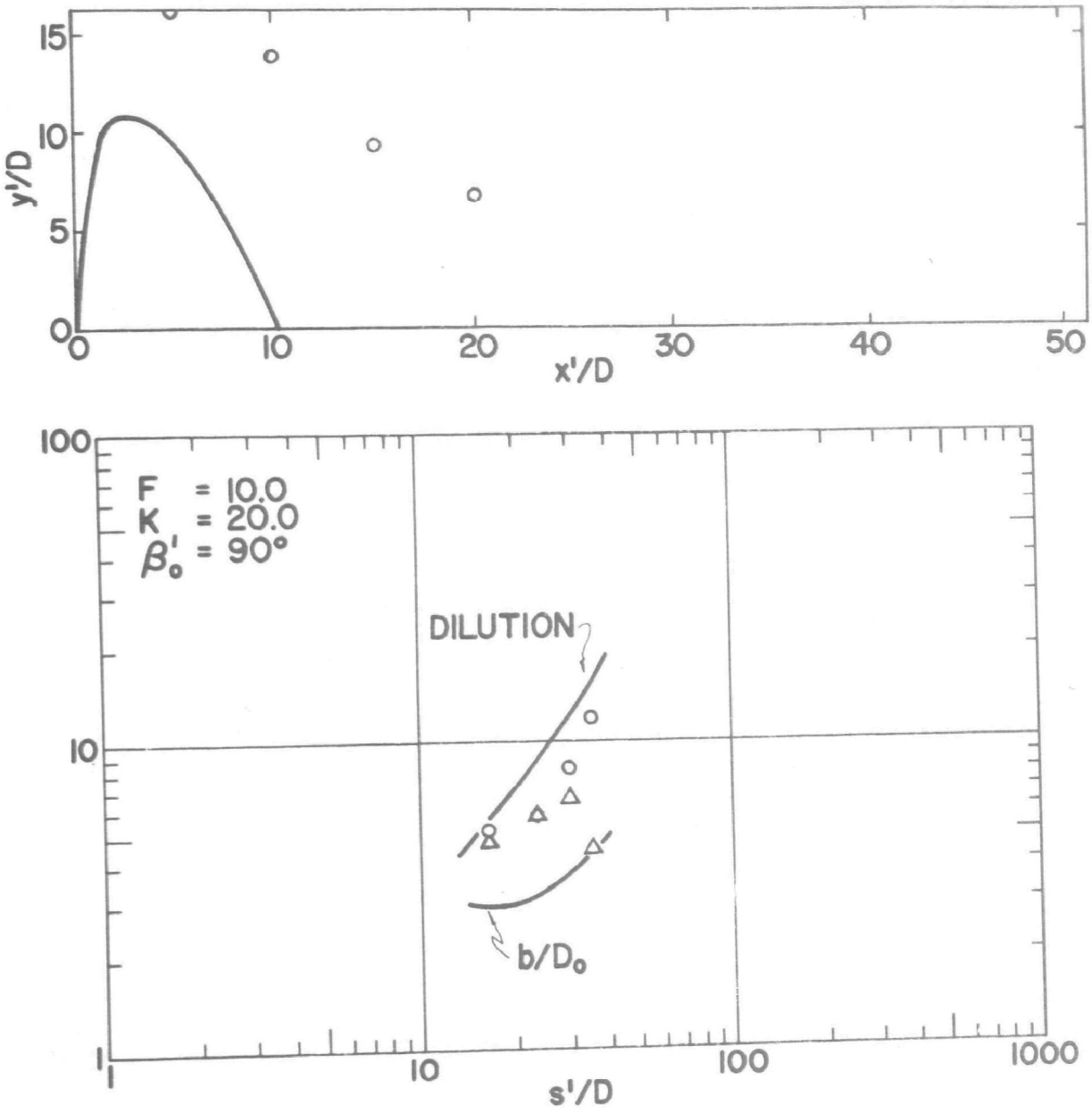

FIGURE 76 - OBSERVED VALUES AND THEORETICAL CURVES
PREDICTED BY ABRAHAM'S MODEL - RUN NO. 15

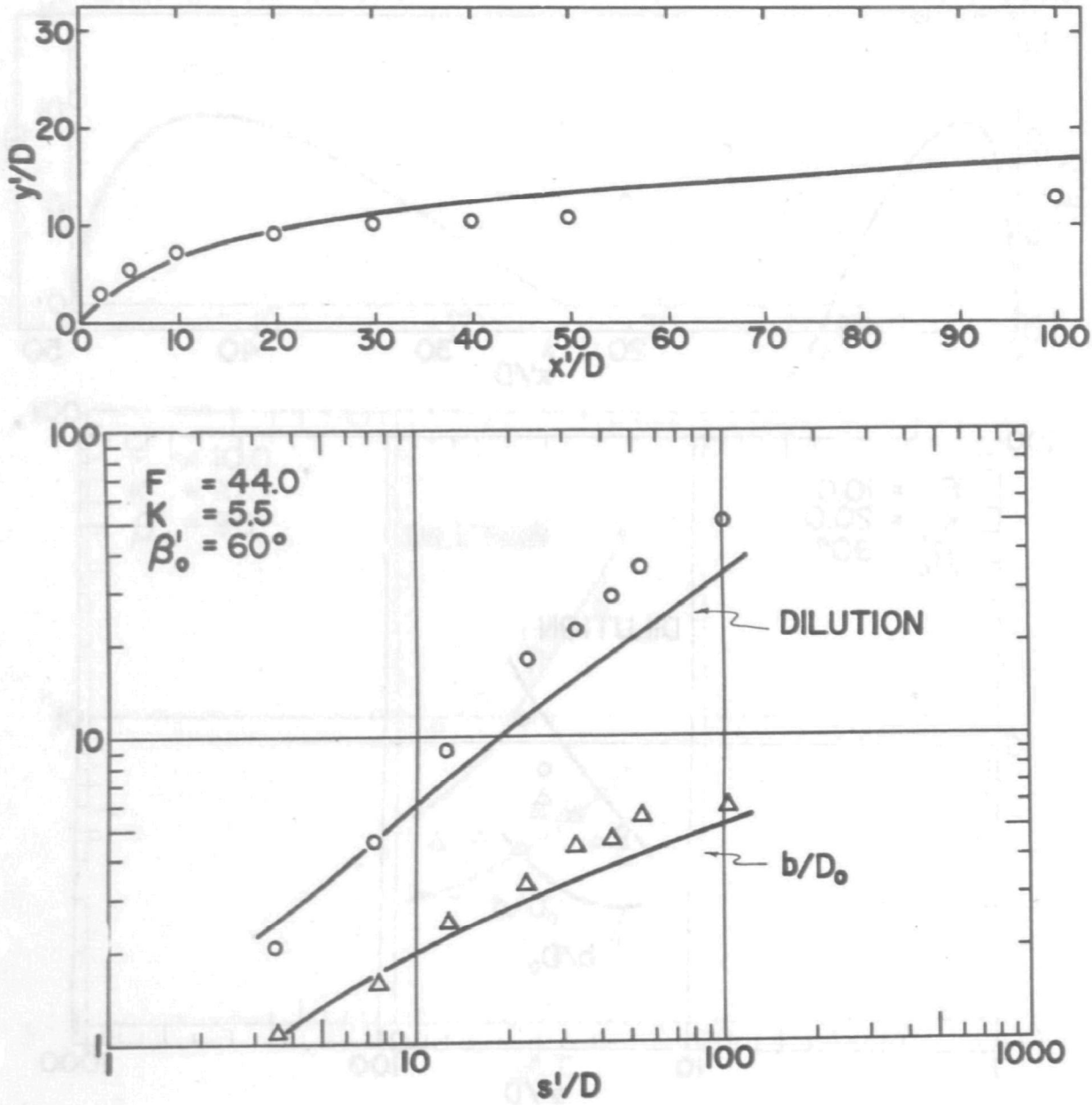

FIGURE 77 - OBSERVED VALUES AND THEORETICAL CURVES
PREDICTED BY ABRAHAM'S MODEL - RUN NO. 34

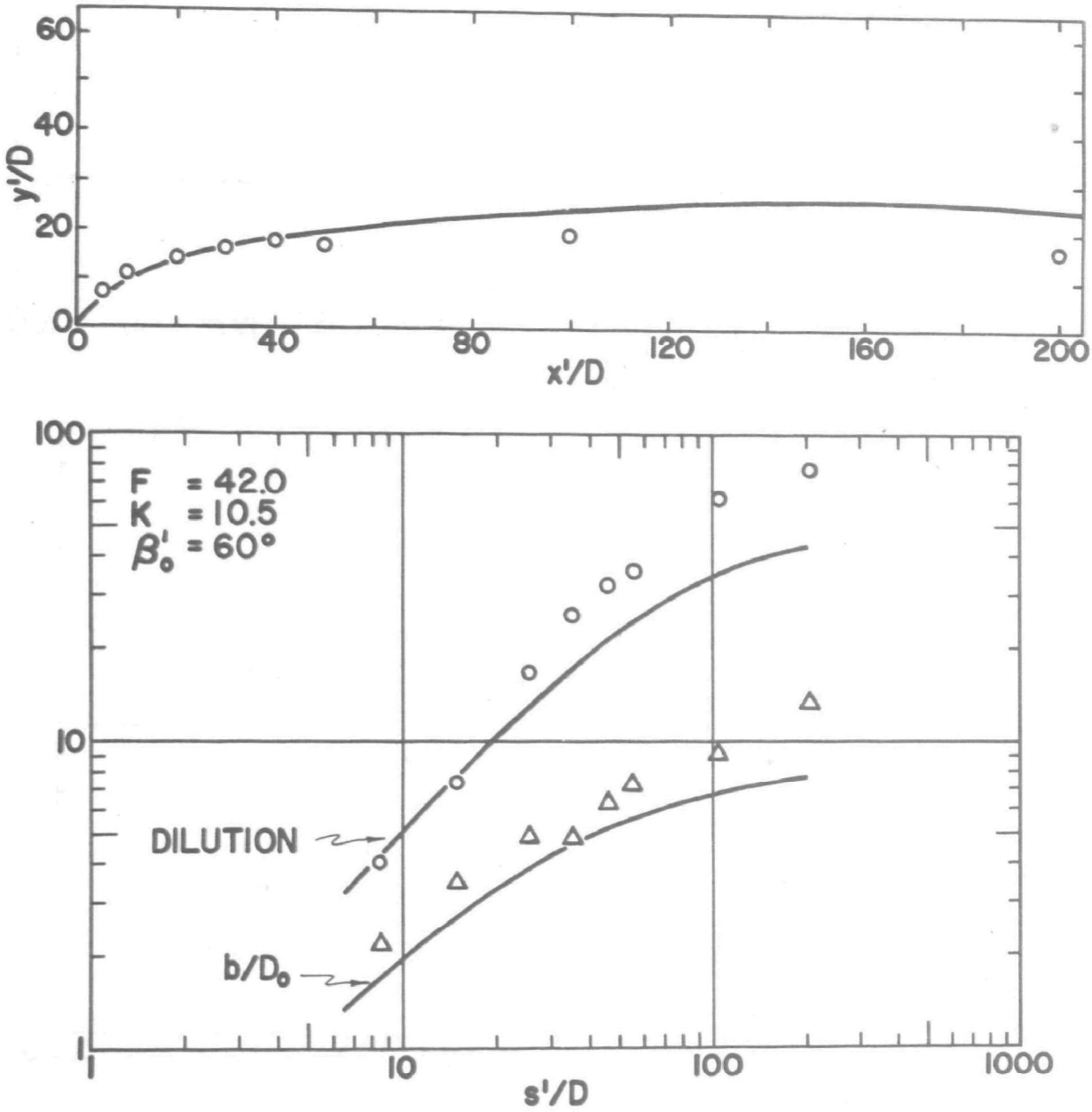

FIGURE 78 - OBSERVED VALUES AND THEORETICAL CURVES
PREDICTED BY ABRAHAM'S MODEL - RUN NO. 33

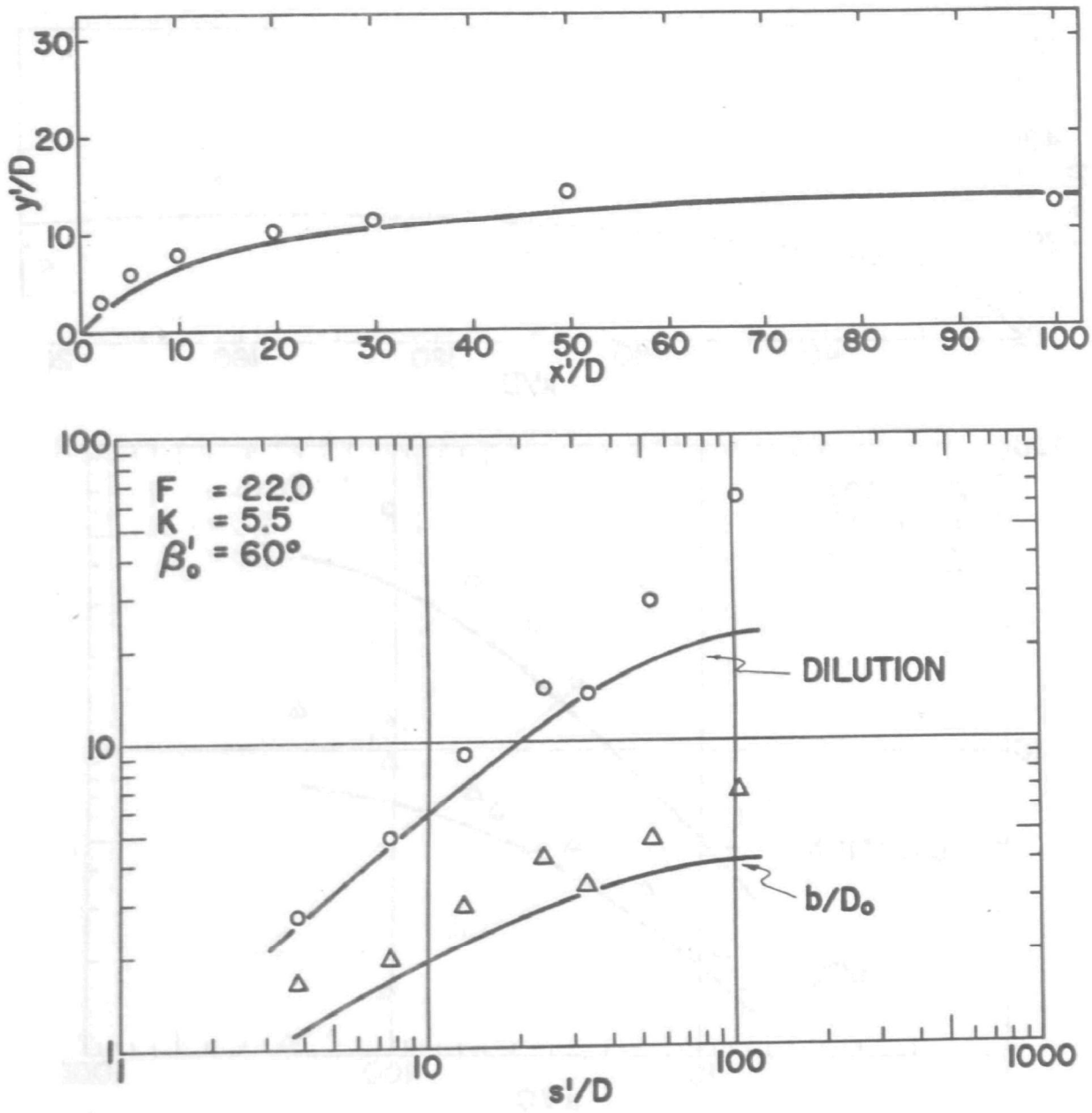

FIGURE 79 - OBSERVED VALUES AND THEORETICAL CURVES
PREDICTED BY ABRAHAM'S MODEL - RUN NO. 32

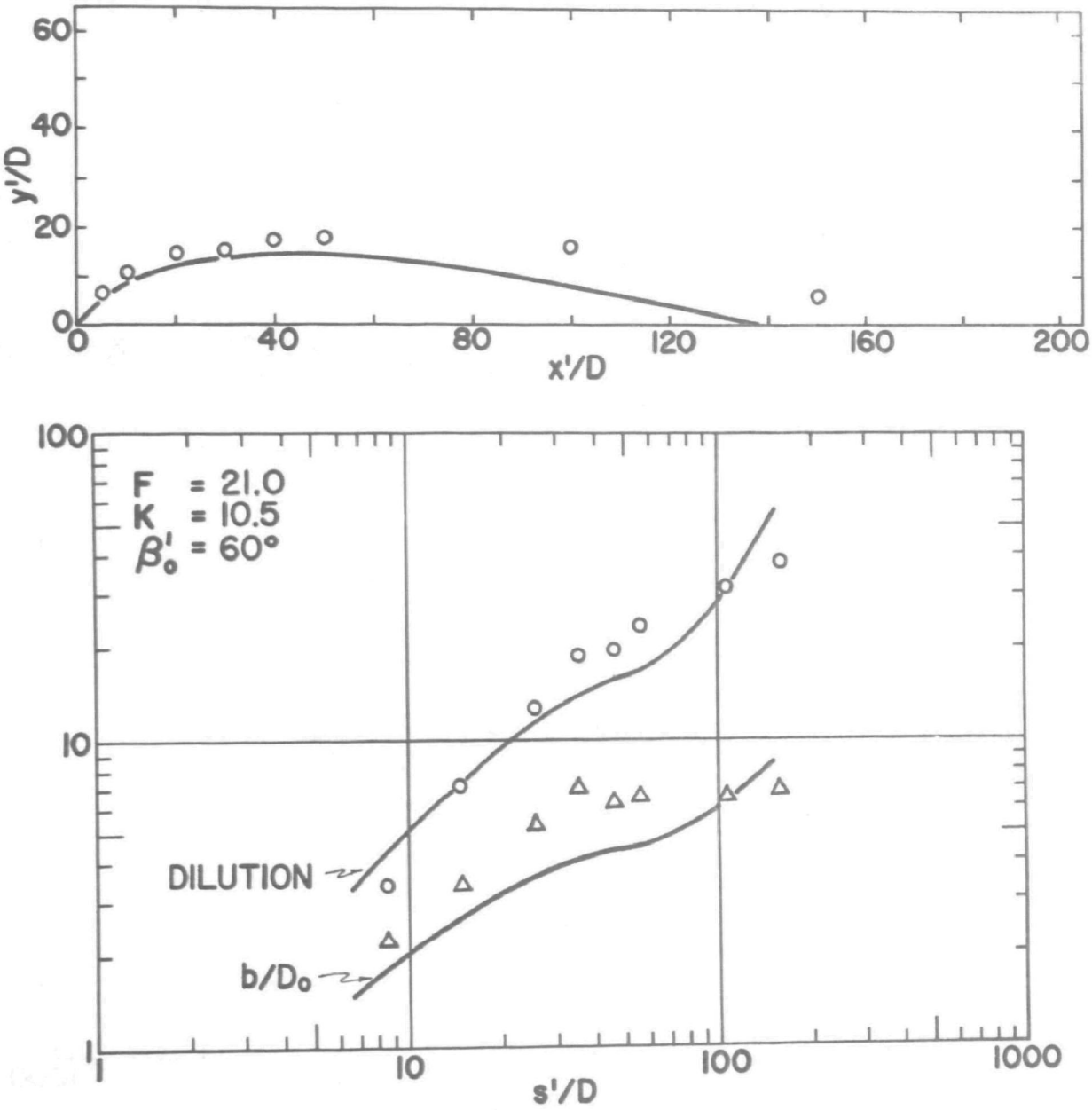

FIGURE 80 - OBSERVED VALUES AND THEORETICAL CURVES
PREDICTED BY ABRAHAM'S MODEL - RUN NO. 28

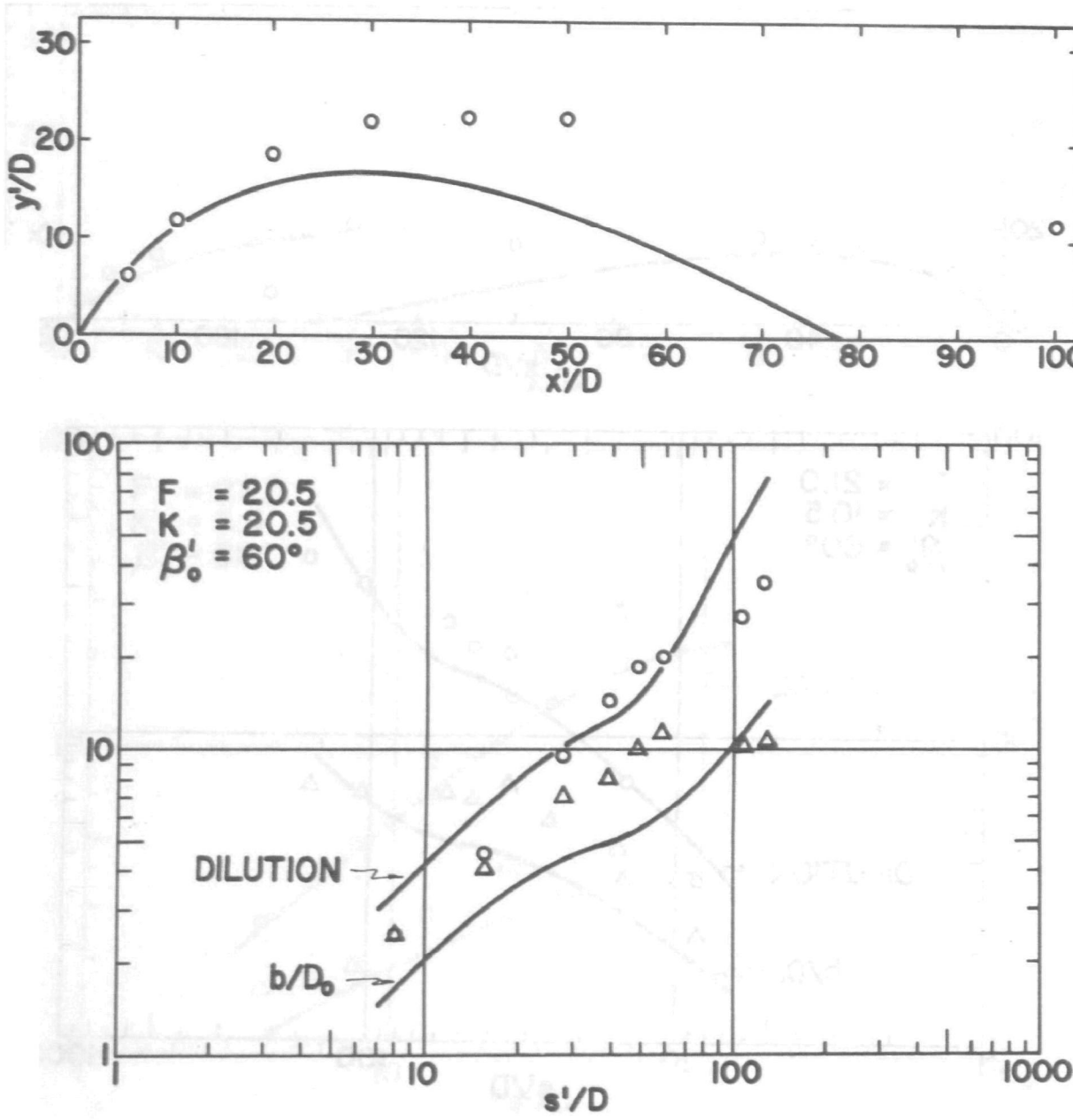

FIGURE 81 - OBSERVED VALUES AND THEORETICAL CURVES PREDICTED BY ABRAHAM'S MODEL - RUN NO. 30

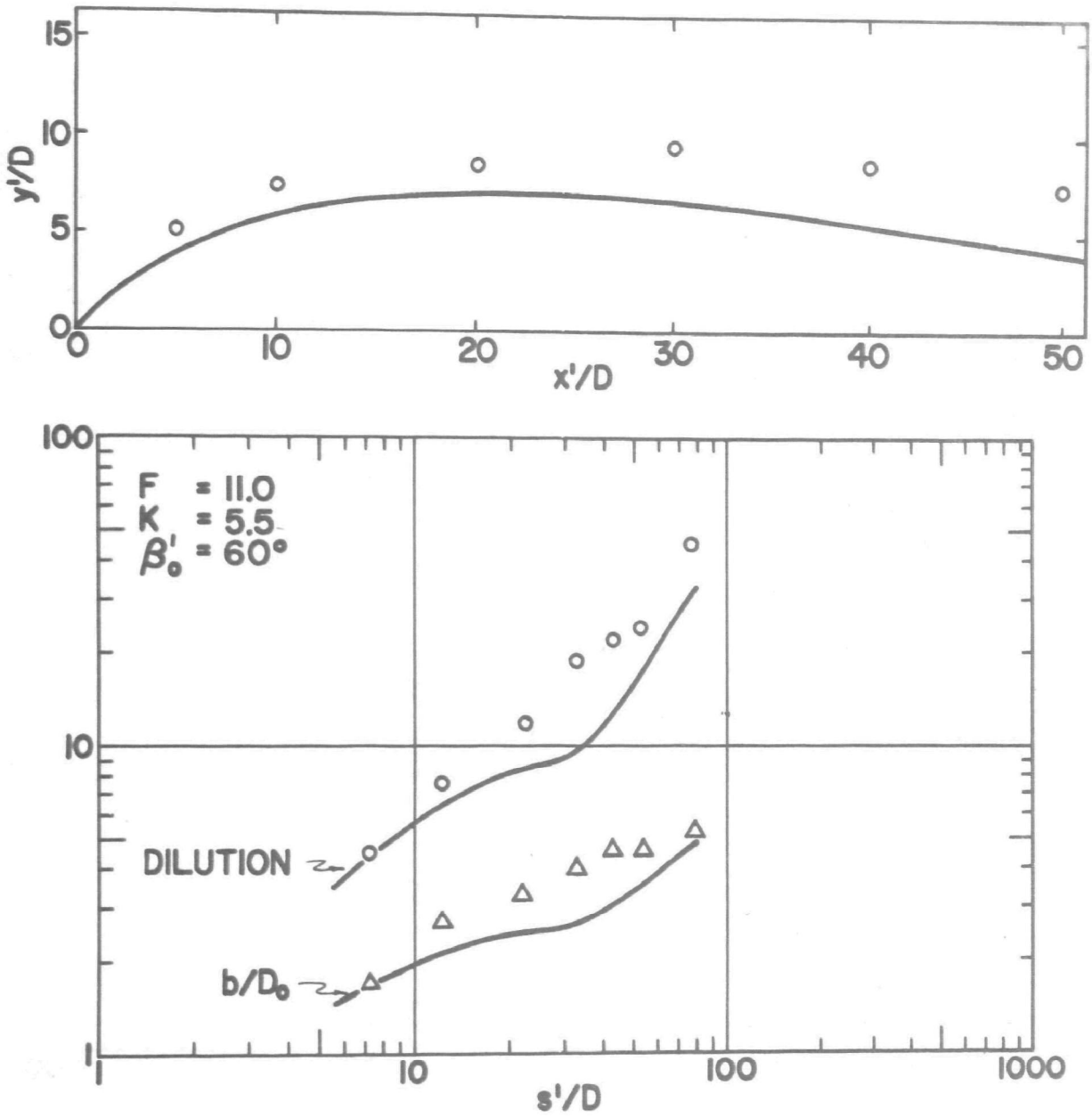

FIGURE 82 - OBSERVED VALUES AND THEORETICAL CURVES
PREDICTED BY ABRAHAM'S MODEL - RUN NO. 27

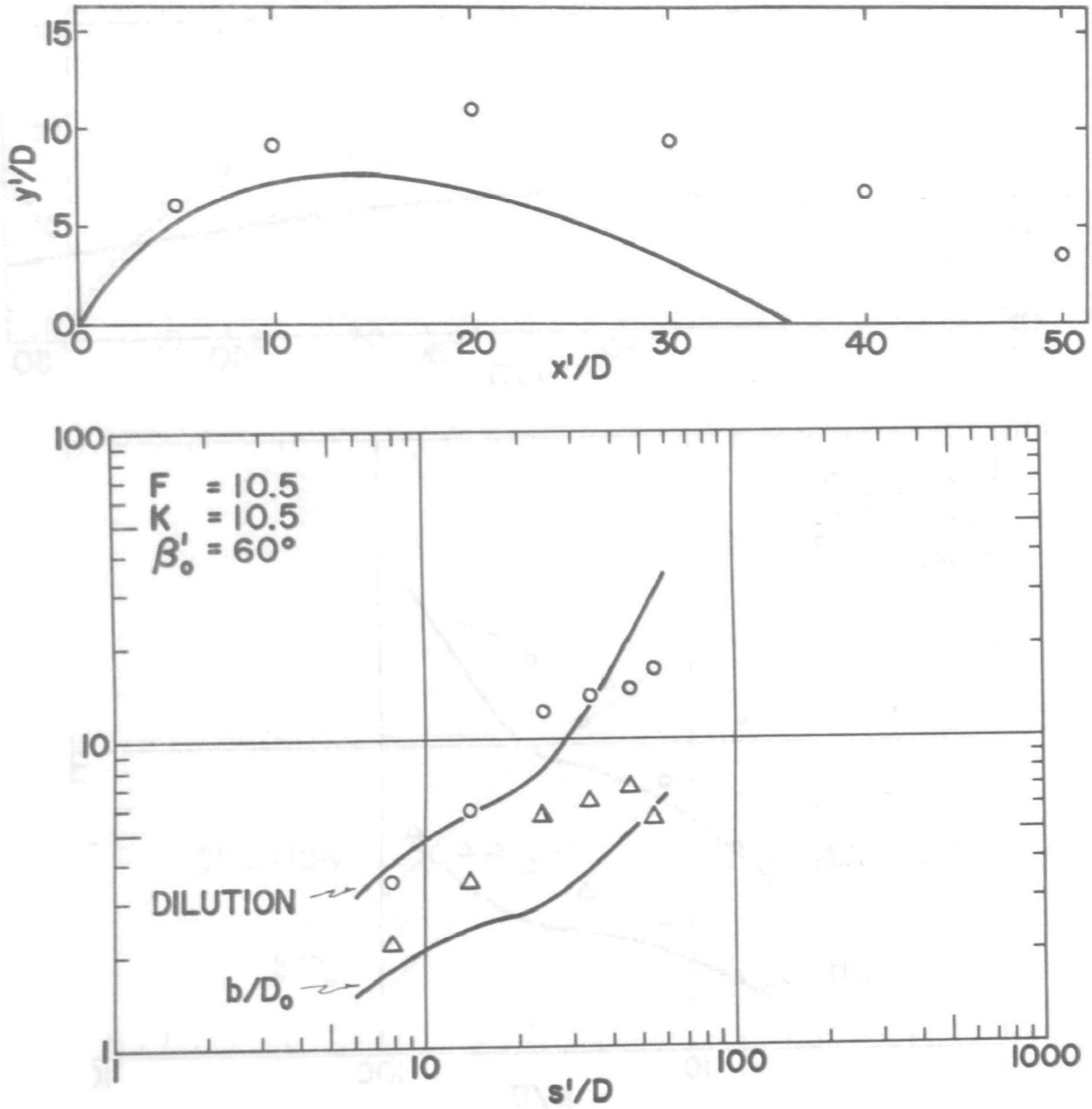

FIGURE 83 - OBSERVED VALUES AND THEORETICAL CURVES PREDICTED BY ABRAHAM'S MODEL - RUN NO. 29

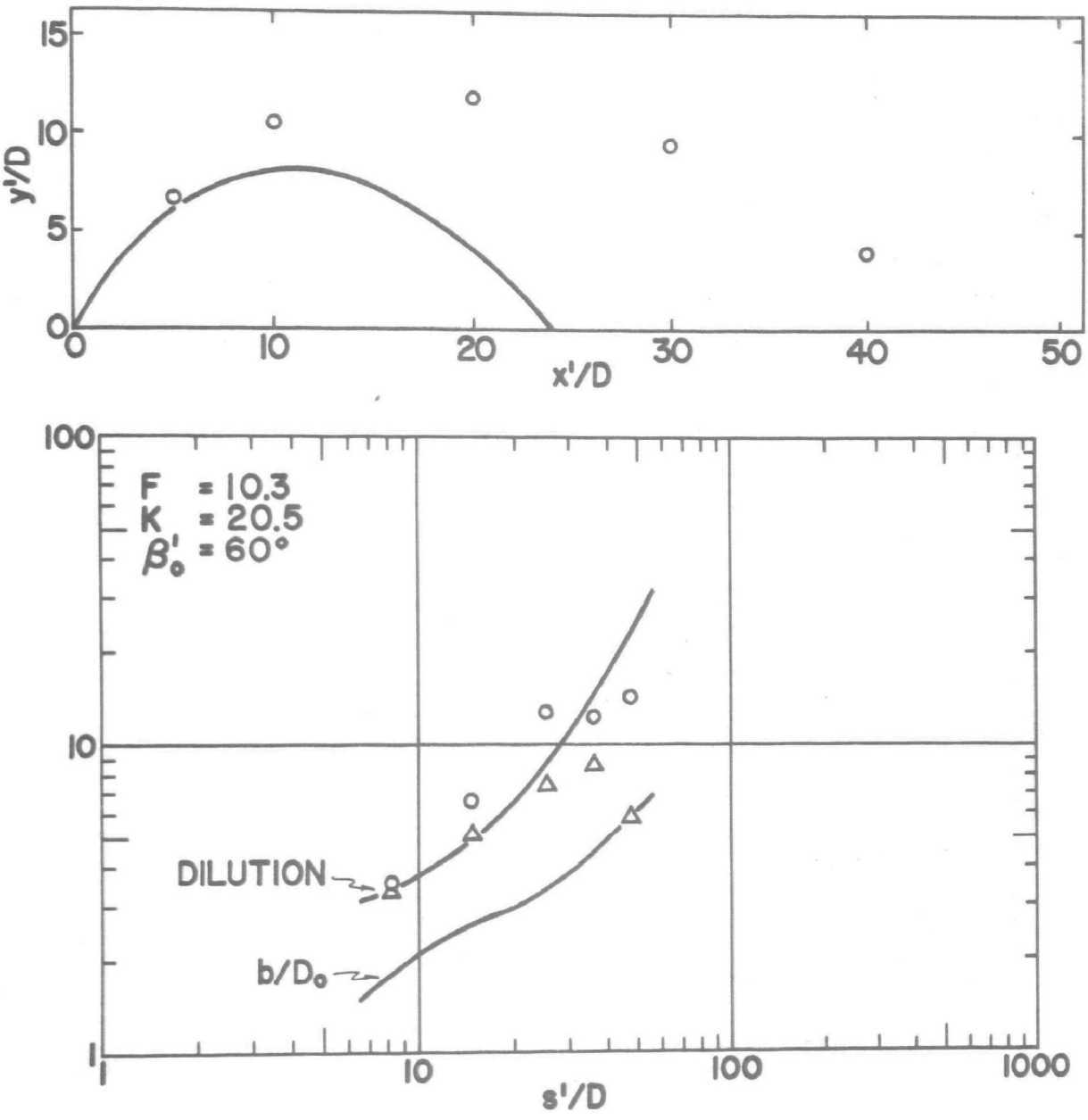

FIGURE 84 - OBSERVED VALUES AND THEORETICAL CURVES
PREDICTED BY ABRAHAM'S MODEL - RUN NO. 31

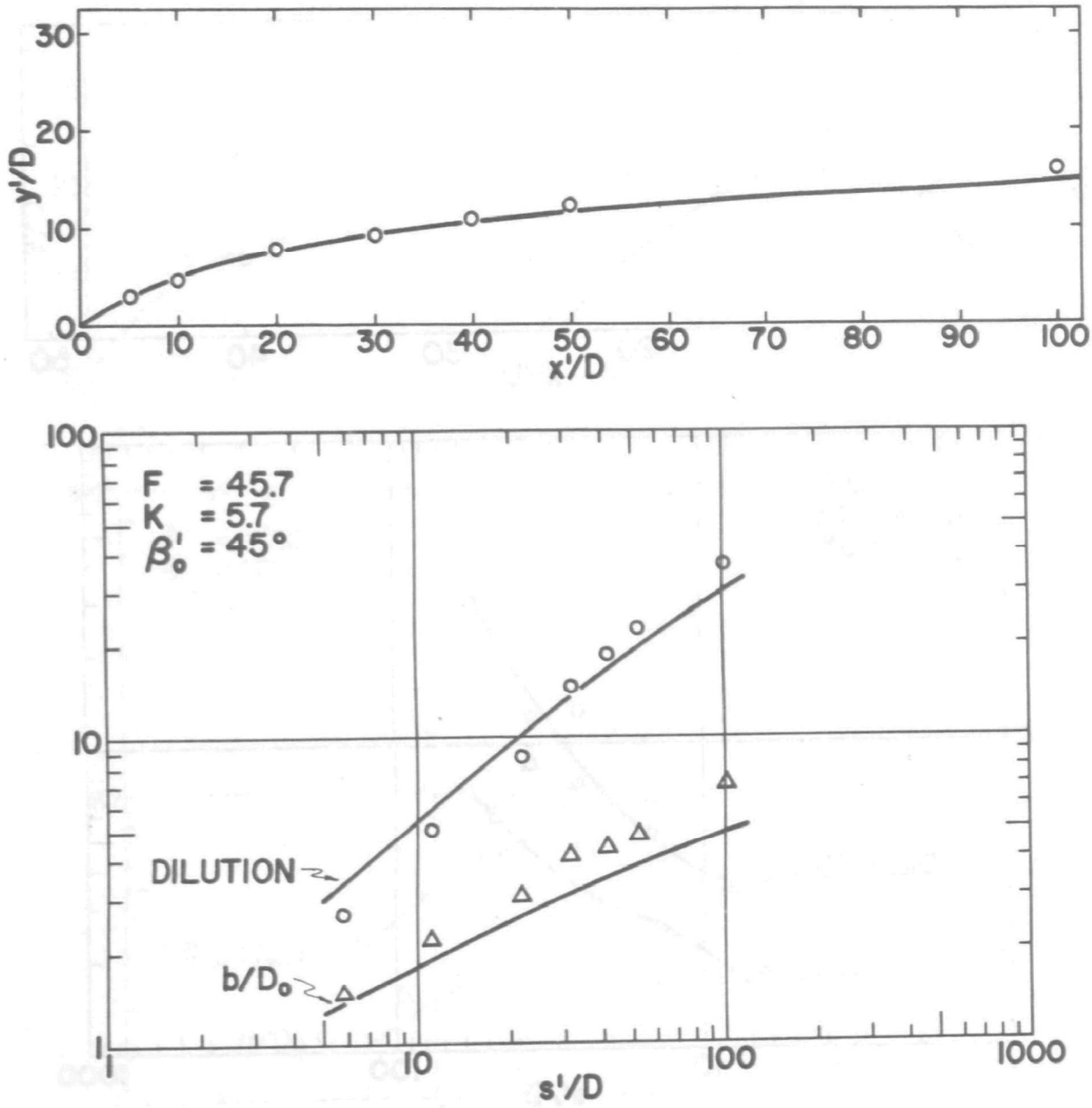

FIGURE 85 - OBSERVED VALUES AND THEORETICAL CURVES PREDICTED BY ABRAHAM'S MODEL - RUN NO. 26

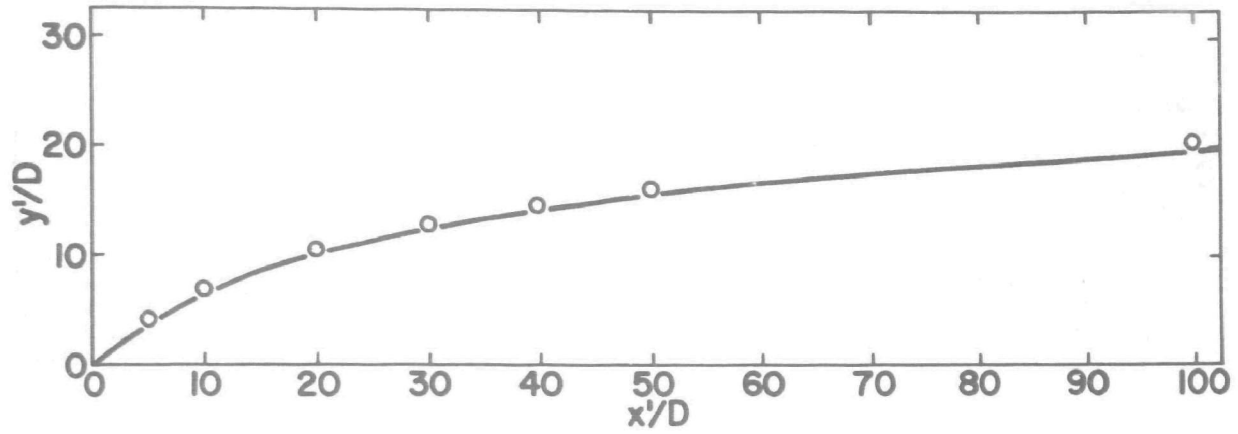

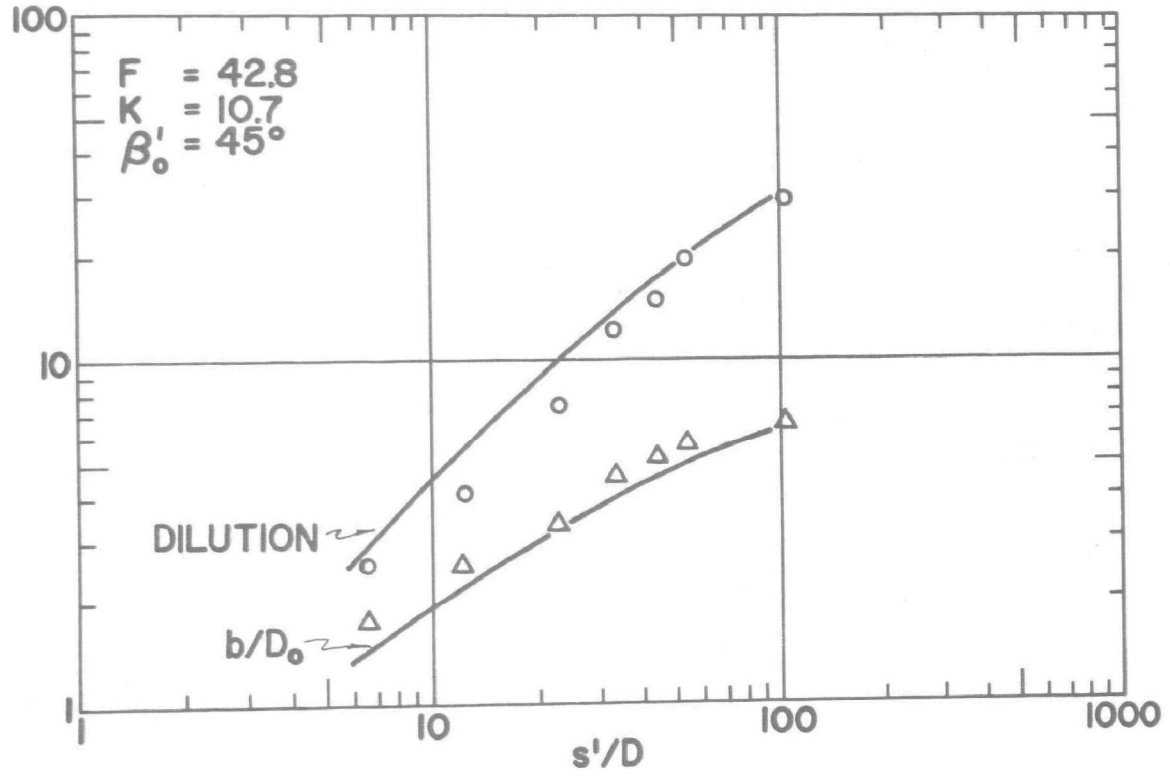

FIGURE 86 - OBSERVED VALUES AND THEORETICAL CURVES
PREDICTED BY ABRAHAM'S MODEL - RUN NO. 22

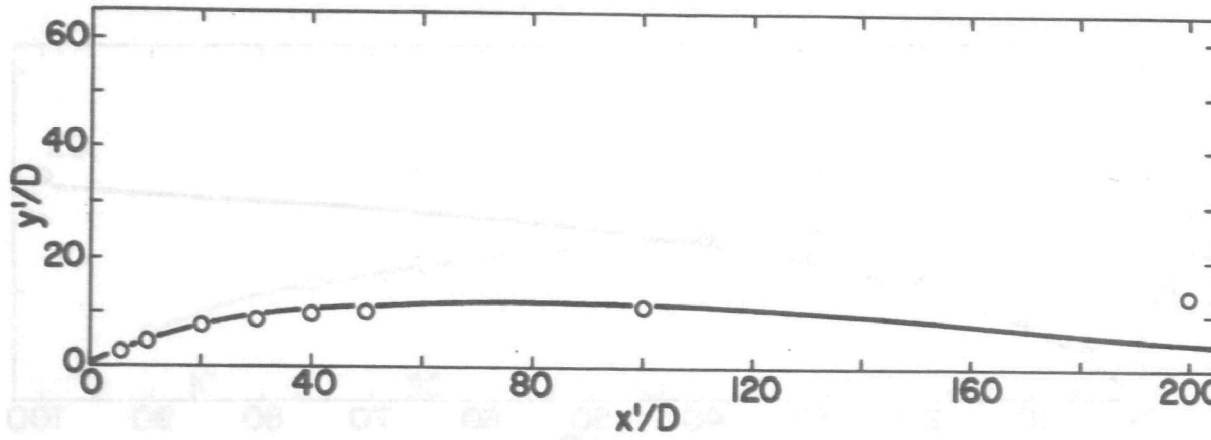

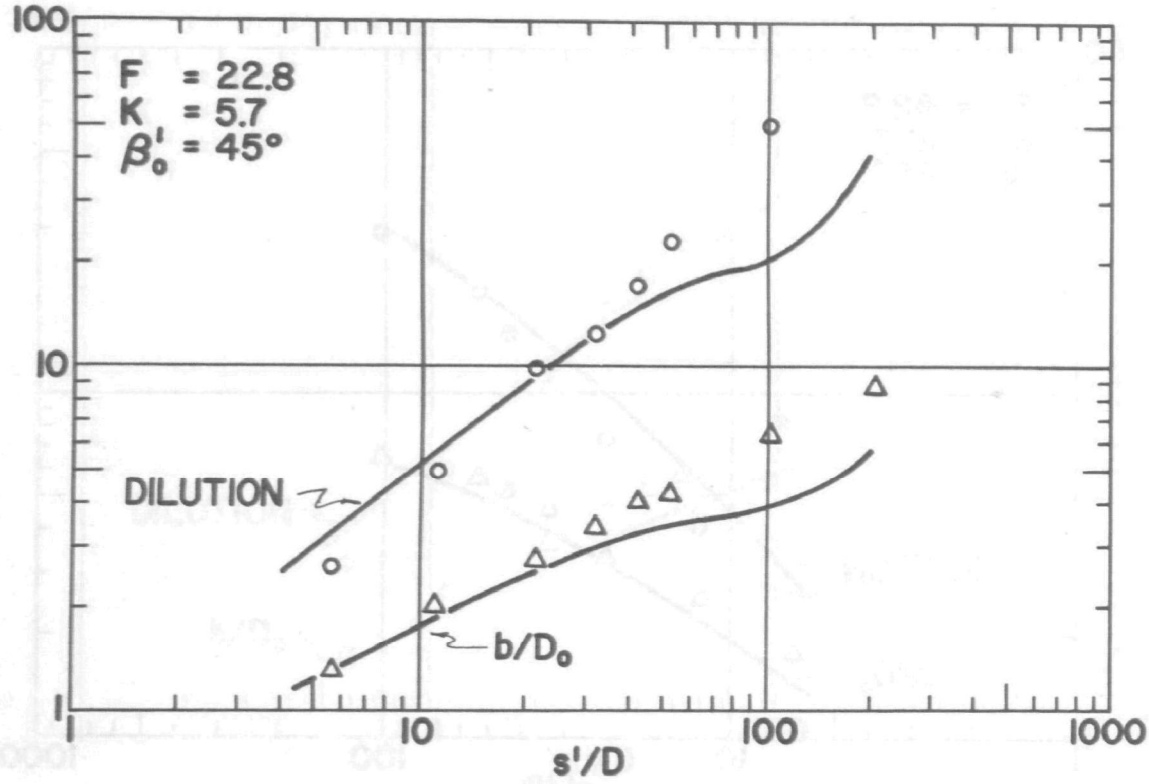

FIGURE 87 - OBSERVED VALUES AND THEORETICAL CURVES
PREDICTED BY ABRAHAM'S MODEL - RUN NO. 21

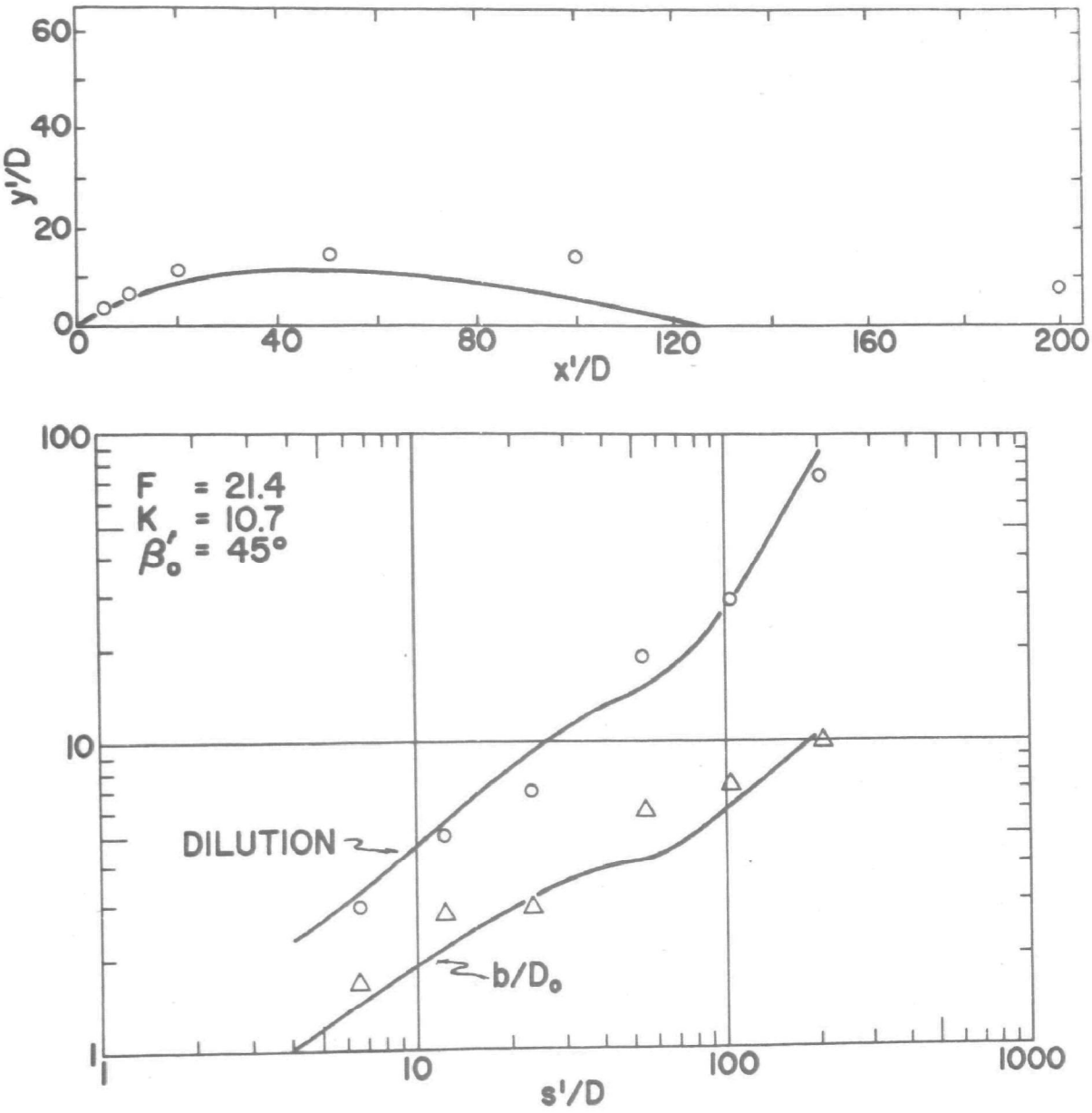

FIGURE 88 - OBSERVED VALUES AND THEORETICAL CURVES
PREDICTED BY ABRAHAM'S MODEL - RUN NO. 20

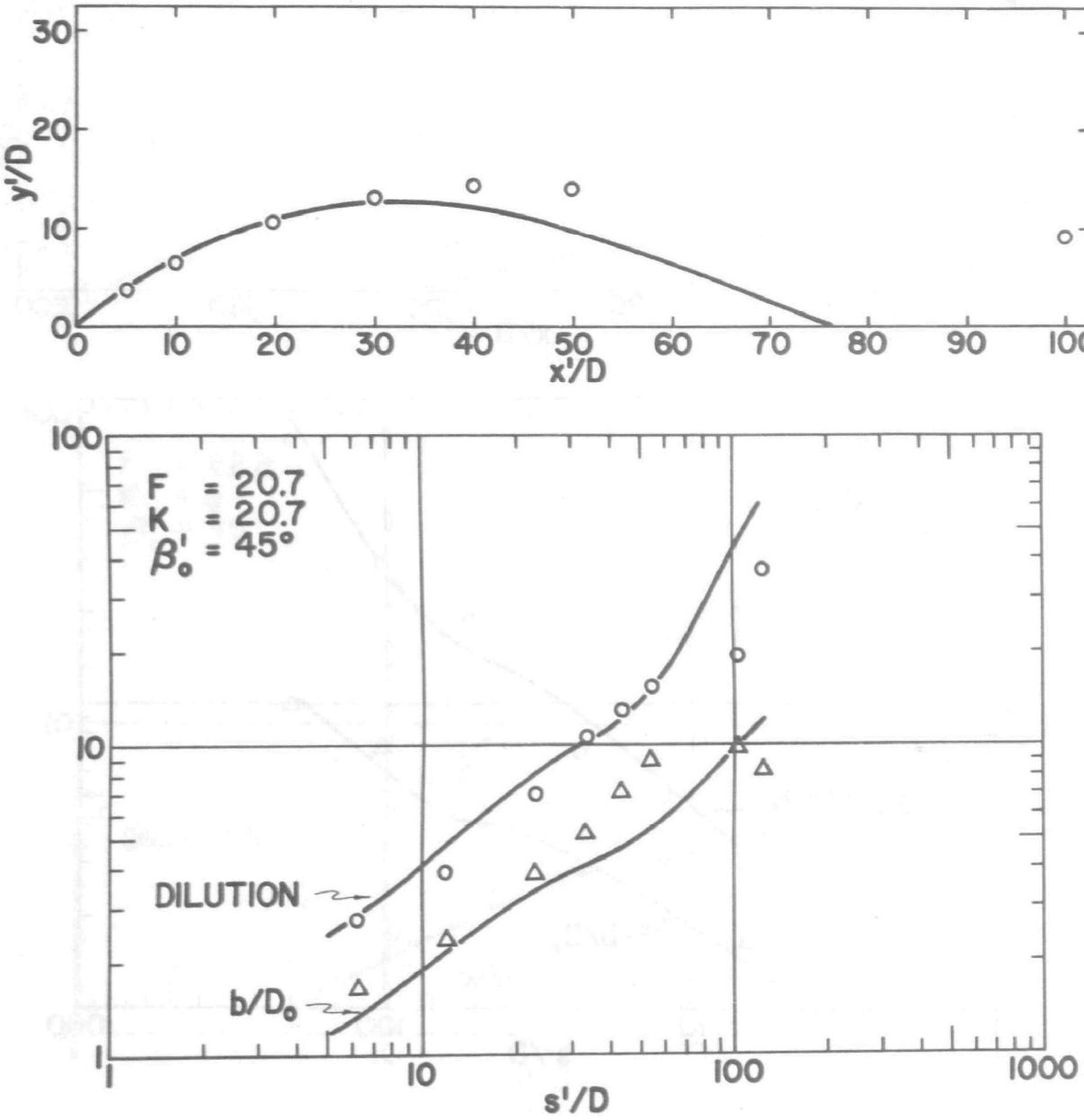

FIGURE 89 - OBSERVED VALUES AND THEORETICAL CURVES
PREDICTED BY ABRAHAM'S MODEL - RUN NO. 24

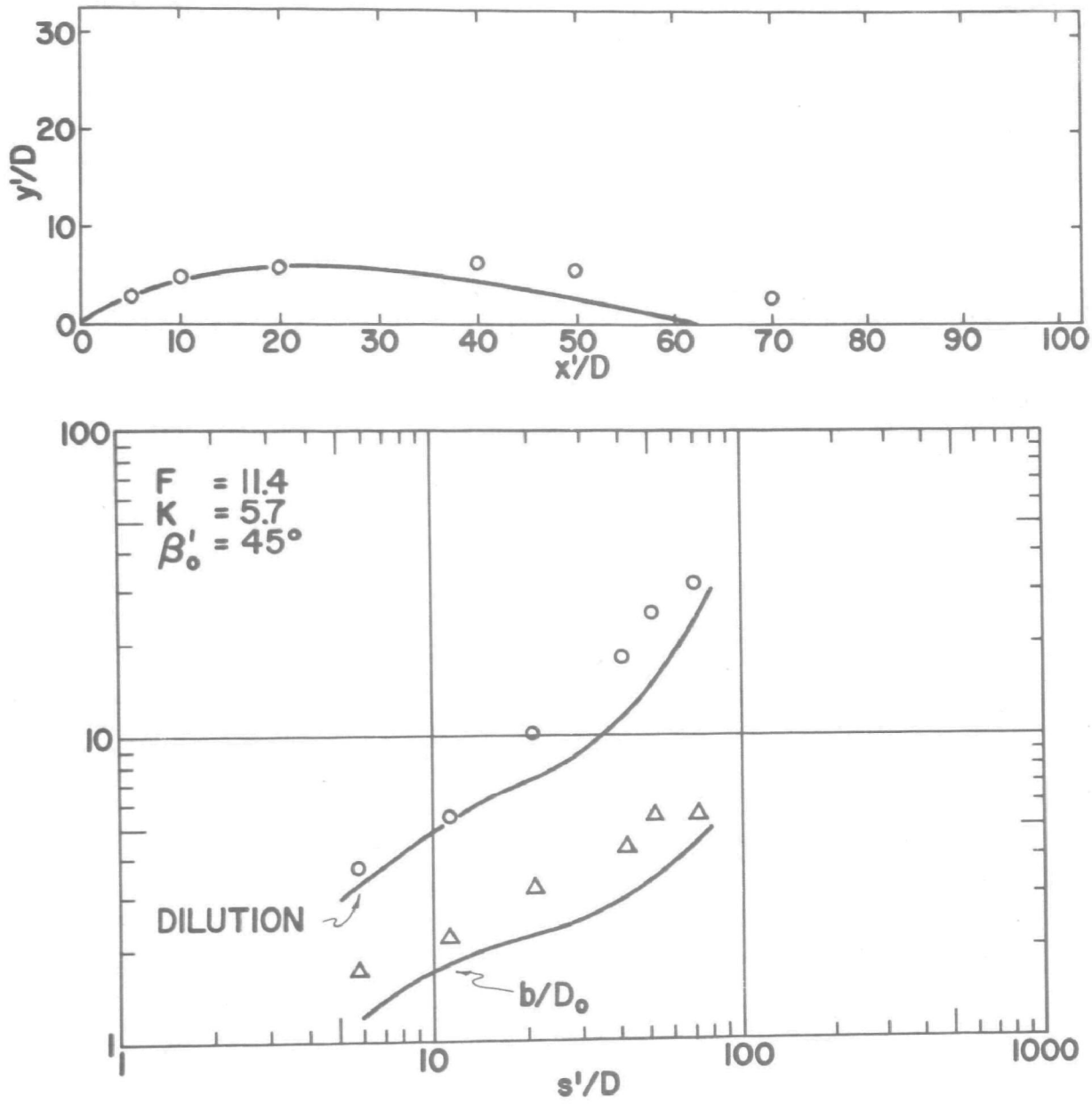

FIGURE 90 - OBSERVED VALUES AND THEORETICAL CURVES
PREDICTED BY ABRAHAM'S MODEL - RUN NO. 19

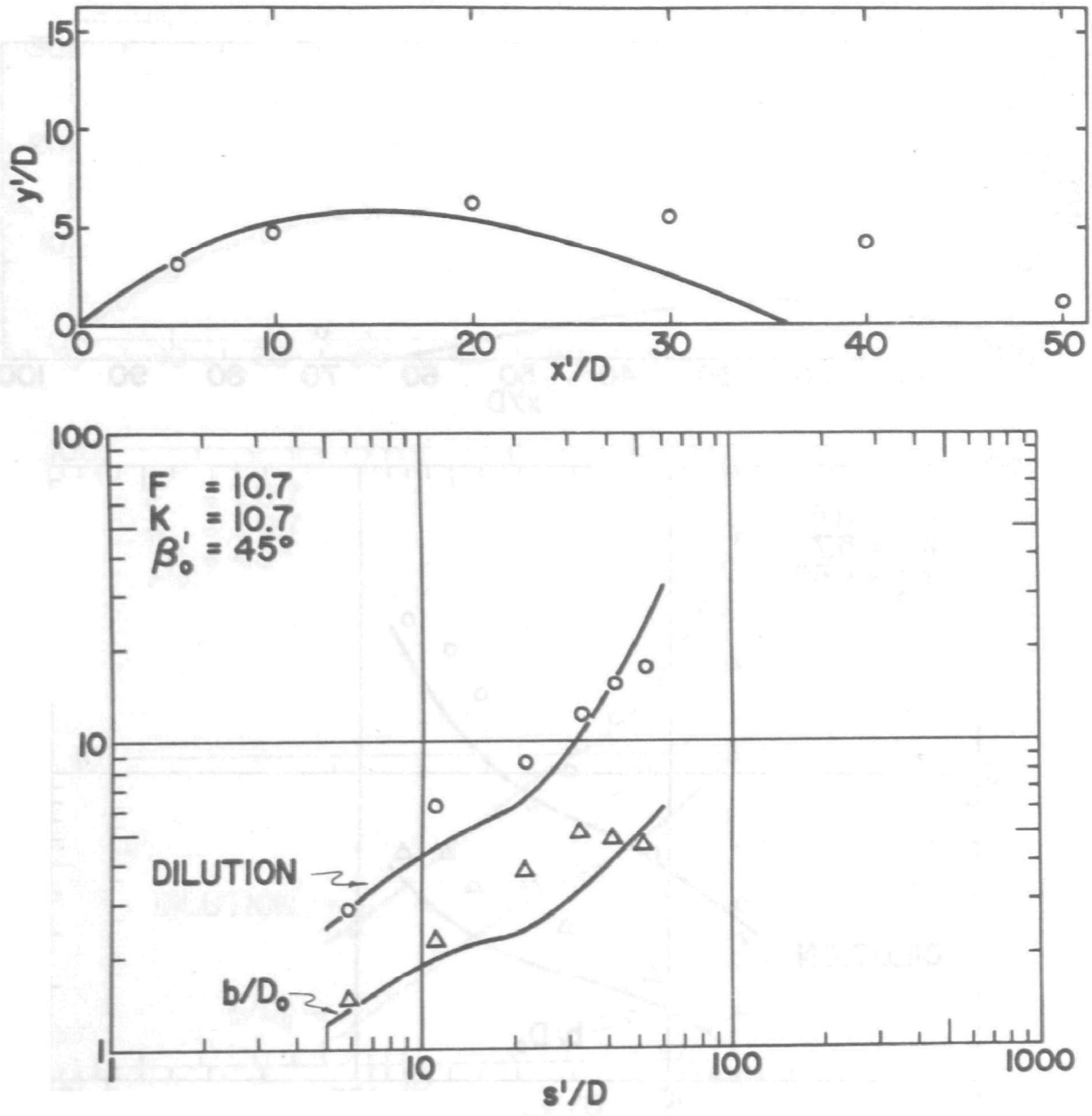

FIGURE 91 - OBSERVED VALUES AND THEORETICAL CURVES PREDICTED BY ABRAHAM'S MODEL - RUN NO. 23

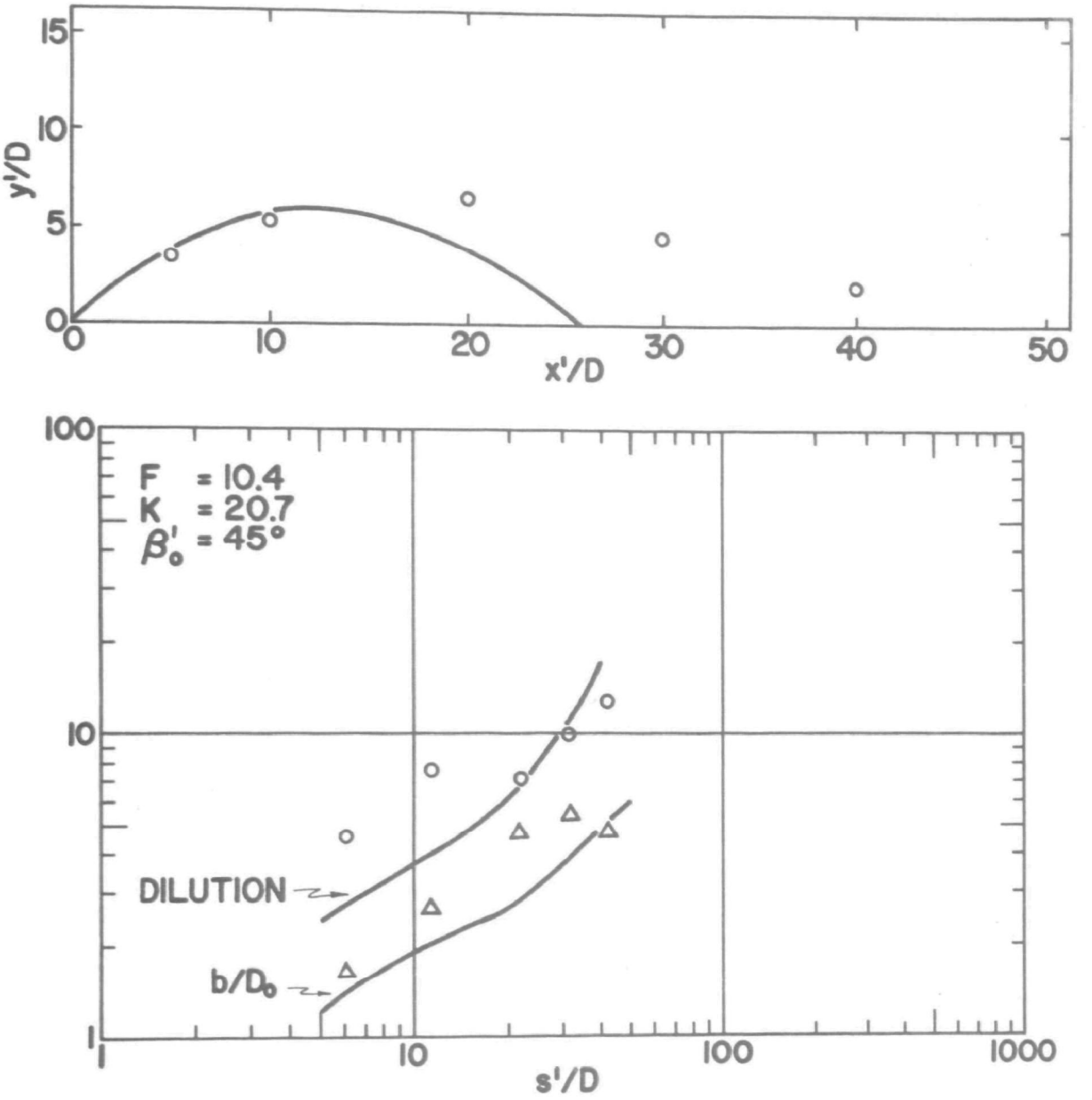

FIGURE 92 - OBSERVED VALUES AND THEORETICAL CURVES
PREDICTED BY ABRAHAM'S MODEL - RUN NO. 25

*U.S. GOVERNMENT PRINTING OFFICE:1974 546-319/385 1-3

SELECTED WATER RESOURCES ABSTRACTS

INPUT TRANSACTION FORM

W

Negatively Buoyant Jets in a Cross Flow

Anderson, J.L., Parker, F.L., & Benedict, B.A.

Vanderbilt University
Environmental & Water Resources Engineering
Nashville, Tennessee

16130 FDQ

Environmental Protection Agency

Environmental Protection Agency No. EPA-660/2-73-012, October 1973.

200 words

Modification of Fan's and Abrahams jet diffusion models were used to predict the trajectory and dilution of a negatively buoyant jet. Such jets can occur when a chemical waste is discharged into a less dense ambient water or when cool, hypolimnetic water is used for condenser cooling water and discharged into less dense surface waters, then a sinking jet would result. Experimental investigations were conducted involving different combinations of densimetric Froude number, velocity ratio, and initial angle of discharge. Salt was used as the tracer, yielding a fluid that was denser than the ambient receiving water and facilitated measuring concentration profiles of the jet plume. The experimental data was then fitted with predicted jet dilution, trajectory, and cross sectional values for each model. The values of the entrainment coefficient were chosen as the one which best fit the experimental data for the particular combination of densimetric Froude number, velocity ratio, and initial angle of discharge. The value of the drag coefficient was chosen as zero for both models since any other value would predict a trajectory whose rise would be less than experimentally observed. Typically, for all angles of discharge the value of entrainment increased with a decrease in the velocity ratio and with an increase in densimetric Froude number. Additionally, there was a marked decrease in the entrainment coefficient with a decrease in the initial angle of discharge.

17a. Descriptors

Thermal Pollution, Thermal Power Plants, Density Currents, Entrainment

17b. Identifiers

Jet Discharge, Near Field, Jet Trajectory, Negative Buoyant Jet, Waste Dilution, Densimetric Froude Number

05B

19. Security Class. (Report)	21. No. of Pages
20. Security Class. (Page)	22. Price

Send To:

WATER RESOURCES SCIENTIFIC INFORMATION CENTER
U.S. DEPARTMENT OF THE INTERIOR
WASHINGTON, D. C. 20240

Dr. Frank L. Parker | Vanderbilt University, Nashville, Tenn.